Universidade Federal do Rio Grande – FURG

Instituto de Oceanografia

Programa de Pós-Graduação em Oceanologia

METABOLISMO AQUÁTICO NO ESTUÁRIO DA LAGOA DOS PATOS: UMA ABORDAGEM MULTIESCALAR

LUÍS HENRIQUE BORDIN

Tese apresentada ao Programa de Pós-Graduação em Oceanologia, como parte dos requisitos para a obtenção do título de Doutor.

Orientadora: *Profa. Dra.* EUNICE DA COSTA MACHADO
Universidade Federal do Rio Grande (FURG), Brasil.

Coorientadora: *Profa. Dra.* ELISA HELENA LEÃO FERNANDES
Universidade Federal do Rio Grande (FURG), Brasil.

Coorientador: *Prof. Dr.* CARLOS RAFAEL BORGES MENDES
Universidade Federal do Rio Grande (FURG), Brasil.

Rio Grande, RS, Brasil

Agosto 2023

METABOLISMO AQUÁTICO NO ESTUÁRIO DA LAGOA DOS PATOS: UMA ABORDAGEM MULTIESCALAR

Tese apresentada ao Programa de Pós-Graduação em Oceanologia, como parte dos requisitos para a obtenção do título de Doutor

por

LUÍS HENRIQUE BORDIN

Rio Grande, RS, Brasil

Agosto 2023

Ficha Catalográfica

B729m Bordin, Luís Henrique.
Metabolismo aquático no Estuário da Lagoa dos Patos: uma abordagem multiescalar / Luís Henrique Bordin. – 2023.
214 f.

Tese (doutorado) – Universidade Federal do Rio Grande – FURG, Programa de Pós-Graduação em Oceanologia, Rio Grande/RS, 2023.
Orientadora: Dra. Eunice da Costa Machado.
Coorientadora: Dra. Elisa Helena Leão Fernandes.
Coorientador: Dr. Carlos Rafael Borges Mendes.

1. Produção primária 2. Respiração 3. Nutrientes 4. Clorofila-a 5. Fitoplâncton 6. Dióxido de carbono I. Machado, Eunice da Costa II. Fernandes, Elisa Helena Leão III. Mendes, Carlos Rafael Borges IV. Título.

CDU 551.46

Catalogação na Fonte: Bibliotecário José Paulo dos Santos CRB 10/2344

SERVIÇO PÚBLICO FEDERAL
MINISTÉRIO DA EDUCAÇÃO
UNIVERSIDADE FEDERAL DO RIO GRANDE - FURG
COORD CUR DE PG EM OCEANOLOGIA

ATA DE REUNIÃO, DE 24 DE JULHO DE 2023

ATA ESPECIAL DE DEFESA DE TESE DE DOUTORADO – 03/2023

Às quatorze horas do dia quatro de agosto do ano de dois mil e vinte e três , por videoconferência e presencial, reuniu-se a Comissão Examinadora da Tese de **DOUTORADO** intitulada **" Metabolismo aquático no estuário da Lagoa dos Patos: uma abordagem multiescalar"**, do **Acad. Luis Henrique Bordin .** A Comissão Examinadora foi composta pelos seguintes membros: Profa. Dra. Eunice da Costa Machado – Orientadora – (IO/FURG), Profa. Dra. Elisa Helena L. Fernandes – Co-orientadora – (IO/FURG), Prof. Dr. Carlos Rafael B. Mendes – Co-orientador (IO/FURG), Prof. Dr. Carlos Augusto F. Schettini – (IO/FURG) e Dra. Nilva Brandini – (UFF). Dando início à reunião, a Coordenadora do Programa de Pós-Graduação em Oceanologia-PPGO, Profa. Dra. Grasiela Lopes L. Pinho, agradeceu a presença de todos e fez a apresentação da Comissão Examinadora. Logo após esclareceu que o Candidato teria um tempo de 45 a 60 min para explanação do tema, e cada membro da Comissão Examinadora, um tempo máximo de 30 min para perguntas. A seguir, passou à palavra ao Candidato que apresentou o tema e respondeu às perguntas formuladas. Após ampla explanação, a Comissão Examinadora reuniu-se em reservado para discussão do conceito a ser atribuído ao Candidato. Foi estabelecido que as sugestões de todos os membros da Comissão Examinadora, que seguem em pareceres em anexo, foram aceitas pelo Orientador/Candidato para incorporação na versão final da Tese. Finalmente, a Comissão Examinadora considerou o candidato **APROVADO,** por unanimidade. Nada mais havendo a tratar, foi lavrada a presente ATA que após lida e aprovada, será assinada pela Comissão Examinadora, pelo Candidato e pela Coordenadora do Programa de Pós-Graduação em Oceanologia.

Documento assinado eletronicamente por **NILVA registrado(a) civilmente como NILVA BRANDINI**, **Usuário Externo**, em 31/07/2023, às 15:52, conforme horário oficial de Brasília, com fundamento no art. 6º, § 1º, do Decreto nº 8.539, de 8 de outubro de 2015 .

Documento assinado eletronicamente por **Carlos Rafael Borges Mendes**, **Servidor**, em 10/08/2023, às 15:39, conforme horário oficial de Brasília, com fundamento no art. 6º, § 1º, do Decreto nº 8.539, de 8 de outubro de 2015.

Documento assinado eletronicamente por **Carlos Augusto Franca Schettini**, **Servidor**, em 10/08/2023, às 15:49, conforme horário oficial de Brasília, com fundamento no art. 6º, § 1º, do Decreto nº 8.539, de 8 de outubro de 2015.

Documento assinado eletronicamente por **Luís Henrique Bordin**, **Usuário Externo**, em 10/08/2023, às 20:55, conforme horário oficial de Brasília, com fundamento no art. 6º, § 1º, do Decreto nº 8.539, de 8 de outubro de 2015.

Documento assinado eletronicamente por **Grasiela Lopes Leaes Pinho**, **Coordenadora de Curso**, em 11/08/2023, às 10:49, conforme horário oficial de Brasília, com fundamento no art. 6º, § 1º, do Decreto nº 8.539, de 8 de outubro de 2015.

Documento assinado eletronicamente por **Elisa Helena Leao Fernandes**, **Servidora**, em 22/08/2023, às 17:14, conforme horário oficial de Brasília, com fundamento no art. 6º, § 1º, do Decreto nº 8.539, de 8 de outubro de 2015.

Documento assinado eletronicamente por **Eunice da Costa Machado**, **Servidora**, em 06/09/2023, às 08:47, conforme horário oficial de Brasília, com fundamento no art. 6º, § 1º, do Decreto nº 8.539, de 8 de outubro de 2015.

A autenticidade do documento pode ser conferida no site https://sei.furg.br/sei/controlador_externo.php?acao=documento_conferir&acao_origem=documento_conferir&lang=pt_BR&id_orgao_acesso_externo=0 informando o código verificador **0090056** e o código CRC **9CBB2F6C**.

Referência: Caso responda este documento Ata de Reunião, indicar o Processo nº 23116.013637/2023-69 SEI nº 0090056

"Dance with the waves, move with the sea, let the rhythm of the water set your soul free."

Christy Ann Martine

Índice

Agradecimentos

Agradeço primeiramente à minha mãe, Jurema Maria Longhi, meu pai Rolindo José Bordin e irmão Giuliano André Bordin, por sempre me apoiarem e me incentivarem nas minhas escolhas e decisões, e principalmente, a seguir os meus sonhos. Agradeço também aos meus familiares, de forma geral, que da sua forma sempre estiveram ao meu lado, me dando forças e apoio moral.

Gostaria também de agradecer à minha companheira Gabrielle, quem esteve mais diretamente comigo, me acompanhando, me apoiando, incentivando, e me dando força nos momentos conturbados. Obrigado meu amor, pelo seu cuidado, carinho, dedicação e compreensão.

Não menos importantes, aliás, cruciais ao longo de toda a minha moradia em Rio Grande, foram os meus amigos. E quantos amigos incríveis eu ganhei nesse período, são tantos, que eu tenho receio de citar nomes e acabar esquecendo de incluir alguém. Eu cheguei em Rio Grande cheio de incertezas, sem conhecer quase ninguém, e vocês me recepcionaram e me integraram na primeira semana. Que turma bacana, unida, animada, festeira, mas também companheira e solidária nos momentos difíceis. Vocês são incríveis.

À minha orientadora Eunice Machado, quem me inspirou e motivou a seguir especialização em biogeoquímica marinha, quem me acompanhou durante toda a minha formação, da graduação ao doutorado, meu muito obrigado. Agradeço também aos meus coorientadores Elisa Fernandes e Rafael Mendes, por todo apoio, paciência, compreensão e ensinamentos. Vocês três me inspiraram e continuarão me inspirando ao longo da minha carreira acadêmica e profissional. Admiro muito vocês.

Sou também muito grato ao Programa de Pós-Graduação em Oceanologia da FURG, aos coordenadores nesse período, Rodrigo Kerr e Grasiela Pinho, ao secretário Clabisnei, e a todo o corpo docente que foram meus professores direta ou indiretamente. Agradeço também a minha banca de acompanhamento, professores Rodrigo, Monica e Guto.

Agradeço aos colegas de laboratório e de curso, que me ajudaram em diversas etapas do meu doutorado, seja de forma prática e/ou intelectual. Aos

colegas do Laboratório de Hidroquímica Renata, Elis, Alessandra, Gabriel, Carlos, Camila, Aline, Paco, Theo, Priscila, Yasmin e Matheus. Aos colegas do Laboratório de Oceanografia Costeira Pablo, Paulo Victor, Roberto, Monique, Ítele, Carol, Thaís, Cristal, Rafael, Ana.

Muito obrigado aos colegas de outros laboratórios da FURG que também contribuíram pro andamento do projeto dessa tese, Rubens, André, Iole, Andrea, Cíntia, Mariah, Ella, Camila, Augusto, Pedro, Thiago.

Sou imensamente grato ao programa Sistema de Monitoramento da Costa Brasileira (SiMCosta), à coordenação professor Garcia e Ella, e aos demais integrantes que me ajudaram, Rubens, André, Camila e Marília. Obrigado pelo empréstimo da sonda multiparamétrica, pelas instruções, pelo apoio, e pela manutenção das boias meteoceanográficas, equipamentos que foram cruciais em fornecer dados para essa tese.

Finalmente, agradeço à CAPES (Programa CAPES PROEX bolsa de doutorado, processo n◦ 88887.342954/2019-00) pela concessão da bolsa de doutorado, ao projeto LOAD (Projeto n° N62909- 19-1-2145), financiado pela *Office of Naval Research*, que subsidiou a embarcação durante a campanha amostral que compôs a primeira etapa/artigo dessa tese.

Lista de Figuras

Lista de Tabelas

Lista de Acrônimos e Abreviações

A

ADCP – Perfilador acústico de efeito Doppler

AIC – Critério de informação de Akaike

ANA – Agência nacional de águas

B

BrOA – Grupo Brasileiro de Pesquisa em Acidificação dos Oceanos

C

Chl-*a* – Clorofila-*a*

CO_2 – Dióxido de carbono

CR – Respiração da comunidade

C:P – Razão entre carbono e fósfoto

CTD – Sensor para medição de condutividade, temperatura e profundidade da água

CHEMTAX – Quimiotaxonomia

$C_6H_{12}O_6$ – Fórmula química da glicose (matéria orgânica)

D

DIN – Nitrogênio inorgânico dissolvido total

DIP – Fósforo inorgânico dissolvido total

DO – Oxigênio dissolvido

E

ETE – Estação de tratamento de esgoto

F

FCO_2 – Fluxos de dióxido de carbono entre água e a atmosfera

G

GAM – Modelo aditivo generalizado

GPP – Produção primária bruta

H

H_20 – Fórmula química da água

I

INMET – Instituto Nacional de Meteorologia

K

KW – Análise de variância de Kruskal-Wallis

L

LOICZ – *Land Ocean Interaction in the Coastal Zone*

N

NO_2^- - Fórmula química do nitrito

NO_3^- - Fórmula química do nitrato

NH_4^+ - Fórmula química do amônio

N:P – Razão entre nitrogênio e fósforo

N:Si – Razão entre nitrogênio e silício

NPP – Produção primária líquida

O

O_2 – Fórmula química do oxigênio

P

PELD – Pesquisa Ecológica de Longa Duração

PL – Lagoa dos Patos

PLE – Estuário da Lagoa dos Patos

PCA – Análise de componentes principais

***p*CO_2** – Pressão parcial do dióxido de carbono

pH – Potencial hidrogeniônico

PO_4^{3-} - Fórmula química do fosfato

psu – Unidade prática de salinidade

R

R – Respiração

RDA – Análise de redundância

S

SAX – Symbolic Aggregate Approximation

SD – Desvio Padrão

SE – Erro padrão

SiMCosta – Programa de monitoramento da costa brasileira

T

TRIX – Índice de estado trófico TRIX

Δ

∆DIP - Variação do fósforo inorgânico dissolvido total

∆DIN - Variação do nitrogênio inorgânico dissolvido total

Resumo

O metabolismo aquático em ecossistemas estuarinos apresenta grande importância para a ciclagem de nutrientes e carbono na interface continente oceano, estando sujeito às pressões antrópicas. No entanto, a abordagem metodológica comumente utilizada é limitada no tempo e no espaço. Neste contexto, essa tese buscou compreender o metabolismo aquático do estuário da Lagoa dos Patos de forma inédita, através de três metodologias complementares, capazes de expandir as estimativas espaço-temporalmente. Além disso, buscou ainda compreender as principais forçantes meteoceanográficas controladoras do metabolismo aquático em diferentes escalas de tempo e espaço. Ambas as estações amostradas pelos dois primeiros métodos (ambos baseados na variação do oxigênio dissolvido, M1 através de incubações com garrafas, e M2 através do método do oxigênio livre) se encontram em regiões de canal. O metabolismo líquido do ecossistema nestes locais foi predominantemente heterotrófico ao longo de todo o período analisado, com um valor médio anual de -168.6 mmol O_2 m^{-2} d^{-1}. As taxas de produção primária e respiração foram diretamente proporcionais. Os períodos com maior heterotrofia líquida foram a primavera e o verão, e os menores, o outono e o inverno. A elevada heterotrofia líquida foi atribuída à profundidade das estações onde foram realizadas as medições. Nessas regiões, a maior parte da coluna de água se encontrou limitada por luz, favorecendo a predominância da respiração. Em escala diária, os principais fatores que controlaram os processos metabólicos foram os ventos NE/SO, que induzem a saída/entrada de água estuarina/marinha do estuário, e influenciam a salinidade e os aportes de nutrientes e material particulado em suspensão, alóctones (rios) e autóctones (ressuspensão de fundo e mistura vertical). O final do verão austral apresentou limitação por nitrato associada à baixa drenagem continental que caracteriza este período. Em escala sazonal, a salinidade novamente foi um fator determinante, mas modulado pelo regime de chuvas, com menores salinidades e maior disponibilidade de nutrientes nos períodos chuvosos (fim de inverno, início de primavera), e maiores salinidades e menor disponibilidade de nutrientes no verão. Ambas as fontes de nutrientes também fornecem material particulado em suspensão, que diminuem a transparência da água. Assim, a produção

primária no estuário da Lagoa dos Patos é colimitada por luz e nutrientes, com condições alternantes entre maior limitação por um dos fatores, a depender das condições meteoceanográficas. A escala interanual foi examinada apenas pela comparação entre as primaveras de cada ano. Nessa escala, a salinidade e processos hidrográficos foram novamente determinantes. Contudo, o efeito foi intensificado devido aos extremos dos regimes hidrológicos, provavelmente relacionados ao fenômeno El Niño Oscilação Sul. Na primavera de 2016 um ciclone extratropical na região sul do Brasil apresentou precipitações e vazão muito acima das médias, elevando as taxas metabólicas, principalmente as respiratórias, aos maiores níveis encontrados de todo o período (líquido: -1382 mmol O_2 m^{-2} d^{-1}). Estes resultados evidenciam os potenciais efeitos das mudanças climáticas na biogeoquímica do estuário da Lagoa dos Patos, e destacam a importância de programas de monitoramento complementares e de longa duração. Por fim, o terceiro método (M3: modelagem de caixas LOICZ), permitiu extrapolar o metabolismo aquático para toda a área do estuário da Lagoa dos Patos, porém, apenas para os períodos de verão/estiagem. O metabolismo líquido foi heterotrófico no estuário da Lagoa dos Patos. O balanço de massa (LOICZ), juntamente com os resultados da campanha amostral realizada no verão de 2021, também evidenciou o aporte de fosfato para o interior do estuário e região lagunar, através da intrusão de água marinha costeira. Essa intrusão, cujos índices termohalinos correspondem à Água da Pluma do Prata, representa, portanto, um fator importante para a biogeoquímica do estuário da Lagoa dos Patos.

Palavras-chave: Produção primária, respiração, nutrientes, clorofila-*a*, fitoplâncton, dióxido de carbono.

Abstract

The aquatic metabolism in estuarine ecosystems presents a huge importance to the carbon and nutrient cycling in the interface between land and ocean, being subject to anthropogenic pressures. However, the methodological approach commonly applied is space and time limited. In this way, this thesis sought to understand the Patos Lagoon Estuary ecosystem metabolism in an unprecedent way, by applying three complementary approaches, capable of expanding the estimates in space and time. It also sought to assess the main meteoceanographic forcing factors in those different scales. Two stations sampled by two of the applied approaches (both based on dissolved oxygen variation, M1 by oxygen bottle-based experiments, and M2 by the Open water-method) were located in channel-sites. The net ecosystem metabolism at these sites was predominantly heterotrophic throughout the studied period, presenting an annual average of -168.6 mmol O_2 m^{-2} d^{-1}. The primary production and respiration rates were directly proportional. The most heterotrophic periods were spring and summer, and the least, autumn and winter. The high heterotrophy was mainly attributed to the depth of the sampled sites, whose water column was light-limited, leading respiration to predominate. In a daily basis, the main ecosystem metabolism forcing factors was NE/SO wind, which induces the ebb/intrusion of estuarine/marine waters into the estuary, influencing the salinity and the inputs of nutrients and particulate suspended matter, allochthonous (continental discharge) and autochthonous (bottom resuspension and vertical mixing). The late austral summer was nitrate-limited due to the low continental runoff characteristic of this season. In a seasonal scale, salinity was a determinant factor too, but in this case modulated by the rain regime, presenting lower (higher) salinities and higher (lower) nutrients availability during the rainy (dry) late austral winter and early spring (summer). Both nutrient sources were also sources of suspended particulate matter, which decrease the water transparency. Thus, the primary production at Patos Lagoon is co-limited by light and nutrients availability, with alternating conditions between larger limitation by one of the factors, depending on the meteoceanographic conditions. The interannual scale was assessed by comparisons between springs of each year only. At this scale, salinity and hydrographic processes were determinant too, however, due to

extremes of hydrological regimes, likely related to El Niño Southern Oscillation phenomena. In the spring of 2016, an extratropical cyclone in the southern Brazil showed high rainfall and river discharge above the average, increasing the metabolic rates, especially respiration, to the highest values found throughout the studied period (net: -1382 mmol O_2 m^{-2} d^{-1}). These findings demonstrate the potential effects of climate change in the biogeochemistry of Patos Lagoon, and highlight the importance of complementary, long-term, monitoring programs. Finally, the third approach (M3: LOICZ box model/mass balance approach) allowed to extrapolate the ecosystem metabolism to the whole Patos Lagoon Estuary, although just for the summer draught conditions. The net ecosystem metabolism was heterotrophic at the Patos Lagoon estuary. The applied LOICZ mass balance as the third approach, as well as the results by the sampling campaign carried out in the late austral summer of 2021, also evidenced the phosphorus inputs into the estuarine region, possibly by intrusions of the Plata Plume Water, representing, therefore, an important factor to the biogeochemistry of Patos Lagoon estuary.

Keywords: Primary production, respiration, nutrients, chlorophyll-*a*, phytoplankton, carbon dioxide.

Prefácio

O metabolismo de um ecossistema é definido como o balanço entre as suas taxas totais de produção e de consumo de matéria orgânica. É resultado de uma complexa interação entre múltiplos processos meteoceanográficos e características biogeoquímicas de um sistema aquático. A geomorfologia, batimetria, o regime sazonal de chuvas, descarga dos rios, ventos e incidência solar, as variações de temperatura, salinidade, nutrientes, oxigênio e material em suspensão, são exemplos de fatores que podem influenciar o metabolismo de um ecossistema aquático em diferentes escalas espaço-temporais. Além da variabilidade natural, múltiplas pressões antrópicas têm afetado drasticamente os processos biogeoquímicos, principalmente em ambientes costeiros densamente povoados. Não é trivial compreender tamanha complexidade, onde múltiplos fatores interagem entre si.

Essa tese buscou desvendar o universo do metabolismo aquático do estuário da Lagoa dos Patos, a maior lagoa costeira estrangulada do mundo, de imensa importância ecológica e econômica para o estado do Rio Grande do Sul, estados e países adjacentes, e Oceano Atlântico Sudoeste. Através de uma abordagem multidisciplinar, os resultados obtidos contribuíram para a compreensão dos principais fatores controladores do metabolismo aquático, nas diferentes escalas espaciais e temporais, cobrindo desde a variabilidade diária e local, até a interanual e para todo o sistema lagunar.

Capítulo I:

Introdução

Situados em regiões transicionais entre ambientes de água doce e marinhos, os estuários são componentes chave porque agem como filtros de nutrientes e carbono, contribuindo de forma significativa para o balanço de massa destes elementos [Bianchi, 2007; Laruelle *et al.* 2013]. Ao longo do gradiente estuarino, o carbono e os nutrientes de origem continental e oceânica são modificados através de processos biogeoquímicos, tais como a incorporação em estruturas biogênicas, sedimentação e enterramento nos sedimentos, regeneração bentônica e pelágica da matéria orgânica e, no caso de gases tais como o oxigênio dissolvido e o dióxido de carbono (CO_2), também por trocas com a atmosfera [Bianchi, 2007]. Todas essas transformações são conduzidas por uma interação complexa entre processos físicos, químicos, biológicos e geológicos que, por sua vez, são modulados por um conjunto de forçantes, tais como a temperatura da água, intensidade luminosa, ondas, marés, vento e descarga fluvial [Bianchi, 2007; Regnier *et al.* 2013a,b]. Logo, a variabilidade sazonal dos processos meteoceanográficos influencia na produção, consumo e exportação de matéria orgânica nos ecossistemas aquáticos e, portanto, na dinâmica biogeoquímica do carbono [Giering *et al.* 2014].

Em ambientes marinhos e estuarinos, a produção primária de matéria orgânica realizada por organismos autótrofos, sustenta a cadeia alimentar destes ecossistemas. A produção primária é dependente de condições simultâneas favoráveis de luz e nutrientes, principalmente de macronutrientes, tais como o

nitrogênio inorgânico dissolvido nas formas de nitrito, nitrato e amônio (NO_2^-, NO_3^- e NH_4^+, respectivamente) e fosfato (PO_4^{3-}) [Valiela, 2015].

Em larga escala espacial, a intensidade luminosa varia diariamente, sazonalmente, e com a latitude. Em pequena escala espacial, a disponibilidade de luz que chega a uma determinada profundidade da coluna da água varia de acordo com a turbidez da água, que, por sua vez, é influenciada pelo material particulado em suspensão [Lalli & Parsons, 1997; Valiela, 2015].

O aporte de nutrientes em ecossistemas costeiros se dá através de processos hidrológicos, e.g., em escala de bacia de drenagem, e através de processos hidrográficos e biogeoquímicos locais, representando respectivamente, fontes alóctones e autóctones de nutrientes. A drenagem continental, a descarga de água subterrânea [Niencheski *et al.* 2007], a deposição atmosférica [Casartelli *et al.* 2008], e a advecção de uma massa de água rica em nutrientes [Bordin *et al.* 2019, 2023], são exemplos de fontes alóctones que fertilizam a coluna de água em zonas costeiras. A remineralização pelágica e bentônica da matéria orgânica pelos microrganismos heterotróficos, são exemplos de fontes autóctones, que redisponibilizam os nutrientes para a coluna de água [Valiela, 2015]. A ação local dos ventos e/ou a circulação em maior escala pode ainda causar turbulência na coluna de água e remobilizar material de fundo rico em nutrientes e matéria orgânica, que são disponibilizados na zona eufótica por mistura vertical [Niencheski *et al.* 1999; Odebrecht *et al.* 2005; Bordin *et al.* 2019].

Em ecossistemas aquáticos, é comum que a produção primária seja controlada pela alternância entre condições favoráveis de luz e nutrientes, principalmente pela disponibilidade relativa entre os macronutrientes nitrogenados e fosfatados, denominada razão N:P. Redfield [1963] definiu para ambientes oceânicos a razão média do nitrogênio e fósforo orgânico particulados (N:P) da biomassa fitoplanctônica, de 16:1. Foi assumido que as exigências nutricionais pelo fitoplâncton por nitrogênio e fósforo inorgânico dissolvidos na coluna de água, se dá nessa mesma proporção. Essa razão é amplamente utilizada para definir a limitação por nutrientes nitrogenados ou fosfatados disponíveis na água, quando não se sabe a razão N:P média específica de uma

dada comunidade fitoplanctônica ou da comunidade total de organismos fotossintetizantes de um determinado ecossistema. Quando a razão é menor que 16, diz-se que há limitação por nitrogênio, e quando maior, por fósforo [Gordon *et al.* 1996; Valiela, 2015; Bordin *et al.* 2019, 2023a]. Entretanto, os processos que fertilizam os ecossistemas costeiros também representam fontes de material particulado em suspensão, que afetam a turbidez da água, bem como a disponibilidade de luz para os organismos fotossintetizantes a uma dada profundidade [Lalli & Parsons, 1997; Valiela, 2015; Bordin *et al.* 2019].

A disponibilidade de luz em sincronia com concentrações adequadas de nutrientes promove o incremento das concentrações de clorofila-*a* (chl-*a*) [Reynolds, 2006; Falkowski & Raven 2013], indicativa da biomassa fitoplanctônica, bem como do potencial de produção biológica do ecossistema [Strickland & Parsons, 1968; Holm Hansen & Rieman, 1978]. O potencial de produção biológica pode ainda ser estimado através do índice de estado trófico TRIX [Vollenweider *et al.* 1998], o qual considera parâmetros relacionados às condições nutricionais e à resposta ao metabolismo aquático. O metabolismo de um ecossistema pode ser representado pela medida integrada de suas taxas totais de produção e consumo (R; respiração, mineralização ou ainda regeneração) de matéria orgânica. Quando o balanço entre produção primária e R é positivo, diz-se que o metabolismo líquido é autotrófico e, quando negativo, heterotrófico [Valiela, 2015].

O metabolismo também é controlado pela alternância entre condições favoráveis de luz e nutrientes [Odebrecht *et al.* 2005; Valiela, 2015; Bordin *et al.* 2019, 2023], a depender da geomorfologia e hidrodinâmica de um dado corpo de água. Exemplos de fatores que podem influenciar são o tamanho e profundidade média do sistema. Uma lagoa ou estuário majoritariamente raso pode apresentar autotrofia líquida caso haja disponibilidade de nutrientes, mesmo com elevada turbidez, visto que a baixa profundidade permite que a zona eufótica abranja toda a coluna de água, incluindo o sedimento, e a produção primária exceda a R. Por outro lado, em condições semelhantes de luz e nutrientes, um sistema mais profundo poderá apresentar heterotrofia líquida. Neste caso a produção primária pode ser intensa em superfície, mas limitada à estreita zona eufótica, enquanto no restante da coluna de água abaixo, a R da comunidade excede a produção

primária integrada da coluna de água [Bordin *et al.* 2023a]. O regime hidrológico sazonal, a hidrodinâmica local e variações espaciais em um sistema, também podem controlar a disponibilidade relativa entre luz e nutrientes, e consequentemente, o metabolismo. Em estações chuvosas ocorre maior drenagem continental e aporte de nutrientes e material em suspensão, havendo disponibilidade de nutrientes e limitação por luz, enquanto em estações secas poderá haver condições favoráveis de luz, mas limitação por nutrientes [Abreu *et al.* 1994; Caffrey, 2004]. Essas condições podem ainda variar espacialmente, havendo maior disponibilidade de nutrientes, mas limitação por luz próximo a desembocadura de rios, enquanto à jusante os nutrientes e o material em suspensão poderão diminuir através da sua remoção da coluna de água por assimilação e/ou adsorção, e sedimentação, respectivamente, havendo, portanto, maior disponibilidade de luz, mas limitação por nutrientes [Brandini, 1985; Odebrecht *et al.* 2005].

Além da variabilidade natural dos processos biogeoquímicos em ecossistemas costeiros, as atividades antrópicas e as mudanças climáticas têm mudado de forma significativa a quantidade e a qualidade dos fluxos de material em suspensão, nutrientes e carbono entre os ambientes terrestre, os estuários, o oceano costeiro adjacente e a atmosfera, impactando o metabolismo, os ciclos biogeoquímicos a nível regional e global, e o clima [Mackenzie *et al.* 2000; Regnier *et al.* 2013a]. Podem ser citados como exemplos, alterações no regime de chuvas e ventos, uso intensivo do solo e da água, que podem afetar a hidrodinâmica, os fluxos e suprimento de nutrientes para as zonas costeiras [Chilton *et al.* 2021], e o aporte antropogênico de compostos orgânicos e nutrientes através do despejo de efluentes domésticos e industriais [Niencheski & Windom, 1994; Baumgarten *et al.* 1995, 2021; Wallner-Kersanach *et al.* 2016], desencadeando episódios de eutrofização antropogênica [Baumgarten *et al.* 2010; Abreu *et al.* 2006], mudanças na composição e estrutura de comunidades fitoplanctônicas [Bužančić *et al.* 2016; Baumgarten *et al.* 2021], depleção do oxigênio e formação de zonas mortas [Cabral & Fonseca, 2019; Altieri & Dias, 2019], afetando o metabolismo [Damashek & Francis, 2018]. O diagrama conceitual apresentado por Chilton *et al.* [2021] (Fig. 1) apresenta um resumo

atualizado das principais pressões antrópicas e suas possíveis consequências em ecossistemas estuarinos.

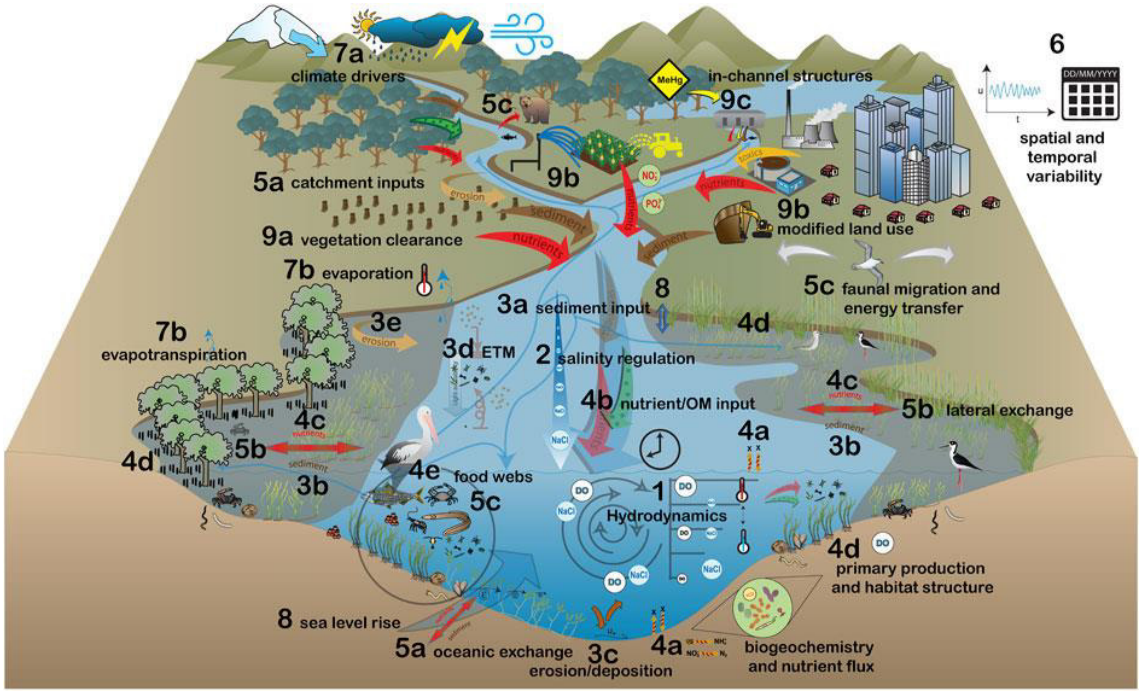

Figure 1. Diagrama conceitual demonstrando as influências dos fluxos de água doce nos processos em ecossistemas estuarinos: 1) hidrodinâmica, 2) regulação da salinidade, 3a-e) dinâmica sedimentar (a: entrada de sedimentos no estuário, b: troca lateral de sedimentos, c: erosão/deposição na desembocadura do estuário, d: zona de máxima turbidez estuarina, e: erosão lateral), 4a-e) ciclagem de nutrientes e transferência trófica (a: processos biogeoquímicos e trocas com os sedimentos, coluna de água e atmosfera, b: aporte de nutrientes e matéria orgânica (OM) pro estuário, c: trocas laterais de nutrientes e energia, d: produção primária, e: cadeia alimentar, e 5a-c) conectividade hidrológica (a: conectividade longitudinal, b: lateral, c: transferência de energia e migração da fauna), 6) variabilidade espaço-temporal, e os fatores que alteram a influência do aporte de água doce nos processos ecossistêmicos: 7a-b) clima (a: chuva, temperatura, degelo de neve, secas e inundações, b: evaporação e evapotranspiração, 8) aumento do nível do mar e 9a-c) fatores antropogênicos diretos (a: desmatamento, b: modificação do uso da terra, c: estruturas nos canais). Fonte: Chilton *et al.* [2021].

Entretanto, tais conhecimentos continuam limitados, principalmente devido aos diferentes padrões de variação espaço-temporal dos processos aos quais estes ambientes estão sujeitos [Abreu *et al.* 2010], e à abordagem metodológica comumente utilizada para estudá-los, i.e., através de observações pontuais, espacial e temporalmente limitadas [Abreu *et al.* 1994, 1995; Proença *et al.* 1994]. Tais informações não permitem uma extrapolação confiável para todo o sistema estuarino em diferentes escalas temporais, limitando o

conhecimento de processos importantes, tais como o metabolismo [Borges & Abril 2011] e a capacidade do estuário em reter e exportar nutrientes e carbono [Nixon *et al.* 1995; Bianchi 2007]. Para tal, são necessárias abordagens espacialmente integradas e com alta resolução temporal [Arndt *et al.* 2009], as quais são viabilizadas através da integração entre a oceanografia discreta, operacional e a modelagem numérica.

Estudos sobre metabolismo têm sido um dos focos da ciência aquática por quase um século [Staehr *et al.* 2012], entretanto, a grande maioria dos trabalhos foram desenvolvidos no hemisfério norte, como destaca Cloern *et al.* [2014] em uma revisão bibliográfica que envolve artigos produzidos em todo o mundo, desde a década de 1950. No Hemisfério Sul os estudos são limitados. Particularmente na Lagoa dos Patos, são poucos os estudos que envolvem o metabolismo aquático [Proença 1990; Abreu *et al.* 1994; Niencheski & Jahnke 2002; Odebrecht *et al.* 2005]. Estudos mais recentes abordam apenas o metabolismo do bacterioplâncton [They *et al.* 2018] e indicativos da produção primária através da dinâmica da chl-*a* [Abreu *et al.* 2017]. De acordo com Staehr *et al.* [2012], estudos sobre metabolismo devem continuar a ser um componente essencial para compreender as complexas mudanças que a biosfera vem sofrendo. Os autores ainda destacam a importância de estudos futuros, que poderão se beneficiar da aplicação de novos métodos, facilitando a integração de processos, calibração de modelos e, portanto, obtendo informações das diferentes escalas dos processos ecossistêmicos. Exemplos são os recentes trabalhos desenvolvidos por Murrell *et al.* [2018] através de metodologias complementares, e de Vaz *et al.* [2019], através de modelagem numérica, representando assim, o estado da arte sobre estudos de metabolismo.

Capítulo II:

Hipóteses

I. O metabolismo aquático no estuário da Lagoa dos Patos é predominantemente autotrófico ao longo do ano;

II. Em escala sazonal, o metabolismo aquático no estuário da Lagoa dos Patos varia principalmente em função da temperatura e radiação solar incidente, enquanto em escalas sinóticas em função do vento atuante.

Capítulo III:

Objetivos

O objetivo geral desse estudo é investigar como o metabolismo aquático no ecossistema do Estuário da Lagoa dos Patos responde às principais forçantes meteoceanográficas em diferentes escalas espaço-temporais. Assim, os seguintes objetivos específicos foram definidos:

I. Estimar a produtividade primária, o consumo e a decomposição da matéria orgânica (respiração/oxidação), em diferentes escalas espaço-temporais;

II. Verificar a relação entre a variabilidade meteoceanográfica, os parâmetros físico-químicos e o metabolismo aquático;

III. Associar o metabolismo aquático à composição e estrutura da comunidade fitoplanctônica;

IV. Avaliar a efetividade da produção primária bruta no potencial de produção biológica (TRIX);

V. Estimar o balanço de massa dos nutrientes entre os ambientes terrestre, lagunar, estuarino e costeiro.

Capítulo IV:

Estuário da Lagoa dos Patos

A Lagoa dos Patos é a maior laguna costeira do tipo estrangulado do mundo [Kjerfve, 1986], sendo alimentada por 3 afluentes continentais: o Rio Guaíba, principal tributário localizado ao norte da Lagoa, que contribui com 86% de toda a entrada de água doce no sistema; o Rio Camaquã, localizado no centro-oeste da Lagoa; e o Canal de São Gonçalo, afluente da Lagoa Mirim, na região estuarina (Fig. 2). A comunicação da Lagoa dos Patos com o Oceano Atlântico ocorre através de um estreito canal (700 m de largura) localizado ao sul da região estuarina. O regime é de micromaré (±0,4 m) [Soares & Möller 2001] e a hidrodinâmica da Laguna é dominada pelos ventos e pela descarga continental. Durante períodos de ventos SO, a entrada de água marinha é favorecida, enquanto os ventos NE favorecem a vazante [Möller *et al.* 2001; Möller & Fernandes, 2010] e a formação de uma pluma costeira [Marques *et al.* 2009; 2011]. O limite teórico de penetração da água salgada é a Ponta da Feitoria (Figura 2c), definindo o limite do estuário da Lagoa dos Patos [Möller & Castaing 1999].

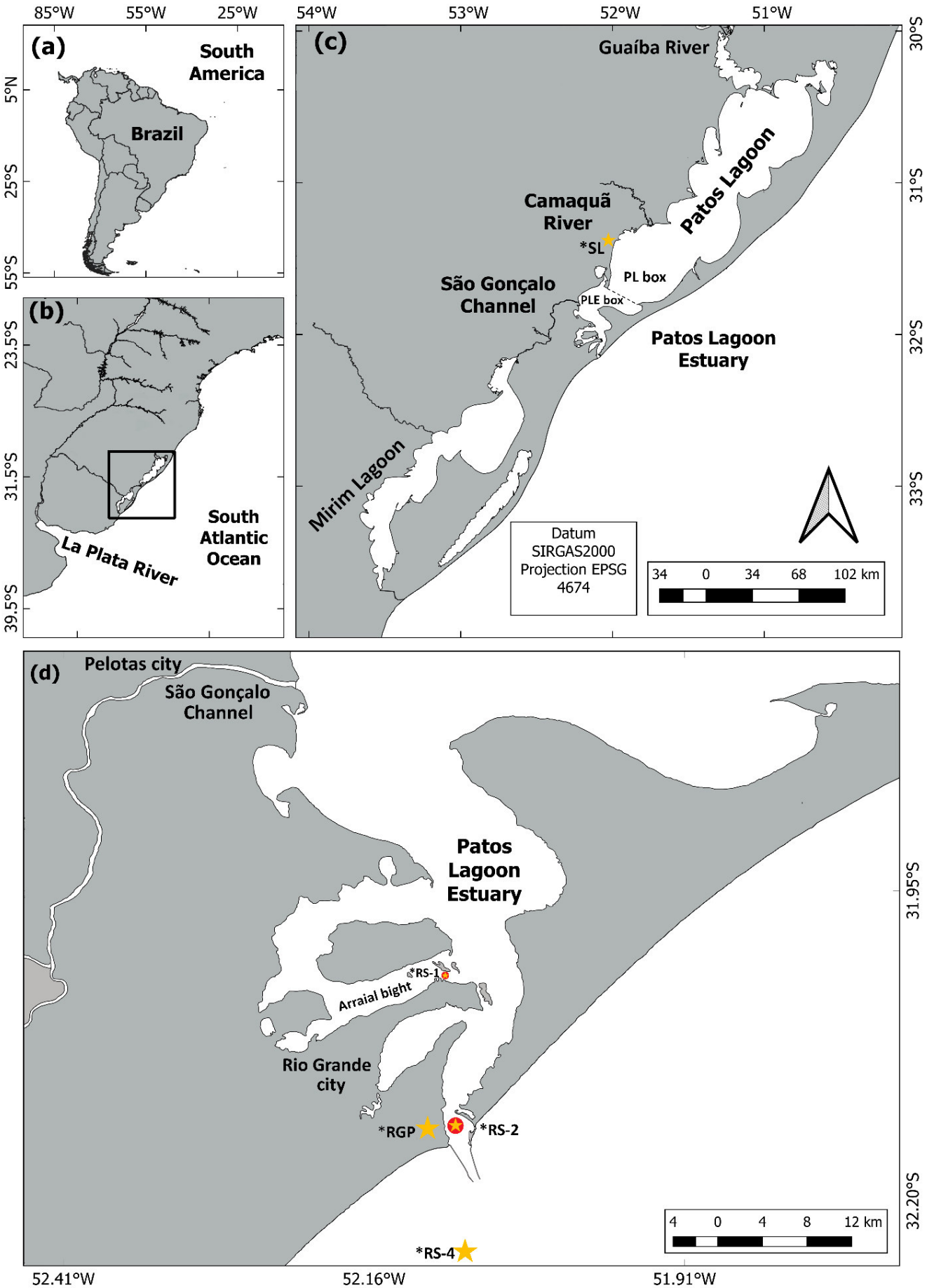
85°W
55°W
25°W
5°N
25°S
55°S
(a)
South America
Brazil
(b)
23.5°S
31.5°S
39.5°S
South Atlantic Ocean
La Plata River
54°W
53°W
52°W
51°W
30°S
31°S
32°S
33°S
(c)
Guaíba River
Patos Lagoon
Camaquã River
*SL
PL box
PLE box
São Gonçalo Channel
Patos Lagoon Estuary
Mirim Lagoon
Datum SIRGAS2000 Projection EPSG 4674
34 0 34 68 102 km
(d)
Pelotas city
São Gonçalo Channel
Patos Lagoon Estuary
*RS-1
Arraial bight
Rio Grande city
*RGP
*RS-2
*RS-4
4 0 4 8 12 km
31.95°S
32.20°S
52.41°W
52.16°W
51.91°W

Figure 2. Mapa da América do Sul (a); sul do Brasil e Uruguai com o Rio da Prata (b); Lagoa dos Patos com os seus principais tributários: Rio Guaíba na porção noroeste, o Rio Camaquã na porção centro-oeste, e o Canal de São Gonçalo na porção sudoeste (c); e em detalhe o Estuário da Lagoa dos Patos (d). As estações amostrais 1 (ou RS-1) e 2 (ou RS-2) estão indicadas por círculos vermelhos (Fig. 1d); os pontos de validação do modelo hidrodinâmico *SL (Fig. 2c), *RGP, *RS-1, *RS-2 e *RS-4 (Fig. 2d) estão indicados por estrelas amarelas. A linha tracejada (Fig. 2c) representa o limite entre a região límnica da Lagoa dos Patos (PL box), e o seu estuário (PLE box). O limite oeste da linha tracejada indica a localização da Ponta da Feitoria.

Sustentada pelos nutrientes inorgânicos dissolvidos de origem continental, a elevada produtividade primária [Windom *et al.* 1999] da Lagoa dos Patos é capaz de exaurir os nutrientes da coluna de água em sua região límnica (salinidade < 7) [Niencheski & Windom 1994]. O tempo elevado de residência (~20 dias) [Fernandes *et al.* 2002] contribui também para a remoção de nutrientes, resultando em um empobrecimento das águas que chegam ao estuário da Lagoa dos Patos [Niencheski *et al.* 1999; Odebrecht *et al.* 2005]. Em salinidades entre 7-27, a demanda nutricional pelos produtores primários ainda é provida majoritariamente por nutrientes de origem fluvial [Windom *et al.* 1999], entretanto, a remineralização bentônica da matéria orgânica oriunda da vegetação aquática acumulada nos sedimentos, torna-se já um importante contribuinte de nutrientes para a coluna de água. Em salinidades maiores que 27, com a elevada hidrodinâmica e as trocas de água entre estuário e oceano, a regeneração bentônica da matéria orgânica torna-se um processo fundamental para suportar a produção primária pelágica [Niencheski & Jahnke, 2002]. Acredita-se que o aumento de nutrientes no baixo estuário pode ainda ocorrer através do retorno de água estuarina com maior salinidade, beneficiando a comunidade bacteriana [They *et al.* 2019] e os produtores primários, resultando em elevadas concentrações de chl-*a* [Abreu *et al.* 1994; 2017]. Além das fontes naturais, desde a industrialização do município na década de 80, os aportes antropogênicos provenientes da cidade de Rio Grande vêm causando desequilíbrios ecológicos, como a eutrofização cultural, [Wallner-Kersanach *et al.* 2015], possivelmente afetando o metabolismo no estuário da Lagoa dos Patos.

A dinâmica biogeoquímica do estuário da Lagoa dos Patos varia em diferentes escalas espaciais [Windom *et al.* 1999; Marreto *et al.* 2017] e temporais [Abreu *et al.* 2010; Haraguichi *et al.* 2015]. As maiores concentrações e variações de nutrientes e chl-*a* ocorrem na primavera e verão em função da produção primária [Proença 1990], da influência da salinidade e interação com o sedimento [Baumgarten *et al.* 1995]. Variações semanais, diárias e/ou horárias em função do vento também ocorrem, sendo estas menores escalas temporais, mais variáveis que as escalas maiores [Abreu *et al.* 2010]. Em concordância com a chl-*a*, o metabolismo sazonal segue o mesmo padrão supracitado. Em zonas rasas, as taxas de produção primária são maiores que a R na maior parte do ano, com baixa variação. Acredita-se que o sistema é predominantemente heterotrófico apenas durante o inverno, em virtude da baixa produção primária associada à baixa intensidade de luz característica dessa época do ano, do elevado teor de seston [Abreu *et al.* 1994], e também pela decomposição da vegetação aquática submersa que entra em senescência nessa época do ano [Abreu *et al.* 1992]. O fitoplâncton é composto principalmente por organismos < 20 µm, tais como diatomáceas, flagelados e dinoflagelados, sendo a produção primária fitoplanctônica responsável por uma parcela importante da produção primária total (até 72%), principalmente no verão [Abreu *et al.* 1994]. A biomassa do fitoplâncton produzida nas áreas rasas do estuário da Lagoa dos Patos pode ser exportada para profundidades maiores [Proença 1990], e possivelmente até o oceano costeiro adjacente.

De forma geral, espera-se que o sistema carbonato também reflita o estado metabólico do ecossistema, visto que durante o processo da fotossíntese, os produtores primários assimilam CO_2 da água para a síntese da matéria orgânica, reduzindo as concentrações de carbono inorgânico total e, consequentemente, aumentando a alcalinidade total. Por outro lado, durante a R da matéria orgânica, ocorre o processo inverso, aumentando o carbono inorgânico total e diminuindo a alcalinidade total. Entretanto, em sistemas cuja produção primária é baseada no consumo de amônio invés do nitrato, pode haver a diminuição da alcalinidade [Middelburg *et al.* 2020]. De acordo com Albuquerque *et al.* [2022], a remineralização da matéria orgânica e a absorção de CO_2 da atmosfera contribuem para elevadas concentrações de carbono

inorgânico total no estuário da Lagoa dos Patos. Entretanto, a variabilidade do sistema carbonato no estuário da Lagoa dos Patos é principalmente governada pela saída de água doce e a entrada de água marinha dirigidas pelo vento. Elevada alcalinidade total e concentrações de carbono inorgânico total são principalmente relacionadas à composição de águas com maiores salinidades advindas da plataforma continental (salinidade > 36 psu) que adentram o estuário [Albuquerque *et al.* 2022]. O sistema carbonato no estuário da Lagoa dos Patos alterna entre condições caracterizadas pela dominância de águas marinhas na primavera e verão, e dominadas por águas doces de origem fluvial no outono e inverno. No primeiro período, em média, prevalece a absorção de CO_2 da atmosfera, enquanto no último, o estuário se comporta como exportador de CO_2 para a atmosfera [Albuquerque 2022].

Capítulo V:

Material e Métodos

O estudo objetivou estimar o metabolismo em diferentes escalas espaço-temporais no estuário da Lagoa dos Patos (Fig. 2). O metabolismo do ecossistema é a diferença entre a produção primária bruta (GPP) e a respiração (R). A produção primária bruta (GPP) é definida como a conversão total de carbono inorgânico em orgânico. A R do ecossistema é a oxidação da matéria orgânica em carbono inorgânico [Valiela 2015]. O metabolismo pode ser estimado através da relação entre a importação, exportação e acumulação de matéria orgânica. Um ecossistema autotrófico (metabolismo > 0) apresenta acumulação líquida e/ou exportação líquida de matéria orgânica, enquanto um ecossistema heterotrófico ocorre o contrário (metabolismo < 0), sendo dependente da matéria orgânica importada de sistemas adjacentes [Lovett *et al.* 2006].

Uma abordagem comumente utilizada para estimar o metabolismo é o uso de técnicas que utilizam as variações nas concentrações de gases tais como o oxigênio dissolvido e CO_2, sob o pressuposto de que mudanças nas concentrações destes gases em um determinado corpo de água, refletem o balanço entre a GPP e a R de toda a comunidade, bem como as trocas físicas entre o oceano e a atmosfera [Staehr *et al.* 2010]. O oxigênio dissolvido pode ser utilizado para esta finalidade, visto que durante o processo de produção primária pelos organismos fotossintetizantes, CO_2 é assimilado para sintetizar a matéria orgânica, e O_2 é liberado na água, enquanto durante a R dos organismos, ocorre o processo inverso, O_2 é consumido para oxidar a matéria orgânica, devolvendo CO_2 para a água, de acordo com a reação química a seguir (Eq. 1):

$$6CO_2 + 6H_2O \leftrightarrow C_6H_{12}O_6 + 6O_2 \quad \text{(Eq. 1)}$$

onde CO_2 é dióxido de carbono, H_2O é água, $C_6H_{12}O_6$ é MO, e O_2 é oxigênio. Partindo deste princípio, o metabolismo foi estimado diariamente por dois métodos baseados nas variações do oxigênio dissolvido. O primeiro método se deu através de experimentos de produção primária e respiração pelo método do oxigênio dissolvido (método 1) [Strickland 1960] nas estações 1 e 2 (Fig. 2), durante uma campanha com duração de aproximadamente um mês, entre os dias 22-Fev-21 e 23-Mar-21. O método 1 (M1) apresenta baixa resolução temporal e espacial, visto que as estimativas compreendem apenas o período e o local do experimento, e apenas a coluna de água, i.e, a comunidade pelágica, negligenciando a bentônica. A segunda abordagem (método 2, M2) se deu através do método do oxigênio dissolvido livre [Odum 1965; Murrel *et al.* 2018] com dados de oxigênio dissolvido da boia meteoceanográfica RS-1 (junto à estação 1) do programa de Monitoramento da Costa Brasileira (SiMCosta), sendo este método de alta resolução temporal e vertical, permitindo expandir as estimativas para toda a comunidade (pelágica + bentônica), e por maiores períodos, que abrangeu os anos entre 2016 e 2021.

Finalmente, um terceiro método (método 3, M3), que permite estimar o metabolismo de forma integrada espacialmente, foi aplicado. Diferentemente dos

dois primeiros métodos, este se baseia na modelagem dos fluxos de nutrientes entre os compartimentos terrestre, lagunar, estuarino e oceano costeiro adjacente, cujos compartimentos são definidos como caixas que trocam fluxos entre si. Este método baseado na modelagem de caixas foi desenvolvido por Gordon *et al.* [1996], denominado *Land Ocean Interaction in the Coastal Zone* (LOICZ). O metabolismo é definido pelo balanço de massa do fósforo inorgânico dissolvido total (DIP), isto é, o resultado entre todos os fluxos de entrada e saída de uma determinada caixa, definida como ΔDIP, multiplicado pela razão C:P média da matéria orgânica daquela caixa. É assumido que os fluxos não conservativos de DIP são uma aproximação do metabolismo líquido do ecossistema, visto que não há uma fase gasosa do fósforo [Gordon *et al.* 1996].

A seguir serão apresentados os materiais e métodos específicos de cada um dos três artigos científicos frutos desta tese, organizados nos subtópicos 5.1 ao 5.3 do Capítulo 5 - Metodologia.

5.1 Campanha amostral

Este subtópico apresenta a metodologia do artigo científico intitulado *Daily variability of pelagic metabolism in a subtropical lagoonal estuary*, publicado na revista *Journal of Marine Systems*, e apresentado no capítulo VI.

5.1.1 Trabalho de campo

Experimentos de metabolismo e amostragens *in situ* de parâmetros hidrográficos e biogeoquímicos foram realizados diariamente nas estações 1 e 2 (Fig. 2), durante 30 dias do verão austral, compreendendo o período entre os dias 24-Fev-21 e 23-Mar-21. A estação 1 é um local de canal com profundidade de 4.5 m, localizada em uma zona biogeoquímica dominada pela remineralização [Windom *et al.* 1999]. O local fica próximo do centro da cidade de Rio Grande, e é sujeito à emissão de esgoto não tratado em suas margens. A estação 2 é um local mais profundo, com aproximadamente 12 m, localizado próximo aos Molhes da Barra, canal principal da conexão do estuário com o oceano costeiro adjacente (Fig. 2d), cuja zona biogeoquímica é dominada por

mistura conservativa [Windom *et al.* 1999]. A profundidade média da Lagoa dos Patos é de aproximadamente 5 m [Calliari *et al.* 1997], enquanto 80% do sul da região estuarina, apresenta profundidade ≤ 1.5 m [Seeliger 2001]. A área no entorno do Porto de Rio Grande é sujeita à descarga difusa de fertilizantes das atividades industriais e portuárias [Baumgarten *et al.* 1995; Wallner-kersanach *et al.* 2016].

Amostras de água foram coletadas com uma garrafa Niskin na superfície (0.5 m), meia profundidade (apenas na estação 2), e próximo do fundo. A profundidade intermediária (7 ± 2 m) foi definida de acordo com a observação da haloclina pela sonda multiparamétrica. Para evitar a interferência do ar com as propriedades da água, as alíquotas foram separadas da garrafa Niskin com auxílio de uma mangueira de silicone, cuidando para não haver formação de bolhas, em garrafas de borossilicato com capacidade de 100 ml, para a determinação do oxigênio dissolvido, e imediatamente fixadas com reagentes Winkler. Após, seguindo os mesmos cuidados, alíquotas foram separadas para determinação do pH, em frascos de borosilicato de 150 ml de cor âmbar, e em frascos de borosilicato de 500 ml para a determinação da alcalinidade total, imediatamente fixadas com cloreto de mercúrio [Dickson *et al.* 2007]. Amostras para pH e alcalinidade total foram tomadas apenas da superfície (estações 1 e 2) e fundo (estação 2). As amostras foram mantidas em caixas térmicas com água do mar para manter a temperatura local até a chegada ao laboratório. Quatorze frascos de borossilicato de todas as profundidades foram separados sem a adição de reagentes Winkler, para o experimento de metabolismo. O restante da água na garrafa Niskin foi separada em frascos de policarbonato, para subsequentes determinações dos pigmentos fotossintéticos e nutrientes inorgânicos dissolvidos nitrito, nitrato, amônio, fosfato e silicato, armazenados em caixa térmica com gelo.

Perfis de velocidade de corrente foram obtidas do programa SiMCosta (SiMCosta 2022; www.simcosta.furg.br), medidos através de perfiladores acústicos de corrente por efeito doppler (ADCP) para as estações do SiMCosta RS-1 (Aquadopp 5 Mhz) e RS-2 (Aquadopp Z-Ccell 600 Mhz), localizados nas estações 1 e 2 do presente trabalho, respectivamente. A vazão de água da seção transversal ao canal adjacente à estação 2 foi medida com um ADCP de 1200

Khz, modelo RDI Workhorse com rastreador de velocidades de fundo. A coluna de água foi perfilada com uma sonda multiparamétrica JFE-Advantech modelo AAQ-Rinko 176, equipada com sensores de temperatura, salinidade, fluorescência da chl-*a*, turbidez, oxigênio dissolvido, pH, matéria orgânica dissolvida colorida, e radiação fotossinteticamente ativa.

A vazão dos rios Jacuí, Taquarí, Caí, Sinos e Camaquã para o período foram obtidas da Agência Nacional de Águas [ANA 2022; www.snirh.gov.br/hidroweb]. O tempo de residência da Lagoa dos Patos foi estimado de acordo com Dyer [1997], considerando o volume da Lagoa dos Patos como 58.5 x 10^6 m^3 [Fernandes *et al.* 2002]. Dados meteorológicos foram obtidos da estação da Praticagem de Rio Grande [RG Pilots 2022; www.rgpilots.com.br]. Os dados de vento (10 m acima do solo) foram rotacionados de acordo com a orientação da linha de costa (32° em relação ao norte geográfico), para melhor obter a influência da componente do vento mais energética (meridional), que força a entrada e saída de água do estuário.

5.1.2 Processamento das amostras

No laboratório, as amostras de oxigênio dissolvido foram analisadas através da técnica de titulação por Winkler [Strickland & Parsons 1972]. A titulação foi feita com uso de uma bureta digital Brand Digital Burette III, com acurácia de 0.2% e coeficiente de variação de 0.01%. O pH foi medido com um phmetro Metrohm 654, equipado com termômetro, tendo como precisão ±0.05 NBS pH. O equipamento foi calibrado diariamente com padrões Mettler Toledo de pH 4 e 7 a 25 °C. O pH foi corrigido somando 0.00114 e depois multiplicado pela diferença entre a temperatura medida em campo e da amostra no momento da análise em laboratório [Gieskes 1969]. O declive da reta foi de 98%. As análises para a determinação da alcalinidade total foram feitas através de titulação potenciométrica em célula fechada [Dickson *et al.* 2007], com uso de um titulador Metrhom Titrando 808, combinado com um eletrodo de vidro (Metrhom 6.0262.100), em temperatura controlada de 25 ± 0.1 °C, sustentado por um banho termostático (Tamson TLC 15). Devido à grande variação de salinidade das amostras (de 0 a ~33 psu), foi adotada uma adaptação no método

da célula fechada [Dickson *et al.* 2007]. Soluções de HCl (0.1 M) com cloreto de sódio em diferentes salinidades foram utilizadas como titulante, para se aproximar da salinidade real da amostra. Um fator de correção foi aplicado nos resultados de cada amostra. A precisão das medidas de alcalinidade total (salinidade > 19 = ± 2.0 µmol kg^{-1} e salinidade < 19 = ± 2.7 µmol kg^{-1}) foi avaliada diariamente durante todo o período das análises, através de várias réplicas de uma mesma amostra. O fator de correção aplicado foi baseado de acordo com valores conhecidos de um material de referência (batch no 177), adquirido do *Scripps Institute of Oceanography*, e diluição da amostra com solução de cloreto de mercúrio [Dickson *et al.* 2007].

Amostras de água foram filtradas com filtros Whatman GF/F (0,70 µm de porosidade) em condições de baixa luz para a determinação das concentrações dos pigmentos fotossintéticos por Cromatografia Líquida de Alta Performance (HPLC) [Zapata *et al.* 2000]. O sistema de HPLC foi calibrado com pigmentos padrões obtidos do *Institute for Water Environment*, Dinamarca (DHI). As alíquotas filtradas foram então utilizadas para a determinação das concentrações dos nutrientes inorgânicos dissolvidos (nitrito, nitrato, amônio, fosfato e silicato), através de espectrofotometria em um SEAL Analytical AutoAnalyzer AA3 HR, de acordo com Grasshoff *et al.* [2007]. O amônio foi determinado separadamente, de acordo com Koroleff & Palmork [1972]. Os limites de detecção foram de 0.006 µM para o nitrito, nitrato e amônio, e 0.016 µM para o silicato e fosfato.

5.1.3 Metabolismo do ecossistema pelágico

O metabolismo do ecossistema pelágico foi estimado por experimentos in situ, através do método do oxigênio com garrafas claras e escuras. Os experimentos foram desenvolvidos diariamente (sempre que possível) durante todo o período da campanha amostral, sendo um dia em cada estação devido a questões logísticas, totalizando onze experimentos na estação 1 e nove na estação 2 (Tab. A.1).

Na embarcação, as garrafas de borossilicato foram dispostas em pares de réplicas, em armações preparadas de tubos de PVC, um totalmente exposto, três totalmente fechados, e outros três cobertos por plásticos filme com

diferentes níveis de irradiância, para simular a atenuação da luz na coluna de água. As garrafas em 100% da radiação fotossinteticamente ativa foram dispostas no tubo exposto, sem película plástica, as escuras nos tubos fechados, totalmente protegidos da luz, e as demais em películas plásticas com filtros conhecidos com 50, 35 e 5% de transmitância. As garrafas escuras foram dispostas em pares de réplicas, para simular as taxas R de três níveis de profundidade, superfície, meio e fundo. Todos os tubos de PVC foram colocados em uma caixa de acrílico totalmente transparente e preenchida com água do estuário para manter a temperatura local constante, até a embarcação chegar ao píer. No píer os tubos foram transferidos para uma armação de madeira, a qual foi amarrada ao píer e deixada flutuando na superfície da água do estuário para manter a temperatura local constante (Fig. 3).

Figure 3. Fotografia da armação de madeira utilizada para dispor os tubos de PVC contendo os frascos de borossilicato utilizados nos experimentos de metabolismo do ecossistema pelágico.

O tempo de incubação foi de aproximadamente 3 horas, quando a armação foi retirada da água, e os frascos de borossilicato imediatamente fixados com reagentes Winkler. As taxas de produção primária líquida (NPP) e a R foram calculadas de acordo com as equações 2 e 3, respectivamente:

$$NPP = \left(DO_{fl} - DO_{il}\right)/Itime; \quad \text{(Eq. 2)}$$

$$R = (DO_{fd} - DO_{id})/Itime; \quad \text{(Eq. 3)}$$

onde *DOfl* e *DOil* são o oxigênio dissolvido final e inicial, respectivamente, considerando as garrafas claras (*l*), enquanto o sobescrito (*d*) se refere às garrafas escuras, e *Itime* o tempo de incubação em fração de horas. As taxas finais de *NPP* e *R* são expressas em mmol O_2 m^{-3} h^{-1}.

Para obter as taxas diárias, a *NPP* integrada foi obtida a partir da integração da irradiância do período luminoso do dia (*Id*) e apenas do período do experimento (*Ie*), através da fórmula da integração trapezoidal (*Id* e *Ie*, Eq. 4):

$$Id\ and\ Ie = \Sigma(T2 - T1) * \left(\frac{I1+I2}{2}\right); \quad \text{(Eq. 4)}$$

onde *Id* é a irradiância integrada para o período luminoso do dia, *Ie* a irradiância integrada apenas durante o tempo do experimento, *T2* é o tempo (segundos) do segundo passo de tempo, *T1* é o tempo inicial, *I* é a irradiância (W m^{-2}) no primeiro (*I1*) e segundo (*I2*) passos de tempo.

A partir das irradiâncias integradas, o NPP_{d12h} foi estimado para o período luminoso do dia, para cada nível de irradiância (*Is*), 100, 50, 35 and 5%, de acordo com a Eq. 5:

$$NPP_{d12h} = \left(\frac{NPP*I_d}{I_e}\right) * \left(\left(\frac{Is}{100}\right) * \%\right); \quad \text{(Eq. 5)}$$

A profundidade correspondente a cada nível de irradiância foi obtida a partir dos perfis verticais de radiação fotossinteticamente ativa medidos com a sonda multiparamétrica. A R para cada nível de profundidade foi também estimada para o período luminoso do dia, multiplicando as taxas por 12 h (R_{12h}), e então para todo o período do dia, multiplicando por 24 h (R_{24h}). As taxas de

NPP e R foram então integradas verticalmente pelo método trapezoidal (ver Eq. 4) até a profundidade da zona eufótica (NPP_{z12h} e R_{z12h}), também obtida da radiação fotossinteticamente ativa da sonda multiparamétrica, e para o período luminoso do dia. A GPP_{z12h} é a soma da NPP_{z12h} e Rz_{12h}, apenas para o período luminoso do dia (12 h) e zona eufótica. As taxas de R também foram estimadas para a camada de fundo, i.e., entre o limite da zona eufótica e o fundo, assumindo a taxa de R da amostra mais profunda como constante ao longo do restante da coluna de água. Finalmente, o metabolismo do ecossistema pelágico foi obtido a partir da Eq. 6:

$$PEM = GPP_{z12h} - (R_{z24h} + R_{b24h}). \quad \text{(Eq. 6)}$$

Onde PEM é o metabolismo do ecossistema pelágico, GPP_{z12h} é a produção primária bruta na zona eufótica durante o dia, R_{z24h} e R_{b24h} são as taxas de R na zona eufótica e no fundo, respectivamente, para o dia inteiro (24 h). Os princípios, detalhes e incertezas do método podem ser encontrados em Fahey & Knapp [2007]. Para converter as taxas em unidades de oxigênio para carbono, foram utilizados quocientes de produção primária de 1,2, e coeficientes R de 0,85 [Almeida *et al.* 2005; Biddanda *et al.* 1994]. Os coeficientes de variação do oxigênio dissolvido das réplicas de incubação foram < 0,01% (n=280).

5.1.4 Composição da comunidade fitoplanctônica

Para avaliar a relação entre as taxas metabólicas e a composição da comunidade fitoplanctônica, os principais grupos de fitoplâncton foram identificados através de quimiotaxonomia baseada em pigmentos. As classes específicas de pigmentos fotossintéticos e acessórios foram estimadas a partir de HPLC [Zapata *et al.* 2000]. Os pigmentos foram extraídos no escuro com 3 mL de uma solução resfriada de metanol padronizado (2% de acetato de amônio), e analisados em um Shimadzu HPLC System, equipado com um módulo dispensador de solvente (LC-20 CE), um sistema controlador (CBM-20ª), um amostrador automático refrigerado (SIL-20 AC), um conjunto fotodiodo

(SPDM20A), e um detector de fluorescência (RF-10AXL). A separação cromatográfica dos pigmentos se deu através de uma coluna C8 monomérica com uma fase móvel contendo piridina [Zapata *et al.* 2000]. Seis grupos fitoplanctônicos foram escolhidos para a análise no CHEMTAX, baseado no diagnóstico dos pigmentos previamente investigados para a região por Mendes *et al.* [2017]. Foram incluídos os grupos diatomáceas, dinoflagelados, criptófitas, prasinófitas, clorófitas e cianobactérias.

5.1.5 Estado trófico

Para avaliar o estado trófico e a relação com os processos metabólicos nas águas do estuário da Lagoa dos Patos, foi aplicado o índice de estado trófico TRIX [Vollenweider *et al.* 1998]. O índice TRIX é calculado de acordo com a Eq. 7:

$$TRIX = [\log(chla * aD\% * O * N * P) - (a)] \,/\, b \qquad \text{(Eq. 7)}$$

onde chl-*a* [mg m^{-3}] representa a condição nutricional para o desenvolvimento do fitoplancton; *aD%O* é o desvio absoluto da saturação do oxigênio dissolvido [%], como medida do balanço entre a produção primária e a R; N é o nitrogênio inorgânico dissolvido N-(NO_3^{-2} + NO_2^{-3} + NH_4^{+}) [µg/L]; P é o fósforo inorgânico dissolvido como P-PO_4^{-3} [µg/L], e os parâmetros a e b são coeficientes de escala usados para fixar os limites mínimos do índice em sua extensão de unidades TRIX de 0 a 10. Para o presente conjunto de dados: a = -0.8 e b = 0.78. As classes de estado trófico são ultra-oligotrófico (0-2), oligotrófico (2.01 – 4), mesotrófico (4.01 – 6), eutrófico (6.01 – 8) e hiper-eutrófico (8.01 – 10) [Vollenweider *et al.* 1998].

5.1.6 Parâmetros do sistema carbonato e fluxos líquidos de CO_2 entre água-ar

O carbono inorgânico total e a pressão parcial do CO_2 na água (pCO_2) foram calculados pelo programa CO_2Sys V2.1 [Pierrot *et al.* 2006; Lewis & Wallace, 1998], utilizando como parâmetros de entrada a pressão hidrostática, temperatura, salinidade, alcalinidade total e pH. A constante de dissociação do ácido carbônico escolhida foi a de Millero *et al.* [2006] por abranger um maior gradiente de salinidade, de 0 a 35 psu. As constantes do sulfato e borato foram as reportadas por Dickson [1990] e Uppstrom [1974], respectivamente. As incertezas nas estimativas do carbono inorgânico total foram calculadas pelo software, de acordo com a rotina de propagação de erros de Orr *et al.* [2018], e foram ± 22 µmol kg^{-1} para o carbono inorgânico total e 45 µatm para a pCO_2.

Os fluxos líquidos de CO_2 entre água-ar foram calculados de acordo com a metodologia descrita por Borges *et al.* [2004], utilizando a constante de solubilidade de Weiss [1974], a qual é apropriada para águas estuarinas e elevada velocidade de correntes. A velocidade do vento variou entre 1.3 e 10.7 m s^{-1} (5.0 ± 2.3) durante o período do estudo, enquanto a velocidade das correntes variou entre 4.7 e 152.5 cm s^{-1} (45.4 ± 38.5). A pCO_2 atmosférica utilizada para o cálculo dos fluxos foi obtida da página do *Ocean Carbon and Acidification Portal* [OCADS 2022; http://www.ncei.noaa.gov/access/ocean-carbon-data-system].

5.1.7 Análises estatísticas

Foram realizadas análises de variância de Kruskal Wallis (KW) [Dodge 2008] para cada variável, para verificar se havia diferenças significativas (α = 0.05) entre as estações e estratos da coluna de água. Uma análise de componentes principais (PCA) foi feita a partir de variáveis normalizadas para extrair a variância entre as amostras baseadas nas taxas metabólicas GPP e R, fatores abióticos temperatura, salinidade, oxigênio dissolvido, turbidez, pH, radiação fotossinteticamente ativa, DIN, fosfato e silicato, e biótico chl-*a*. Foram elaborados modelos aditivos genéricos (GAM) para modelar a resposta das taxas metabólicas GPP e R em relação aos preditores abióticos, extraindo as

principais forçantes que governam as taxas metabólicas [Wood 2018]. O melhor modelo foi escolhido de acordo com a porcentagem de desvio explicado, os resíduos e o menor Critério de Informação de Akaike (AIC) [Akaike 1974]. Transformações Boxcox foram usadas quando necessário para atender às premissas paramétricas. As incertezas foram avaliadas de acordo com o erro padrão (SE) estimado pelo modelo. Além disso, foi realizada uma Análise de Redundância (RDA) [Legendre & Anderson 1999] para visualizar a ordenação das taxas metabólicas GPP e R em relação às variáveis bióticas, i.e., os grupos fitoplanctônicos diatomáceas, dinoflagelados, criptófitas, prasinófitas, clorófitas e cianobactérias. A melhor combinação de variáveis foi escolhida de acordo com a significância ($\alpha < 0.05$) e o AIC. Todas as análises estatísticas foram realizadas no Software R [R Core Team 2022].

5.2 Metabolismo do ecossistema aquático – método do oxigênio livre

Este subtópico apresenta a metodologia do artigo científico intitulado *Total ecosystem metabolism variability in a subtropical lagoonal estuary channel-site*, cujo manuscrito original, submetido à revista *Estuaries and Coasts*, encontra-se apresentado no capítulo VII.

O metabolismo foi também estimado através do um segundo método (método 2), do oxigênio dissolvido livre [Odum 1956; Murrel *et al.* 2018]. Este método também se baseia em variações de oxigênio dissolvido, mas diferentemente do método 1 em que uma parcela de água é incubada em frascos de borossilicato, limitando as estimativas do metabolismo à processos bioquímicos dentro do frasco, sem trocas com o meio, o método 2 parte de variações do oxigênio dissolvido medidas periodicamente por um sensor sujeito às trocas advectivas com o meio. Assim, assume-se que a variação do oxigênio dissolvido representa o resultado integrado dos processos de GPP e R de toda a comunidade, i.e., pelágica e bentônica, sob o pressuposto da homogeneidade de toda a coluna de água. Por utilizar dados coletados por um sistema automatizado, este método permite realizar estimativas do metabolismo de longos períodos em que há disponibilidade de dados com qualidade e que satisfaçam os pressupostos do método. O detalhamento do método, os seus

pressupostos, a aquisição, filtração (controle de qualidade) e seleção (de acordo com os pressupostos) dos dados, são descritos a seguir.

5.2.1 Aquisição dos dados

Dados horários do SiMCosta baixados da página www.simcosta.furg.br, foram utilizados. Devido aos pressupostos de homogeneidade espaço-temporal da massa de água, o método do OD livre pôde apenas ser aplicado à estação 1 (Fig. 2d). A boia RS-1 do SiMCosta no local da estação 1 é um sistema *Seabird Scientific Land/Ocean Biogeochemical Observatory* (LOBO), equipado com diversos sensores. Os seguintes parâmetros foram utilizados: temperatura, salinidade, oxigênio dissolvido, saturação do oxigênio dissolvido, pH, turbidez e chl-*a*. Dados dos parâmetros meteorológicos temperatura do ar, umidade relativa, pressão atmosférica, velocidade e direção do vento e radiação solar, foram obtidos da estação meteorológica da Praticagem do Rio Grande [RG Pilots 2022; www.rgpilots.com.br]. A qualidade dos dados foi assegurada através da filtros de controle de qualidade: teste de variação bruta (limites de leitura), teste de picos (dados anormalmente elevados), teste de taxa de variação (dentro de um determinado número de janelas de tempo), e teste de platô (valores constantes repetidos devido a defeitos nos sensores). Tais testes são sistematicamente realizados pelo SiMCosta e as respectivas bandeiras são informadas juntamente com o conjunto de dados. Os dados de ventos foram corrigidos para 10 metros acima do solo, a partir do perfil logarítmico do vento, Eq. 8:

$$v2 = v1 \frac{ln\left(\frac{h2}{z_0}\right)}{ln\left(\frac{h1}{z_0}\right)} \qquad \text{(Eq. 8)}$$

onde *v2* é a velocidade do vento na altura acima do solo desejada, *v1* é a velocidade do vento na altura em que o sensor está instalado, *ln* é o logaritmo natural, z_0 é a rugosidade da superfície (2×10^{-5} para superfície da água), e *h1* e *h2* é a altura original e a desejada, em metros.

5.2.2 Metabolismo do ecossistema aquático

O metabolismo total foi estimado de acordo com o método do oxigênio livre descrito por Odum [1956], o qual se baseia em variações de oxigênio dissolvido ao longo de um dia, obtidas de estações automáticas com sensores de oxigênio dissolvido. De acordo com o descrito em Caffrey et al [2014] e Murrell *et al.* [2018], a técnica consiste na modelagem dos fluxos de O2 em cada passo de tempo (Eq. 9):

$$\frac{\partial C}{\partial t} = P_e + R_e + D \qquad \text{(Eq. 9)}$$

onde *∂C/∂t* representa os fluxos medidos de oxigênio dissolvido (mmol O_2 m^{-3} h^{-1}), *Pe* é a taxa de fotossíntese, *Re* as taxas de respiração, e *D* é a taxa de troca de oxigênio dissolvido entre água-ar, de acordo com a Eq. 10:

$$D = k_a(C_s - C) \qquad \text{(Eq. 10)}$$

onde *ka* é o coeficiente de reaeração volumétrica (h^{-1}) e *Cs* é a concentração de saturação do O_2 em função da temperatura e salinidade da água [Benson & Krause, 1984]. Para o ka, uma forma modificada da equação desenvolvida por Ro & Hunt [2006] foi usada, de acordo com o implementado por Thèbault *et al.* [2008]:

$$k_a = \frac{1}{h}.1.706\left(\frac{D_w}{v_w}\right)^{\frac{1}{2}}.\left(\frac{p_a}{p_w}\right)^{\frac{1}{2}}.{U_{10}}^{1.81} \qquad \text{(Eq. 11)}$$

onde *h* é a profundidade da coluna de água (m), *Dw* é a difusividade do O_2 na água do mar (m_2 s^{-1}), *vw* é a viscosidade cinemática da água do mar a uma dada temperatura e salinidade (m^2 s^{-1}), *ρa* e *ρw* são as densidades do ar e da água,

respectivamente (kg m^{-3}), e *U10* é a velocidade do vento normalizada a 10 m acima do nível do solo (m s^{-1}).

Os fluxos de oxigênio dissolvido corrigidos pela difusão na interface água-ar foram integrados para o período de 24 h, para calcular a produção primária aparente (Pa) e as taxas respiratórias ao longo do período da noite (Re). As taxas de respiratórias foram multiplicadas por 24 h para obter a respiração de toda a comunidade do ecossistema (CR), enquanto as taxas de GPP foram obtidas pela soma de Pa e Re, multiplicadas pelo tempo do período luminoso do dia e profundidade local. O metabolismo líquido do ecossistema aquático foi finalmente calculado como a GPP menos a CR.

As taxas metabólicas foram computadas com o pacote do R WtRegDO [Beck *et al.* 2015], para os seguintes períodos: de março de 2016 a dezembro de 2017, de abril de 2019 a fevereiro de 2021, com algumas lacunas menores. Tais lacunas se deram em função da retirada dos sensores da água para a limpeza de organismos incrustrados, manutenção e calibração dos sensores. Durante 2018 a boia RS-1 esteve inoperante por um longo período para manutenção.

Devido as premissas e limitações do método do oxigênio livre, tais como a homogeneidade da coluna de água e das suas propriedades ao longo do tempo [Coloso *et al.* 2008; Needoba *et al.* 2012; Staehr *et al.* 2012], o método pôde apenas ser aplicado à estação 1 (boia RS-1 do SiMCosta), em que a homogeneidade vertical pôde ser assumida devido à menor profundidade e os processos de mistura locais [Bordin *et al.* 2023a]. A estação 1 está em um canal com cerca de 4.5 m de profundidade. Está situada em uma área abrigada, na seção intermediária do estuário da Lagoa dos Patos (Fig. 2d). Baseado na sua localização intermediária no estuário da Lagoa dos Patos, na profundidade média da Lagoa dos Patos (5 m) [Calliari 1997], bem como no fato de que as taxas metabólicas medidas pelo método 1 em ambas as estações (abrigada e exposta), apresentaram tendências semelhantes nas taxas do metabolismo, [Bordin *et al.* 2023a], assumiu-se que a estação 1 é representativa das áreas de canal do estuário da Lagoa dos Patos.

O regime de micromaré do estuário da Lagoa dos Patos é de aproximadamente 0,5 m [Soares & Möller 2001]. No entanto, o nível da água no

estuário muda devido à drenagem continental e à direção dos ventos. Os ventos SO forçam a entrada de água costeira para dentro do estuário, enquanto os ventos NE causam a vazante da água estuarina [Möller & Fernandes 2010]. O efeito de mudança de nível da água poderia ter sido removido pela técnica *detide* através de regressão ponderada contida no pacote WtRegDO package [Beck *et al.* 2015], mas não havia dados disponíveis sobre o nível da lagoa para a estação 1. Diferentemente de estações fixas, para o qual o método foi desenvolvido, a boia meteoceanográfica acompanha a subida e descida do nível da água. Além disso, as mudanças de salinidade mencionadas acima ainda poderiam representar um problema, por violarem a premissa de homogeneidade temporal da massa de água [Coloso *et al.* 2008; Needoba *et al.* 2012; Staehr *et al.* 2012]. Portanto, os resultados do metabolismo do ecossistema pelágico foram cuidadosamente filtrados para eliminar os dias cujas variações na salinidade foram > 4 psu (arbitrariamente definido). O primeiro passo foi através do pacote do R DO-Classifier, o qual avalia se os dados são aptos para estimativas de metabolismo através de uma classificação supervisionada por um modelo *Symbolic Aggregate Approximation (SAX)* [Muraoka *et al.* 2018]. Então o conjunto de dados foi manualmente checado para certificar que os dias selecionados pelo SAX eram realmente homogêneos (de acordo com a variação de salinidade), se todos os dados anômalos, i.e., com GPP negativos e CR positivos) haviam sido removidos, e por *outliers* cujos quartis eram < 5% e > 95%, substituídos pelos valores que representavam tais quartis, totalizando 363 dias com estimativas do metabolismo do ecossistema pelágico.

5.2.3 Análise dos dados

As análises foram realizadas com todos os cinco anos de dados (2016, 2017, 2019, 2020 e 2021). Foram feitas análises estatísticas descritivas em escalas de tempo diária, mensal, sazonal e anual, para todos os parâmetros. As análises interanuais referem-se apenas às primaveras austrais, por incluírem dados suficientes para uma comparação de quatro anos. Análises de variância de Kruskal Wallis (KW) [Dodge 2008] foram realizadas para testar as diferenças globais (em todas as escalas de tempo) e a posteriori para analisar diferenças

par a par ($\alpha < 0.05$; apenas interanual/primaveras). Uma PCA foi feita para verificar a associação entre os parâmetros: GPP, CR, temperatura, salinidade, saturação do oxigênio dissolvido, chl-*a*, turbidez, velocidade do vento e radiação fotossinteticamente ativa (inferido através de dados de irradiância medidos por um piranômetro, fora da água). Uma matriz de correlação de Pearson dos parâmetros supracitados foi feita para complementar e corroborar a PCA. Foram computados GAMs [Wood 2011, 2017] (estações do ano e anos adicionados como fatores) para extrair as principais forçantes que governam as taxas metabólicas GPP e CR em cada escala de tempo (diária, mensal, sazonal e interanual/primaveras). O melhor modelo para cada escala de tempo foi selecionado baseado na porcentagem de explicação, menor erro padrão, e AIC [Akaike H. 1974]. Alguns parâmetros foram transformados por Boxcox para diminuir a assimetria dos dados. Para incluir o vento nas análises, ele foi decomposto em componentes meridional e zonal, e apenas a componente meridional foi usada na análise representando tanto a velocidade como a direção do vento. Isso ocorreu porque os principais quadrantes que afetam a entrada (saída) de água marinha salgada (água estuarina) no estuário da Lagoa dos Patos são os de norte (sul) [Möller & Fernandes 2010]. Todas as análises estatísticas foram realizadas com o Software R versão 4.2.1 [R Core Team 2022], usando o pacote mgcv.

5.3 Fluxos e balanço de massa dos nutrientes

Este subtópico apresenta a metodologia do artigo científico intitulado *Nutrient fluxes, budgets and net ecosystem metabolism in the Patos Lagoon under drought conditions*, cujo manuscrito original foi submetido à revista *Estuarine, Coastal and Shelf Science*, e é apresentado no capítulo VIII.

5.3.1 Trabalho de campo e análises laboratoriais

O trabalho de campo e as análises laboratoriais que descrevem os procedimentos de coleta e análise dos dados utilizados nesta etapa, encontram-se nos subtópicos 5.1.1 e 5.1.2.

5.3.2 Modelo numérico Delft3D-FLOW – Lagoa dos Patos

Foram realizados experimentos de modelagem numérica utilizando o software Delft3D. Este é um software modular, e o módulo D-FLOW [Deltares Systems, 2019] foi aplicado neste estudo. O D-FLOW é um software de modelagem que tem sido aplicado com sucesso em diversos estudos para avaliar a hidrodinâmica e os processos de transporte sedimentar [Pokavanish *et al.* 2014; Martyr-Koller *et al.* 2017], em áreas rasas, costeiras, estuários, lagoas e rios. O D-FLOW calcula os fluxos não estacionários e os fenômenos de transporte decorrentes de forçantes de maré astronômica e meteorológicas, em grades retilíneas ou curvilíneas. Ele segue a abordagem de coordenadas σ em simulações 3D, onde as equações de Navier-Stokes são resolvidas para fluxos em superfícies livres incompressíveis [Deltares Systems, 2019].

Foi criada uma malha batimétrica regular para discretizar o domínio da Lagoa dos Patos (Fig. B.1). Foi aplicada uma malha de alta resolução espacial para melhor resolver os processos na região de interesse, i.e., região estuarina. As células da malha foram irregularmente espaçadas, variando de $2{,}3 \times 10^{-5}$ Km^2 na região estuarina, para 8,06 Km^2 nas bordas oceânicas e norte da Lagoa dos Patos, totalizando 261 células na direção X e 279 na direção Y. Cinco camadas σ foram empregadas para discretização vertical.

O estudo foi conduzido para o ano de 2019, com exercícios de calibração (fevereiro) e validação (setembro). O modelo foi forçado por marés, ventos e descarga dos rios. Para as marés astronômicas, foram aplicados dados horários de nível do mar obtidos do modelo regional do mar da Patagônia OSU TPXO [Egbert *et al.* 2002]. Dados horários de nível do mar resultantes da maré meteorológica, dados de temperatura e salinidade, foram obtidos do *Copernicus Marine Service* (www.resources.marine.copernicus.eu/products), modelo *Operational Mercator Global Ocean Analysis and Forecast,* PHY_001_024. Séries temporais de temperatura e salinidade foram aplicadas para cada uma das 5 camadas σ, como forçantes nas condições de contorno oceânicas. Para as forçantes meteorológicas, foram aplicadas séries temporais de ventos e pressão atmosférica na superfície do mar, obtidas do modelo de reanálise ERA-5 do ECMWF (*European Center for Medium-Range Weather Forecasts*; www.ecmwf.int/en/forecasts/datasets/reanalysis-datasets/era5). Foram

utilizados dados diários de vazão dos rios Guaíba (soma dos rios Jacuí, Taquarí, Caí e Sinos) Rio Camaquã (obtidos da ANA; www.snirh.gov.br/hidroweb), e Canal São Gonçalo (fornecidos pelo Laboratório de Oceanografia Costeira da FURG). Após validado, o modelo foi aplicado para o período da campanha amostral (de Fev-22 a Mar-23 de 2021). Todos os arquivos de setup do modelo da Lagoa dos Patos pelo Delft3D-FLOW podem ser obtidos através do repositório disponível em www.github.com/graoceano/Patos-Lagoon-Delft3D-FLOW-model.

5.3.3 Avaliação do modelo Delft3D-FLOW – Lagoa dos Patos

O modelo hidrodinâmico foi calibrado através da variação dos coeficientes de fricção, fórmula de rugosidade, coeficientes de rugosidade, viscosidade turbulenta e difusividade verticais e horizontais, modelo de turbulência 3D e coeficientes de arrasto do vento. O melhor arranjo entre os resultados do modelo e os dados medidos, foram encontrados para os coeficientes de arrasto do vento A $1{,}55 \times 10^{-3}$ a 0 m/s, B $8{,}55 \times 10^{-3}$ a 19,22 m/s e C 8.55×10^{-3} a 19,22 m/s (os coeficientes entre 0 e 19,22 m/s são automaticamente interpolados), fórmula de rugosidade de White-Colebrook, coeficiente de 1×10^{-5}, viscosidade horizontal turbulenta de 11,25 m^2/s e difusividade de 25 m^2/s, viscosidade vertical turbulenta de 1×10^{-4} m^2/s e difusividade de 1×10^{-5} m^2/s. O melhor modelo de turbulência 3D foi o algébrico. O melhor arranjo entre os parâmetros físicos foi aplicado na validação do modelo. A Tabela B.1 apresenta um resumo demonstrativo, com o *set-up* de 25 das mais de 100 simulações realizadas nas fases de calibração, juntamente com os respectivos valores de RMAE.

A validação do modelo hidrodinâmico foi realizada através da comparação entre os dados de nível do mar calculados e medidos (Fig. B.1) e velocidade de corrente longitudinal (Fig. B.2), para os mesmos locais. Para o nível do mar os locais foram os pontos de controle *SL (Fig. 2c, Fig. B.1a), localizado na região lagunar, e o ponto de controle *RGP (Fig. 2d, Fig. B.1b), localizado na região estuarina, canal de acesso principal do estuário da Lagoa dos Patos. Para as velocidades de corrente longitudinais, os pontos de controle foram as boias meteoceanográficas do SiMCosta *RS-1, *RS-2 e *RS-4 (Fig. 2d, Figs. B.2a,

B.2b e B.2c, respectivamente). As duas primeiras estavam localizadas na região estuarina (próximas das estações RS-1 e RS-2, respectivamente), enquanto a terceira estava na plataforma continental adjacente (Fig. 2d).

O modelo hidrodinâmico foi avaliado quantitativamente através do erro relativo médio absoluto (RMAE) sugerido por Van Rijn *et al.* [2003], cujas cinco classes representam a qualidade do modelo em reproduzir a realidade do ambiente: excelente (< 0,2), bom (0,2 – 0,4), razoável (0,4 – 0,7), pobre (0,7 – 1,0) e ruim (> 1,0). O RMAE para o nível do mar variou entre 0,06 (*SL) e 0,13 (*RGP), e para a velocidade de corrente longitudinal entre 0,15 (*RS-1), 0,17 (*RS-2) e 0,35 (*RS-4). Portanto, o modelo foi considerado apto a representar a hidrodinâmica da Lagoa dos Patos de forma satisfatória.

5.3.4 Análise dos dados

Apesar dos fluxos de água terem sido estimados durante a campanha amostral na seção transversal à estação RS-2 com um ADCP, o uso dos fluxos estimados através da modelagem numérica é justificado pela falta de dados para a seção adjacente à estação RS-1. Para uniformidade das estimativas entre os canais das duas estações, os fluxos de água foram obtidos através de modelagem numérica. Foram obtidas séries temporais horárias dos fluxos de água nos canais, dos dados de saída de uma simulação do modelo D-FLOW entre o período da campanha amostral (Fev-22 a Mar-23 de 2021), de seções transversais dos canais onde as estações RS-2 e RS-1 estão localizadas. Os fluxos de água da simulação pelo D-FLOW foram processados com a ferramenta do Delft3D, QUICKPLOT versão 2,15 [Deltares Systems, 2014]. Os fluxos de nutrientes (nitrito, nitrato, amônio, fosfato e silicato) médios foram estimados por interpolação, de acordo com a Equação 12:

$$\text{Flux} = \frac{1}{n}\sum_{i=1}^{n} Q_i C_i \qquad \text{(Eq. 12)}$$

onde *Ci* é a concentração instantânea (mol m^3; das amostragens *in situ*) dos nutrientes no tempo $_i$, *Qi* é o fluxo de água (m^3 s^{-1}; da simulação com o D-FLOW) no tempo $_i$, e *n* é o número de amostras.

Séries temporais dos fluxos de água e nutrientes, gráficos de dispersão entre salinidade e nutrientes, e um gráfico de curva frequência da normal climatológica de descarga dos rios Guaíba e Camaquã, foram plotadas através da biblioteca do Python Matplotlib Pyplot versão 3.7.1 [Hunter, 2007].

5.3.5 Modelo biogeoquímico de caixas – LOICZ

O modelo LOICZ de balanço de massa [Gordon *et al.* 1996] foi aplicado para os parâmetros: água, sal, DIN e DIP. A Lagoa dos Patos foi dividida em duas caixas, uma para representar a região límnica, i.e., dominada por água doce, com salinidades < 3, chamada de PL box, e outra para representar a região estuarina, cuja salinidade é > 3, denominada de PLE box. O limite geográfico entre as duas caixas foi definido como sendo uma seção transversal da lagoa a partir da Ponta da Feitoria (Fig. 2d), visto que este é o limite teórico médio das intrusões de águas marinhas para dentro da Lagoa dos Patos [Möller & Castaing, 1999]. Foi aplicado um modelo de uma camada vertical, assumindo o sistema como verticalmente homogêneo e estável. Esta abordagem é comumente aplicada em sistemas que não possuem uma estrutura física vertical bem definida [Gordon *et al.* 1996], como observado para a Lagoa dos Patos [Möller & Castaing, 2001]. Portanto, foram usadas as médias verticais dos parâmetros salinidade, DIN e DIP.

A área e o volume das duas caixas foram obtidos através da ferramenta de pré-processamento QUIKIN versão 4.00 [Deltares Systems, 2020], a partir da malha batimétrica regular da Lagoa dos Patos, como descrito na seção 3.3.1. Os dados de descarga dos rios foram obtidos da ANA (ver seção 3.1.1) para as estações localizadas nos rios Jacuí, Caí, Taquarí e Sinos, cuja soma representam o Rio Guaíba, e Rio Camaquã. Foram selecionados apenas dados dos períodos do verão austral (dez a mar), dos anos entre 1991 e 2021. As descargas do Canal São Gonçalo foram fornecidas pelo Laboratório de Oceanografia Costeira e Estuarina (LOCOSTE – FURG), e representam as médias climatológicas mensais. Para representar os fluxos de água dos rios para

dentro da PL box, foram obtidas as médias climatológicas mensais, e então somadas as vazões de cada mês do verão austral dos rios Guaíba e Camaquã, e finalmente calculada a média geral da vazão do verão austral para este compartimento. Para representar os fluxos de água para a PLE box, os dados de vazão do Canal São Gonçalo já estavam representados por médias climatológicas mensais, tendo sido necessário apenas calcular a média dos meses do verão austral. Dados de normais climatológicas de precipitação e evaporação foram obtidos da página web do Instituto Nacional de Meteorologia (INMET; www.portal.inmet.gov.br/normais) para o período entre os anos de 1981 e 2010. Para representar estes fluxos, foram calculadas as médias dos meses de verão austral das estações do INMET localizadas na cidade de Porto Alegre (n° 83967) e Pelotas (n° 83985), para a PL box, e as médias entre as estações de Pelotas e Rio Grande (n° 83995) para a PLE box. Os fluxos de água subterrânea não foram considerados devido a insuficiência de dados.

Foram calculados os balanços de massa para o DIP e DIN, considerando as fontes externas (rios, efluentes e oceano) e as concentrações internas, usadas para estimar os fluxos de entrada e saída desses elementos. Apenas dados representativos do verão austral foram considerados. Dados de nutrientes para o Rio Guaíba e Camaquã, bem como para determinar as concentrações internas da PL box, foram obtidos do Programa Pró Mar de Dentro (superfície e fundo), dos cruzeiros realizados nos meses de Fev-1999, Mar-1999 e Jan-2000. Havia uma estação em cada rio (n = 12), e seis estações (n = 36) dispostas sobre o eixo N-S da Lagoa da PL box. As concentrações dos nutrientes de aporte fluvial para a PL box foram obtidas através das médias de todas as amostras dos rios Guaíba e Camaquã. Dados de nutrientes do Projeto Espinha, coletados em Jan-1986 em 37 estações (superfície e fundo; n = 74) distribuídas ao longo dos eixos N-S e W-E da PL box, foram somados ao conjunto de dados das estações internas da PL box (total n = 110). Ambos os conjuntos de dados foram apresentados por Pereira [2003]. Dados de DIP e DIN para representar as entradas pelo Canal São Gonçalo foram obtidos a partir da média de cinco estações (n = 5) localizadas próximo da desembocadura com a PLE box [de Souza, 2015]. As concentrações internas dos nutrientes na PLE box foram representadas pela média do conjunto total de dados (n = 188), compostos pelo

Programa Mar de Dentro (2 estações, n = 12), Projeto Espinha (13 estações, n = 26) e do presente trabalho (2 estações, amostras com salinidade < 30, n = 93). As concentrações de referência para o oceano costeiro adjacente foram obtidas através da média de 1 estação do projeto Pró Mar de Dentro (n = 6), e das amostras da estação 2 do presente conjunto de dados, cuja salinidade foi > 30. As concentrações de referência para o oceano costeiro adjacente (total n = 57) foram obtidas da média entre os dados de 1 estação do programa Pró Mar de Dentro (n = 6) e dos dados da estação 2 da campanha amostral, sujas salinidades foram > 30 (n = 51). Para representar o aporte através da água da chuva, dados de DIP e DIN foram obtidas pela média anual de 3 estações localizadas na cidade de Porto Alegre (n = 36) e quatro estações em Rio Grande (n = 48) para representar os fluxos pra PL box (total n = 74). Para a PLE box foram utilizadas apenas as médias das estações localizadas na cidade de Rio Grande [Casartelli *et al.* 2008].

Para representar o aporte de efluentes para a PL box, assumiu-se que a vazão do Rio Guaíba, localizado na região mais populosa deste compartimento (Porto Alegre), já é composto pela somatória dos aportes naturais e antrópicos, visto que os efluentes tratados e não tratados, são lançados neste rio. Os aportes da cidade de Pelotas para a PLE box, foram estimados de forma similar, visto que os efluentes são lançados no Canal São Gonçalo. Para a cidade de Rio Grande, foram aplicadas as concentrações utilizadas por Seiler *et al.* [2020] para representar os aportes de nutrientes das estações de tratamento de esgoto (ETE Navegantes e ETE Parque Marinha), aplicando uma vazão de água de 0,15 e 0,05 m^3 s^{-1}, respectivamente. As fontes difusas e outras fontes pontuais clandestinas de 17 emissários identificados por Baumgarten *et al.* [2021] nas margens da cidade de Rio Grande, foram consideradas, utilizando as mesmas concentrações registradas nas ETEs, somando um adicional de fluxo de água de 0,01 m^3 s^{-1}, totalizando 0,21 m^3 s^{-1}. Os dados de vazão e concentrações de DIP e DIN para representar os aportes antropogênicos foram computados como “outras descargas de rios” e “outras fontes de nutrientes” para a PLE box. Os balanços de massa foram computados com a LOICZ toolbox [Gordon *et al.* 1996], disponível em https://nest.su.se/mnode/Toolbox/LOICZ_Toolbox.htm.

5.3.6 Processos metabólicos e potencial para produção primária

O metabolismo líquido do ecossistema e o balanço entre a fixação de nitrogênio e desnitrificação N-fix – denit, respectivamente, foram estimados através do modelo de caixas LOICZ [Gordon *et al.* 1996]. O metabolismo líquido é estimado multiplicando o ΔDIP pela razão C:P de Redfield [Redfield, 1963] de 106:1, devido à insuficiência de dados de carbono e fósforo orgânicos para representar a razão C:P medida de cada caixa do modelo. O balanço entre N-fix – denit é determinado como a diferença entre o ΔDIN calculado e aquele esperado que, por sua vez, é o produto da razão N:P (estimada pela média do DIN/DIP) e o ΔDIP [Gordon *et al.* 1996]. Finalmente, 4 diagramas de balanço de massa (água, sal, DIP e DIN) foram gerados com o toolbox do LOICZ, para sumarizar os resultados. Os detalhes completos dos dados de entrada para as caixas PL e PLE, são apresentados na Tabela B.2. O metabolismo líquido também foi computado considerando a razão C:P (457) da grama marina *Ruppia marítima* [Atkinson *et al.* 1983], uma vez que é a principal espécie, cuja cobertura se estende por uma área de aproximadamente 120 km^2 [Costa *et al.* 1997]. O metabolismo líquido para o fitoplâncton foi aplicado para a área restante (759 km^2), com ração C:P de 106 [Redfield, 1963]. O metabolismo líquido para a *Ruppia marítima* não foi computado para a região límnica da Lagoa dos Patos, pois as gramas marinhas não apresentam cobertura significativa nesta região, devido a maior profundidade média deste compartimento.

O potencial de produção primária foi estimado para a zona costeira adjacente, a partir dos fluxos de DIN (nutriente limitante), baseado nas razões estequiométricas C:P:N = 106:16:1 [Redfield *et al.* 1963], assumindo que todo o DIN foi assimilado em biomassa fitoplanctônica. O potencial foi computado para a região límnica (caixa PL: 9.660 km^2), região estuarina (caixa PLE: 879 km^2), e plataforma continental adjacente, considerando uma faixa de 0,1 x 90 km (9 km^2).

Capítulo VI:

Variação diária do metabolismo pelágico em um estuário lagunar subtropical

O primeiro manuscrito apresenta, em síntese, a variabilidade diária das taxas metabólicas do ecossistema pelágico na zona inferior do estuário da Lagoa dos Patos. Neste contexto, foram investigados os principais processos meteoceanográficos que governam o metabolismo aquático na área de estudo. Este estudo contribuiu com uma visão interdisciplinar do tema, partindo do conhecimento da variabilidade em pequena escala temporal do metabolismo aquático, dos parâmetros físico-químicos (e.g., vazão, temperatura, salinidade, nutrientes), biológicos (i.e., comunidade fitoplanctônica), do sistema carbonato, e como essas variáveis se relacionam entre si em pequena escala temporal. De autoria de Luís Henrique Bordin, Eunice da Costa Machado, Carlos Rafael Borges Mendes, Elisa Helena Leão Fernandes, Maurício Garcia de Camargo, Rodrigo Kerr e Carlos Augusto França Schettini, intitulado "***Daily variability of pelagic metabolism in a subtropical lagoonal estuary***", foi publicado no periódico "***Journal of Marine Systems***" em janeiro de 2023. A campanha amostral, análise laboratorial dos parâmetros oxigênio dissolvido, nutrientes inorgânicos dissolvidos, pigmentos fotossintéticos, a análise e interpretação dos resultados, e a redação deste manuscrito foram feitas por mim, como parte da minha tese de doutorado. Eunice da Costa Machado, fez toda a supervisão para que chegássemos à conclusão desse estudo. Carlos Rafael Borges Mendes contribuiu como especialista em ecologia de produtores primários. Elisa Helena Leão Fernandes e Carlos Augusto França Schettini contribuíram como especialistas em oceanografia física. Rodrigo Kerr contribuiu nas análises químicas das amostras para determinação da Alcalinidade Total e Carbono Total, e como especialista em sistema carbonato.

Abstract

The influence of meteoceanographic variability on pelagic ecosystem metabolism was evaluated during late austral summer (from February to March 2021), through a daily survey for one month, at two channel sites in the subtropical Patos Lagoon Estuary, Brazil — the largest choked (restricted connection to the sea) coastal lagoon of South America. Heterotrophic predominance prevails in the studied area, with an overall mean of −205 ± 143 mmol O_2 m^{-2} d^{-1}, with 78 ± 67 mmol O_2 m^{-2} d^{-1} from gross primary production (GPP) and 285 ± 178 mmol O_2 m^{-2} d^{-1} from respiration (R). Generalized additive models were used to identify the most relevant driving forces for GPP, which were nitrate, salinity, chlorophyll-a (chl-*a*), wind speed and direction, water flow rate, silicate, and turbidity. The main driving mechanisms for R were photosynthetically active radiation, temperature, wind speed, chl-*a*, turbidity, and nitrate. GPP was potentially co-limited by dissolved inorganic nitrogen (very low nitrogen to phosphorus ratio, N:P = 3.1 ± 2.0) throughout the period and by light in some events due to material resuspension from the bottom by wind-induced salt-wedge intrusions. Evidence of intrusions of Plata Plume Water into the estuary were observed, likely contributing as a key factor to local biogeochemistry. The main phytoplankton groups, in decreasing order of abundance, were diatoms, cryptophytes, and cyanobacteria, with their variability being controlled mainly by wind-induced salinity changes. Diatoms responded as the main contributor to metabolic rates, water carbon dioxide (CO_2), carbon dioxide partial pressure (pCO_2), and water-air CO_2 fluxes (FCO_2) by its higher biomass and uptake of total inorganic carbon. Inlet (70%) and sea-exposed (95%) stations behaved mainly as net CO_2 sinks from the atmosphere during most of the study period (−7.9 ± 30.6 mmol C m^{-2} d^{-1}). The inlet inner station had a median FCO_2 of −9.8 and an average of 4.4 ± 41.2 mmol C m^{-2} d^{-1}, while the sea-exposed station had −17.0 and −15.4 ± 17.3 mmol C m^{-2} d^{-1}, respectively. Although total inorganic carbon and chl-*a* were negatively correlated, which indicates carbon assimilation by primary production, no correlation was observed between metabolic rates and FCO^2. These results suggest the need for additional investigation into the driving factors and/or sources of carbon species in the Patos Lagoon Estuary to better understand the role of aquatic ecosystem metabolism in the carbon budget. Finally, the daily

investigation of pelagic ecosystem metabolism and its driving factors was unprecedented for the Patos Lagoon Estuary and showed the importance of short-term monitoring for a better understanding of highly dynamic estuarine environments.

6.1 Introduction

Continental and meteoceanographic processes influence the dynamics of water properties in aquatic coastal ecosystems, such as suspended particulate matter concentration and euphotic zone depth, which are affected by the biogeochemical dynamics of carbon, nutrients, and organic matter production and consumption [Valiela 2015]. Estuaries are key zones between freshwater and saltwater environments, and are responsible for the cycling of nutrients and carbon from land and ocean, which contributes significantly to the mass balance of these elements [Bianchi 2007; Laruelle *et al.* 2013]. Along the estuarine haline gradient, carbon and nutrients from different origins are transformed by complex multi-interactions of physical, chemical, biological, and geological processes. These processes are modulated by a set of forces, such as continental runoff, tides, waves, light intensity, and water temperature and salinity changes [Bianchi 2007; Regnier *et al.* 2013a, 2013b].

Organic matter primary production supplies the food web in marine and estuarine environments [Bianchi 2007; Valiela 2015]. Primary production and ecosystem potential for biological production can be estimated using chl-*a* as a biomass proxy. Similarly, chl-*a* combined with nutrient concentrations and the deviance of dissolved oxygen from its saturation index, provide an estimation of trophic state, a parameter related to aquatic metabolism [Vollenweider *et al.* 1998]. The whole of aquatic ecosystem metabolism can be expressed as integrated rates of primary production and organic matter consumption (R; also called respiration, regeneration, remineralization, or organic matter degradation).

Although aquatic metabolism has been the focus of aquatic science for more than a century [Staehr *et al.* 2012], habitats of the Northern Hemisphere have been studied more intensively [Cloern *et al.* 2014], such as Chesapeake Bay [Kemp *et al.* 1997]; Apalachicola, Weeks, and Grand bays [Caffrey *et al.*

2014]; Pensacola Bay [Murrell *et al.* 2018]; Urdaibai Estuary [Iriarte *et al.* 1997]; and Douro Estuary [Azevedo *et al.* 2006]. In the Southern Hemisphere, the Patos Lagoon Estuary has been intensively studied for about fifty years, with studies mainly focused on hydrodynamics [Costa *et al.* 1988; Möller *et al.* 2001; Möller & Fernandes 2010] biogeochemical dynamics [Niencheski *et al.* 1999; Odebrecht *et al.* 2015], biological and ecological aspects [Closs 1962; Odebrecht *et al.* 1987; Zago 1976], and suspended particulate matter and sediments [Calliari *et al.* 1997; Niencheski *et al.* 1999]. Early studies on aquatic metabolism in the Patos Lagoon Estuary were conducted by Abreu *et al.* [1994; 1995; 2010], Proença *et al.* [1994], and Haraguchi *et al.* [2015], but they did not report R rates nor the status of integrated aquatic ecosystem metabolism. Therefore, in the present study, we aimed to: i) estimate pelagic ecosystem gross primary pro- duction (GPP) and R rates, at high sampling frequency; ii) evaluate the relationship between meteoceanographic variability (i.e., wind speed and direction, water-flow, and photosynthetically active radiation), physico-chemical parameters (i.e., temperature, salinity, dissolved inorganic nutrients, and chl-*a*), and metabolic rates; iii) associate metabolic rates with phytoplankton community structure and composition; and iv) evaluate the association between the biological component (i.e., metabolic rates and biomass of phytoplankton groups) and water-air net CO_2 fluxes in the Patos Lagoon Estuary.

6.2 Patos Lagoon Estuary: hydrodynamics and biogeochemistry

The Patos Lagoon Estuary is located in south Brazil, with its hydrodynamics governed by wind and continental runoff. The influence of tides (± 0.5 m) is minor in the region, because it is located in a micro- tidal regime zone [Soares & Möller Jr 2001]. The Guaíba and Camaquã Rivers and the São Gonçalo Channel are the main tributaries, with a combined mean annual discharge of 2400 $m^3\ s^{-1}$. Drought periods occur during summer-autumn, while peaks of river discharge occur during winter-spring [Vaz *et al.* 2006]. The water dynamics of the estuarine system is controlled by the wind when the combined river discharge is lower than 2000 $m^3\ s^{-1}$, while higher rates allow freshwater flow domains to occur in the region [Möller *et al.* 2001; Möller & Fernandes 2010].

During periods of higher river discharges, the reversal of the outflow condition only occurs with intense southwestern winds [Möller *et al.* 2001].

Southwesterly winds promote seawater inflow conditions and advection into the estuary [Möller *et al.* 2001; Möller & Fernandes 2010]. Abreu *et al.* [1994, 2017] hypothesized that southwestern winds promote fertilization of the southern section of the Patos Lagoon Estuary because regenerated nutrients, which previously left the estuary towards the inner shelf during outflow (ebb) conditions, re-enter into the estuary. This process also brings marine phytoplankton species into the estuary, such as diatoms and dinoflagellates [Fujita & Odebrecht 2007; Haraguchi *et al.* 2015; Mendes *et al.* 2017]. Nutrient-rich Plata Plume Water [Braga *et al.* 2008; Bordin *et al.* 2019], which spreads across the southern Brazilian Shelf during southwestern winds [Möller *et al.* 2008], is also a key source of nutrients entering the Patos Lagoon Estuary under these conditions. On the other hand, northeastern winds promote ebb conditions [Möller *et al.* 2001; Möller & Fernandes, 2010], which reduce the salinity of the Patos Lagoon Estuary by bringing freshwater and nutrient depleted waters from the northern limnic region of Patos Lagoon [Niencheski *et al.* 1999; Odebrecht *et al.* 2015]. The northeasterly winds also insert freshwater microalgae species into the estuarine zone, such as cyanobacteria and chlorophytes [Fujita & Odebrecht 2007; Haraguchi *et al.* 2015; Mendes *et al.* 2017]. Nutrients, chl-*a* and primary production rates are higher and more variable during the spring and summer, decreasing throughout the autumn and reaching the lowest values during the winter, due to lower temperatures and light intensities. Abreu *et al.* [1994] showed that higher turbidity, caused from continental runoff during the rainy season, is associated with a decrease in primary production rates. Despite the existing knowledge gap regarding aquatic ecosystem metabolism in the Patos Lagoon Estuary, the system is considered autotrophic most of the year, and heterotrophic during winter, when organic matter from senescent seagrass is regenerated on the sediments [Abreu *et al.* 1994].

The wind-induced outflow of freshwater and inflow of seawater governs carbonate system variability in the Patos Lagoon Estuary. High surface total alkalinity and total inorganic carbon concentrations are mainly associated with the composition of salty shelf waters (salinity > 36) that intrude into the estuary

[Albuquerque *et al.* 2022]. Organic matter remineralization and CO_2 ingassing also contribute to increased total inorganic carbon in the estuary. The CO_2 system in the Patos Lagoon Estuary swings between an ocean-dominated (spring/summer) and riverine- dominated (autumn/winter) estuarine behavior [Albuquerque *et al.* 2022]. On average, during the former period, CO_2 ingassing prevails, whereas in the latter period, the system behaves as a source of CO_2 to the atmosphere [Albuquerque *et al.* 2022]. Although a net CO_2 uptake of −2 mmol m^{-2} d^{-1} prevailed in the Patos Lagoon Estuary between 2017 and 2021, with higher sink rates during the austral summer, CO_2 emission to the atmosphere is more pronounced during winter/spring period in the inner protected zones of the estuary [Albuquerque *et al.* 2022].

6.3 Material and methods

6.3.1 Field sampling

Daily hydrographic and biogeochemical samplings and in situ experiments on pelagic metabolism were carried out at two stations, station (station) 1 (32◦01′24.6”S 52◦06′19.8”W) and station 2 (32◦08′04.5”S 52◦05′52.9”W), during 30 days of the late austral summer spanning from Feb-24 to Mar-23-2021 (Fig. 2). St. 1 is a channel-site with a depth of 4.5 m, located in a biogeochemical zone where organic matter remineralization is the dominant process [Windom *et al.* 1999]. This site is next to the city of Rio Grande, and subject to sewage on littoral areas. St. 2 is a deeper site (~ 12 m), located next to the bar jetties in the main Patos Lagoon Estuary access channel (Fig. 2d), where the biogeochemical zone is dominated by conservative mixing [Windom *et al.* 1999]. The mean depth of Patos Lagoon is about 5 m [Calliari *et al.* 1997], while 80% of the area in the southern estuarine region is <1.5 m [Seeliger 2001]. Being located next to Rio Grande Harbor, the area is subject to diffuse release of fertilizers by industries and harbor activities [Baumgarten *et al.* 1995; Wallner-Kersanach *et al.* 2015].

Water was collected with a Niskin bottle at surface (0.5 m), intermediate (only at station 2), and bottom (near-bottom depth) layers. The intermediate layer (average of 7 ± 2 m) was defined according to the halocline observed by multiparametric sonde. To avoid air interference with water properties, aliquots

from the Niskin bottle were first separated with a hose, avoiding bubble formation, in 100 mL borosilicate bottles for the determination of dissolved oxygen (immediately fixed with Winkler reagents). Then water for pH was sampled in 150 mL amber borosilicate bottles, while that for total alkalinity was sampled in a 500 mL borosilicate bottles and immediately fixed with mercury chloride [Dickson *et al.* 2007]. pH and total alkalinity were sampled only at the surface (for station 1 and 2) and bottom (station 2) layers. These samples were kept in a thermic box until analysis at the laboratory. Fourteen biochemical oxygen demand bottles for all depths were separated without Winkler reagents for the metabolism experiment. The remaining water in the Niskin bottle was separated into polycarbonate bottles for subsequent determination of photosynthetic pigments and the dissolved inorganic nutrients of nitrite, nitrate, ammonium, phosphate, and silicate, and stored in a thermal box with ice packs.

Water column current profiles were obtained from the Brazilian Coastal Monitoring System, [SiMCosta 2022; www.simcosta.furg.br]. Acoustic Doppler Current Profilers (ADCP) for their RS-1 (Aquadopp 5 Mhz) and RS-2 (Aquadopp Z-Cell 600 Khz) sites, exactly next to our stations 1 and 2, respectively. The cross-section water flow at station 2 was measured with a 1200-kHz ADCP RDI Workhorse with bottom track water velocities. The water column was profiled with a multiparametric sonde by JFE-Advantech model AAQ-Rinko 176 equipped with temperature, salinity, chl-*a* fluorescence, turbidity, dissolved oxygen, pH, colored dissolved organic matter and photosynthetically active radiation sensors.

The river discharge data for Jacuí, Taquarí, Caí, Sinos, and Camaquã rivers was obtained from Brazilian National Water Agency [ANA 2022; www.snirh.gov.br/hidroweb]. Water residence time for Patos Lagoon was estimated according to Dyer [1997], considering a lagoon volume of 58.5 × 106 m^3 [Fernandes *et al.* 2002]. The meteorological data was obtained from Rio Grande Port Pilotage [RG Pilots 2022; www.rgpilots.com.br]. Wind data (10 m above ground) were rotated to the main coastline orientation in relation to geographic north (32◦) to take the most energetic wind component that forces the estuary inflow/outflow conditions.

6.3.2 Sample processing

In the laboratory, dissolved oxygen was analyzed by the Winkler titration technique [Strickland & Parsons 1972]. Titration was per- formed with a Brand Digital Burette III, with an accuracy of 0.02% and a coefficient of variation of 0.01%. The pH was measured with a pH Meter (Metrohm 654) equipped with a thermometer (precision ±0.05 pH NBS units). Daily calibration was made with buffers (Mettler Toledo) of pH 4 and 7 at 25 °C. The pH was corrected by summing 0.0114 and then multiplying by the difference among the sample temperatures [Gieskes 1969], i.e., that taken during the pH Meter reading, minus those measured in the field. The resulting slope was 98%. Analysis for total alkalinity determination followed the potentiometric titration in a closed cell described by Dickson *et al.* [2007]. The titration was performed in an automated titrator (Metrohm® Titrando 808) with a combined glass-reference electrode (Metrohm® 6.0262.100) at a controlled temperature of 25 ± 0.1 °C sustained by a thermostatic bath (Tamson® TLC 15). Due to the high salinity range in the estuary (from 0 to ~33), an adaptation of the closed-cell method [Dickson *et al.* 2007] was adopted. Solutions of HCl (0.1 M) with NaCl backgrounds of different salinities were used as titrants to approximate the actual salinity of the samples. The precision of total alkalinity measurements (for salinity >19 = ±2.0 μmol kg^{-1} and salinity <19 = ±2.7 μmol kg^{-1}) was evaluated daily, throughout the analysis period, with replicate analysis of a single sample. A correction factor was applied to the measured values based on the readings of the certified reference material values (batch no. 177, acquired from Scripps Institution of Oceanography) and dilution of the sample by mercury chloride solution [Dickson *et al.* 2007].

Water samples were filtered with Whatman GF/F filters (0.70 μm of porosity) in low light conditions for the determination of photosynthetic pigments by High-Performance Liquid Chromatography (HPLC), according to Zapata *et al.* [2000]. The HPLC system was calibrated with pigment standards from the Institute for Water and Environment, Denmark (DHI). The filtered water samples were then used to determine the concentrations of dissolved inorganic nutrients (nitrite, nitrate, phosphate and silicate) by the spectrophotometry technique, in a SEAL Analytical AutoAnalyzer AA3 HR, according to Grasshoff *et al.* [2007]; and ammonium separately, according to Koroleff & Palmork [1972]. The detection

limits were 0.006 µM for nitrite, nitrate and ammonium, and 0.016 µM for silicate and phosphate.

6.3.3 Pelagic ecosystem metabolism

Pelagic ecosystem metabolism was estimated by in situ experiments through the oxygen-based bottles technique. The *in-situ* experiments were carried out daily (whenever possible) during the sampling campaign, and one day in each station due to field logistics, totaling eleven experiments at station 1 and nine at station 2 (experimental days at each station are provided in Table A.1). In the vessel, borosilicate bottles were disposed in replicate pairs, according to respective sampling depth and approximate observed photosynthetically active radiation, in transparent (100% of irradiance) and semitransparent plastic films of 50, 35 and 5% of irradiance, representing the vertical light attenuation in the water column. Samples were also put in replicate pairs in dark tubes to estimate R rates at each of the sampled depths. All tubes were kept in a transparent box filled with local water to keep the temperature constant until assembling the experiment on the pier. At the pier, the tubes were transferred to a wooden frame, tied on the pier, and put floating on the surface to keep flasks at the local water temperature. The incubation time was approximately 3 h, after which the frame was taken from the water and the Winkler reagents inserted into the borosilicate bottles. Net primary production (NPP) and R rates were then obtained by Eq. 13 and Eq. 14, respectively:

$$NPP = \left(DO_{fl} - DO_{il}\right)/Itime; \quad (13)$$

$$R = \left(DO_{fd} - DO_{id}\right)/Itime; \quad (14)$$

where DO_{fl} and DO_{il} are final and initial dissolved oxygen, respectively, considering the light ($_l$) bottles, while the subscript ($_d$) refers to the dark bottles, and *Itime* is the incubation time in hours. Final NPP and R rates are expressed in

mmol O_2 m^{-3} h^{-1}. To obtain the daily rates, NPP daily integration was obtained from the irradiance integration throughout the day (*Id*) and just during the experiment time (*Ie*), by the trapezoidal formula (*Id* and *Ie*, Eq. 15):

$$Id\ and\ Ie = \Sigma(T2 - T1) * \left(\frac{I1+I2}{2}\right) \quad (15)$$

where *Id* is the irradiance integrated for full daylight, *Ie* the irradiance integrated just during the experiment time, *T2* is time (seconds) in the second timestep, *T1* is time in the first timestep, *I* is irradiance (W m^{-2}) in the first (*I1*) and second (*I2*) timesteps.

From the integrated irradiances, NPP_{d12h} was estimated for the daylight period for each percentage of irradiance incident on the surface (*Is*), 100, 50, 35 and 5%, according to Eq. 16:

$$NPP_{d12h} = \left(\frac{NPP*I_d}{I_e}\right) * \left(\left(\frac{Is}{100}\right) * \%\right) \quad (16)$$

The depth corresponding to each irradiance was obtained from the vertical profiles of the photosynthetically active radiation probe. The R for each depth was also estimated by the daylight period by multiplying the rate by 12 h (R_{12h}), and for the entire day by multiplying by 24 h (R_{24h}). NPP and R rates were then vertically integrated by the trapezoidal method (see Eq. 4) until euphotic zone depth (NPP_{z12h} and R_{z12h}) for the daylight, also obtained from the photosynthetically active radiation probe. The GPP_{z12h} is the sum of NPP_{z12h} and R_{z12h}, only for the daylight period (12h) and euphotic zone. The R rates were also estimated for the bottom layer, i.e., from the euphotic zone depth to the estuarine floor, assuming the R rate of the deepest sample as constant along the rest of the water column. Finally, net pelagic ecosystem metabolism was obtained from Eq. 17:

$$PEM = GPP_{z12h} - (R_{z24h} + R_{b24h}) \quad (17)$$

where GPP_{z12h} is the gross primary production in the euphotic zone during the daylight, R_{z24h} and R_{b24h} are the R rates in the euphotic zone and in the bottom layer, respectively, for the entire day (24 h). The principles, details and uncertainties of the method can be found on Fahey & Knapp [2007]. To convert the rates from oxygen to carbon units, the primary production quotient of 1.2, and the respiratory coefficient of 0.85 were used [Almeida *et al.* 2005; Biddanda *et al.* 1994]. The coefficients of variation in the dissolved oxygen incubation replicates were < 0.01% (n = 280).

6.3.4 Phytoplanktonic community composition

To evaluate phytoplankton and metabolic rates, the main phytoplankton taxonomic groups were identified by pigment-based chemo- taxonomy where class-specific photosynthetic accessory pigments are estimated through HPLC. The pigments were extracted in the dark with 3 mL of 95% cold-buffered methanol (2% ammonium acetate) and analyzed using a Shimadzu® HPLC system, equipped with a solvent dispenser module (LC-20 CE), a system controller (CBM-20A), a refrigerated auto-sampler (SIL-20 AC), a photodiode array (SPDM20A), and a fluorescence detector (RF-10AXL). The gradient elution program used was slightly modified from that proposed by Zapata *et al.* [2000]. Further details of the HPLC method (using a monomeric C8 column with a pyridine-containing mobile phase) are described in Mendes *et al.* [2007]. The CHEMTAX matrix factorization software routine was used to determine phytoplankton community composition from HPLC pigment concentrations [Mackey *et al.* 1996]. The basis and procedures are fully described in Mendes *et al.* [2017]. Six algal groups were chosen for CHEMTAX analysis, based on identified diagnostic pigments and previous experience in the region [Mendes *et al.* 2017]. The groups resolved include diatoms, dinoflagellates, cryptophytes, prasinophytes, chlorophytes, and cyanobacteria.

6.3.5 Trophic status

The TRIX trophic index [Vollenweider *et al.* 1998] was applied to classify the trophic status and its relationship with the metabolic processes. The TRIX index was calculated by Eq. 18:

$$TRIX = [\log(chla * aD\% * O * N * P) - (a)] / b \quad (18)$$

where *chla* [mg m^{-3}] is the effect of nutritional conditions for phytoplankton growth; *aD%O* is dissolved oxygen as an absolute deviation of saturation [%], as way of measuring the balance between production and respiration; *N* is dissolved inorganic nitrogen N-(NO_3^{-2} + NO_2^{-3} + NH_4^{+}) [µg/L]; *P* is dissolved inorganic phosphorus as P-PO_4^{-3} [µg/L], and parameters *a* and *b* are scale coefficients used to fix the lower limit value of the index and the extension of the trophic scale from 0 to 10 TRIX units. Here, *a* and *b* were determined from the current dataset as: a = −0.8 and b = 0.78. The trophic classes were ultra-oligotrophic (0–2), oligotrophic (2.01–4), mesotrophic (4.01–6), eutrophic (6.01–8) and hyper-eutrophic (8.01–10) [Vollenweider *et al.* 1998].

6.3.6 Carbonate system variables and water-air net CO_2 fluxes

The total inorganic carbon and water CO_2 partial pressure (pCO_2) was computed through the CO_2Sys V2.1 Microsoft Excel program [Pierrot *et al.* 2006; Lewis & Wallace 1998], using hydrostatic pressure, temperature, salinity, TA, and pH as input parameters. The dissociation constants of carbonic acid from Millero *et al.* [2006] were chose because they are indicated for the salinity range of 0 to 35. Sulfate and borate constants were those reported by Dickson [1990] and Uppstrom [1974], respectively. Uncertainties of the derived carbonate variables were computed according to the propagation error routines proposed by Orr *et al.* [2018] and were ± 22 µmol kg^{-1} for total inorganic carbon and 45 µatm for pCO_2. The water–air net CO_2 flux (FCO_2) was calculated following Borges *et al.* [2004], with the CO_2 constant of solubility from Weiss [1974], which is proper for estuarine waters with high wind and current velocities. The wind velocity ranged

from 1.3 to 10.7 m s^{-1} (5.0 ± 2.3) during the study period, while the current velocity ranged from 4.7 to 152.5 cm s−1 (45.4 ± 38.5). The pCO_2 in the atmosphere used in the calculation was 412.3 ppm and was obtained from the Ocean Carbon and Acidification Portal website [OCADS 2022; www.ncei.noaa.gov/access/ocean-carbon-data-system].

6.3.7 Statistical analysis

Kruskal Wallis analysis of variance [KW - Dodge 2008] was performed for each variable to test differences between means (α = 0.05) of the two stations and among means of the layers of the two stations. A principal component analysis (PCA) was performed on normalized variables to extract variance among samples based on metabolic rates GPP, R, and the abiotic factors of temperature, salinity, dissolved oxygen, chl-*a*, turbidity, pH, photosynthetically active radiation, dissolved inorganic nitrogen (DIN: nitrite + nitrate + ammonium), phosphate and silicate. Generalized additive models (GAM) were performed to model the response variables GPP and R to the predictor abiotic variables, extracting the main forcing factors that drive metabolic rates [Wood 2018]. The best model was chosen by explanatory percentage, residuals, and lower Akaike's Information Criterion [AIC – Akaike 1974]. Boxcox transformations were used when necessary to fulfill parametric premises. Uncertainties were evaluated from the model standard error (SE). Otherwise, to visualize the ordination of the metabolic rates GPP and R as response variables against the constraining biotic variables, i.e. the phytoplankton groups, a redundancy analysis (RDA) [Legendre & Anderson 1999] was performed, in which the best set of constraining variables was chosen according to their significances (α < 0.05) and by AIC to verify differences among models. All statistical analyses were performed in R software [R Core Team 2022].

6.4 Results

6.4.1 Meteoceanographic conditions

Total river discharge of the main tributaries of the Patos Lagoon for the eight months preceding the sampling period varied from 32.3 to >5000 $m^3\ s^{-1}$ (931 ± 904 $m^3\ s^{-1}$; Fig. 3a) [ANA 2022]. The lowest water residence time for the lagoon was 99.6 days on Sep-15-2020, and the maximum was 20,937 days on Dec-30-2020 (1567 ± 2231 days). Drought conditions were observed during the austral summer of 2021, with a minimum water residence time of 279 days (Fig. 4a). The wind timeseries showed the alternance between SW and NE winds during the sampling campaign (Fig. 4b), and predominance of SW winds with maximum intensity of 13.0 m s^{-1} on Mar-21. The SW winds (positive values, Fig. 4b) promote the predominance of coastal water inflow into the estuary (negative values, Fig. 4c). The Pearson's correlation was 0.55, with *p-value* (p) < 0.01, between meridional wind speed and water flow rate. The mean water flow rate during the outflow periods was 5200 $m^3\ s^{-1}$, reaching up to 9900 $m^3\ s^{-1}$, while during seawater inflow the averaged rate decreased to 2800 $m^3\ s^{-1}$ and did not exceed 6000 $m^3\ s^{-1}$.

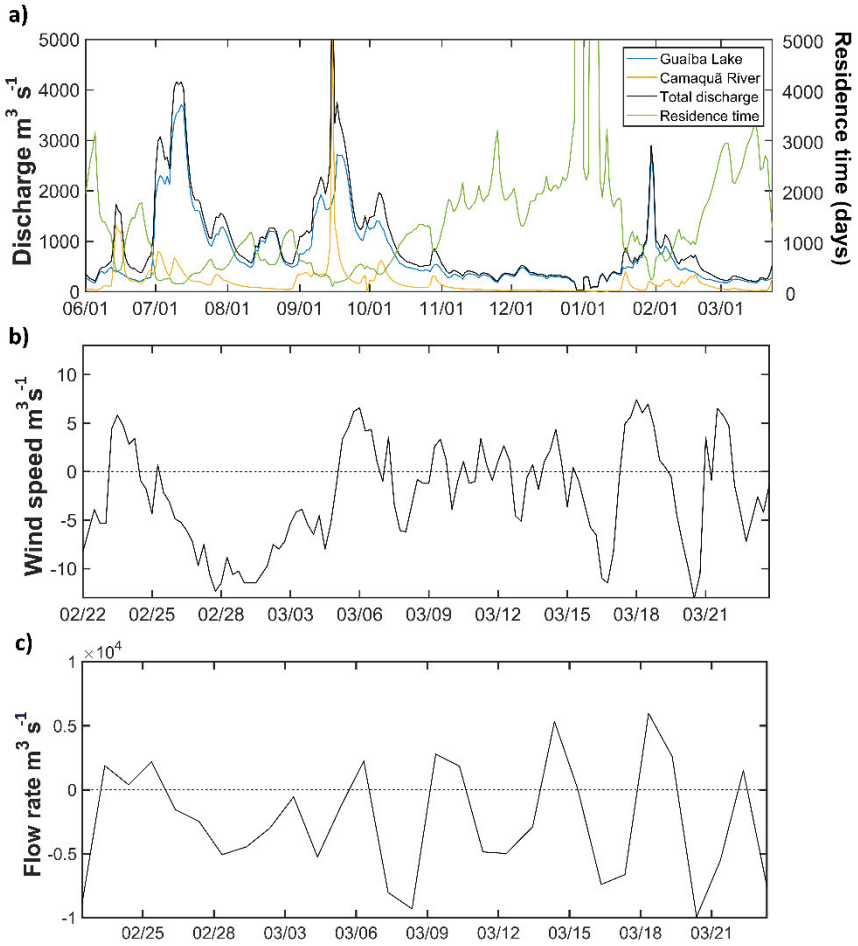

Figure 4. a) Guaíba and Camaquã rivers and Total Flow rates (m^3 s^{-1}), and Patos Lagoon water residence time (days) from Jun-01–2020 to Mar-23–2021. b) Meridional wind speed (m s^{-1}) from Feb-22-2021 to Mar-23–2021. Positive values indicate winds from NE, and negative from SW. c) Flow rate (m^3 s^{-1}) timeseries on the channel cross section (next to station 2). Positive values indicate outflow and negative values indicate inflow conditions.

Despite the higher intensity of water outflow during the sampling period promoted by the NE winds, the estuary was mainly dominated by euryhaline conditions at station 2 (closer to the estuary mouth), with an average salinity of 25.9 ± 9.2. This condition was also observed at station 1, with an averaged salinity of 20.7 ± 11.3. Thus, confirming the dominance of seawater intrusions with salinities >20 into the Patos Lagoon Estuary most of the time (Fig. 5a). The minimum salinity observed in the study region was 5.2 (on Mar-02) at the surface of station 1, which coincided with NE winds on the previous days (Fig. 5b). The maximum salinity was 33.6 at the bottom at station 2 (Tab. A.2). On Mar-04, the surface salinity at station 2 was 6.4, evidencing strong vertical stratification

(vertical amplitude of 27.2) with a salt wedge entering the estuary at the bottom. On the other hand, the haline vertical amplitude was lower (≤ 10) at station 1.

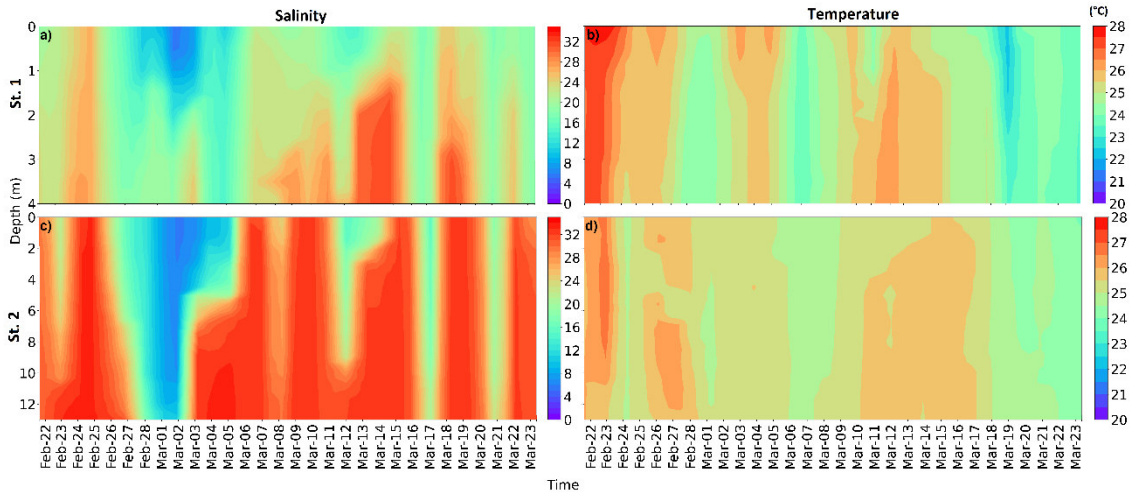

Figure 5. HovMöller plots for temporal and spatial salinity and temperature (°C) profiles for station 1 (5a and 5b) and station 2 (5c and 5d), in the Patos Lagoon Estuary from Feb-22-2021 to Mar-23–2021 (late austral summer).

The temperature vertical profile showed both stations as vertically homogenized (Fig. 5). The minimum (23.45 °C) and maximum (27.67 °C) water temperatures were observed at station 1 (Fig. 5b), while higher mean temperature occurred at station 2 (Fig. 5d) for the entire water column. The higher temperature variability at station 1 *vs*. station 2 is evident by the higher deviations from the mean (Tab. A.2).

Euphotic zone depth was greater at station 2 with an average of 3.8 ± 1.5 m, and a maximum of 6.7 m (Feb-27). The average at station 1 was 2.7 ± 1.3 m, with a maximum of 5 m (Feb-26). Euphotic zone depth decreased at both stations from Mar-01 to Mar-10, maintaining values < 2 and < 4 m at station 1 and 2, respectively, subsequently increasing until Mar-15 at both stations, then decreasing to low values until the end of the sampling campaign.

6.4.2 Pelagic ecosystem metabolism

Pelagic ecosystem metabolism was mostly heterotrophic throughout the entire month (Fig. 6), at both stations (station 1: −132.7 ± 109.7; station 2: −402.9 ± 185.7 mmol O_2 m^{-2} d^{-1}). The most heterotrophic condition at station 1 occurred

at the end of February (−383.0 mmol O_2 m^{-2} d^{-1}) while that for station 2 was at the beginning of the sampling campaign (−784.3 mmol O_2 m^{-2} d^{-1}). On Mar-17 (station 1) and Mar-18 (station 2), GPP rates were 30.0 and 10.5 mmol O_2 m^{-2} d^{-1} and R rates were 10.4 and 73.4 mmol O_2 m^{-2} d^{-1}, respectively. These were the minimum GPP and R rates observed, which led to the only autotrophic episode at station 1, and the least heterotrophic condition at station 2 (10.6; −62.9 mmol O_2 m^{-2} d^{-1}, respectively). Overall, both GPP and R rates decreased over-time. Only pelagic ecosystem metabolism and R rates differed significantly between stations (KW: pelagic ecosystem metabolism and R $p < 0.05$). The averaged NPP was 16.4 ± 12.5 mmol O_2 m^{-2} d^{-1} at station 1 and 25.9 ± 28.7 mmol O_2 m^{-2} d^{-1} at station 2 during the entire period.

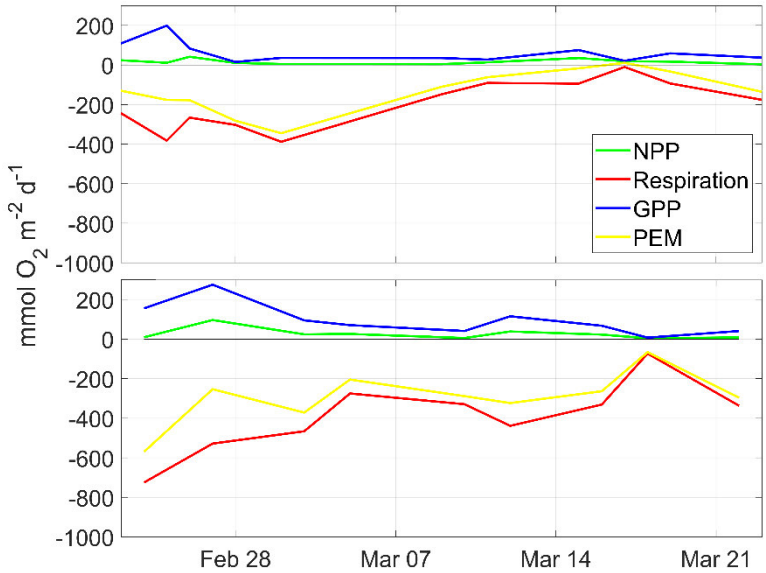

Figure 6. Time series of the metabolic rates gross primary production (GPP), net pelagic production (NPP), respiration and net pelagic ecosystem metabolism (PEM) in mmol O_2 m^{-2} d^{-1}, for station 1 (upper) and station 2 (bottom) in the Patos Lagoon Estuary from Feb-24-2021 to Mar-23–2021 (late austral summer). Negative PEM values indicate net heterotrophy. Respiration values are always negative.

6.4.3 Dissolved inorganic nutrients, dissolved oxygen and TRIX trophic status

Silicate was the only nutrient that presented a significative difference in concentration among layers and between stations, with higher silicate in the surface of station 1. Regarding nutrient concentration between stations, in general, only nitrite and nitrate were higher at the surface of station 2, while nitrate, ammonium, phosphate and silicate were higher at the bottom of station

1. The TRIX trophic index indicated that both stations were mostly mesotrophic (overall: 5.4 ± 1.0) during 58% of the period. TRIX was higher at the bottom at both stations. Considering the entire water column, a higher average (KW $p < 0.05$) was found at station 1, with a mean index of 5.8 ± 1.2, versus 5.2 ± 0.8 at station 2 (Tab. A.3). St. 2 had a higher frequency of the mesotrophic state (60%) — respective to these mean values (both between 4.0 and 6.0) — compared to station 1 (only 51%). On the other hand, the eutrophic condition was mostly observed at station 1, where the frequency was about twofold (39%) that at station 2 (23%). Specific descriptive statistics and KW differences among layers and between stations for dissolved inorganic nutrients, dissolved oxygen, dissolved oxygen saturation and the TRIX trophic index can be seen in Table A.3 and Figures. A.4 to A.7.

6.4.4 Phytoplankton community composition

A total of 17 phytoplankton pigments were identified: chl-*a*, chl-*b*, chl-*c1*, chl-*c2*, peridinin, Mg DVP, fucoxanthin, neoxanthin, prasinoxanthin, violaxanthin, diadinoxanthin, alloxanthin, diatoxanthin, zeaxanthin, lutein, a-carotene, and ß-carotene. The concentration of chl-*a* ranged from 1.05 to 20.1 µg/L during the studied period (Fig. 7). The averaged chl-*a* concentration at station 1 was 5.8 ± 2.7 µg/L, which was approximately twofold higher than the 2.7 ± 2.4 µg/L at station 2 (KW $p < 0.01$).

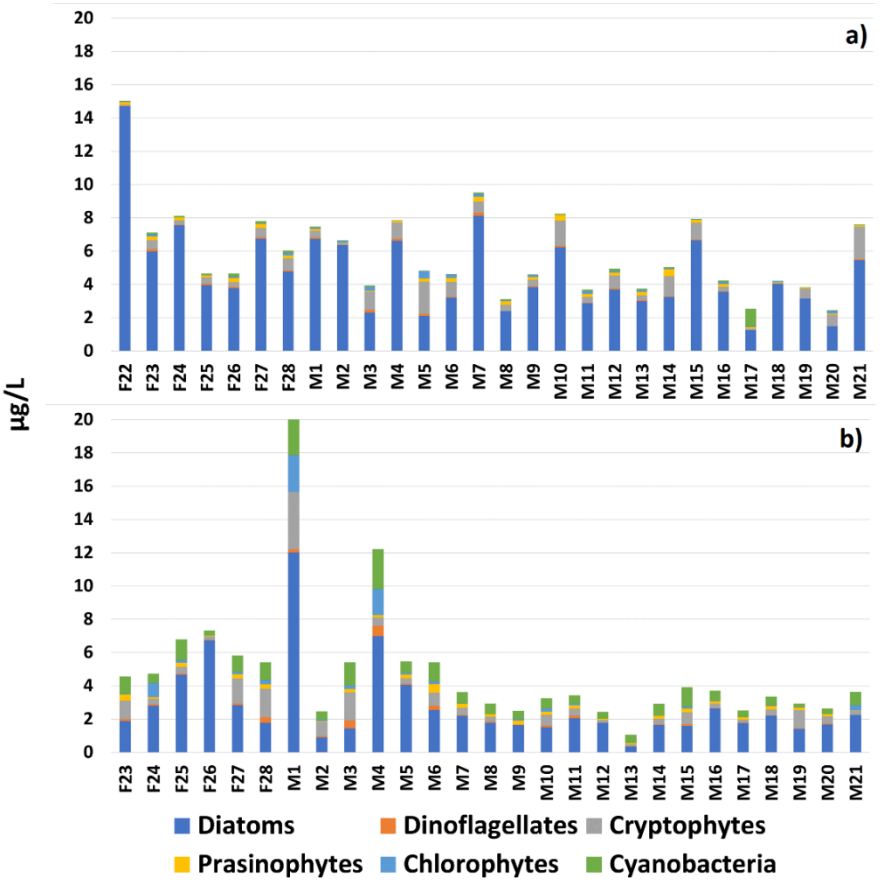

Figure 7. Daily biomass contribution of phytoplankton groups at the surface (the complete bar corresponds to total chl-a concentration) during late austral summer. The results were calculated by CHEMTAX application at (a) station 1 and (b) station 2 in the Patos Lagoon Estuary from Feb-23–2021 (F23) to Mar-21–2021 (M21).

Diatoms was the dominant phytoplankton group at both stations (Fig. 7) throughout the sampling period, with an averaged percentage for all groups considered of 78.3 ± 13.3% at station 1 and 56.2 ± 15.0% at station 2 (Fig. A.1). Cryptophytes was the second dominant group at station 1, with an averaged contribution of 12.3 ± 9.8%, while cyanobacteria was such at station 2 with an averaged contribution of 18.8 ± 7.6%. However, cryptophytes was also representative as a secondary group at station 2, with an averaged contribution of 14.6 ± 10.1%.

6.4.5 Carbonate system variables and water-air net CO_2 fluxes

Both stations had a pH of 7.9 ± 0.2, with no significant differences between stations and among layers (Tab. A.4). However, TA, total inorganic carbon, pCO_2

and FCO_2 did differ significantly between sites and among layers. There was evident salinity and depth influence on the spatial distribution of total alkalinity and total inorganic carbon (Fig. A.2). The pCO_2 ranged from 169.5 (station 1) to 1173.9 µatm (station 2) at both stations. Higher values did not exceed 612.5 µatm at station 2, thus, leading to a lower mean value (284.7 µatm) than at station 1 (450.3 µatm). The CO_2 outgassing behavior prevailed at station 1, with an averaged FCO_2 of 4.4 ± 41.2 mmol C m^{-2} d^{-1}, while at the station 2 the CO_2 ingassing behavior prevailed, with an averaged FCO_2 of −15.4 ± 17.3 mmol C m^{-2} d^{-1} (Fig. A.5 and A.7). However, when looking at the frequency, behavior as net CO_2 sink from the atmosphere prevailed at both stations, during 70.5% (station 1) and 95.4% (station 2) of the time (medians, station1: −9.8; station 2: −17.0 mmol C m^{-2} d^{-1}). Lower FCO_2 values were similar at both stations (station 1: −42.5; station 2: −38.9 mmol C m^{-2} d^{-1}). Specific descriptive statistics and KW differences between stations and among layers for all carbonate system parameters can be seen in the Table A.4.

6.4.6 Factors drivinging metabolism

6.4.6.1 Abiotic factors

The metabolic rates GPP, NPP and R, were positively colinear, therefore, only GPP was included in the PCA (Fig. 8a). GPP rates were mainly positively related to photosynthetically active radiation, but limited by higher turbidity, mainly at the bottom. Water flow rate was modulated by wind direction, which induced the outflow of fresher, phosphate and silicate (DIN) poor (rich) waters. The wind-induced inflow of marine salty waters into the estuary was associated with higher turbidity and concentrations of silicate, phosphate and chl-*a*. The opposition of GPP against silicate and phosphate, indicates its removal by phytoplankton assimilation in the euphotic zone. On the other hand, the short phosphate vector in relation to DIN and silicate, suggests that primary production was limited by nitrogen (low N:P ratio, mean of 3.10 ± 2.0, and median of 2.5).

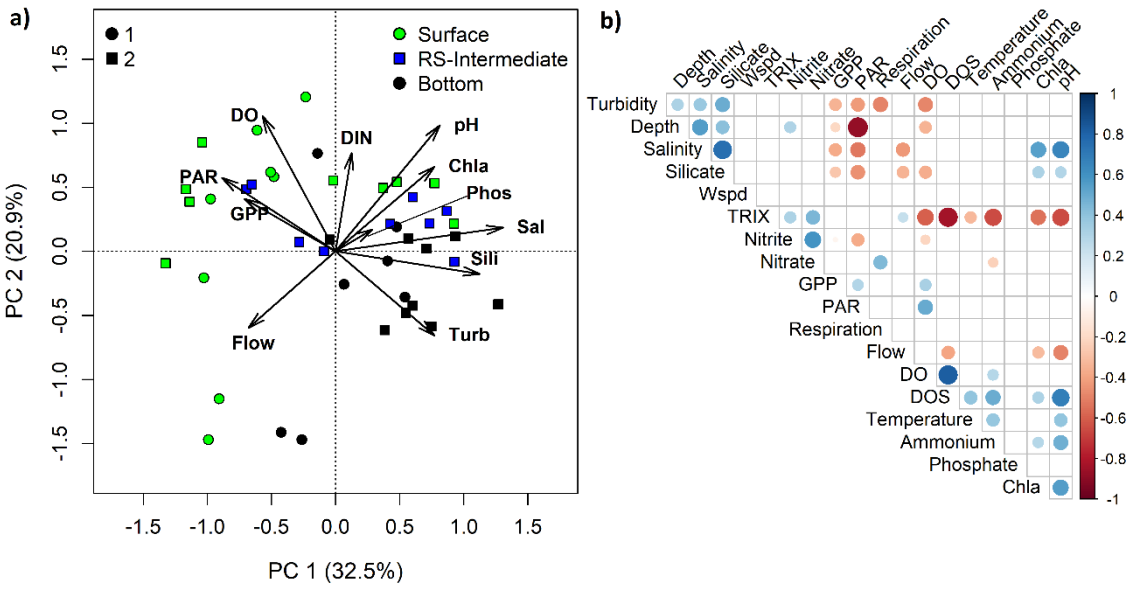

Figure 8. a) Principal component analysis of the main variables of gross primary production (GPP), respiration (R) salinity (Sal.), temperature (Temp.), pH, dissolved oxygen (DO), photosynthetically active radiation (PAR), water flow rate (Flow), turbidity (Turb.), chlorophyll-a (chla), dissolved inorganic nitrogen (DIN), phosphate (Phos) and silicate (Sili.), at station 1 and station 2 in the Patos Lagoon Estuary from Feb-24-2021 to Mar-23–2021 (late austral summer). Circles represent samples from station 1 and squares from station 2. Green symbols represent surface samples, blue intermediate (only station 2), and black bottom layer samples. b) Pearson's correlation matrix of the main variables, as in a). Only significant correlations are presented in the graph ($p < 0.05$). Positive correlations are indicated by blue circles, and negative by red circles. Colour intensity represents the strength of the correlation from 0 to 1 for positive, and 0 to −1 for negative correlations. Other abbreviations not present in Fig. 6a are dissolved oxygen saturation (DOS) and wind speed (Wspd). Sample n = 46.

The set of GAM independent variables that best describe GPP were, in order of significance, nitrate, salinity, chl-*a*, wind speed and direction and flow rate ($p < 0.01$), explaining up to 95.3% of the deviance, with an R^2 of 0.88 (Tab. A.5). Silicate concentration and turbidity were also important driving factors ($p < 0.05$). Of the remaining variables, only wind speed expressed a significant influence on the primary production processes. It is important to note that p was only significant (< 0.01) for the bottom (represented by the intercept) and intermediate layers, suggesting that other sources of non-sampled environmental variability are driving GPP at the surface. For R rate as the dependent variable (Tab. A.6), the best set of descriptive variables were, in decreasing order of significance, photosynthetically active radiation, nitrate, temperature, chl-*a*, wind

speed and phosphate. Different than for GPP as the independent variable, water flow rate was not significant.

6.4.6.2 *Biotic factors (phytoplankton groups)*

The most significant set of independent variables, was that considering all phytoplankton groups, i.e., diatoms, cryptophytes, cyanobacteria, chlorophytes, dinoflagellates and prasinophytes. Between them, diatoms had highly significant ($p < 0.01$) influence on GPP and R rates (Fig. 9). The pattern of abundant phytoplankton groups was clear in the RDA with the spatial grouping mainly separated by cryptophytes (cyanobacteria) at station 1 (2), while diatoms remained the dominant group at both stations (Fig. 9). Most of the variability was explained by RDA component 1 (RDA 1), which divided the samples between stations. Despite the predominance of diatoms, the samples of Mar-11 pulled the GPP next to cryptophytes and prasinophytes, exactly on the day of highest GPP. The R rate was more related to RDA component 2 (RDA 2), and was clearly influenced by cyanobacteria, dinoflagellates and chlorophytes, whose rates and group biomasses were justly the highest on the sample of Feb-23, Feb-24, Mar-03 and Mar-05 (Fig. 9).

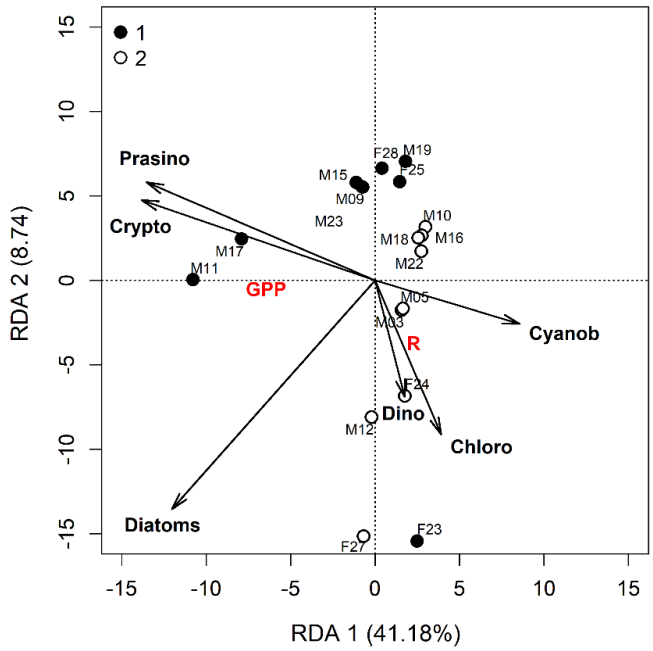

Figure 9. Redundancy analysis (RDA) of the metabolic rates of gross primary production (GPP) and respiration (R) as dependent variables (red font), and as independent variables (black font) the taxonomic phytoplankton groups di- atoms, dinoflagellates (Dino), chlorophytes (Chloro), cryptophytes (Crypto), cyanobacteria (Cyanob) and

prasinophytes (Prasino). Surface layer samples from station 1(filled circles) and station 2 (open circles) of the Patos Lagoon Estuary from Feb-24-2021 to Mar-23–2021 (late austral summer). Aside the circles, F and M represent February and March samples, while the number represents the day of sampling. Samples n = 18.

6.5 Discussion

6.5.1 Metabolic rates

Pelagic ecosystem metabolism was mainly net heterotrophic at both channel-sites (stations) during the late austral summer of 2021 (Fig. 6). The mean pelagic ecosystem metabolism for the two studied stations was −205.5 ± 143.2 mmol O_2 m^{-2} d^{-1}, of which 78.0 ± 67.0 mmol O_2 m^{-2} d^{-1} is GPP and 285.0 ± 177.6 mmol O_2 m^{-2} d^{-1} is R. Spatial differences between the shallow (station1) and deeper (station 2) areas can be determined by comparing the metabolic rates of the two stations, indicating that compensation depth is similar at the two stations. However, R rate was higher at station 2, mainly due to the greater depth providing more available area for the R process. Secondly, euphotic zone depth is more likely to reach the bottom at station 1, as was observed three times during the studied days, wherein GPP can exceed R. A similar pattern was observed by Kemp *et al.* [1997] at the Chesapeake Bay Estuary, with net autotrophy around shallow littoral areas, and net heterotrophy in channels. The higher metabolism at deeper sites is fueled by the high phytoplankton biomass produced in, and imported from, shallow areas, as observed in other estuaries worldwide [Cloern *et al.* 2014; Bukaveckas *et al.* 2011; Kemp *et al.* 1997]. Therefore, in even shallower areas at the Patos Lagoon Estuary — as in the vast shoals and bights — it is likely for the metabolism to be autotrophic [Abreu *et al.* 1994, 1995].

Although Abreu *et al.* [1994] did not report R rates and net metabolism, they concluded that shoal areas of the Patos Lagoon Estuary are mainly autotrophic during the austral summer season. The heterotrophic condition was mostly attributed to high water turbidity and depth because high turbidity prevents the euphotic zone from reaching the bottom, whereas Abreu *et al.* [1994; 1995] experimented in a shallow area (~ 0.5 m). When comparing the mean daily NPP rate of 21.2 ± 20.6 mmol O_2 m^{-2} d^{-1} with that obtained by Abreu *et al.* [1994] (0.04 mmol O_2 m^{-2} d^{-1}) by the 14C technique and the acidification-bubbling method, we observed a higher value, but at a depth 9- (station 1) to 14-fold (station 2)

greater in the present study. However, when the comparison is made with rates by volume and hourly, i.e., before daily and vertical integration, we reach similar results, with a mean of 2.3 and maximum of 13.2 mmol O_2 m^3 h^{-1} (station 1), versus the 2.0 and 11.1 mmol O_2 m^3 h^{-1} of Abreu *et al.* [1994], respectively.

The GPP and R rates of the Patos Lagoon Estuary in late austral summer, however, were higher in comparison to the Brazilian sub- tropical estuary of Babitonga Bay [Parizzi *et al.* 2016] — a much smaller estuary than the Patos Lagoon Estuary (160 *vs.* 10,000 km^2, respectively). Different from the Patos Lagoon Estuary, the Babitonga Bay is influenced by the rainy season in the spring-summer, while in winter- spring the hydrodynamics is mainly controlled by tides. The mean depth of both estuaries is ~6 m. Comparing the results of station 1 with a similar depth in Babitonga Bay, Parizzi *et al.* [2016] found a monthly-averaged GPP of 67.68 mmol O_2 m^{-2} d^{-1} and a R of 38.80 mmol O_2 m^{-2} d^{-1}, while in present study found 101.32 mmol O_2 m^{-2} d^{-1} for GPP and 298.81 mmol O_2 m^{-2} d^{-1} for R. As can be noted, both, but mainly R, were much higher for Patos Lagoon Estuary than for Babitonga Bay. Net pelagic ecosystem metabolism was not provided by the authors.

Carmouze *et al.* [1991] estimated the entire aquatic ecosystem metabolism (including the benthos) in two sub-systems of the Saquarema Lagoon (Urussanga and Fora), Brazil, by the Open Water Method [Odum 1956], although much smaller in area (only 24 km^2), shallower (mean 1.15 m) and eutrophicated than the Patos Lagoon Estuary. Different from the present study, they found mainly net autotrophy, with few net heterotrophic episodes during February and March, possibly due to the shallower studied areas. Both GPP and R rates reached up to ~200 mmol O_2 m^{-2} d^{-1}, with net ecosystem metabolism ranging from −68.0 to 83.33 mmol O_2 m^{-2} d^{-1}. Due the inclusion of benthic metabolism, care should be taken when comparing the results. Bordin *et al.* [2023b] estimated the entire aquatic ecosystem metabolism for station 1 of Patos Lagoon Estuary through the Open Water Method using monthly data from 2016 to 2021. Their rates are close to those reported here, although they did not find conditions of net autotrophy, which is likely due to the benthic contribution to R rates. Considering their rates for the months of February and March from 2016 to 2021, the authors found a mean net heterotrophic condition of −168.60 mmol O_2

m^{-2} d^{-1}, of which 80.71 mmol O_2 m^{-2} d^{-1} was GPP and 250.93 mmol O_2 m^{-2} d^{-1} was R.

Murrell *et al.* [2018] studied the entire aquatic ecosystem metabolism by the same method as Carmouze *et al.* [1991] for the Pensacola Bay Estuary, U.S. (at the Gulf of Mexico coast), with one station in a shallow seagrass dominated site, and another in a bare-bottomed channel site. As for the Patos Lagoon Estuary, this is a subtropical estuary where its margins are dominated by seagrass, although there are some remarkable differences, since the Pensacola Bay Estuary presented many net autotrophic periods, even in the deeper channel site. Their boreal spring period was drier, like studied austral summer period of the present study, when their mean pelagic ecosystem metabolism approximated a neutral condition (16.9 mmol O_2 m^{-2} d^{-1}), presenting some net heterotrophic periods, mainly when considering the entire ecosystem. The boreal spring mean net pelagic ecosystem metabolism in their 6 m channel site was −3.3 mmol O_2 m^{-2} d^{-1}, caused mainly by the intensive benthic R of −36.70 mmol O_2 m^{-2} d^{-1}, ~32% of the total ecosystem, while benthic GPP represented only about 14% (15.7 mmol O_2 m^{-2} d^{-1}). In opposition to the Pensacola Bay Estuary, three other subtropical estuaries along the Gulf of Mexico coast showed net heterotrophy most of the year, with neutral or slightly net autotrophy just in the boreal winter [Caffrey *et al.* 2014]. The metabolic rates of these and other estuaries can be seen in Table 1.

Table 1. Summary of the metabolic rates of gross primary production (GPP), respiration (R), net primary production (NPP) and net ecosystem metabolism (NEM), of summer season or other depending on the rainy season and/or polyhaline zones (averaged values when needed and possible) for different world estuarine systems. The asterisk "*" in the references indicates the method considers the entire ecosystem metabolism, instead of just the pelagic. When needed, units were standardized in mmol O_2 m^{-2} d^{-1}, by the same photosynthetic coefficient and respiration quotient applied in the present work, and/or divided/multiplied by 12 (carbon atomic mass) to transform from mg to mmol O_2. Values presented in this study represent mean values (± standard deviation) for station 1 and station 2 in the Patos Lagoon Estuary from February-24-2021 to March-23-2021 (late austral summer).

Estuary	GPP	R	NPP	NEM	Season	Reference
Patos Lagoon (1), BR	63.1± 53.4	199.8 ± 126.1	16.5 ± 12.5	-135.4 ± 111.9	Summer	This study
Patos Lagoon (2), BR	96.2 ± 80	389.2 ± 181.2	25.9 ± 28.7	-291.1 ± 134.1	Summer	This study
Patos Lagoon (both), BR	78.0 ± 67.0	285.0 ± 177.6	21.2 ± 20.6	-205.4 ± 143.1	Summer	This Study
Patos Lagoon (1), BR	80.7 ± 50.0	250.9 ± 139.7	-	-168.6 ± 145.8	Annual	Bordin *et al.* [2023b]*
Patos Lagoon, BR	-	-	0.04 ± 0.04	-	Annual	Abreu *et al.* [1994]
Babitonga Bay, BR	67.7	38.8	-	-	Spr+Su	Pazzini *et al.* [2016]
Saquarema Lagoon, BR	14.6	13.8	-	1	Annual	Carmouze *et al.* [1991]*
Pensacola Bay, US	93.3 ± 13.7	76.5 ± 6.8	-	17.2 ± 11.9	Summer	Murrel *et al.* [2018]
Grand Bay, US	138.9	159.9	-	-	Annual	Caffrey *et al.* [2014]*
Apalachicola, US	225	224.9	-	-	Annual	Caffrey *et al.* [2014]*
Weeks Bay, US	300	375.0	-	-	Annual	Caffrey *et al.* [2014]*
Chesapeake Bay, US	491.9	471.7	-	34.5	Annual	Kemp *et al.* [1997]*
Urdaibai, ES	199.7	45.4	-	-	Summer	Iriarte *et al.* [1996]
Douro, PT	~35	~70	-	~-35	Annual	Azevedo *et al.* [2006]

Finally, it is important to keep in mind that the metabolic rates presented here are representative for the channel-sites of the Patos Lagoon Estuary, where the trophic status is distinct from the shallow and coastal areas, where sewage is released [Marreto *et al.* 2017], and where the euphotic zone reaches the bottom often and easier, resulting in different vertically integrated GPP and R rates, as well as net pelagic ecosystem metabolism [e.g., Abreu *et al.* 1994; 1995]. The oxygen-based bottle experiments limit the estimates to the water column only, neglecting the benthos contribution, and includes “bottle effects” introduced by sample confinement in a limited volume [Gieskes *et al.* 1979]. However, according to the GAM models, the uncertainties were quantified as being very small, with a standard error for GPP of <0.3% and for R of <0.1%.

6.5.2 Abiotic factors driving metabolism

Starting from the main limiting factors that control primary production, the availability of light and dissolved inorganic nutrients are the most important [Valiela 2015], as observed here by the co-limitation of DIN concentration and light availably (Fig. 8). During the sampling campaign, the dominant freshwater flow (from Feb-27 to Mar-03, Fig. 7) was not associated with significantly higher turbidity, suggesting autochthonous sources of materials into the water column. According to Niencheski *et al.* [1994], the suspended particulate matter in the Patos Lagoon Estuary is mainly from resuspension caused by wind-induced turbulence, increasing its concentration towards the estuary mouth when southerly winds promote the entrance of saltwater and consequently resuspends material from the bottom. The more intense and frequent SW winds caused the entrance of shelf (sometimes turbid, depending on the circumstances) waters into the estuary, in which a bottom salt-wedge intrusion caused resuspension of benthic material, contributing to the elevated turbidity (Fig. 8a). This trend was corroborated by the cross-section flow rate, determined next to station 2 (Fig. 4), that coincides with the highest turbidity, as already observed in the vicinities of the mouth of the Patos Lagoon Estuary [Hartmann & Schettini 1991; Niencheski *et al.* 1994, 1996; Ávila *et al.* 2021], as well as in other estuaries [McSweeney *et al.* 2017]. Both, GPP and R variability seems to be associated with this trend, evidenced by the negative correlation of both metabolic rates with turbidity (Fig.

8). The relationship between estuarine hydrodynamics, suspended material and turbidity in the Patos Lagoon Estuary (Ávila *et al.* 2021] and other estuaries [McSweeney *et al.* 2017], has already been established, as well as its effects on water column light attenuation [Kirk 2003] and consequently limitation on primary production [Murrell *et al.* 2018].

The silicate association with salinity was attributed to the shelf turbid waters and sediment resuspension by the salt-wedge intrusion. Even though the other nutrients do not correlate with turbidity and salinity, they presented higher concentrations at station 2 at the bottom (nitrite, nitrate and phosphate); it is likely that the origin is bottom resuspension [Abreu *et al.* 2010; They *et al.* 2019]. Another possibility could be due to the entrance of nutrient-rich salt/brackish water resulting from the exportation of nutrient-rich freshwater that mixes with saltwater and re-enters the estuary, as hypothesized by Abreu *et al.* [1995]. Moreover, it is possible that the coastal water intrusion is composed of a mixture of the Subtropical Shelf Water and the turbid and nutrient-rich (mainly phosphate and silicate) Plata Plume Water [Braga *et al.* 2008], which is pushed northward during southerly winds and may dominate the Southern Brazilian Continental Shelf [Piola *et al.* 2005; Möller *et al.* 2008]. Saltier than the Patos Lagoon Estuary brackish waters, the mixture of Plata Plume Water (salinity ≤ 33.5) and Subtropical Shelf Water (35.3 < salinity < 36) [Möller *et al.* 2008], characterized here by salinity ≤34, phosphate around 1.5 µM and silicate around 40 µM, could have caused the bottom resuspension in the mentioned events, contributing with its turbidity and nutrients content. The salinity, phosphate and silicate concentrations observed during the inflow periods are in accordance with that characteristic of the Plata Plume Water for the austral summer season on the southern continental shelf of Brazil [Möller *et al.* 2008; Braga *et al.* 2008; Bordin *et al.* 2019]. Therefore, we attribute the main content of dissolved inorganic nutrients (phosphate and silicate) to be from the Plata Plume Water that enters the estuary forced by southerly winds, and by the remineralization of the organic matter (ammonium and nitrate) produced by phytoplankton blooms during the nutrient-rich rainy spring season. Conversely, it is likely that the inverse relation of silicate with GPP occurred due to the co-variation of this nutrient with turbidity — mainly in the bottom at station 2 — which caused light-limitation for primary

producers (Fig. 8), evidencing another possible effect of the Plata Plume Water intrusion into the Patos Lagoon Estuary during the late austral summer of 2021.

Besides light-limitation, primary production is also potentially limited by nitrogen availability (Fig. 8) [Abreu *et al.* 1994], by nitrate as the most significant variable identified in the GAM models (Table A.5), and by the Redfield ratios N:P < 16 and N:Si < 1 (N:P = 4.84 ± 2.99; N: Si = 0.07 ± 0.05), as observed in other studies [Abreu *et al.* 1994; Proença *et al.* 1994]. The low nitrate is attributed to low continental runoff and low dissolved oxygen, which prevent/reduce the nitrification [Niencheski *et al.* 2006] of the exceeding ammonium concentrations (Tab. A.3) during the austral summer [Niencheski & Windom 1994; Fujita *et al.* 2004]. This is caused by the greater residence time characteristic of drought [Baumgarten *et al.* 1995] summer [Abreu *et al.* 1994] and La Niña periods [Abreu *et al.* 2010; Haraguichi *et al.* 2015], which hampers the exportation of the sewage of the city of Rio Grande, as happens in other estuaries under similar conditions [Wang *et al.* 2004]. Moreover, the high ammonium during this season at the Patos Lagoon Estuary is also due to elevated pelagic [Jesus & Odebrecht 2001] and benthic [Bemvenuti 2012] herbivore activity, which in-creases its mineralization. Besides the Patos Lagoon Estuary [Abreu *et al.* 1994], nitrogen limitation during dry periods also occurs in other estuaries [Murrell *et al.* 2007].

Regarding the R driving factors, the trend observed by the most significant variables included in the four best GAM models could be due to some reasons: lower temperatures towards March, which decreases bacterial activity, as observed in the Patos Lagoon Estuary [Abreu *et al.* 1994] and other estuaries [Carmouze *et al.* 1991; Apple *et al.* 2008]. The inclusion of photosynthetically active radiation and turbidity can be related to the greater R rates for the bottom layer at station 2, where turbidity was higher and radiation lower (Fig. 8). Furthermore, the salt-wedge bottom intrusion may also resuspend organic substrates, such as benthic algae [Abreu *et al.* 2010], from sediments (indicated by turbidity and chl-*a*), fueling bacterial activity and increasing R rates during these episodes. Despite the material resuspended from the bot-tom may limit the euphotic zone to the first 0.5 m [Niencheski *et al.* 1994], it fertilizes the euphotic zone with bottom rich waters, fueling primary production at the surface [Abreu *et al.* 2010; They *et al.* 2019] (Figure 6), as also observed in other estuaries [Santos

et al. 2014]. According to Niencheski & Jhanke [2002], remineralization within sediments may dominate nutrient regeneration at the estuary, which return to the water column to support pelagic primary producers.

Light availability was the main driver of primary production in deeper channel-sites, whereas nutrients have already been observed as such by Odebrecht *et al.* [2005] in shoal sites in the Patos Lagoon Estuary. The occurrence of light-limitation is due to high turbidity [Kocum *et al.* 2002; McSweeney *et al.* 2017] and the greater distance from the surface to the bottom, generally preventing light from reaching sediments, limiting phytobenthic production [Murrell *et al.* 2018].

6.5.3 Biotic factors driving metabolism

The composition of the phytoplankton assemblage in Patos Lagoon Estuary is mainly associated with salinity fluctuation, which is controlled by wind direction [Fujita & Odebrecht 2007]. SW winds promote inflow with the entrance of marine diatoms and dinoflagellates into the estuary, while NE winds promote outflow carrying freshwater species, such as cyanobacteria and chlorophytes [Abreu *et al.* 1994; Fujita & Odebrecht 2007]. This pattern was evidenced in the present study by wind speed and water flow (Fig. 4), salinity (Fig. 5), and phytoplankton group composition (Fig. 8). Higher mean chl-*a*, but with lower phytoplankton group variability, occurred at station 1. The higher group variability observed at station 2 was mainly associated with its proximity to the more dynamic region in the estuary mouth, which is subject to the more frequent exchange of water and salinity gradient [Abreu *et al.* 2017]. Conversely, the higher mean chl-*a* at station 1 may be have been due the position of the station in the inner-estuary, where the greater retention time could favor the accumulation of phytoplankton biomass [Odebrecht *et al.* 2015], as evidenced by higher chl-*a* concentrations coinciding with the saltiest days at station 1. This behavior may directly affect metabolic rates. The higher chl-*a* at station 2 occurred together with low salinity but high DIN and N:P ratios. The high biomass and nutrient content came from the limnic region, as corroborated by the higher biomass of freshwater species (Fig. 7), and had not been converted into high

GPP rates (Fig. 6), being directly exported out of the estuary due the intense outflow [Odebrecht *et al.* 2015; Abreu *et al.* 2017].

In spite of the lower biomass of cryptophytes and prasinophytes in relation to diatoms during days of high GPP rates (Fig. 9), their occurrence suggests they represent a significative portion of the metabolic rates. This behavior may result from a combination of factors such as light [Domingues *et al.* 2011] and nutrient availability [Zhao & Quigg 2014], vertical mixing of cells in the water column [MacIntyre & Geider 1996], and distinct properties intrinsic to each phytoplankton group concerning its physiology and metabolic rates, such as the cell-size (López-Sandoval *et al.* 2014], maximum nutrient uptake and growth rates [Litchman & Klausmeier 2008; Marañon *et al.* 2013]. Nitrogen supply is expected to especially favor greater growth rates of diatoms and prasinophytes, as found by Zhao & Quigg [2014] for the Mississippi-Atchafalaya River Plume, suggesting their advantage over other taxonomic groups when DIN becomes available.

The higher R rates coincided with the highest GPP rates and phytoplankton biomass, and/or greater contributions of cyanobacteria and chlorophytes, as observed by López-Sandoval *et al.* [2014]. This is a possible reason for decoupling of GPP and R, since on other days with increased GPP rates and when these groups were not abundant, the R rates did not accompany GPP rates proportionally. To conclude, it is important to highlight that it was on only one day that such groups were more abundant coinciding with GPP and R rates and so it is not enough to perform a robust statistical analysis or even to assert about these observed trends, making it a future challenge to be properly investigated.

6.5.4 Metabolism and CO_2-carbonate chemistry

No coupling was found between metabolic rates and carbonate system parameters at the Patos Lagoon Estuary during the late austral summer of 2021, suggesting other driving factors than pelagic metabolism, and/or other sources of total alkalinity and total inorganic carbon than those quantified in the present study. High quantities of nutrients and organic matter from autochthonous and allochthonous sources are known to promote marked and fast cycling of materials

in estuaries [Bianchi *et al.* 2007; Libes 2009]. Among such processes, organic matter remineralization leads to a heterotrophic state and CO_2 supersaturation in estuarine waters [Sunda & Cai 2012; Cloern *et al.* 2014]. An increase in pH and decrease in pCO_2 occurs during photosynthesis, while the contrary occurs during respiration. As a result, the direction of CO_2 fluxes can change [Bianchi *et al.* 2007; Libes 2009].

As a proxy for primary production, chl-*a* and its negative correlation with total inorganic carbon reflects inorganic carbon assimilation during photosynthesis [Bianchi *et al.* 2007; Libes 2009]. The dominance of diatoms and the groups relation with total inorganic carbon may indicate its high efficiency at assimilating CO_2 from the water (Fig. A.3). However, this could only be true if the diatom community was dominated by microphytoplankton species [Hopkinson *et al.* 2011], which was not evaluated in this study. Therefore, we suggest that future studies confirm the cell-size of the community. Finally, the lack of a relationship between metabolic rates and pH, total alkalinity, total inorganic carbon and pCO_2, indicates the inflow (outflow) of salty coastal (freshwater) waters as the main modulating factor for carbonate system parameters in the Patos Lagoon Estuary [Albuquerque *et al.* 2022]. Albuquerque [2022] found the estuary to act as a net CO_2 sink during austral summer. However, in the inlet inner station1 evaluated here, the averaged FCO_2 rates show the predominance of water-air net CO_2 source to the atmosphere.

Albuquerque [2022] attributed the outgassing at the inlet inner station during winter and spring to its location, since it is more subject to freshwater influence, with high heterotrophy rates due the organic matter produced on a larger scale in less saline areas [Niencheski & Jahnke 2002]. Moreover, the sheltered station of Albuquerque [2022] was in the margin, while the station 1 of the present study was in a channel-site, where R rates prevail. Near station 1, but in a salt-marsh area, Souza *et al.* [2022] found daily net CO_2 sink from the atmosphere during the summer period, the net CO_2 fluxes of which were modulated by transient atmospheric systems (as observed here) and by the level of variation of adjacent areas. This behavior has also been observed in other tidal marshes during summer periods [Schafer *et al.* 2014]. Therefore, it is likely that the extensive areas with salt-marshes next to station 1 are an important source

of variability that could affect the carbonate system in the permanently flooded areas of the Patos Lagoon Estuary. Finally, other sources of organic and inorganic carbon species should be considered to better understand the specific contribution of each to carbonate system dynamics and its relationship with metabolic rates.

6.6 Concluding remarks

The evaluation of the influence of multi meteoceanographic and biogeochemical processes on pelagic ecosystem metabolism through a daily, whole-month sampling design showed to be useful for understanding short-term variability in complex estuarine systems. By presenting GPP and R rates, and their combined net metabolism, new insights were gained on the biogeochemistry of the Patos Lagoon Estuary. We identified heterotrophic predominance in the channel-sites of the Patos Lagoon Estuary during the late austral summer, yet also highlighted huge short-term variability induced by wind direction rotation and its effects on estuarine and shelf waters exchanges, leading to important shifts in the processes driving pelagic ecosystem metabolism variability. In addition, we found evidence of Plata Plume Water intrusion into the Patos Lagoon Estuary, which likely changes estuarine properties. We showed the importance of nutrients in having a major influence on primary production by DIN limitation, and secondly by light availably, which is attenuated by turbidity, induced resuspension of sediments and intrusions of turbid shelf waters (Plata Plume Water). Although it was not possible to make conclusions regarding the role of the main phytoplankton groups in contributing to pelagic ecosystem metabolism variability, the importance of diatoms, cryptophytes, and cyano- bacteria as the main microalgae assemblage at the Patos Lagoon Estuary during this time of the year was evident, and its dynamics linked to the wind-induced salinity on the estuary. The same can be stated about the influence of pelagic ecosystem metabolism on water-air CO_2 exchanges, which is not clear yet, but was relevant by encompassing the short-term variability and wind- induced salinity on the Patos Lagoon Estuary. Moreover, the results open several challenges for further investigations to better comprehend carbon cycling in Patos Lagoon Estuary and other similar environments worldwide. Thus, we suggest that future efforts

combine longer monitoring programs [e.g., BrOA 2022: Kerr *et al.* 2016; and PELD-ELPA 2022: Odebrecht *et al.* 2003; Lemos *et al.* 2022] with the evaluation of entire ecosystem metabolism, to embrace all scales and sources of variability.

Capítulo VII:

Variabilidade do metabolismo total do ecossistema em um canal de um estuário lagunar subtropical

O segundo manuscrito, em síntese, apresenta estimativas do metabolismo total do ecossistema em uma área interna do Estuário da Lagoa dos Patos, em diferentes escalas temporais, e estabelece quais as principais forçantes meteoceanográficas que controlam os processos metabólicos nas escalas diária, sazonal e interanual. De autoria de Luís Henrique Bordin, Eunice da Costa Machado, Carlos Rafael Borges Mendes, Elisa Helena Leão Fernandes e Maurício Garcia de Camargo, intitulado "Total Ecosystem Metabolism Variability in a Subtropical Lagoonal Estuary Channel-site", publicado no periódico "***Estuaries and Coasts***" em setembro de 2023. A análise e interpretação dos resultados, e a redação deste manuscrito foram feitas por mim, como parte da minha tese de doutorado. Eunice da Costa Machado, fez toda a supervisão para que chegássemos à conclusão desse estudo. Carlos Rafael Borges Mendes contribuiu como especialista em ecologia de produtores primários. Elisa Helena Leão Fernandes contribuiu como especialista em oceanografia física, e Maurício Garcia de Camargo contribuiu como especialista em oceanografia biológica e estatística.

Abstract

Daily, seasonal, and interannual/austral spring (among austral springs only) responses in total ecosystem metabolism (EM) were studied for the first time for the Patos Lagoon Estuary using Odum's Open Water-method. The method was applied from 2016 to 2021 for a channel site in the inner part of the estuary. The main objective was to evaluate what driving factors control the EM at different timescales. The net EM (net ecosystem metabolism) was heterotrophic throughout the year (mean; standard error: -193.8; 7.8 mmol O_2 m^{-2} d^{-1}), with gross primary production (GPP) of 89.7 ± 3.7 mmol O_2 m^{-2} d^{-1} and community respiration (CR) of -281.6 ± 10 mmol O_2 m^{-2} d^{-1}. Annual GPP was estimated at 298.8 g C m^{-2} y^{-1}. Higher EM rates were observed during the austral spring/summer and lower rates during the fall/winter. Smaller timescales and spring/summer exhibited greater fluctuations than long-term and other seasons. The high net heterotrophy was attributed to the high turbidity and local depth, in which the majority of water column to be below the euphotic zone, where respiration prevails. The EM rates were mainly controlled by the hydrodynamics: daily by the wind-induced short-term salinity changes due to shifts on the inflow/outflow of marine/estuarine waters, and photosynthetically active radiation; seasonally by the freshwater flow regime (draught and flood seasons), which induce changes in the primary production co-limiting factors turbidity and nutrients availability, as well as organic matter supply and decomposition (nutrients and organic matter inferred from turbidity); interannual/austral spring also by the freshwater flow regime, but related to extreme conditions caused by weather/climatic phenomena. In the spring of 2016, an extratropical cyclone occurred with heavy rainfall and freshwater flow, resulting in unusually high EM rates over the following two months. The first total EM estimates for the Patos Lagoon Estuary from daily to interannual/austral spring basis, showed the importance of total EM estimates to provide the basis for studies on the effects of climate change on the EM of the Patos Lagoon Estuary.

Keywords: Ecosystem metabolism; primary production; community respiration; estuary; driving factors.

7.1 Introduction

Estuarine and other shallow coastal ecosystems are subject to meteoceanographic and biogeochemical variability on a variety of timescales, especially in regions with pronounced seasonality, as reflected in the availability of light, temperature, freshwater flow, salinity, and nutrients. On smaller timescales, other sources of variability such as the passage of cold fronts and other extreme meteorological events can also be considered [Wolfe, 1986; Bianchi, 2007; Day *et al.* 2012], while on longer timescales, climate change and natural climatic oscillations such as the El Niño-Southern Oscillation (ENSO) affect estuarine ecosystems by altering wind patterns and pluviometry [Grimm 2009]. Extreme meteorological events are directly related to climate change and have the potential to strongly influence biogeochemical dynamics, especially in shallow systems such as estuaries [Lopes *et al.* 2021]. It is becoming increasingly important to understand their impacts in these systems.

These meteoceanographic changes directly affect the dynamics of properties such as freshwater flow, salinity, nutrients, suspended sediment concentrations, euphotic zone depth, and thus aquatic ecosystem metabolism (EM) [Bianchi, 2007; Testa *et al.* 2012; Day *et al.* 2012] and contribute significantly to carbon mass balance and biogeochemical dynamics locally and globally [Bianchi, 2007; Laruelle *et al.* 2013; Regnier *et al.* 2013a,b]. EM consists of the processes of primary production of organic matter, carried out by chemo- and photosynthesizing organisms, and organic matter decomposition, also referred to as remineralization or community respiration (CR) [Valiela 2015]. Primary production consumes carbon dioxide and releases oxygen, whereas the opposite is true for CR [Reynolds 2006; Valiela 2015]. Therefore, EM can be evaluated based on the changes in dissolved gases, such as dissolved oxygen. The balance between them represents the net state of the ecosystem, which is called autotrophic when it is positive and accumulates and/or exports organic matter, and heterotrophic when it is negative and depends on organic matter imported from adjacent systems [Bianchi 2007; Valiela 2015].

Although EM studies are of great importance to aquatic science [Staehr *et al.* 2012], few studies have been conducted in the Southern Hemisphere, mainly

due to high cost for deployment and maintenance of automatic-systems for the developing countries. This is the case of Patos Lagoon Estuary, Brazil. In this area are few studies on primary production rates [Abreu *et al.* 1994; Niencheski & Jahnke, 2002; Proença, 1994], which focus on the use of chl-*a* as a proxy for primary production, with limited temporal resolution [Abreu *et al.* 2010, 2017; Haraguchi *et al.* 2015]. Furthermore, none of the previous studies report respiration rates (CR) or net ecosystem metabolic status, i.e., primary production minus CR. A recent study by Bordin *et al.* [2023a] estimated pelagic ecosystem metabolism using oxygen-based bottle experiments, and although their approach did not include the entire EM (neglecting benthic metabolism), their results are the most recent advances in this direction, showing the channel-sites of Patos Lagoon Estuary to be net heterotrophic during the late austral summer.

In order to capture and understand the whole EM, the present study aims to: i) estimate the rates of gross primary production (GPP) and CR and consequently the net ecosystem metabolism; ii) verify the relationship between the meteoceanographic factors influencing the rates of EM, from daily to the interannual/austral spring scale. This study was the first attempt to assess the overall EM status in the Patos Lagoon Estuary and to examine which meteoceanographic factors drive metabolic processes from daily to interannual/austral spring timescales. It contributes to the limited knowledge of EM rates in the southern hemisphere/subtropical South America, and also provides insight into how estuarine systems worldwide might respond to extreme events such as those caused by ENSO and climate change.

7.1.1 Study site

Patos Lagoon in south Brazil (Fig. 2a), is the largest choked coastal lagoon (connected to the sea by a narrow channel) in South America. The lagoon receives water from many subwatersheds. To the northwest is the Guaíba River (Fig. 2b), a lake that flows into Patos Lagoon, where the main tributaries are the Jacuí, Taquarí, Caí, and Sinos rivers and whose watershed covers 84.7 km^2 [Scottá *et al.* 2019]. To the west is the Camaquã River, with a drainage basin of 21.6 km^2. Finally, in the southwest is the São Gonçalo Channel, a narrow channel that connects the Patos Lagoon and the Mirim Lagoon, whose watershed

comprises 28.5 km^2. The direction of waterflow between the lagoons is determined by the wind direction [Oliveira *et al.* 2019]. The runoff pattern is characteristic of temperate regions and has the maximum flows from winter to spring. On an annual basis, the mean freshwater flow is 2,400 $m^3 s^{-1}$. Between years, the system is modulated by climatic processes [Marques & Möller, 2009; Marques 2012], such as the ENSO [Grimm 2009], where extreme discharge events can reach up to 25,000 $m^3 s^{-1}$ [Marques 2012]. To the southeast is the Patos Lagoon Estuary (Fig. 2c). Because of the microtidal regime (±0.5 m) [Möller *et al.* 2001], hydrodynamics is governed by wind and freshwater flow [Möller *et al.* 1996]. When river discharge (Q) is > 2,000 $m^3 s^{-1}$, the system is controlled by freshwater flow, and when Q is < 2,000 $m^3 s^{-1}$, by a bidirectional wind system. Southwesterly winds promote flood flows and thus estuarine salinization, while northeasterly winds promote ebb flows and estuarine salinity reduction [Möller & Castaing, 1999]. River discharge also affects the residence time of water in Patos Lagoon, which is about 135 days at a flow of 5,000 $m^3 s^{-1}$, 85 days at 8,000 $m^3 s^{-1}$, and 68 days at 10,000 $m^3 s^{-1}$ [Fernandes *et al.* 2002]. Watersheds are development areas with land use and land cover of about 20% of the total area [IBGE 2022]. The main source of nutrients for Patos Lagoon is from the Guaíba River in the northern lagoon, whose nutrients are removed during the 250 km journey to the estuary in the southern lagoon [Niencheski & Windom, 1994a]. In the estuarine region, the anthropic nutrient input is the primary cause of eutrophication [Niencheski & Windom 1994a]. Nutrient, chl-*a*, and primary production rates are higher and more variable in spring and summer, decrease in fall, and reach the lowest values in winter, when lower temperatures and light intensities, as well as higher turbidity from freshwater flow due to the rainy season, lead to a decrease in primary production rates [Abreu *et al.* 1994; Proença 1990]. Patos Lagoon is a shallow system with a mean depth of 5 m [Calliari 1997]. The shallow and littoral areas are autotrophic most of the year and heterotrophic only in winter when, in addition to the factors already mentioned, organic matter is regenerated from senescent seagrass on the sediments [Abreu *et al.* 1994; Proença 1990]. In addition, the biogeochemical dynamics of the Patos Lagoon Estuary are subject to the intrusion of Plata Plume waters, especially during southerly winds and low freshwater flow [Bordin *et al.* 2023a]. The Plata Plume Water is a nutrient-rich water mass [Braga *et al.* 2008; Bordin *et al.* 2019]

composed by water discharges of La Plata River (35°S) into the southwestern Atlantic Ocean (Fig. 2b), whose drainage basin is the second largest of South America, following that of the Amazon [Acha *et al.* 2008].

7.2 Methods

7.2.1 Data acquisition

Hourly data from the Brazilian Coastal Monitoring System (SiMCosta) were used. Due to the conditions of water column homogeneity, the station RS-1 (Fig. 2d) was selected for the application of the overall approach EM. More details about the SiMCosta project, the buoy systems, and their specific probes for RS-1, a Seabird Scientific Land/Ocean Biogeochemical Observatory (LOBO), can be found on the project website (www.simcosta.furg.br). The following parameters were used in this study: Temperature (C°), salinity (psu), dissolved oxygen (DO; µmol), DO saturation (DO%; %), pH (seawater – logarithmic scale), turbidity (NTU), and chl-*a* (µg L^{-1}). Meteorological parameters were: Air temperature (°C), relative humidity (%), atmospheric pressure (µatm), wind speed and maximum speed (m s^{-2}), wind direction (degrees - N), precipitation (mm), and solar radiation (W m^{-2}) and were obtained from the Rio Grande Pilots (RG Pilots; www.rgpilots.com.br). Data quality for all variables was ensured by filtering with quality control filters: Gross Range Test (reading limits), Spike Test (anomalous protruding data), Rate of change (variability limit between certain time windows), test and flat line test (repeated values due to probe errors). Wind data was corrected to 10 m above ground (U10) from the logarithmic wind profile (v2):

$$v2 = v1 \frac{ln\left(\frac{h2}{z_0}\right)}{ln\left(\frac{h1}{z_0}\right)} \qquad \text{(Eq. 18)}$$

where *v2* is the wind speed at the desired height above the ground, *v1* is the wind speed at the height where the probe is installed, ln is the natural logarithm, z_0 is the roughness length ($2x10^{-5}$ for water surfaces), and *h1* and *h2* are the original and desired heights above the ground in meters.

7.2.2 Aquatic ecosystem metabolism

The total EM was estimated by Odum's Open Water-method [Odum 1956], based on diel changes in DO obtained from automatic stations with oxygen probes. As described in Caffrey *et al.* [2014] and Murrell *et al.* [2018], the technique is to model the DO flux at each time step according to the equation 19:

$$\frac{\partial C}{\partial t} = P_e + R_e + D; \quad \text{(Eq. 19)}$$

where $\partial C/\partial t$ is the measured DO flux rate in mmol O_2 m^{-3} h^{-1}, P_e is the photosynthesis rate, R_e is the respiration rate, and D is the volumetric air-sea exchange rate (D), according to equation 20:

$$D = k_a(C_s - C); \quad \text{(Eq. 20)}$$

where k_a is the volumetric reaeration coefficient in hours and C_s is the concentration of DO saturation due to the water temperature and salinity effect [Benson & Krause 1984]. The k_a was calculated by the equation of Ro & Hunt [2006], modified by Thèbault *et al.* [2008] as:

$$k_a = \frac{1}{h}.1.706\left(\frac{D_w}{v_w}\right)^{\frac{1}{2}}.\left(\frac{p_a}{p_w}\right)^{\frac{1}{2}}.{U_{10}}^{1.81}; \quad \text{(Eq. 21)}$$

where h is the local depth in meters, Dw is the O_2 diffusivity in seawater (m^{-2} s^{-1}), vw is the kinematic viscosity of seawater respective to a specific temperature and salinity (m^{-2} s^{-1}), ρa and ρw are, in order, the air and seawater densities (kg m^{-3}), and U_{10} is the wind speed at 10 m above ground level (m s^{-1}).

The DO fluxes corrected by the air/water diffusion were then averaged over daytime to calculate apparent primary production (P_a) and over nighttime to

calculate respiration rates (R_n). Respiration rates were multiplied by 24 hours to obtain the daily ecosystem CR, while GPP was the sum of P_a and R_n multiplied by daylight hours and local depth. Finally, net ecosystem metabolism was computed as GPP minus CR.

The metabolism rates were computed with the R package WtRegDO [Beck *et al.* 2015], from March 2016 to December 2017, and from April 2019 to February 2021, with some minor gaps. These gaps occur during the probes cleaning of encrusted organisms, its maintenance and calibration. During 2018, the buoy was inoperative for a longer period for maintenance.

Due to the premises and limitations of Odum's Open-Water method, such as water column homogeneity and water properties over time [Coloso *et al.* 2008; Needoba *et al.* 2012; Staehr *et al.* 2012], the method could only be applied at the SiMCosta RS-1 station, where vertical homogeneity could be assumed due to the shallower depth and the observed local mixing process [Bordin *et al.* 2023a]. The RS-1 is a channel site with 4.5 m depth. It is located in the middle section of the Patos Lagoon Estuary in a protected area (Fig. 2d). Based on its intermediate location second biogeochemical zone [Windom *et al.* 1999] far from direct fresh- and salt-water influence, local depth near the mean depth of Patos Lagoon (5 m) [Calliari 1997], and the fact that metabolic rates show similar trends to those observed in an area exposed to the sea [Bordin *et al.* 2023a], we assume the RS-1 station as representative of channel sites in Patos Lagoon Estuary.

The microtide regime of Patos Lagoon Estuary is only about 0.5 m [Soares & Möller 2001], but the water level in the Patos Lagoon Estuary changes due to freshwater flow and wind direction, which causes the inflow of salty coastal water into the estuary during SW winds and the outflow of fresher water during NE winds [Möller & Castaing 1999]. The effect of water level changes could be accounted for using the detide technique through weighted regression in the WtRegDO package [Beck *et al.* 2015], but we do not have water level data for the RS-1 station. Unlike fixed probes, for which the detide method was developed, meteoceanographic buoys accompany the rise and fall of water level. Nevertheless, the salinity changes (advection) mentioned above are still a problem due to the violation of temporal water mass homogeneity [Coloso *et al.*

2008; Needoba *et al.* 2012; Staehr *et al.* 2012]. Therefore, the results from EM had to be carefully sifted to eliminate all days where significant changes in salinity occurred (arbitrarily defined as > 4 psu). The first step was performed using the R package DO - Classifier, which assessed the suitability of the data to the metabolism analysis through a supervised classification model called Symbolic Aggregate Approximation (SAX) implemented by Muraoka *et al.* [2018]. Then, the dataset was manually checked to see if the days classified by the last step were haline-homogeneous, if all anomalous data (i.e., negative GPP and positive CR rates) were removed, and for outliers < 5% and > 95% quartiles, replaced by them, a total of 345 days of EM rates covering the entire period from 2016 to 2021.

7.2.3 Data analysis

The analyses were performed with all corresponding data from the five years (2016, 2017, 2019, 2020 and 2021). Daily, monthly, seasonal, and annual descriptive statistics were performed for all the parameters and timescales (monthly, seasonal and annual). For the interannual/austral spring analysis, only the austral spring season was considered due the great data availability, which includes sufficient data for a four-year analysis. Kruskal Wallis analysis of variance (KW) [Dodge 2008] were performed to test for global (all timescales analysis) and posteriori (only seasonal and interannual/austral spring) pairwise differences ($\alpha < 0.05$). A principal component analysis was performed to verify the association between the parameters: GPP, CR, temperature, salinity, DO%, chl-*a*, turbidity, wind speed and direction, and photosynthetic active radiation (PAR; inferred from a pyranometer out of the water). Pearson's correlation matrix of these parameters was made to complement and corroborate the PCA. Generalized additive models (GAM) were conducted to model the response of the GPP and CR variables to the predictors at the timescales daily, seasonal, and yearly, to take the main forcing factors which drives the rates under each timescale [Wood S.N. 2017]. Multicollinearity and concurvity between the appropriate independent variables in GAM were analyzed. When multicollinearity was detected in the linear part of the model, only one of the collinear explaining variables was kept. The concurvity [Wood S.N. 2017] was analyzed to avoid

redundancy in the non-linear part of the model [Kovács 2022]. No concurvity was found. The seasons and years were added as factors, however, since the quality control sifting and mining (haline heterogenous-days randomly distributed over time) steps removed several unsuitable data, resulting in seasons and years with unbalanced number of samples for each factor. The best model for each timescale was selected by a formal backward approach, based on the high explanatory percentage and adjusted R^2, and lower standard error (SE) and Akaike's Information Criterion (AIC) Akaike H. [1974]. Boxcox transformations were used when necessary to reduce the asymmetry of the data. To include wind in the analysis, it was decomposed into meridional and zonal wind components and only the meridional component was used to represent both wind speed and wind direction, since the main wind quadrants affecting the inflow (outflow) of marine saltwater (freshwater) into the Patos Lagoon Estuary are southern and northern [Möller & Castaing 1999]. All statistical analyzes were performed with R software version 4.2.1 [R Core Team 2022] using the packages mgcv [Wood S.N. 2017].

7.3 Results

7.3.1 Total ecosystem metabolism

7.3.1.1 Daily variability

The net ecosystem metabolism at station RS-1 was heterotrophic throughout the study period, with an average of -193.8 mmol O_2 m^{-2} d^{-1}. Overall, GPP and CR rates followed a trend in which both rates were positively collinear. The most heterotrophic state (net ecosystem metabolism: -1,382 mmol O_2 m^{-2} d^{-1}) occurred in November 2016, when GPP was 272.8 mmol O_2 m^{-2} d^{-1}, and CR reached its highest value (-1,665 mmol O_2 m^{-2} d^{-1}) during the studied period. The least variable metabolic rate was GPP, with a SD of 80.1 mmol O_2 m^{-2} d^{-1}, while CR had a SD of 214.9 mmol O_2 m^{-2} d^{-1}. GPP, CR, and net ecosystem metabolism rates are shown in Figure 10. Annual GPP was determined by trapezoidal integration for the entire year 2017 only due to data availability and representativeness for each season (which was not observed for the other periods studied) as being 298.8 g C m^{-2} y^{-1} (mean; SE: 0.72; 0.05 g C m^{-2} y^{-1}), converted to C units assuming PQ = 1.

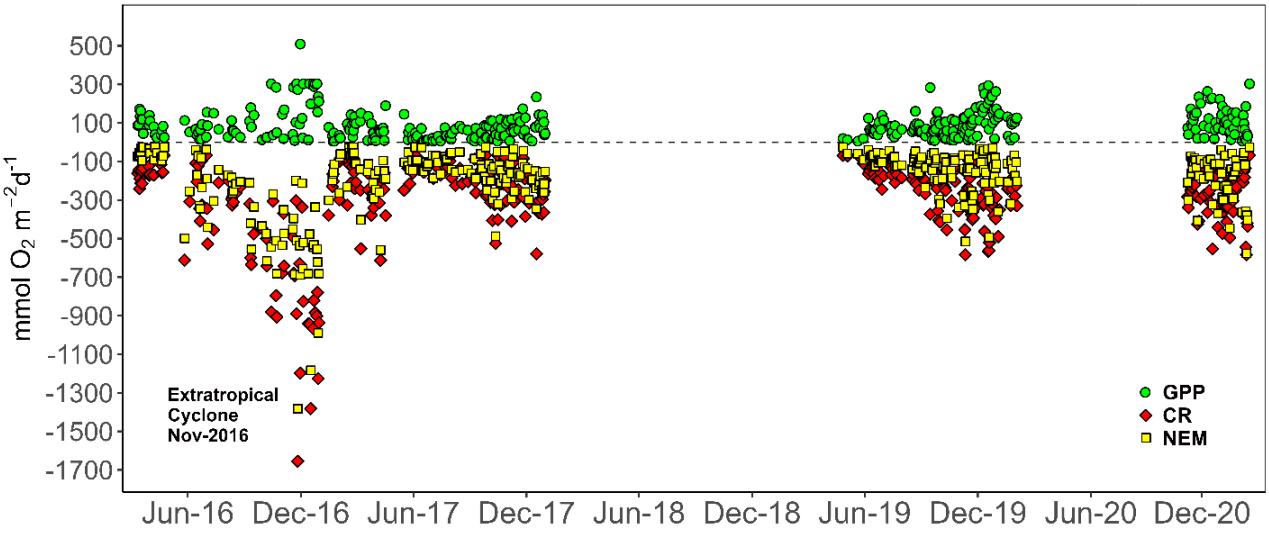

Figure 10. Daily aquatic ecosystem metabolism at station RS-1, in the middle section of the Patos Lagoon Estuary. Data from March-16 to December-17; April-19 to February-20; and November-20 to February-21 (with small gaps). Gross primary production (GPP: circles), community respiration (CR: rhombus), and net ecosystem metabolism (NEM: squares). Samples n = 345.

7.3.1.2 Monthly variability

To assess monthly variability, rates from EM, caused by the extreme climatic event in November and December 2016, were removed to avoid contamination and to show normal rates from EM. The data for the three metabolic rates are summarized in monthly time series in Figure 11. The most heterotrophic months were October, November, and December with a maximum of up to -687.8 mmol O_2 m^{-2} d^{-1}, while the average in December was -256.2 mmol O_2 m^{-2} d^{-1}, resulting in intense CR rates. However, the higher CR rate (-968.2 mmol O_2 m^{-2} d^{-1}) and average (-394.2 mmol O_2 m^{-2} d^{-1}) were observed in December, when the higher GPP maximum (304.4 mmol O_2 m^{-2} d^{-1}) and average (157.8 mmol O_2 m^{-2} d^{-1}) occurred. On the other hand, June was the least heterotrophic month with an average of -118.7 mmol O_2 m^{-2} d^{-1}. As for variability, the months from October to January were the most variable, when net ecosystem metabolism SD reached a maximum value of 188.4 mmol O_2 m^{-2} d^{-1} (December), mainly driven by the strongly varying CR rates (SD: 253.2 mmol O_2 m^{-2} d^{-1}), but also by GPP (SD: 92.3 mmol O_2 m^{-2} d^{-1}). The lower variability for the three metabolic rates occurred in the August months (SD: net ecosystem metabolism 62.1; GPP 29.9; CR -60.8 mmol O_2 m^{-2} d^{-1}). After monthly global KW analysis, all

metabolic rates were statistically different between months, whose respective p and n are presented in Figure 11. No pairwise KW was performed between months.

Figure 11. Monthly averaged time series and standard errors (error bars) of EM rates of

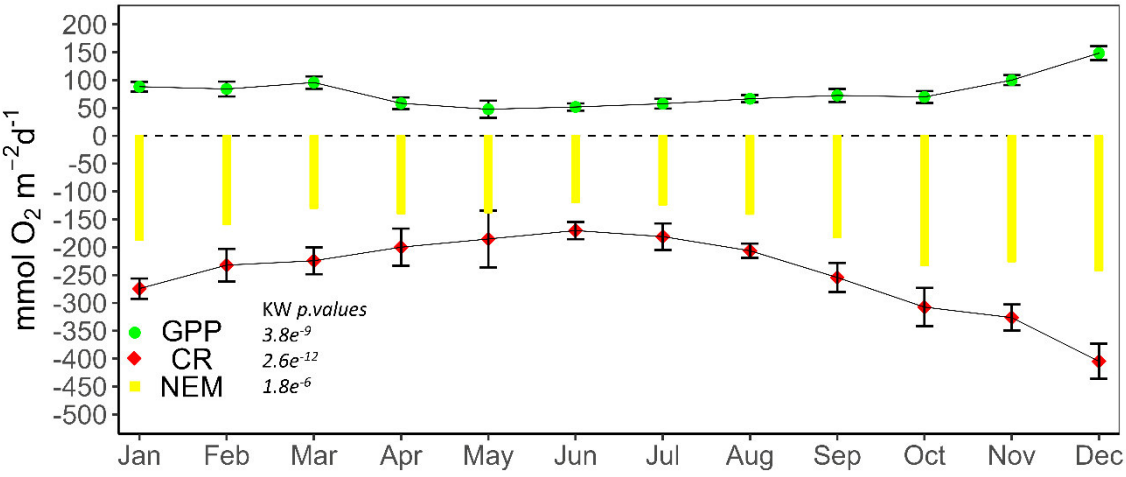

gross primary production (GPP: green circles), community respiration (CR: red rhombus), and net ecosystem metabolism (NEM: yellow drop lines) at station RS-1, in the middle section of the Patos Lagoon Estuary. Kruskal-Wallis test (KW) shows significant differences between months. Samples n: Jan = 33; Feb = 19; Mar = 20; Apr = 17; May = 10; Jun = 29; Jul = 23; Aug = 23; Sep = 30; Oct = 36; Nov = 53; Dec = 51.

7.3.1.3 Seasonal variability

The least heterotrophic condition occurred in summer (minimum net ecosystem metabolism -16.2 mmol O_2 m^{-2} d^{-1}). However, the lowest mean values occurred in the autumn and winter with ~ -130 mmol O_2 m^{-2} d^{-1}. In spring and summer, despite the highest mean GPP values (≥ 100.0 mmol O_2 m^{-2} d^{-1}), the net ecosystem metabolism reached the most heterotrophic state (net ecosystem metabolism mean, in order: -211.3 and -183.7 mmol O_2 m^{-2} d^{-1}). This resulted from the increased CR rates with mean values of -308.4 and -291.5 mmol O_2 m^{-2} d^{-1}, respectively, and with maximum values around -820.0 mmol O_2 m^{-2} d^{-1}. As can be seen from the error bars in Figure 4 (SE), autumn and winter had the most homogeneous rates, with net ecosystem metabolism SD of 115.0 and 98.1 mmol O_2 m^{-2} d^{-1}, respectively, while the most variable data were observed in spring (SD: 143.1 mmol O_2 m^{-2} d^{-1}). The GPP and CR followed the same pattern.

Detailed results of pairwise KW among seasons for all three metabolic rates are shown in Figure 12.

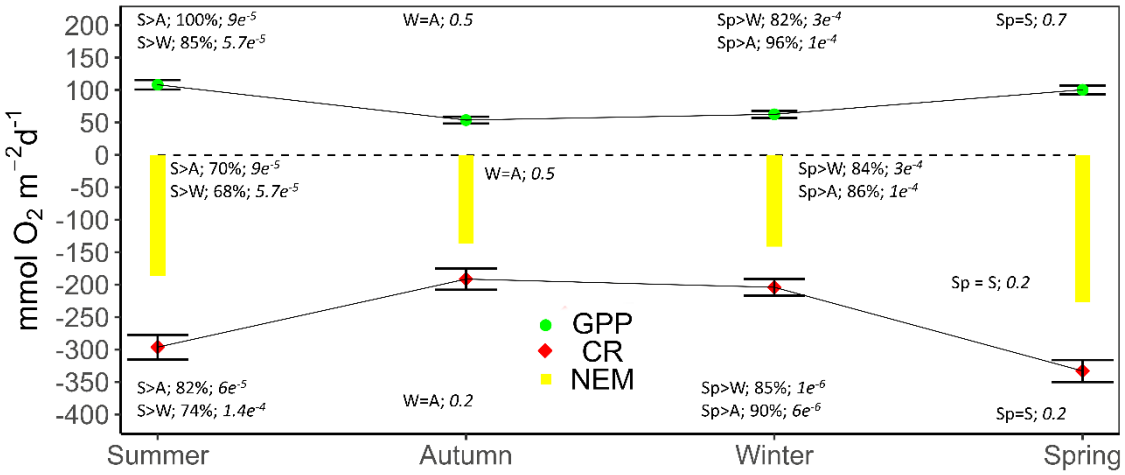

Figure 12. Seasonal averages and standard errors (error bars) of the EM rates, gross primary production (GPP: green circles), community respiration (CR: red rhombus), and net ecosystem metabolism (NEM: yellow drop lines) at station RS-1, in the middle section of the Patos Lagoon Estuary. Posteriori Kruskal-Wallis for each EM rate reveal differences between seasons, followed by the percentage of difference, and by the p.value (italic) among pairwise seasons: summer (S), autumn (A), winter (W), and spring (Sp). Samples n: summer = 90; autumn = 53; winter = 77; spring = 125.

7.3.1.4 Interannual/austral spring variability

The least heterotrophic spring was in 2020 with an average of -159.4 mmol O_2 m^{-2} d^{-1}, while the averages for GPP and CR were 127.4 and -286.8 mmol O_2 m^{-2} d^{-1}, respectively. On the other hand, the heterotrophic spring was strongest in 2016. In such period, the net ecosystem metabolism reached -1,382 mmol O_2 m^{-2} d^{-1}, mainly caused by intense CR rates (up to -1,655; mean -764.1 mmol O_2 m^{-2} d^{-1}), ~ threefold higher than normal. The GPP was also high, reaching up to 509.2, with a mean of 180.6 mmol O_2 m^{-2} d^{-1}. The year with the greatest variation was 2016 (SD: net ecosystem metabolism 160.5; GPP 329.9; CR -277.3 mmol O_2 m^{-2} d^{-1}), while the other years had 116.4 (2019), 73.6 (2020), and 132.6 (2019) mmol O_2 m^{-2} d^{-1} of net ecosystem metabolism, GPP, and CR, respectively. The GPP and CR followed the same pattern. Detailed results of pairwise KW among years/austral springs for all three metabolic rates are shown in Figure 13.

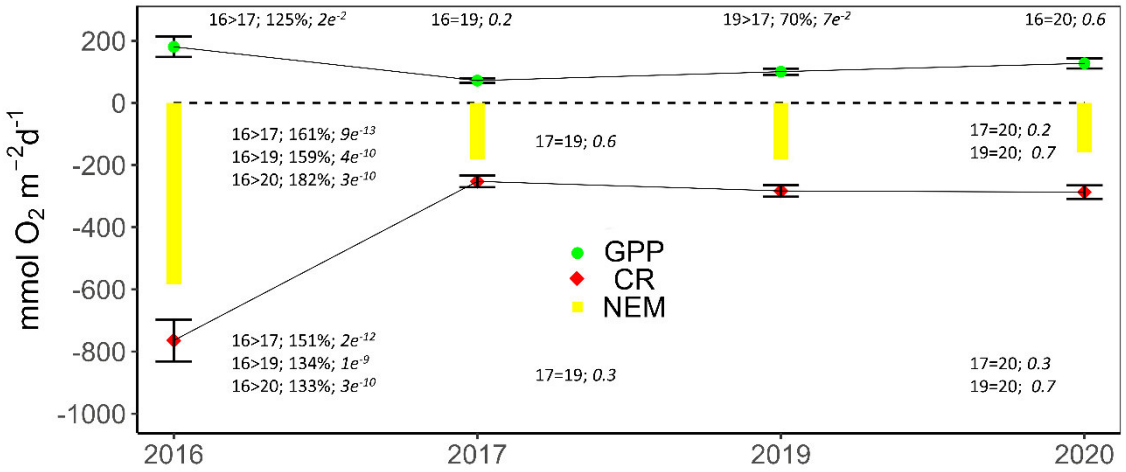

Figure 13. Interannual/austral spring averages and standard errors (error bars) of EM rates, gross primary production (GPP: green circles), community respiration (CR: red rhombus), and net ecosystem metabolism (NEM: yellow drop lines) at station RS-1, in the middle section of the Patos Lagoon Estuary. Posteriori Kruskal-Wallis for each EM rate reveal differences between seasons, followed by the percentage of difference, and by the p.value (italic) among pairwise years. Samples n: 2016 = 24; 2017 = 41; 2019 = 50; 2020 = 20.

7.3.1.5 Metabolism driving factors

According to the principal component analysis (Fig. 14a) — with some relations corroborated by the Pearson's correlation matrix (Fig. 14b) — the grouping of the data by pairs of seasons is noteworthy: spring+summer and autumn+winter. The GPP and CR rates were higher in austral spring and summer and were mainly influenced positively by the photosynthetically active radiation, temperature, salinity, wind, and chl-*a* and negatively by turbidity. Other patterns and relations can be seen in the Figures 14a and 14b. The descriptive statistics for the meteoceanographic variables are shown in Table 2 for each of the timescales.

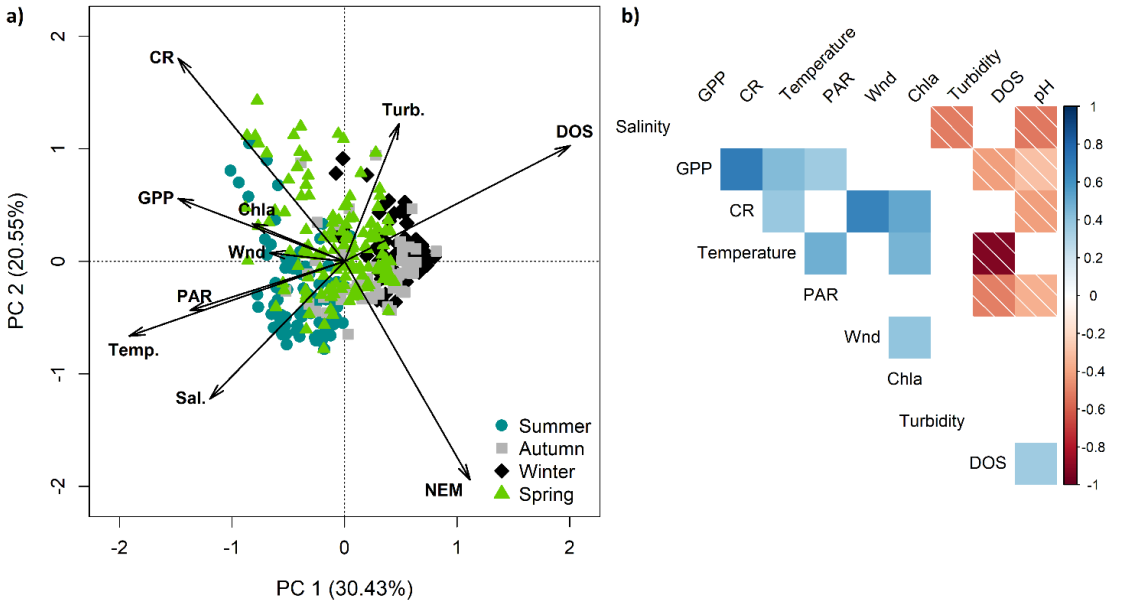

Figure 14. a) Principal component analysis of the EM rates gross primary production (GPP), community respiration (CR), net ecosystem metabolism (NEM), and variables temperature (Temp.), salinity (Sal.), dissolved oxygen saturation (DOS), turbidity (Turb.), chlorophyll-a (Chla), wind meridional component (Wnd) and photosynthetically active radiation (PAR); and b) Pearson's correlation matrix of the same variables, plus pH. Data for 2016 to 2021 for Station RS-1, in the middle section of the Patos Lagoon Estuary. Filled squares represent positive correlations, and striped ones represent negative correlations. Samples n = 349.

Table 2. Minimum, maximum, mean ± standard deviation (SD) – and mode for the wind direction – for the meteoceanographic variables temperature (Temp °C), salinity (Sal), dissolved oxygen (DO – µmol L^{-1}), DO saturation (DO%), chlorophyll-a (Chl-a – µg L^{-1}), turbidity (Turb – NTU), wind speed (Wspd – Kt), wind direction (Wdir degrees), and photosynthetically active radiation (PAR µE m^{-2} s^{-1}). Data from Station RS-1, in the middle section of the Patos Lagoon Estuary. Data from 2016 to 2021. The yearly data are only for the spring season. Samples n: overall = 345; summer = 90; autumn = 53; winter = 77; spring = 125; 2016 = 22; 2017 = 38; 2019 = 48; 2020 = 18.

		Temp	Sal	DO	DO%	Chl-*a*	Turb	Wspd	Wdir	PAR
Overall	Range	12.0-28.3	0.1-30.9	187.9-319.7	65.0-129.2	1.5-8.8	3.9-107	1-17.4		0.1-1.6
	Mean±SD	21.3±4.2	7.1±8.6	244±34.5	88.9±8.08	3.3±1.5	28.1±23.6	6.4±3.3	68.4	0.8±0.4
Summer	Range	21.4-28.3	0.4-31	187.9-289.7	72.9-116.7	1.5-8.8	3.9-87.7	1.3-17.4		0.4-1.6
	Mean±SD	25.7±1.7	14.1±10	214.7±22.1	88.8±8.4	3.3±1.7	17.5±15	6.6±3	67.5	1.1±0.3
Autumn	Range	12-24.6	0.4-31	187.9-315.5	65.1-129.3	1.6-8.8	3.9-107	1-13		0.3-1.6
	Mean±SD	19.5±3.6	5.9±9.1	250.3±40.5	88.1±11.9	3.7±2.4	27.5±18.6	5.3±3.1	90	0.6±0.3
Winter	Range	12-20.8	0.2-22	210.8-319.2	73.9-103.6	1.5-5.2	4.7-84	1-17.4		0.1-1.2
	Mean±SD	15.8±2.3	3.9±4.1	279.9±26	90.2±5.7	2.6±0.7	27.8±20.8	5.4±2.8	236.2	0.6±0.2
Spring	Range	16.1-27.7	0-31	196.8-292	74.5-119.6	1.6-7.3	5.4-107	1-17.4		0.3-1.6
	Mean±SD	22±2.3	4.5±6.2	242.5±21.3	88.57± 7	6.3±1	36.2±28.6	7±3.5	111.1	1±0.5
2016	Range	17.5-24.4	0.3-27.4	197-284.3	74.5-98.3	2.2-4.2	13.7-82.8	2.6-17.4		0.3-1.4
	Mean±SD	21.3±2	4.1±5.7	242.9±23.1	87±5.2	3.3±0.6	47.4±21.7	11.3±4.6	157.5	0.9±0.3
2017	Range	18.3-27.6	0.1-18.9	200.2-257.9	76.9-99.3	1.9-7.3	6.2-107	1-11.6		0.3-1.6
	Mean±SD	21.5±2.1	2.7±3.8	230.2±14.4	82.9±4.7	3.7±0.9	61.9±32.5	6.4±2.6	160.3	1±0.6
2019	Range	16.1-27	0.-17.9	215.6-292	84.1-119.8	2.4-6.5	7.5-24.8	1.3-11.6		0.3-1.6
	Mean±SD	22.3±2.7	2.4±3.7	258.1±16.7	93.5±6.3	4.2±1	19.9±2.8	6.4±2.6	92.8	1.2±0.3
2020	Range	18.9-26.2	4-31	203.2-261.6	84.1-102.2	1.6-4.1	5.4-20.1	1.3-9.4		0.4-1.6
	Mean±SD	23.3±1.5	13.8±7.6	228.5±14.9	89.5±5.4	2.5±0.7	11.2±4	5.9±2.3	106.8	1.1±0.4

Regarding the GAM models, with GPP as a dependent variable (Tab. 3), the best model-describing variables, in decreasing order of significance, were salinity, photosynthetically active radiation and wind. In the seasonal analysis, the parameters that better described the GPP variability were the same, but wind were much more significative with *p* decreasing from 0.02 to $6e^{-3}$, and the GAM with turbidity instead of salinity (not included in Table 3), presented similar results. By including the season as a factor, the model best described GPP in the autumn and spring. The interannual/austral spring analysis were performed using only spring data of 2016, 2017, 2019, and 2020 due to the large data availability. On this timescale, wind, salinity and temperature were significative (p $3e^{-3}$, $1e^{-3}$ and $1e^{-3}$, respectively). The SE was small for most parameters (≤ 0.2). Although the adjusted R^2 and explained variance (dev.exp) were not as meaningful, we can validate the analysis by finding statistical significance (*p* in Table 3) and low SE. In addition, we note that the adjusted R^2 and percentage of dev.exp was lower for the daily model (R^2 0.19; dev.exp 21.7%) and increase toward the interannual/austral spring model (R^2 0.3; dev.exp 34.6%), indicating greater heterogeneity at this timescale, i.e., the data is more susceptible to greater variation at the daily than at the longer timescales (Tab. 3).

Table 3. Details of the generalized additive model for gross primary production (GPP) as the dependent variable, for the timescales daily, seasonal, and interannual/austral spring (just the austral springs for the inter-annual analysis). Data from 2016 to 2021, for Station RS-1, in the middle section of the Patos Lagoon Estuary. As independent variables: temperature (Temp), salinity (Sal), turbidity (Turb), photosynthetically active radiation (PAR), meridional wind component (Wnd). Others: Akaike information criterion (AIC), r-squared (R2), deviance explained (Dev.exp), standard error (SE), degrees of freedom (df), and F statistics (F), intercept (Itcp). Samples n: total = 345; summer = 90; autumn = 53; winter = 77; spring = 125; 2016 = 22; 2017 = 38; 2019 = 48; 2020 = 18.

Model and diagnostics	Term	Parametric coefficients			GAM analysis of variance		
		Estimate	SE	p.value	df	F	p.value
Daily							
GPP ~ PAR + s(Sal) + s(Wnd)	Itcp	3.50	0.13	$< 2e^{-16}$			
AIC: 1084; R^2: 0.19; Dev.exp: 21.7%	PAR	0.67	0.13	$1.6e^{-6}$			
	Salinity				6.46	6.35	$2e^{-6}$
	Wnd				7.51	2.24	0.02
Seasonally							
GPP ~ PAR + s(Sal) + s(Wnd) + Season	Autu. (Itcp)	3.30	0.17	$< 2e^{-16}$			
AIC: 1070; R^2: 0.21; Dev.exp: 25%	Spring	0.76	0.19	$6e^{-3}$			
	Summer	0.34	0.21	0.1			
	Winter	0.16	0.19	0.39			
	PAR	0.41	0.15	$6e^{-3}$			
	Salinity				4.40	8.21	$1.5e^{-6}$
	Wnd				7.52	2.79	$6e^{-3}$
Interannual/austral spring							
GPP ~ Temp + s(Sal) + s(Wnd) + Year	2016 (Itcp)	1.94	0.71	$7e^{-3}$			
AIC: 329; R^2: 0.30; Dev.exp: 34.6%	2017	–0.81	0.22	$3e^{-3}$			
	2019	–0.62	0.21	$4e^{-3}$			
	2020	–1.12	0.31	$4e^{-3}$			
	Temperature	0.10	0.03	$1e^{-3}$			
	Salinity				2.16	6.96	$1e^{-3}$
	Wnd				3.96	5.55	$3e^{-3}$

For the CR as dependent variable (Tab. 4), the daily model shows that the wind, temperature and photosynthetically active radiation were the variables that better described the CR processes. With the inclusion of the season as a factor, the wind remained as the only significative descriptive variable, and PAR changed for salinity, which better described the CR data during autumn, spring and summer. In the interannual/austral spring basis, besides the wind, the temperature also appeared as an important driving factor, and the model was

able to describe the data variability in all of the years. Similar to the GPP models, the increase in the adjusted R^2 and dev.exp from the daily (R^2 0.19; dev.exp 21.5%) to the interannual/austral spring (R^2 0.47; dev.exp 49.3%), also seems to indicate its high variability on small timescales. The SE were always < 0.1.

Table 4. Details of the GAM (generalized additive model) for the community respiration (CR) as the dependent variable, for the timescales daily, seasonally and interannual/austral spring (just the austral springs for the interannual analysis). Data from 2016 to 2021, for Station RS-1, in the middle section of the Patos Lagoon Estuary. As independent variables: temperature (Temp), salinity (Sal), photosynthetically active radiation (PAR), wind meridional component (Wnd). Others: Akaike information criterion (AIC), r squared (R2), deviance explained (Dev.exp), standard error (SE), degrees of freedom (df), and F statistics (F), intercept (Itcp). Samples N: overall = 345; summer = 90; autumn = 53; winter = 77; spring = 125; 2016 = 22; 2017 = 38; 2019 = 48; 2020 = 18.

Model and diagnostics	Term	Parametric coefficients			GAM analysis of variance		
		Estimate	SE	p.value	df	F	p.value
Daily							
CR ~ PAR + Temp + s(Wnd)	Itcp	0.53	$9e^{-3}$	$< 2e^{-16}$			
AIC: –1386; R^2: 0.19; Dev.exp:	PAR	$-1e^{-2}$	$4e^{-3}$	$2e^{-2}$			
21.5%	Temp	$-1e^{-3}$	$4e^{-4}$	$5e^{-3}$			
	Wnd				7.59	8.22	$< 2e^{-16}$
Seasonally							
CR ~ s(Sal) + s(Wnd) + Season	Autum (Itcp)	0.51	$4e^{-3}$	$< 2e^{-16}$			
AIC: –1416; R^2: 0.26; Dev.exp:	Spring	-0.03	$5e^{-3}$	$8e^{-10}$			
28.6%	Summer	-0.02	$6e^{-3}$	$3e^{-4}$			
	Winter	$-5e^{-3}$	$6e^{-3}$	0.32			
	Salinity				3.47	1.84	0.15
	Wnd				5.77	9.69	$< 2e^{-16}$
Interannual/austral spring							
CR ~ Temp + s(Wnd) + Year	2016 (Itcp)	1.86	0.08	$< 2e^{-16}$			
AIC: –578; R^2: 0.47; Dev.exp:	2017	–0.21	0.02	$1e^{-14}$			
49.3%	2019	–0.21	0.02	$4e^{-15}$			
	2020	–0.21	0.03	$5e^{-10}$			
	Temperature	$9e^{-3}$	$3e^{-3}$	0.01			
	Wnd				3.13	6.18	$5e^{-4}$

7.4 Discussion

The assessment of the entire aquatic ecosystem metabolism (i.e., pelagic + benthic), from daily to interannual/austral spring timescales, is an unprecedented contribution to the Patos Lagoon Estuary. The net ecosystem metabolism in the

studied channel of the Patos Lagoon Estuary (RS-1 station) was completely net heterotrophic throughout the year. The EM was dominated by the CR process and had wind, temperature and photosynthetically active radiation as driving factors, while for the GPP process the same plus salinity, with photosynthetically active radiation contributing to shorter timescales, and turbidity and temperature contributed to longer timescales. No less important, but not measured in this study, are dissolved inorganic nutrients, which are a critical factor in EM processes in the Patos Lagoon Estuary, evidenced by low N:P ratios [Abreu *et al.* 1994; Bordin *et al.* 2023a], especially during dry periods [Odebrecht *et al.* 2005] and by increased primary production [Abreu *et al.* 1994; Odebrecht *et al.* 2005; Bordin *et al.* 2023a] and bacterial density [They *et al.* 2018] when nutrients become available.

Overall, the GPP and CR rates obtained in this study fell within the range obtained from other Brazilian and worldwide subtropical and temperate estuaries (see citations in Tab. 5). However, when net ecosystem metabolism is considered, it is found that net heterotrophy is much higher in the Patos Lagoon estuary (Tab. 5). While the CR rates are within values found in other estuaries, such as Pensacola Bay [Murrel *et al.* 2018], where high CR rates were observed in their channel-site, they found high GPP rates, with several days of net autotrophy. On the other hand, the Patos Lagoon Estuary channel-sites presents much higher CR than GPP rates, as also observed by Bordin *et al.* [2023a] in the oxygen-based bottle experiments, mainly due to the euphotic zone rarely reaching the bottom, resulting in a net heterotrophic state prevailing throughout the year, leading to high averaged negative net ecosystem metabolism values. In addition, the results obtained for the summer period (net ecosystem metabolism: -178.4; GPP: 107.9; CR: -289.9 mmol O_2 m^{-2} d^{-1}) and those obtained by Bordin *et al.* [2023a] for the same season show slightly lower rates in their study (Tab. 6) since the oxygen-based bottle method includes only the pelagic EM [Bordin *et al.* 2023a], while the Open Water-method, includes the benthos. A summary of metabolic rates from the literature review for some estuaries worldwide can be seen in Table 5.

Table 5. Net ecosystem metabolism (NEM) and its metabolic rates gross primary production (GPP) and community respiration (CR) for different worldwide estuarine systems. Surveyed values represent mean, or mean (± SD), or mean (± SE%), or the range (minimum – maximum). Values for this study are for Station RS-1, located at the Patos Lagoon Estuary middle section. * denotes that only the pelagic ecosystem metabolism was considered.

Estuary	Lat.	Long.	Season	NEM	GPP	CR	Reference
Patos Lagoon (RS-1), BR	-32.02	-52.10	Annual	-193.87 ± 7.82%	89.70 ± 3.71%	281.64 ± 10.04%	This study
Patos Lagoon (RS-1), BR	-32.02	-52.10	Summer	-135.41 ± 34.7%	63.14 ± 16.9%	199.82 ± 39.88	Bordin *et al.* [2023a]*
Babitonga Bay, BR	-26.23	-48.65	Sum+Spr	-	0.87 – 150	0.75 – 95	Parizzi *et al.* [2016]*
Saquarema Lagoon, BR	-22.91	-42.56	Annual	3	105 ± 65	102 ± 50	Carmouze *et al.* [1991]
Pensacola Bay, US	30.35	-87.19	Spring	-3.3 ± 4.5%	110.2 ± 10.1%	113.5 ± 9.4%	Murrell *et al.* [2018]
Pensacola Bay, US	30.35	-87.19	Summer	0.3 ± 7.7%	283.4 ± 16.5%	283.1 ± 16.9%	Murrell *et al.* [2018]
Grand Bay, US	30.35	-88.46	Annual	~-30 – ~10	~5 – 160	~5 – 170	Caffrey *et al.* [2014]
Apalachicola, US	29.66	-85.00	Annual	~-10 – ~5	~0 – 250	~0 – 300	Caffrey *et al.* [2014]
Weeks Bay, US	30.39	-87.83	Annual	~-30 – ~10	~0 – 400	~0 – 450	Caffrey *et al.* [2014]
Chesepeak Bay, US	37.48	-76.08	Annual	-	~30 – 480	0 – ~200	Kemp *et al.* [1997]
Scheldt Estuary, NL	51.38	3.74	Annual	-39 ± 8	0 – ~300	0 – ~400	Gazeau et. al. [2005]

7.4.1 Metabolism driving factors

7.4.1.1 Short-term variability

Short-term changes in the EM rates were greater than the long-term ones, as observed by Abreu *et al.* [2010] from chl-*a* dynamics in the Patos Lagoon Estuary. The best set of independent variables driving EM rates on small timescales according to the GAM, can be interpreted into short-term hydrodynamic changes. The main driving factor of such changes for the Patos Lagoon Estuary is the shift in wind direction and the passage of southerly cold fronts in the region on a timescale of 6-11 days [Stech & Lorenzetti, 1992; Möller *et al.* 1996]. It changes the direction of waterflow entering/exiting the estuary, which triggers changes in several other parameters and processes. Southerly winds lead to inflow intrusion of saltwater, while northerly ones, to outflow of fresh/brackish water [Möller *et al.* 2001; Fernandes *et al.* 2002]. Southerly winds can promote the intrusion of coastal waters composed by the nutrient-rich (mainly P) Plata Plume Water [Bordin *et al.* 2023a], and release of nutrients from bottom

resuspension and desorption of phosphate [Niencheski *et al.* 1999; Odebrecht *et al.* 2005]. Northerly winds also promote the estuary fertilization with allochthonous nutrients from freshwater sources, mainly N-nutrients and silicate [Abreu *et al.* 1994; Niencheski *et al.* 1999; Fujita & Odebrecht, 2007; Odebrecht *et al.* 2005; Bordin *et al.* 2023a].

Other factor affecting short-term light-availability could be the alternation between sunny and cloudy days, as the Patos Lagoon Estuary region has a high frequency of cloudy/rainy days throughout the year, mainly during the rainy season (late austral winter and spring) and during the passage of cold fronts [Stech & Lorenzetti, 1992]. Although our photosynthetically active radiation data were converted from a pyranometer, i.e., out of the water, Bordin *et al.* [2023a] noted a light limitation to primary production in the Patos Lagoon Estuary throughout the water column that was related to turbidity but may also be related to cloud cover as observed for the Babitonga Bay Estuary [Parizzi *et al.* 2016].

Finally, although not included in the best set of GAM independent descriptive variables, turbidity from resuspension can also be an important factor influencing EM rates in Patos Lagoon Estuary, by contributing with nutrients from wind- and salt wedge-induced resuspension [Niencheski & Windom, 1994; Abreu *et al.* 2017] on the one hand, and on the another, by inducing light-limitation for primary production [Abreu *et al.* 1994; Proença *et al.* 1994; Odebrecht *et al.* 2005].

7.4.1.2 Monthly and seasonal variability

The primary production in the Patos Lagoon Estuary is co-limited by N-nutrients and light availability [Bordin *et al.* 2023a], with more expressive light-limitation upstream, and N-limitation on the southern section, with changes between conditions over the seasons [Odebrecht *et al.* 2005]. The main factor determining those conditions on a seasonal scale, is the rain/freshwater flow regime. The seasonal influence of freshwater flow on EM rates is a common feature of estuaries worldwide, e.g., Babitonga Bay Estuary [Parizzi *et al.* 2016], Saquarema Lagoon [Carmouze *et al.* 1991], Weeks Bay [Caffrey *et al.* 2014],

Pensacola Bay Estuary [Murrel *et al.* 2018], Copano Bay Estuary [Bruesewitz *et al.* 2013], and many others [Cloern *et al.* 2014].

The primary source of nutrients in Patos Lagoon is from the continental discharge [Abreu *et al.* 1994; 2010; Niencheski *et al.* 1994; Windom *et al.* 1999]. During the rainy season (late austral winter/early-spring), heavy rainfall causes a positive anomaly in the river discharge [Marques *et al.* 2009], resulting in large amounts of dissolved inorganic nutrients and organic matter entering the lagoon [Abreu *et al.* 1994; 2010; Niencheski *et al.* 1994; Windom *et al.* 1999]. From the main northern tributary (Guaíba River, Fig. 10c), the freshwater flow takes about two months to reach the estuarine zone during a medium flow rate (2,400 m^{-3} s^{-1}) [Fernandes *et al.* 2002], which is characteristic of this time of year. During the water travel from the northern lagoon towards the estuary, the nutrients are almost exhausted still in the limnic region [Niencheski *et al.* 1999; Windom *et al.* 1999; Odebrecht *et al.* 2005]. From the Patos Lagoon Estuary first biogeochemical zone (salinity 0 to 7) till its third and last zone (salinity > 27), the importance of allochthonous nutrients changes, and the autochthonous supply by the benthic organic matter regeneration becomes more important to maintain the primary production [Windom *et al.* 1999]. However, during large continental discharges, the allochthonous nutrients can play an important role in supplying the primary producers at the Patos Lagoon Estuary [Windom *et al.* 1999], since the freshwater flow dominates the entire estuary during flow rates higher than 3,000 m^{-3} s^{-1} [Möller *et al.* 2001].

During the rainy season in the early austral spring, besides the freshwater to fertilize the Patos Lagoon Estuary with new and regenerated nutrients, there is also an increase of suspended solids [Bitencourt *et al.* 2020], particulate matter [Távora *et al.* 2020; Bortolin *et al.* 2022] and turbidity [Ávila *et al.* 2021]. The turbidity is also increased due to higher wind intensity in the spring [Möller & Castello, 2009] and during high southerly winds [Abreu *et al.* 1994; Niencheski *et al.* 1999; Ávila *et al.* 2021] due to resuspension of particulate matter. Despite the euphotic zone is limited to the first half meter [Niencheski *et al.* 1994] due to high turbidity, new and regenerated nutrients boost the primary production in the surface where light is available [Abreu *et al.* 1994; Odebrecht *et al.* 2005]. Therefore, the most productive season is the austral spring due to the large

freshwater flow, with light limitation being surpassed by the nutrients availability, with high GPP rates on the thin euphotic zone. However, the CR is also high by the phytoplankton blooms and whole community higher metabolism [Hopkinson & Smith, 2005], which is stimulated by the large allochthonous, as well as newly autochthonous organic matter decomposition. As most of the water column is under light-limitation, the contribution of CR overlaps the GPP resulting in the highest net heterotrophic rates as well. Moreover, it is likely the wind-induced resuspension, to increase the CR as the decomposition of resuspended organic matter is favored in the more oxygenated water column. Nutrients were not measured, but the turbidity (not shown in Table 4, but played similarly to salinity in the GAM) could be an indicative of nutrient input by both allochthonous [Niencheski & Windom *et al.* 1994; Abreu *et al.* 2017] and autochthonous sources [Niencheski & Windom, 1994; Abreu *et al.* 1995; Odebrecht *et al.* 2005]. However, such an interpretation may be tricky, because turbidity can play a negative role by light-limitation for primary production [Proença *et al.* 1994].

Under drought conditions such as in the austral summer, despite desorption and intrusions of the Plata Plume Water into the estuary to supply phosphate and to increase the water transparency, the estuary is nutrient-limited [Baumgarten *et al.* 1995], mainly by N-nutrients [Bordin *et al.* 2023a]. The EM decreases from early fall to its minimum in austral autumn and winter, probably drived by the temperature fall [Abreu *et al.* 1994]. Temperature was not among the most important driving factors by the GAM analysis, but was positively correlated with both GPP and CR rates (Fig. 15b), suggesting its influence on the EM processes [Abreu *et al.* 1994], as observed by Caffrey [2004] for 22 U.S. estuaries on a seasonal basis.

7.4.1.3 Interannual/austral spring trends

Similar than in a seasonal basis, the freshwater flow regime was also the main driving factor explaining the variability between years/austral springs, but as a modulating factor, i.e., by extremes of freshwater flow (mainly for GPP, signal from salinity in the GAM). In early November 2016, an extratropical cyclone occurred, causing heavy rainfall in southern Brazil. The freshwater flow of the

Guaíba River (Fig. 2c) during this period was about 12,000 m^{-3} s^{-1}. This high freshwater flow is twice the observed value during the rest of the study period (6,000 m^{-3} s^{-1}) and four times the values observed in spring (3,000 m^{-3} s^{-1}) [Möller *et al.* 2001]. This extreme event was followed by elevated GPP and CR rates in the Patos Lagoon Estuary during the following two months (Fig. 10), which is the Patos Lagoon mean residence time during medium to large freshwater flow [Fernandes *et al.* 2002]. Temperature was the most important factor for CR as the dependent variable, possibly due to an uptrend (+2 °C in year/austral spring averages; Tab. 3] from 2016 to 2021. Temperature is a common factor positively influencing EM rates in the Patos Lagoon Estuary [Abreu *et al.* 2004; Bordin *et al.* 2023a] other estuaries [Caffrey, 2004].

The effects of extreme meteorological events due to climate/weather phenomena, such as the ENSO [Grimm, 2009] and climate change [Stott, 2016] is well stablished. Although we do not have sufficient data to draw conclusions about ENSO processes and characteristics in the Patos Lagoon Estuary in this study, previous studies show the influence of its positive (El Niño) and negative (La Niña) phases on reduced and increased rainfall, respectively, in the southern Brazil [Grimm, 2009], as well as on reduced [Odebrecht *et al.* 2005] and increased [Fernandes *et al.* 2002; Möller *et al.* 1996] freshwater inflow in the Patos Lagoon Estuary on the respective conditions. Moreover, similar values of freshwater flow (12,000 m^{-3} s^{-1}) have been recorded during El Niño periods [Möller *et al.* 1996; Marques, 2012].

Other studies in this area have still shown the effects of increased precipitation rates and freshwater inflow during ENSO periods, on the primary production limiting factors in the Patos Lagoon Estuary. Flood-fresher conditions with higher turbidity [Bitencourt *et al.* 2020; Bortolin *et al.* 2022], nutrients and chl-*a* during periods of El Niño [Abreu *et al.* 2010, 2017; They *et al.* 2015; Seiler *et al.* 2015], and drought-saltiest conditions with lower turbidity [Bitencourt *et al.* 2020; Bortolin *et al.* 2022], nutrients and chl-*a* during La Niña periods [Abreu *et al.* 2010, 2017; They *et al.* 2015; Seiler *et al.* 2015].

These findings suggest that extreme weather/climatic conditions have the potential to affect the EM rates in the Patos Lagoon Estuary. As a consequence,

the distinct climatic periods can lead to many distinct biotic responses [Odebrecht *et al.* 2015], such as in the community composition of macroalgae [Lanari & Copertino, 2017], microalgae [Haraguchi *et al.* 2015; Abreu *et al.* 2017] and bacteria [They *et al.* 2015], impacting the organic matter respiration by the heterotrophic bacteria in the Patos Lagoon Estuary [They *et al.* 2015]. This may lead to the significant EM changes observed in this study and was also observed for the Río de la Plata Estuary [Nagy *et al.* 2002]. Furthermore, the ENSO effects have the potential to affect the fishery stocks and related economic activities [Pereira & D'Incao, 2012; Haimovici & Cardoso, 2017; Möller & Castello, 2009]. Thus, these highlight the importance of long-term monitoring programs that makes possible more robust interannual evaluation, especially those related to climate changes.

7.4.1.4 Methodological considerations

In the present study, the application of the Open Water-method represented a powerful alternative to the oxygen-based bottle experiment, firstly because it makes possible to carry out a long-term monitoring, and secondly because it avoids the container artifacts and error propagation related to incubations [Staehr *et al.* 2012]. Nevertheless, this technique also needs constant maintenance and calibration of the probes, and finally the data mining for quality control, which usually generates incomplete time-series that can hamper some statistical analysis and the adequate answer to research questions. Coloso *et al.* [2008], Needoba *et al.* [2012], Staehr *et al.* [2012] discusses in detail about the errors and uncertainties of this method, especially the need for water column and time homogeneity of water mass passing through the oxygen probe, properly addressed here. However, since the Station RS-1 probes were at the surface, they may not capture the benthic metabolism, as pointed out by Murrel *et al.* [2018] for the Pensacola Bay Estuary at their deeper channel-site station during vertical stratification.

Other source of error can still come from nitrification, since this process consumes O_2 [Gazeau *et al.* 2005], and the Open Water-method does not distinguish it from aerobic respiration. This could occur mainly in ammonium-rich

estuaries, as observed for the Patos Lagoon Estuary during summer periods with mean values varying from 2.6 µM [Bordin *et al.* 2023a] to 25.6 µM [Fujita & Odebrecht, 2007]. In this season, the sewage of Rio Grande City [Marreto *et al.* 2017] is retained in the estuary due to the drought conditions [Baumgarten *et al.* 1995] and the marine water inflow, that prevents the outflow of the ammonium-rich estuarine water [Abreu *et al.* 1995; Odebrecht *et al.* 2015]. On the other hand, the lower DO during this season (Tab. 3) hampers the nitrification, helping to maintain the high-ammonium and low-nitrate concentrations [Niencheski *et al.* 2006], not being a significant source of DO variation.

Thus, to apply the Open Water-method, it is very important to consider its premises and limitations to choose a suitable site for the EM evaluation, e.g., at the center of well-mixed estuaries far from freshwater sources and less influenced by the tidal exchanges [Caffrey *et al.* 2014]. That was the reason for choosing a single Station (RS-1), due to its location in the mid-estuary second biogeochemical zone [Windom *et al.* 1999], far from direct continental and marine influence. In systems with vertical stratification, the deployment of probes also at the bottom layer is desirable to produce more accurate estimates. Moreover, in systems with lateral stratification, and/or formed by distinct zones and waterbodies, the deployment of several probes at different sites is desirable to make possible spatial integrations [Staehr *et al.* 2012; Caffrey *et al.* 2014].

The GAM method also has some premises, such as the number of non-linear descriptive variables, that should not exceed three [Zurr, 2012]. By limiting the number of non-linear parameters, the model had reduced the adjusted R^2 and dev.exp. Its R^2 and dev.exp increased as temporal factors were being added to the models, suggesting that when the iterations are performed with the whole dataset (i.e., in the daily analysis) that contains more variance, the model reduces its capacity to explain the variability of the dependent variable, reaching low parameters values. As the temporal factors were being included, the model improved its fit, reaching to greater R^2 and dev.exp. Finally, it is likely that the absence of dissolved inorganic nutrients, an important driving factor for the metabolic process [Staehr *et al.* 2012; Caffrey *et al.* 2014], which can be limiting for the primary producers at the Patos Lagoon Estuary [Abreu *et al.* 1994; 1995; Bordin *et al.* 2023a], has reduced the model fit, differently from Bordin *et al.*

[2023a], which found much higher model performance by including the nutrients to explain the pelagic EM rates also by the GAM.

7.5 Conclusions

The EM in the RS-1 station was consistently net heterotrophic throughout the year. The EM on a daily basis was mainly controlled by the short-term wind-induced hydrodynamic variability by shifts between inflow/outflow of marine/estuarine waters, and photosynthetically active radiation, while on longer timescales by the freshwater flow regime including turbidity and temperature. Salinity was modulated by the freshwater flow and winds, which controls the inflow and outflow of marine saltwater and estuarine fresh/brackish water, respectively. In turn, it also modulates the turbidity (plus the wind-induced particulate matter resuspension). Although spatially limited, the use of the Open Water-method to estimate the total EM at the Patos Lagoon Estuary, was useful for evaluate the rates of important processes and its trends from daily to interannual/austral spring timescales, and also in determining the main driving factors that modulate these oscillations.

This study represents the first complete total EM assessment for the Patos Lagoon Estuary and demonstrates the importance of EM evaluations in these and other coastal systems. In addition, the results highlight the importance of long-term monitoring programs based on continuous and automatized probe-systems, which makes possible to observe processes and trends in different timescales, especially at very short (hourly) and medium/long term (interannual and interdecadal), and especially in the context of climate changes. Therefore, it is emphasized the need for further monitoring systems in this area, covering more sites and depths, to better comprehend the EM and the overall biogeochemistry dynamics of the system in an integrated manner.

Capítulo VIII:

Fluxos de nutrientes, balanço de massa e metabolismo líquido do ecossistema em um sistema costeiro brasileiro sob condições de seca

O terceiro manuscrito, em síntese, apresenta o balanço de massa de água, sal e nutrientes, os fluxos dos nutrientes entre os compartimentos terrestre, a Lagoa dos Patos, o estuário da Lagoa dos Patos, e oceano costeiro adjacente. Apresenta ainda o potencial de produção primária, o metabolismo líquido e o balanço entre fixação de nitrogênio e desnitrificação, para os diferentes compartimentos acima mencionados. Este método permitiu uma visão integrada espacialmente do metabolismo líquido do estuário da Lagoa dos Patos. De autoria de Luís Henrique Bordin, Eunice da Costa Machado, Carlos Rafael Borges Mendes, Elisa Helena Leão Fernandes e Carlos Augusto França Schettini, intitulado "***Nutrient fluxes, budgets and net ecosystem metabolism in a Brazilian coastal system under drought conditions***", encontra-se em revisão no periódico "***Estuarine, Coastal ans Shelf Science***", submetido em julho de 2023. A análise e interpretação dos resultados, e a redação deste manuscrito foram feitas por mim, como parte da minha tese de doutorado. Eunice

da Costa Machado fez toda a supervisão para que chegássemos à conclusão desse estudo. Carlos Rafael Borges Mendes contribuiu como especialista em ecologia marinha. Elisa Helena Leão Fernandes e Carlos Augusto França Schettini contribuíram como especialistas em oceanografia física e modelagem numérica.

Graphical Abstract

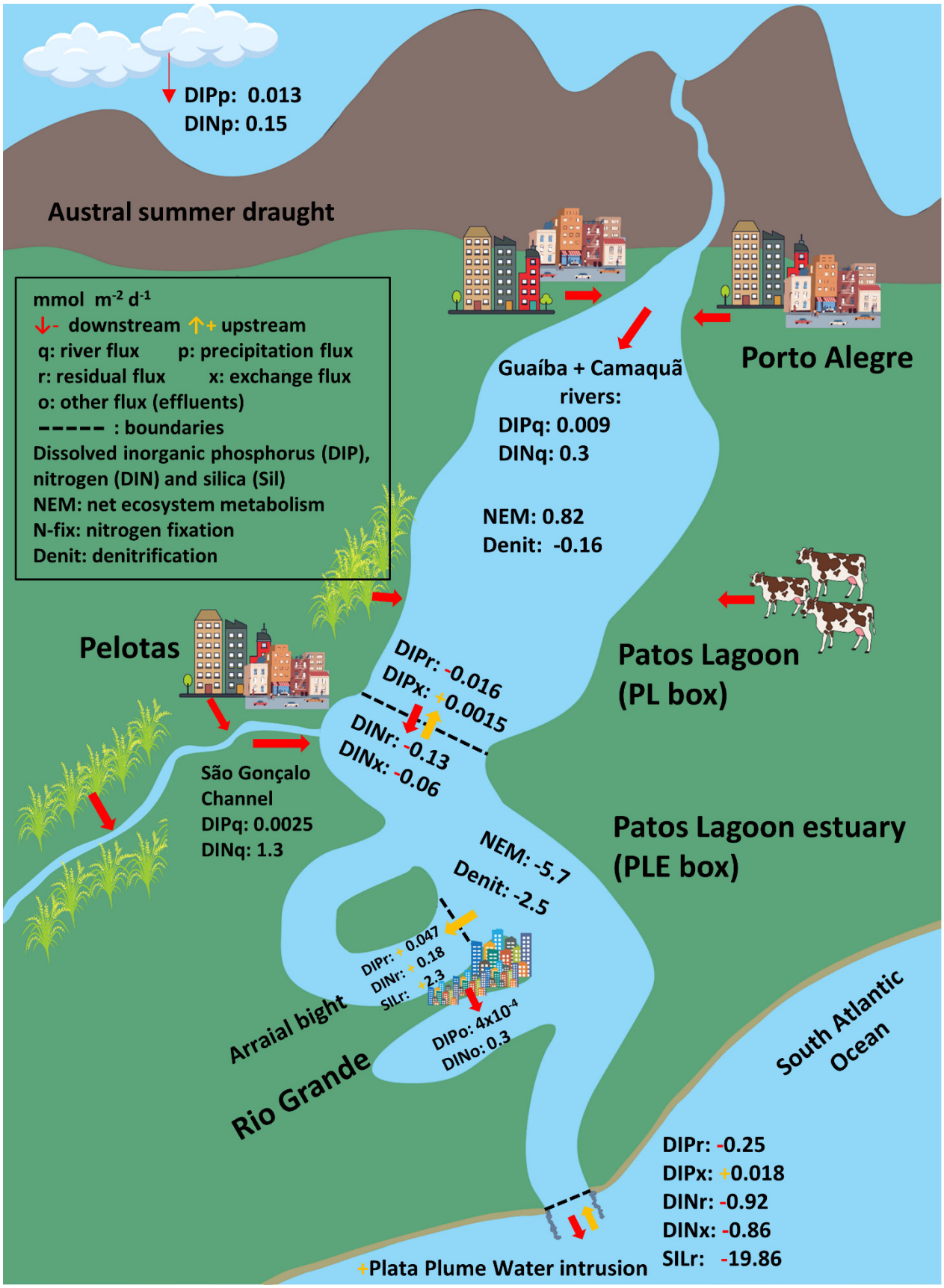

Abstract

Integrated dissolved inorganic nutrient fluxes (nitrite, nitrate, ammonium, phosphate and silicate) between Patos Lagoon estuary (PLE), Brazil, and the inner continental shelf of the southwest Atlantic Ocean, were estimated from averaged water column nutrient concentrations and water fluxes (method 1 – M1). Daily surveys were carried out for 30 days, spanning from Feb-22 to Mar-23 of 2021 during late austral summer drought, at two stations — one next to the estuary mouth, the other in the inner estuary, at the interface between the estuary main channel and a shallow embayment called the Arraial bight. On average, PLE delivered dissolved inorganic phosphorus (DIP), nitrogen (DIN) and silicate outfluxes to the adjacent continental shelf at rates of 22.4 ± 596.1, 89.8 ± 207.3 and 1,715.9 ± 3,283.2 x10^3 mmol m^{-2} d^{-1}, respectively. Budgets for DIP and DIN were computed by the LOICZ box model approach (method 2 – M2) considering Patos Lagoon divided into its limnic (fresh, mean salinity 2 psu) and estuarine (brackish, mean salinity 18.5 psu) regions. The residual fluxes for DIP and DIN from PLE to the inner continental shelf were similar to those of M1, but the complete budget (M2) revealed that PLE also imported DIP, at a positive exchange rate between PLE and coastal waters. There is evidence that DIP is supplied by Plata Plume Water. Net ecosystem metabolism (NEM) and N-fixation - denitrification were assessed through the LOICZ budgets for DIP and DIN, respectively. Denitrification prevailed in both limnic and estuarine regions. Estimated NEM indicated weak autotrophy in the limnic region, and net heterotrophy in the estuarine region. The net heterotrophy in the estuarine region was mainly attributed to nitrogen limitation due to low allochthonous supply by river discharge, and N-loss by denitrification during austral summer drought conditions.

8.1 Introduction

Estuaries are key environments between land and ocean, as they are responsible for the cycling of elements from adjacent environments [Bianchi 2007], contributing significantly to mass balance, e.g., of nutrients [Zeldis & Swaney 2018; Dan *et al.* 2019] and carbon [Laruelle *et al.* 2013; Yao *et al.* 2022]. Along an estuary, nutrients from different origins are transformed by complex and multi-interactions of physical, chemical, biological, and geological processes [Bianchi 2007], which in turn are modulated by a set of physical forcing factors such as river discharge, tides, waves, light intensity, water temperature, and salinity [Bianchi, 2007; Bukaveckas *et al.* 2018].

The increasing world human population has led to growing intensive land-use, fertilization and soil leaching with a consequent increase in suspended solids, nutrients and organic matter ending in rivers, estuaries and the coastal ocean, causing many disturbances, e.g., to biological metabolism [Damashek & Francis 2018; Bordin *et al.* 2023a,b], eutrophication [Wurtsbaugh *et al.* 2019], and dead zones [Altieri & Diaz 2019; Cabral & Fonseca 2019]. Extreme hydrologic conditions due to climate change have also been impacting element cycling in estuarine environments [Yao *et al.* 2020]. Due the increasing vulnerability of coastal areas to global changes, many efforts have been gathered to understand the fluxes and cycling of nutrients between land and ocean [Gordon *et al.* 1996; Bukaveckas *et al.* 2017; Jutras *et al.* 2020].

Although the Patos Lagoon (PL) and its estuarine zone (PLE) have been intensively studied for the last fifty years, with many studies on hydrodynamics [Costa *et al.* 1988; Möller *et al.* 2001; Franzen *et al.* 2023], biogeochemical dynamics [Niencheski *et al.* 1999; Odebrecht *et al.* 2015; Bordin *et al.* 2023a], nutrient fluxes between water and sediments [Niencheski & Jahnke, 2002], and from freshwater to the estuarine zone [Niencheski *et al.* 1994], none have reported these fluxes between Patos Lagoon estuary (PLE) and the adjacent coastal ocean and its bights, nor net ecosystem metabolism integrated over the system. Therefore, the present study intended to: i) estimate fluxes of dissolved inorganic nutrients between PLE and Arraial bight, and between PLE and the adjacent continental shelf; ii) estimate nutrient (DIP and DIN) budgets between land, PL, PLE and the adjacent coastal zone; iii) estimate net ecosystem

metabolism (NEM) and N-fixation - denitrification (N-fix – denit) for PL and PLE; and iv) estimate the potential for primary production (PP) in PL, PLE and the coastal zone.

8.2 Patos Lagoon estuary hydrodynamics and biogeochemical features

Located in southern Brazil, Patos Lagoon (PL) is the largest choked lagoon of South America [Kjerfve 1986], connected to the South Atlantic Ocean by a narrow channel (~550 m) [Cunha & Calliari, 2009; Franzen *et al.* 2023]. Patos Lagoon receives water from a drainage basin of 200,000 km^2, with the main tributaries being the Guaíba and Camaquã rivers and the São Gonçalo Channel, with a combined mean annual discharge of 2,400 $m^3\ s^{-1}$ [ANA 2023]. Drought periods occur during summer-autumn, while peaks of river discharge occur during winter-spring [Vaz *et al.* 2006].

These rivers drain effluents from many inhabited areas. The most densely populated region is in its northern portion, where the city of Porto Alegre is located, with ~2,800 inhabitants/km^2; Pelotas and Rio Grande are the main cities in the southern area with 203 and 72 inhabitants/km^2, respectively [IBGE 2023]. Despite being less populated, the southern region receives effluents from agricultural (mainly rice crops), harbor and industrial activities, such as from fertilizer factories on the margins of PLE. The wastewater causes contamination with organic compounds and nutrients, leading to eutrophication [Baumgarten *et al.* 1995; Baumgarten 2010; Wallner-Kersanach *et al.* 2016; Bordin *et al.* 2023a]. Nutrient depuration is favored in the main PLE body, where a strong dynamic occurs in the deeper channels [Marreto *et al.* 2017; Wallner-Kersanach *et al.* 2016].

The hydrodynamics of PLE are governed by river discharge and local and remote winds due to its microtidal regime [Möller *et al.* 1996]. When river discharge is less than 2,000 $m^3\ s^{-1}$, the system is controlled by wind, and when it is higher than 2,000 $m^3\ s^{-1}$, it is controlled by river discharge itself. During high river discharge, only intense SW winds can reverse the outflow condition. The predominant wind condition in PL is from the NE [Möller *et al.* 2001].

Marine water inflow into the estuary is SW wind-induced [Möller *et al.* 2001; Möller & Fernandes 2010], which may promote the intrusion of the nutrient-rich

Plata Plume Water [Braga *et al.* 2008] that spreads along the Southern Brazilian Continental Shelf under SW winds [Möller *et al.* 2008; Bordin *et al.* 2019], and could be an important fertilizing process for PLE under these conditions [Bordin *et al.* 2023a]. On the other hand, estuarine water outflow is NE wind-induced [Möller & Fernandes 2010]. This ebb condition reduces the salinity in PLE by bringing freshwater and nutrient depleted waters from the northern limnic region of PL [Niencheski *et al.* 1999; Odebrecht *et al.* 2005].

Nutrients, chlorophyll-a (chl-a; an index of primary producer biomass) and PP rates are higher and more variable during austral spring and summer, decreasing throughout autumn and reaching their lowest values during winter, due to lower temperatures and lower light intensity. Higher turbidity from river discharge during the rainy season causes a decrease in PP rates [Abreu *et al.* 1994; 1995; Bordin *et al.* 2023a,b]. Aquatic NEM in shallow areas of PLE is considered autotrophic most of the year, and heterotrophic during winter, when organic matter from senescent seagrass is regenerated in sediments [Abreu *et al.* 1994], while in deeper areas such as in channel-sites, the system is predominantly heterotrophic [Bordin *et al.* 2023a,b]. The mean depth of PL is about 5 m [Calliari *et al.* 1997], and ~80% of the area in the southern estuarine region is less than 1.5 m [Seeliger 2001]. In its channel-sites, however, the depth reaches up to 16 m. Different zones are characterized along the estuarine saline gradient by distinct biogeochemical trends, which influence nutrient cycling [Windom *et al.* 1999].

8.3 Material and methods

8.3.1 Fieldwork

Daily samplings and in situ experiments on pelagic metabolism were carried out at stations RS-2 (mouth: 32°08'04.5"S 52°05'52.9"W) and RS-1 (bight: 32°01'24.6"S 52°06'19.8"W) during 30 days of the late austral summer spanning from Feb-22 to Mar-23 2021. Station RS-2 is a channel-site station with 12 m of depth, located next to the Molhes da Barra jetties, in the main PLE access channel (Fig. 2). Station RS-1 is a shallow embayment-site (4.5 m), located next to the city of Rio Grande, which is subject to sewage at the margins.

Intermediate depth (mean 7 ± 2 m) was defined according to the halocline observed by a JFE-Advantech model AAQ-Rinko 176 multiparametric sonde, based on temperature and salinity vertical profiles. Water was collected with a Niskin bottle at surface (0.5 m), intermediate (only at station RS-2), and bottom layers (12 m), and respective aliquots separated in polycarbonate bottles for determination of dissolved inorganic nutrients (nitrite, nitrate, ammonium, phosphate, and silicate) and stored in a thermal box with ice. Cross-section water flux at station RS-2 was measured with a RDI Workhorse 1200 kHz Acoustic Doppler Current Profiler (ADCP) with bottom tracking.

In the laboratory, water samples were filtered with Whatman GF/F filters (0.70 µm porosity), which were then used to determine the concentrations of dissolved inorganic nutrients (nitrite, nitrate, phosphate and silicate) by the spectrophotometry technique using an AA3 HR SEAL Analytical AutoAnalyzer, according to Grasshoff *et al.* [2007]; and ammonium, separately, according to Koroleff & Palmork [1972]. The detection limits were 0.006 µM for nitrite, nitrate and ammonium, and 0.016 µM for silicate and phosphate. Further details of fieldwork are presented by Bordin *et al.* [2023a].

8.3.2 Delft3D-FLOW Model – Patos Lagoon

Numerical experiments were designed using the Delft3D numerical model. Delft3D is a modular software, and the D-FLOW module [Deltares Systems 2019] was applied in this study. D-FLOW has been successfully applied in several studies to evaluate hydrodynamics and transport phenomena [Pokavanish & Alosairi 2014; Martyr-Koller *et al.* 2017], in shallow seas, coastal areas, estuaries, lagoons, lakes and rivers. D-FLOW calculates the non-steady flow and transport phenomena that result from tidal and meteorological forcing on a rectilinear or curvilinear boundary-fitted grid, following the σ coordinate approach for 3D simulations, solved by Navier-Stokes equations for incompressible free surface flow. Its time discretization uses a semi-implicit scheme and a finite spatial volume [Deltares Systems 2019].

A representative regular mesh (Fig. B.1) of the entire PL was created to discretize the domain. To better solve the processes in the estuarine region, a high-resolution mesh was applied in these regions, where the mesh cells were

irregularly spaced, ranging from 0.00002 Km^2 in the estuarine region, to 8.06 Km^2 in the oceanic boundaries and northern PL, totaling 261 cells in the X-direction and 279 cells in the Y-direction. Five σ layers were applied for vertical discretization.

Calibration (February) and validation (September) experiments were carried out in 2019 and, in both cases, the model open boundaries were forced with the respective tides, winds and river discharge for the period. For astronomical tides, hourly water level data were obtained from OSU TPXO Tide Models for the Patagonian barotropic tide regional model [Egbert *et al.* 2002]. Hourly water level data of meteorological tide, temperature and salinity were downloaded from the Copernicus Marine Service (www.resources.marine.copernicus.eu/products), Operational Mercator Global Ocean Analysis and Forecast System, PHY_001_024 model. Offshore boundary conditions were defined by the temperature and salinity in each of the five σ layers, and water level from the sum of astronomical and meteorological tides. For the meteorological forcings, wind and atmospheric surface pressure time-series were applied, obtained from the European Center for Medium-Range Weather Forecasts [ECMWF 2023], ERA-5 reanalysis data (www.ecmwf.int/en/forecasts/datasets/reanalysis-datasets/era5). Hourly river discharge was considered for Guaíba River (sum of Jacuí, Taquarí, Caí and Sinos rivers) and Camaquã River, obtained from ANA - Brazilian National Water Agency (www.snirh.gov.br/hidroweb), and São Gonçalo-Channel, obtained from the Coastal and Estuarine Oceanography Lab, FURG. All setup files for the Patos Lagoon Delft3D-FLOW model and files to run a simulation example, can be download from the repository at www.github.com/graoceano/Patos-Lagoon-Delft3D-FLOW-model.

8.3.3 Hydrodynamic model assessment

The hydrodynamic model was calibrated by varying wind drag coefficients, friction law coefficient, roughness formula, roughness coefficients, horizontal and vertical eddy viscosity and diffusivity, and model for 3D turbulence. The best agreement between model results and the measured data was observed for wind drag coefficients of A $1.55x10^{-3}$ at 0 m/s, B $8.55x10^{-3}$ at 19.22 m/s and C 8.55 $x10^{-3}$ at 19.22 m/s (coefficients between 0 and 19.22 m/s are automatically interpolated), White-Colebrook roughness formula, roughness coefficient of $1x10^{-}$

^{5}, horizontal eddy viscosity of 11.25 m^2/s and diffusivity of 25 m^2/s, and vertical eddy viscosity of $1x10^{-4}$ m^2/s and diffusivity of $1x10^{-5}$ m^2/s. The best model for 3D turbulence was the algebraic. The best set of physical parameters was applied for model validation.

Validation of the hydrodynamic model was carried out by comparing measured and modeled water levels (Fig. B.2) and longitudinal current velocities (Fig. B.3) with available data for the same locations and period. Two points were used for water level, one located in the lagoonal area (*SL, Fig B.2a) and the other in the main PLE access channel (*RGP, Fig B.2b). Longitudinal current velocity used current data from *Sistema de Monitoramento da Costa Brasileira* [SiMCosta 2023; www.simcosta.furg.br] for *RS-1, *RS-2, and *RS-4 meteoceanographic buoys (Figs. B.3a, B.3b and B.3c, respectively), the first two located in the estuarine region, and the last in the adjacent coastal ocean (Fig. 2d).

The ability of the hydrodynamic model to reproduce the measurements was quantitatively evaluated by comparing measured and computed estuarine water levels and current velocities. The methods Relative Mean Squared Error (RMSE) and Relative Mean Absolute Error (RMAE) [Walstra *et al.* 2001] were chosen for comparing the data. According to Van Rijn *et al.* [2003], the RMAE measures whether the computed values fall within the envelope of the measurement error and is less susceptible to outliers than the RMSE. Walstra *et al.* [2001] proposed five ranges of RMAE classification: excellent (<0.2), good (0.2 – 0.4), reasonable (0.4 – 0.7), poor (0.7 – 1.0) and bad (>1.0). The RMSE/RMAE for water level were 0.04/0.06 at *SL and 0.09/0.13 at *RGP (Fig. B.2a and B.2b, respectively); and for longitudinal current velocity were 0.06/0.15 at *RS-1, 0.16/0.17 at *RS-2 and 0.25/0.35 at *RS-4 (Fig. B.3). Therefore, the model was considered able to satisfactorily represent PL hydrodynamics. The RMAE values for the calibration exercise are presented in Table B.1.

8.3.4 Data analysis

Although water fluxes were estimated at station RS-2 with an ADCP during the sampling campaign, they were not measured at station RS-1. Thus, the use

of water flux estimates from numerical modeling for both stations is justified. Hourly water flux timeseries were obtained from the D-FLOW output data for the sampling period (Feb-22-2021 to Mar-23-2021), in the cross-sections of the channel where stations RS-2 and RS-1 (Fig. 2d) are located. Water flux from the D-FLOW simulation was processed with the Delft3D post-processing tool QUICKPLOT version 2.15 [Deltares Systems 2014]. Time averaged dissolved inorganic nutrient (nitrite, nitrate, ammonium, phosphate and silicate) fluxes were estimated by interpolation (method 1: M1), as follows (Eq. 1):

$$\text{Flux} = \frac{1}{n}\sum_{i=1}^{n} Q_i C_i \qquad \text{(Eq. 1)}$$

where C_i is the instantaneous concentration (mol m^{-3}; from in situ sampling) of the nutrient at time $_i$, Q_i is the water flux (m^3 s^{-1}; from D-FLOW simulation) at time $_i$, and n is the number of samples.

8.3.5 LOICZ biogeochemical model approach

Water, salt, DIN and DIP concentrations were applied to the LOICZ (Land Ocean Interaction in the Coastal Zone) biogeochemical mass-balance model approach [Gordon *et al.* 1996]. Patos Lagoon was divided into two boxes for modeling (Fig. 2c), one to represent the limnic region with salinity < 3 psu (PL box), and another to represent the estuarine region with salinity > 3 psu (PLE box). The boundary between boxes was defined at Ponta da Feitoria, which is considered the average limit for seawater intrusion into the system [Möller & Castaing 1999]. Water column mean salinity, DIN and DIP were used to apply the one-layer model, assuming the system as vertically homogenous and in steady-state. This approach is commonly implemented for systems that do not have a defined vertical physical structure [Gordon *et al.* 1996], as observed for PLE [Möller & Castaing 1999; Möller *et al.* 2001].

The area and volume of the two boxes were obtained using the Delft3D pre-processing tool QUICKIN version 4.00 [Deltares Systems 2020], from the bathymetric regular mesh (Section 3.2.). River discharge data was obtained from the ANA website (www.snirh.gov.br/hidroweb) for Jacuí, Caí, Taquarí and Sinos stations, which together represent the Guaíba River), and the Camaquã River,

for the austral summer period (Dec-21 to Mar-21) from 1991 to 2021. The discharge for the São Gonçalo Channel was estimated based on daily-averaged climatological data for the austral summer period. Mean data of climatological normal precipitation and evaporation (1981-2010) for the austral summer period was acquired from INMET [INMET 2023; https://portal.inmet.gov.br/normais], for stations located in the cities of Porto Alegre (n° 83967) and Pelotas (n° 83985) to represent the PL box, and the cities of Pelotas and Rio Grande (n° 83995), to represent the PLE box. No fluxes from groundwater were considered.

Non-conservative budgets were calculated for DIP and DIN, considering external (rivers, wastewater and ocean) and internal concentrations used to estimate fluxes (method 2: M2) of sources and sinks of these elements. Only data representative of summer drought periods was selected. Nutrient data for Guaíba and Camaquã rivers (PL box region) and for the PL box internal concentrations were obtained from data collected by *Programa Pró Mar de Dentro* (surface and bottom) on monthly cruises carried out in Feb-1999, Mar-1999 and Jan-2000 with one station at each river (n = 12), and six stations (n = 36) disposed over the N-S axis of PL. Data for river discharge were the sum of those of Guaíba and Camaquã rivers, and nutrient concentrations were the mean (the sum of all concentrations of all datasets, divided by the n) of all samples for the respective stations on both rivers. Nutrient data from *Projeto Espinha* sampled during Jan-1986 at thirty-seven stations (surface and bottom) (n = 74) distributed over the N-S and W-E axes of PL, were combined with the former dataset and then averaged to represent the internal concentration of PL box (total n = 110). The datasets were described by Pereira [2003], and a map with the stations is presented in Figure B.4. DIP and DIN for the São Gonçalo Channel inputs were averaged from data sampled at five stations (n = 5) close to the mouth [de Souza 2015]. PLE internal nutrient concentrations were the averages of the dataset (total n = 188) composed of *Programa Pró Mar de Dentro* (two stations, n = 12)*, Projeto Espinha* (thirteen stations, n = 26) and the current study (two stations, samples with salinity < 30, n = 92). The coastal concentrations were the averages of the dataset of the current study (samples with salinity > 30 psu, only from Station RS-2, n = 58). Concentrations of DIP and DIN in rainfall were the annual averages of three stations at the city of Porto Alegre (n = 36) and four stations at the city of Rio

Grande (n = 48) for the PL box (total n = 74) and the averages for the Rio Grande stations only for the PLE box [Casartelli *et al.* 2008].

To represent wastewater disposal, since treated and untreated effluents from the most populated region next to the PL box (city of Porto Alegre) flow into Guaíba River, it was assumed that concentrations for this river are already composed of natural and anthropogenic inputs. The same approach was considered for the São Gonçalo Channel, in the PLE box. For Rio Grande city wastewater, nutrient data presented by Seiler *et al.* [2020] for the Rio Grande Effluent Treatment Stations (ETE Navegantes and ETE Pq. Marinha) was applied, with discharge flows of 0.15 and 0.05 $m^3\ s^{-1}$, respectively. To represent point source and diffuse effluent disposal of seventeen sites on the margins of the city of Rio Grande [Baumgarten *et al.* 2021], the same nutrient concentrations as for the ETEs were considered, with an additional water flux of 0.01 $m^3\ s^{-1}$, totalizing 0.21 $m^3\ s^{-1}$. These water fluxes and nutrient concentrations were inserted as other river discharge and sources of nutrients, respectively, for the PLE box. The budgets were computed with the LOICZ budget toolbox [Gordon *et al.* 1996; https://nest.su.se/mnode/Toolbox/LOICZ_Toolbox.htm].

8.3.6 Metabolic processes and potential for primary production

NEM and N-fix – denit were assessed by the LOICZ model [Gordon *et al.* 1996]. NEM is ΔDIP multiplied by the C:P ratio. N-fix – denit is the difference between ΔDIN and the expected ΔDIN, which is the product of the N:P ratio (estimated as the mean of DIN/DIP) and ΔDIP [Gordon *et al.* 1996]. Input data for PL and PLE boxes are presented in Table B.2. Seagrass NEM for the PLE box was computed considering the *Ruppia maritima* C:P ratio of 457 [Atkinson *et al.* 1983], since it is the main species and covers an area of 120 km^2 [Costa *et al.* 1997]. For the phytoplankton in the remaining area (759 km^2), the C:P ratio of 106 [Redfield 1963] was applied. NEM was spatially integrated by weighted average. Since seagrass does not represent a significant coverage in the PL box, due to its greater mean depth, seagrass NEM wasn't computed for this compartment.

The potential for PP was estimated for the adjacent coastal zone based on limiting nutrient (DIN) flux and Redfield Ratio stoichiometry [Redfield *et al.* 1963],

assuming that all DIN content was transformed into algae biomass. It was computed for both the limnic (PL box: 9,660 km^2) and estuarine (PLE box: 879 km^2) regions, and for the adjacent continental shelf along a 0.1 x 90 km (9 km^2) strip of coastline.

8.4 Results

8.4.1 Water and nutrient fluxes

The average river discharge from the sum of Guaíba and Camaquã rivers, which represents 86% of total river discharge to PL [Niencheski *et al.* 1994], was 501 m^3 s^{-1} for the austral summer of 2021, which represents ~8% of climatology flow frequency (Fig. B.5). Based on river discharge, it was assumed that the estimates are representative of 8% of the time.

The integrated water and nutrient fluxes at the station RS-2 cross-section show a predominance of outflow for all variables (Tab. 6, Fig. 15). Considering station RS-2 as representative of the PLE endmember, the estimated fluxes represent the exchange of water and nutrients between the estuary and the continental shelf. Silicate was the nutrient with the largest export flux, followed by the sum of N-nutrients (DIN; mostly composed of ammonium and nitrate), and then by DIP.

Table 6. Mean (±SD) water flux (m^3 s^{-1}) and dissolved inorganic nutrients (nitrite, nitrate, ammonium, DIN, DIP and silicate) fluxes (mmol s^{-1} and mmol m^{-2} d^{-1}), in the cross-sections of stations RS-2 (Patos Lagoon Estuary access channel) and RS-1 (Arraial bight access channel). Data from Feb-22-2021 to Mar-23-2021 (late austral summer), Patos Lagoon Estuary, Brazil. Sample *n*: RS-2 = 90; RS-1 = 60. Positive/negative values indicate inflow/outflow conditions.

Station	Water	Nitrite	Nitrate	Ammonium	DIN	DIP	Silicate
RS-2							
mmol s^{-1}	-1,900 ± 4775	-171.0 ± 513	-4,865.1 ± 11,119	-5,494.4 ± 13,057	-10,602.7 ± 24697	-2,685.5 ± 7043	-20,208 ± 38,780
mmol m^{-2} d^{-1}	-	-0.016 ± 0.05	-0.47 ± 1	-0.54 ± 1.3	-1.04 ± 2.4	-0.26 ± 6.9	-19.86 ± 38
RS-1							
mmol s^{-1}	327 ± 495	16.1 ± 35	623.4 ± 1226	1,087.5 ± 1707	1,710.9 ± 1793	476.6 ± 753	23,55.3 ± 37727
mmol m^{-2} d^{-1}	-	1.6e^{-3} ± 3x10^{-3}	0.062 ± 0.12	0.1 ± 0.16	0.18 ± 0.17	0.047 ± 0.07	2.3 ± 3.7

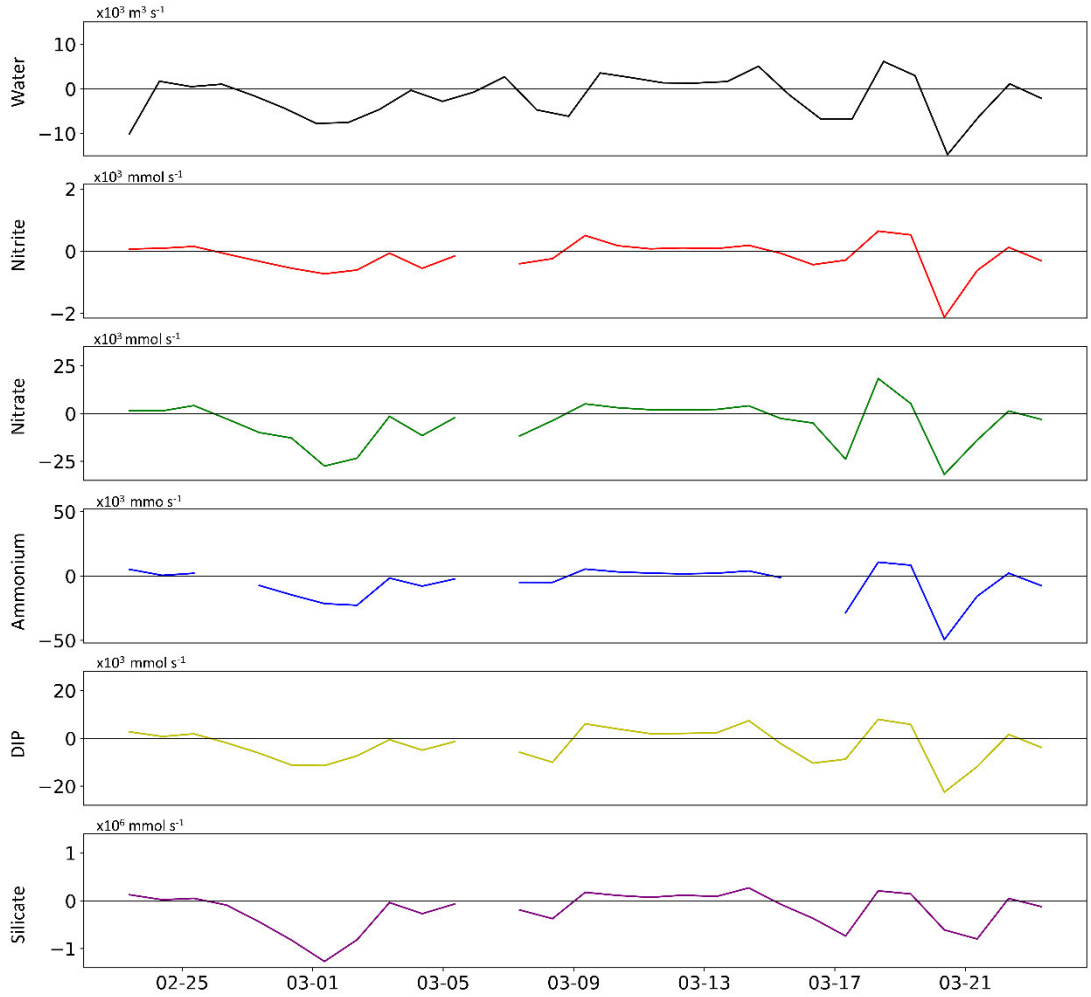

Figure 15. Instantaneous water flux and dissolved inorganic nutrients (nitrite, nitrate, ammonium, DIP and silicate) fluxes, in the cross-sections of station RS-2 (main Patos Lagoon estuary access channel). Data from Feb-22-2021 to Mar-23-2021 (late austral summer), Patos Lagoon estuary, Brazil. Sample $n = 90$. Positive/negative values indicate inflow/outflow conditions. There was no sampling on 03-06-2021.

The integrated water and nutrient fluxes in the cross-sections of station RS-1 show the predominance of inflow from the main estuary into the Arraial bight. The magnitudes of both fluxes were lower than at station RS-2, but the relative contribution of each nutrient followed the same magnitude as at station RS-2 (Tab 6, Fig. 16).

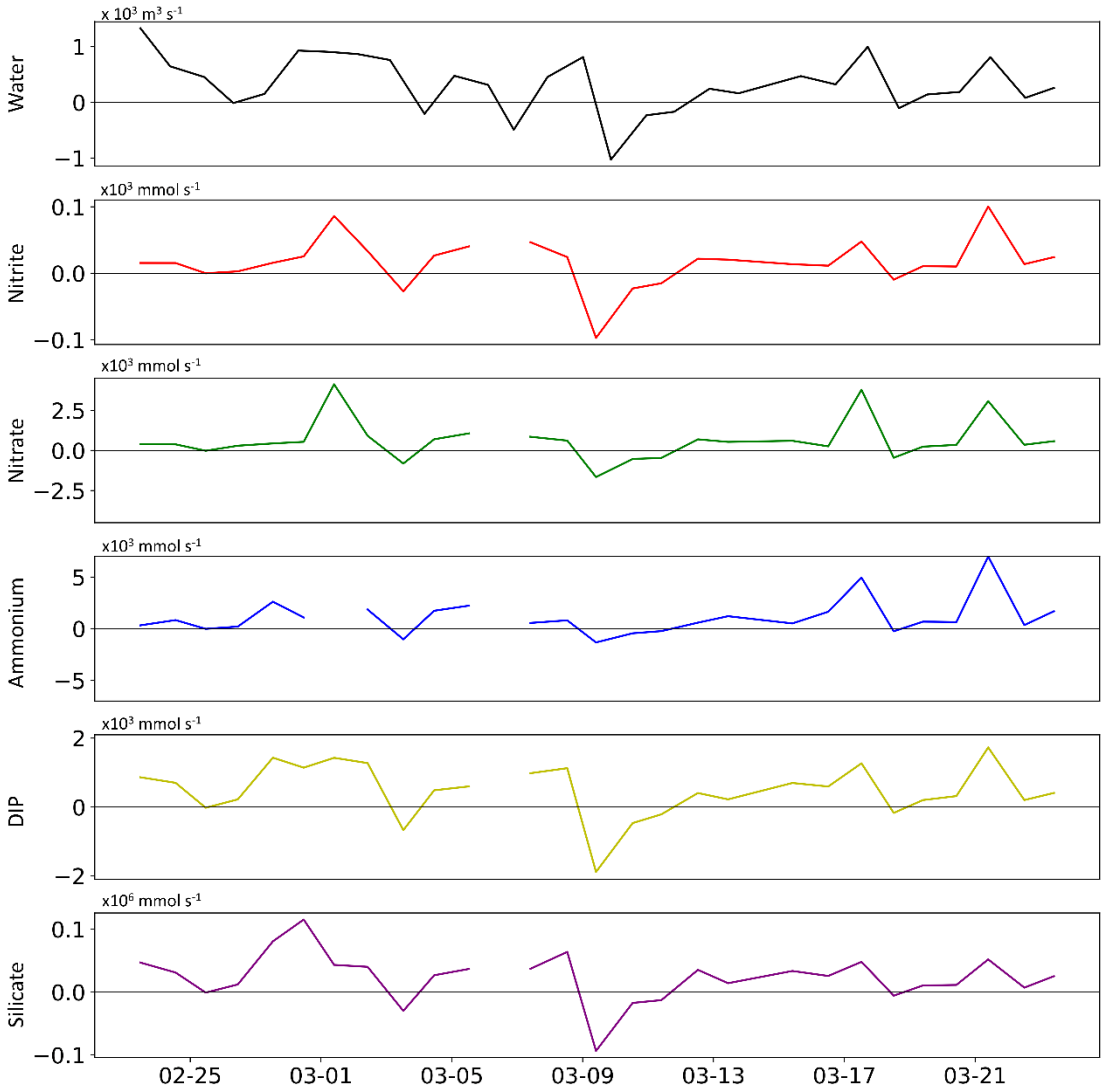

Figure 16. Instantaneous water flux and dissolved inorganic nutrients (nitrite, nitrate, ammonium, DIP and silicate) fluxes, in the cross-sections of station RS-1 (Arraial bight access channel). Data from Feb-22-2021 to Mar-23-2021 (late austral summer), Patos Lagoon estuary, Brazil. Sample n = 60. Positive/negative values indicate inflow/outflow conditions into the Arraial bight. There was no sampling on 03-06-2021.

Nutrients vs. salinity boxplots (Fig. 17) and scatterplots (Fig. B.6) indicate a clear negative relationship only for silicate (r = -0.84; p = 1.2x10^{-38}), with the highest concentrations being related to low salinity, and lower concentrations to salty waters, as fresh is being mixed with coastal waters. For N-nutrients, only nitrate (r = -0.37; p = 4.4x10^{-6}) and ammonium (r = -0.30; p = 3.2x10^{-4}) showed a

slight negative relationship, while nitrite (r = 0.03; p = 0.24) and phosphate (r = 0.07; p = 0.39) showed no pattern of distribution over the haline gradient.

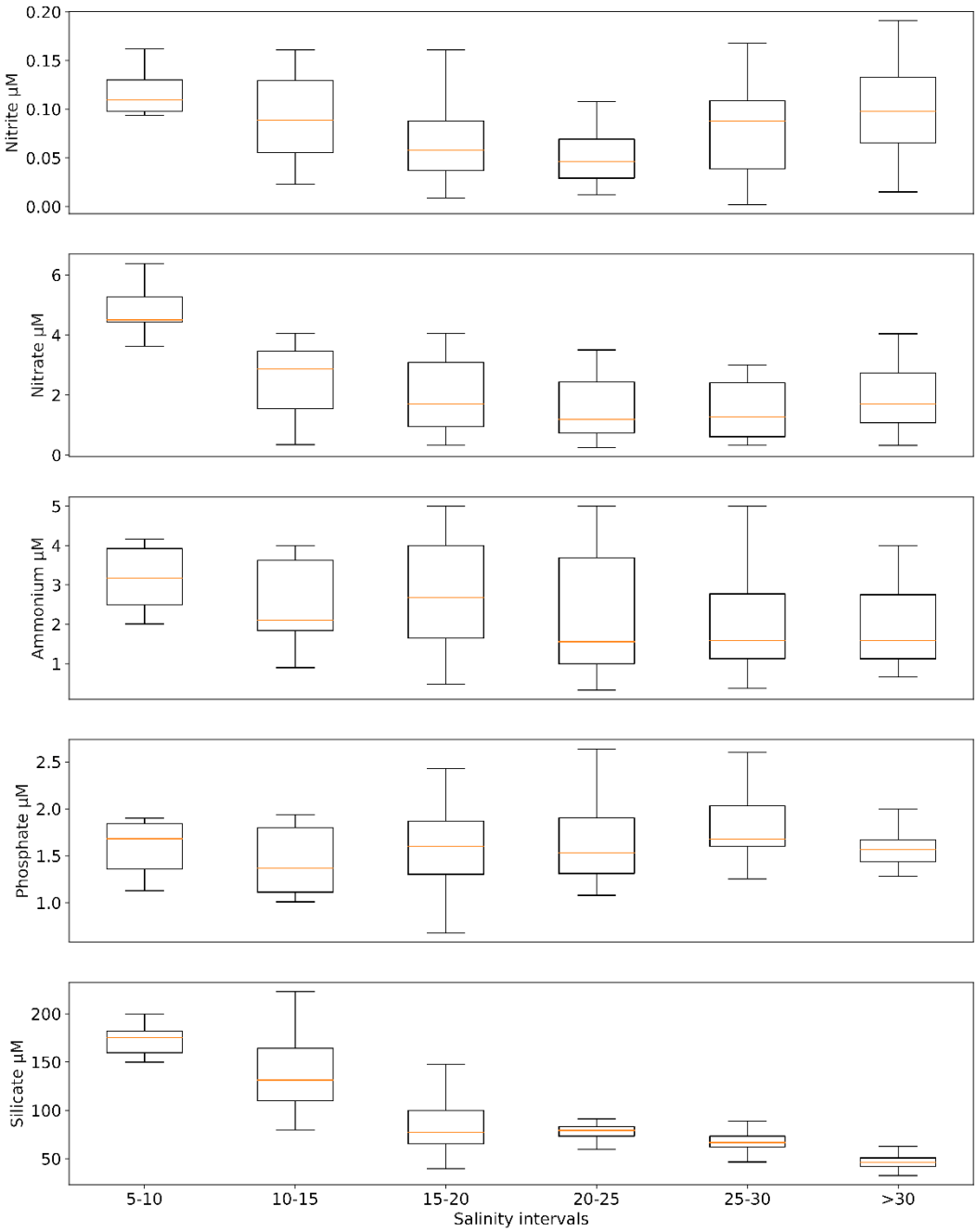

Figure 17. Boxplots of dissolved inorganic nutrients by salinity class intervals. Data from Feb-22-2021 to Mar-23-2021 (late austral summer), stations RS-2 and RS-1, Patos Lagoon estuary, Brazil. Sample n = 150. Median (orange line) values are shown in the boxplot; hinges are 25th and 75th percentiles; whiskers are 5th and 95th percentiles.

8.4.2 Water, salt and nutrient budgets

Water and salt residual flow from the PL box to the PLE box were -118.3 x10^6 m^3 d^{-1} and -1,207.9 x10^6 psu m^3 d^{-1}, respectively. Water and salt residual flows from the PLE box to the coast were -153.4 x10^6 m^3 d^{-1} and -3,888.8 x10^6 psu m^3 d^{-1}, respectively. Estimated residence time according to LOICZ for the PL and PLE boxes were 256.7 ± 8.8 and 3.3 ± 0.1 days, respectively. Complete budgets of water and salt are presented in Figure 18 and Table B.2.

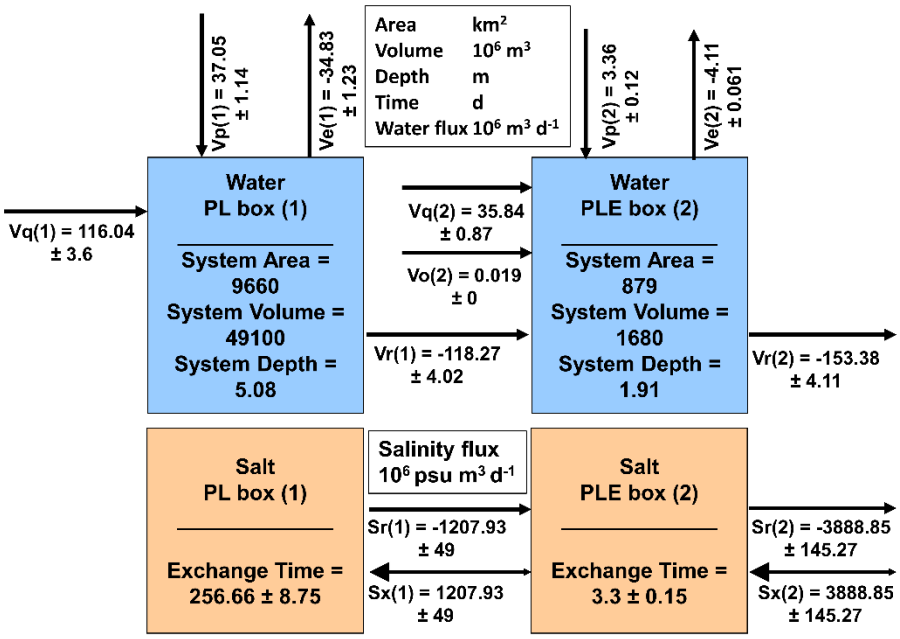

Figure 18. *Summary conceptual model of LOICZ budgets* (mean ± SD) of water (upper - blue) and salt (bottom – orange), for Patos Lagoon, southern Brazil, during austral summer drought conditions. Fluxes of water (V) from river (q), precipitation (p), evaporation (e), other sources (o: wastewater) and residual flow (r); and of salt (S) from the coast to Patos Lagoon through exchange (x), and between PL box (1), PLE box (2) and the coast through residual flow (r). Negative values are downstream, and positive upstream.

The DIP budgets reveal that the majority of its inputs to the PL box were from riverine sources and precipitation. The inputs of DIP from the coast into the PLE and PL boxes were positive, providing 9.3 ± 17.6 and 14.5 ± 5.1 x10^3 mol d^{-1}, from the coast into the estuary, and from the estuary into the lagoon, respectively. The DIP fluxes in river discharge and precipitation for the PL box were 95.1 ±7.7 and 126.4 ± 6.7 x10^3 mol d^{-1}, respectively. Complete DIP budgets are presented in Figure 19 and Table B.2.

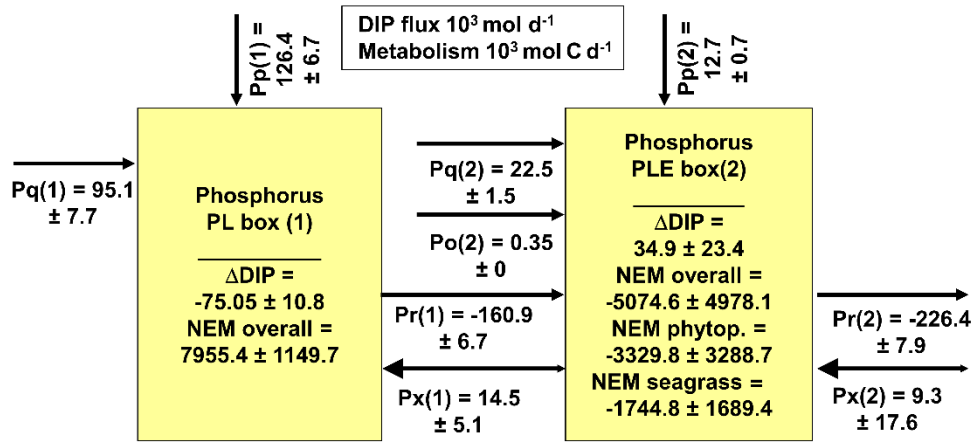

Figure 19. *Summary conceptual model of LOICZ budgets* (mean ± SD) of DIP for Patos Lagoon, southern Brazil, during austral summer drought conditions. P denotes DIP fluxes from river (q), precipitation (p), evaporation (e), other sources (o: wastewater), residual (r) and exchange (x) between PL box (1), PLE box (2) and the coast. Negative values are downstream, and positive upstream. Negative ΔDIP means less DIP than expected, and negative net ecosystem metabolism is net heterotrophic.

For DIN, river discharge was the main source, providing the majority of DIN to the PL box, and then to the PLE box. There was no positive influx of DIN from the coast into the estuary. Complete DIN budgets are presented in Figure 20 and Table B.2.

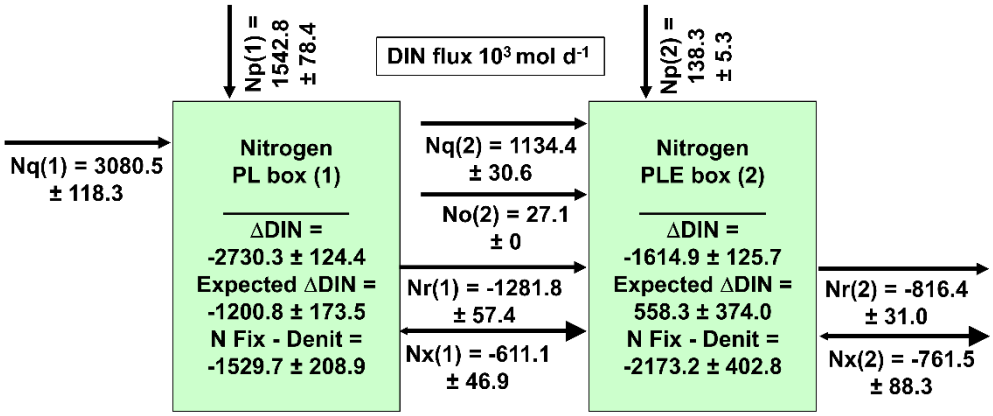

Figure 20. *Summary conceptual model of LOICZ budgets* (mean ± SD) of DIN from land, atmosphere, and between the limnic lagoon (PL box), estuary (PLE box) and adjacent coastal ocean, for Patos Lagoon, southern Brazil, during austral summer drought conditions. N denotes DIN fluxes from river (q), precipitation (p), evaporation (e), other sources (o: wastewater), residual (r) and exchange (x) between PL box (1), PLE box (2) and the coast. Negative values are downstream, and positive upstream.

8.4.3 Net ecosystem metabolism and N-cycling

NEM for the PL box was estimated as 0.8 ± 0.1 mmol C m^{-2} d^{-1}, classifying it as net autotrophic, but very close to balanced (≈ 0) (Fig. 19, Table B.2). Regarding DIN, the PL and PLE boxes had a negative balance, with denitrification prevailing at rates of -0.16 ± 0.02 mmol m^{-2} d^{-1} and -2.50 ± 0.70 mmol m^{-2} d^{-1}, respectively. Weighted average NEM for the PLE box was net heterotrophic, with -5.7 ± 5.6 mmol C m^{-2} d^{-1}. Detailed phytoplanktonic and seagrass NEM rates are presented in Figure 19 and Table B.2.

8.4.4 Potential for primary production

The potential for PP was based on the total DIN input fluxes to each box and the coastal zone. DIN for the PL box was computed from river discharge plus precipitation; that for the PLE box was from river discharge plus the residual DIN flux of the PL box, precipitation and effluents; and that for the coast from the residual DIN flux of PLE box. PP potentials for the PL and PLE boxes were 2.7 ± 0.1 and 9.2 ± 0.4 mmol C m^{-2} d^{-1}, respectively. The PP potential for the adjacent continental shelf in a 0.1 x 90 km strip of coastline (9 km^2) was 515.1 ± 19.6 mmol C m^{-2} d^{-1}.

8.5 Discussion

8.5.1 Water and nutrient fluxes

PLE hydrodynamics is modulated by the combination of freshwater flow and winds [Möller *et al.* 2001; Möller & Castaing, 1999]. When freshwater flow is greater than 3,000 m^3 s^{-1}, the wind cannot invert the outflow direction. However, during drought conditions of the austral summer (freshwater flow less than 3,000 m^3 s^{-1}), the wind is expected to have greater influence in controlling the direction of water flow, allowing even infrequent and weak southerly winds to promote marine water inflow [Möller *et al.* 2001; Möller & Castaing, 1999] far into the estuary, causing its salinization [Möller *et al.* 2001; Odebrecht *et al.* 2005]. It is likely that the predominant mean outflow condition observed during the austral summer of 2021 (Tab.6, Fig. 15), was due to more intense currents than observed during inflow periods. Nonetheless, the drought condition was confirmed by greater residence time compared to wet periods (1.4 days, simulated with a river

flow of 3,500 m^3 s^{-1}), and the predominance of saltwater (20.7 on average) within the estuary [Bordin *et al.* 2023a].

Fluxes at station RS-1 were from the main body of PLE into the Arraial bight. Despite the magnitudes of water and nutrient fluxes being lower than at station RS-2, the results suggest that the effect of wind on water circulation acts distinctly in each location. During drought conditions, the influence of wind and marine salty water intrusion into the Arraial bight is greater than during higher river discharges [Giordano 2008], likely supplying nutrients from the estuary into the Arraial bight and retaining nutrients from the ETEs inside the bight. Moreover, station RS-1 is within the second biogeochemical zone proposed by Windom *et al.* [1999], which is dominated by remineralization. Net pelagic heterotrophy found by Bordin *et al.* [2023a] at the same station also points to the predominance of remineralization against nutrient uptake, the regenerated nutrients of which seem to have been advected to the Arraial bight, contributing to nutrient demand by primary producers in its shallow autotrophic shoals [Abreu *et al.* 1994; 1995].

The relationship of nutrients vs. salinity (Fig. 17 and B.6) can indicate fluvial or marine coastal inputs [Statham 2012], but a lack of relationship may indicate other sources, and/or that biogeochemical cycling is removing or introducing them. The negative relationship of nitrate, ammonium and silicate vs. salinity indicates freshwater as the main source of these nutrients, correcting that stated by Bordin *et al.* [2023a] for silicate. It is likely that the observed lack of a relationship for nitrite and phosphate vs. salinity, may indicate biogeochemical processes, such as nutrient uptake by primary producers [Abreu *et al.* 1994, Bordin *et al.* 2023a], organic matter mineralization on sediments [Niencheski & Jahnke, 2004], and anthropogenic sources [Baumgarten *et al.* 1995, Wallner-Kersanach *et al.* 2016], as can be observed in the LOICZ budget results. Bordin *et al.* [2023a] assessed the influence of nutrients, PP and meteoceanographic factors, and pointed out that DIP and silicate were assimilated by PP, while DIN was limiting for PP. They also attributed the low nitrate concentrations to low freshwater inputs, which, along with high ammonium and low dissolved oxygen concentrations, prevent/reduce nitrification [Niencheski *et al.* 2006], and to denitrification, as will be addressed in the next sections. Therefore, since ammonium was the main DIN, and it had a weak relationship with river discharge,

it is likely that its main source was anthropogenic inputs from the city of Rio Grande, accumulated in the estuarine zone (Tab. 1) due to the higher residence time characteristic of this time of year [Baumgarten *et al.* 1995; Fujita & Odebrecht, 2007], as also observed for other estuaries under similar conditions [Wang *et al.* 2004]. Large residence times can favor the development of algal blooms within estuaries, with potential to significantly remove nutrients from the water column, impacting fluxes to the coastal zone, as observed in UK estuaries [Jickells *et al.* 2014]. This was previously observed in PLE by Odebrecht *et al.* [2015], and there is evidence it occurred at station RS-1 [Bordin *et al.* 2023a].

8.5.2 Nutrient budgets

PL acts as a sink of both DIP and DIN (negative deltas, Figs. 19 and 20, and Tab. B.2). On the other hand, PLE behave as a sink for only DIN, and as a source for DIP, likely supplied from intrusions of Plata Plume Water [Bordin *et al.* 2023a], organic matter mineralization and/or desorption of phosphate from the sediments [Windom *et al.* 1999] and inputs from the fertilizer factories [Baumgarten *et al.* 1995; Niencheski *et al.* 2006; Wallner-Kersanach *et al.* 2016]. However, PLE exports relatively less DIN than DIP from to the coast, while the export from PL to PLE was proportional for both nutrients (Figs. 19 and 20, and Tab. B.2]. Since the PL region was net autotrophic, and with lower rates of denitrification, it is likely that the DIN retained within this box was removed from the water column by PP [Niencheski *et al.* 1994]. On the other hand, denitrification was higher in PLE, favoring N-limitation for PP, possibly increasing net heterotrophy. This is why less DIN relative to DIP was exported for the coast, and the fate of such an amount being loss by denitrification.

DIP exhibited a behavior distinct from DIN — an upstream flux component. Looking upstream from the coast, PLE also received a DIP contribution of 8.6 $x10^3$ mol d^{-1} from exchange fluxes with the continental shelf, and PL a contribution of 17.1 $x10^3$ mol d^{-1} from exchanges with PLE. Bordin *et al.* [2023a] showed the influence of coastal water intrusions on PLE biogeochemistry, possibly composed of Plata Plume Water. The nutrient-rich (mainly phosphate and silicate) [Braga *et al.* 2008; Bordin et al, 2019] Plata Plume Water is forced northward by SW winds

and spreads over the Southern Brazilian Continental Shelf, especially on the surface, but it may dominate the water column [Möller *et al.* 2008; Piola *et al.* 2005; Bordin *et al.* 2019]. It is likely that these waters are advected into the estuary [Bordin *et al.* 2023a], which corroborates the DIP delivery from this water mass to PLE [Bordin *et al.* 2023a], and shows it goes further upstream, to the limnic region. However, it is likely that these inputs are less significant to riverine, as well as groundwater, sources. Moreover, despite not having time for biogeochemistry transformations from the mouth until station RS-2, it is noteworthy that oceanic nutrient concentrations were estimated just from data taken inside the estuary (only station RS-2) with salinities > 30 psu.

Niencheski & Windom [1994] presented the only previous nutrient budget estimate for PLE, on an annual basis, but they did not consider exchanges with continental shelf waters. Their budget was based on exchange across boxes within the estuarine region, assuming nutrients as conservative and considering only riverine discharges as a nutrients source. The DIP input values found in the present study for the PLE box were 2.3 times higher considering all input sources (river, effluents and precipitation), and 1.9 times higher considering only the residual flux of DIP from the PL box. For DIN, in the same order, the present study was 1.2 times higher and proportional if only riverine sources are considered. Moreover, both estimates of export fluxes from PLE to the coast presented in the present study (M1 and M2) and the residual fluxes of the LOICZ approach, were in accordance, with values of the same magnitude.

8.5.3 Net ecosystem metabolism and N-cycling

The assessment of NEM and N-fix – denit revealed that the system was slightly net heterotrophic in both regions, but mainly in the estuary. N-fix prevailed in the limnic region, while denitrification prevailed in the estuary. Despite some differences in magnitude, the rates found by the present study are within the range of those for other Brazilian [Landim & Knoppers, 2000; M.F.L Souza *et al.* 2009; Cabral & Fonseca, 2019] and worldwide [Giordani *et al.* 2008; Dan *et al.* 2019] estuaries (Tab. 7).

Table 7. Net ecosystem metabolism (NEM), nitrogen fixation minus denitrification (N-fix - denit) in mmol m^{-2} d^{-1}, and water residence time (days) for estuaries worldwide. Positive values represent autotrophic (NEM) and N-fixation conditions, while negative represent heterotrophic and denitrification conditions. NEM values of the present study represent the averaged phytoplankton and seagrass values, for details see Fig. 19.

	Lat/Long	NEM	N-fix – denit	Residence time	Reference
Patos Lagoon, BR	-31.0/-51.3	0.82 ± 0.1	-0.16 ± 0.02	257	Present study
Patos Lagoon estuary, BR	-32.0/-52.0	-5.7 ± 5.6	-2.5 ± 0.7	3.3 ± 8.8	Present study
Piratininga-Itaipu lagoon system, BR	-22.9/-43.0	-0.44	0.01	23	Landim *et al.* [2000]
Marica-Guarapina lagoon system, BR	-22.9/-42.8	5.07	0.77	185	Landim *et al.* [2000]
Araruama, BR	-22.9/-42.1	-2.03	-0.33	985	Landim *et al.* [2000]
Piauí River Estuary, BR	-11.4/-37.3	-0.02	-0.13	6	M.F.L Souza *et al.* [2009]
Madre Estuarine System, BR	-27.9/-48.6	-0.40	-0.20	30 ± 10	Cabral & Fonseca [2019]
Sacca di Goro lagoon, IT	44.8/12.3	3.40	-19.5	2	Giordani *et al.* [2008]
Cross River Estuary system, NG	4.64/8.41	-58	-14	3.5	Dan *et al.* [2019]

Until recently, PLE was thought to be net autotrophic during the spring, summer and autumn, and net heterotrophic just during winter, when lower temperatures and sun irradiation, and the decomposition of senescent seagrass, lead respiration to prevail [Abreu *et al.* 1994]. In a recent assessment of the pelagic NEM of PLE by oxygen-based bottle experiments, Bordin *et al.* [2023a] showed that the channel-sites where stations RS-2 and RS-1 are located are net heterotrophic during the austral summer drought. Another study that estimated NEM at station RS-1 by the Open-Water method, showed the channel to be net heterotrophic throughout the year [Bordin *et al.* 2023a,b]. The authors attributed this metabolic state to N- and light-limitation (high turbidity) [Bordin *et al.* 2023a], and the high net heterotrophy to the great depth of the experimented sites, with most of the water column being under the aphotic zone, where respiration prevails against PP [Bordin *et al.* 2023a,b]. The rates found by Bordin *et al.* [2023a] varied from -135.4 (RS-1) to -291.1 mmol C m^{-2} d^{-1} (RS-2), and Bordin *et al.* [2023b] found an annual average of -168.6 mmol C m^{-2} d^{-1} (O_2:C conversion factor = 1). Despite the current findings being in accordance with net heterotrophy [Bordin *et al.* 2023a,b], the magnitude differs. Therefore, cross comparisons must be done with caution because methodologies, as well as spatial and temporal scales, differ. While the mentioned studies only measured at channel-sites deeper than average system depth (where respiration prevails), the current approach encompassed the whole system, considering average PLE depth (1.9

m). Since shoals (< 1.5 m in depth) represent ~80% of the area of PLE [Seeliger, 2001; present study), it is more likely for the euphotic zone to reach the bottom of these extensive areas, where PP represents a greater fraction, leading overall NEM from high to slight net heterotrophy. Finally, it is likely that the greater amount of submerged aquatic vegetation [Copertino & Seeliger, 2010; Lanari & Copertino, 2017] and microphytobenthos [Abreu *et al.* 1994; Odebrecht *et al.* 2005; Bordin *et al.* 2023a,b] play an important role in reducing net heterotrophy in PLE during the austral summer. This observation is consistent with many shallow microtidal Italian lagoons, where NEM was also assessed using the LOICZ approach [Giordani *et al.* 2008].

The metabolic process in sediments plays an important role in nutrient budgets of shallow systems, due the greater sediment area:water volume ratio [Castel *et al.* 1996], as previously observed for PLE [Niencheski & Jahnke, 2002]. However, no exchanges with the sediment were considered here due to insufficient data. It is known that denitrification is directly related to DO concentration in the water column and sediments [Risgaard-Petersen, 2004]. Unlike the limnic region, where vertical haline stratification does not occur, the estuarine region experiences stratification of the water column, particularly during the austral summer when the intrusion of salty marine waters into PLE is common [Möller *et al.* 2001; Odebrecht *et al.* 2005]. Therefore, it is likely for the water column to be stratified by the haline gradient in some regions, reinforced by warming on the surface. In the PL region, it is more likely for the vertical mixing layer to be deeper and the bottom oxygenated, favoring bacterial mineralization of organic nitrogen, as well as the nitrification of large amounts of ammonium from rivers that drain sewage from the city of Porto Alegre. On the other hand, in the PLE region, particularly in channel-sites and pits, the greater residence time typical of austral summer droughts, along with the salt effect and subsequent intensified vertical stratification, are likely to reduce the vertical mixing layer and lower the concentration of dissolved oxygen at the bottom [Odebrecht *et al.* 2005; Bordin *et al.* 2023a]. These conditions could promote denitrification, as previously observed for PLE by Abreu *et al.* [2006] and Patterson [2016].

Increased ammonium concentrations have, until now, been attributed to the accumulation of sewage from the city of Rio Grande [Baumgarten *et al.* 1995]

within PLE during the longer residence time typical of austral summer [Abreu *et al.* 1994; Odebrecht *et al.* 2005] and La Niña periods [Abreu *et al.* 2010; Haraguchi *et al.* 2015], and to reduced nitrification associated with lower oxygen saturation [Niencheski *et al.* 2006]. However, there is evidence that high ammonium concentrations, low nitrate levels, and low N:P ratios can also result from denitrification in PLE. Denitrification plays a crucial role in determining the availability of nitrogen nutrients for primary producers in estuaries worldwide [Risgaard-Petersen 2004]. Therefore, it is likely that the limitation of PP by N is caused not only by reduced nutrient supply through river discharge [Odebrecht *et al.* 2005; Bordin *et al.* 2023a], but also by N-loss by denitrification. Moreover, this process may be the primary factor contributing to PLE being net heterotrophic under such conditions.

8.5.4 Potential for primary production

One of the main sources of nutrients entering estuarine and coastal zones is river discharge [Bianchi *et al.* 2007], which supports PP in these areas [Valiela, 2015]. DIN is the main nutrient that controls PP in PLE [Abreu *et al.* 1994; Bordin *et al.* 2023a] and in Cassino beach [Piedras & Odebrecht 2012]. Moreover, scenarios with different availabilities among DIN, DIP and silicate, control phytoplankton community composition and abundance [Reynolds, 2006] in both PL [Odebrecht *et al.* 2005] and PLE [Odebrecht *et al.* 2005; Mendes *et al.* 2017].

The potential for PP was higher in the estuarine region than in the limnic region, contrasting with the findings of Odebrecht *et al.* [2005]. Those authors found higher maximum rates in the PL region [180 mg C m^{-3} h^{-1}) than in the PLE region (90 mg C m^{-3} h^{-1}), but higher gross productivity per unit of chl-a in PLE. This may have been due to differences in phytoplankton community composition under distinct light-conditions in the two regions, since light is the main limiting factor, except during dry periods, when N-limitation turns to play a major role as a co-limiting factor, especially in the PLE region [Odebrecht *et al.* 2005]. The potential for PP in the PLE region was 9.2 ± 0.4 mmol C m^{-2} d^{-1}, slightly lower than the 16.5 mmol C m^{-2} d^{-1} net PP estimated by Bordin *et al.* [2023a] at station RS-1 (4.5 m depth), and higher than the 0.04 mmol C m^{-2} d^{-1}estimated by Abreu

et al. [1994] in a shallower area (0.5 m). If extrapolated yearly (3,358 ± 146 mmol C m^{-2} y^{-1}), the potential PP would classify PLE as oligotrophic according to Nixon [1995]. However, Bordin *et al.* [2023b] found 24,900 mmol C m^{-2} $year^{-1}$ by the Open-Water method, which would classify PLE as mesotrophic [Nixon, 1995] and in accordance with the mesotrophic state estimated with the TRIX trophic index [Vollenweider *et al.* 1998] by Bordin *et al.* [2023a]. This value of PP potential is plausible, since this estimate considers a fixed source of nutrients for a determined area. Other non-accounted-for sources of nutrients may exist, such as benthic organic matter mineralization [Niencheski & Jahnke, 2002] and submarine groundwater [Souza *et al.* 2021], that cause such differences.

The potential for PP was also assessed for the adjacent continental shelf area. Considering the surface waters exported by PLE as the only source of nutrients for an adjacent continental shelf area of 9 km^2, the PP potential was 515.1 ± 19.6 mmol m^{-2} d^{-1}, higher than PL and PLE due the much smaller area considered. Submarine groundwater fluxes also represent significant inputs of nutrients to the coast, as the concentration of DIN, DIP and silicate can be much higher in groundwater fluxes compared to surface waters [Andrade *et al.* 2012]. Niencheski *et al.* [2007] and Souza *et al.* [2021] estimated nutrient fluxes from submarine groundwater from PLE to the adjacent continental shelf and estimated PP potential based on the same approach (but from DIP fluxes) and same area (9 km^2) as the present study and reached similar rates.

8.5.5 Caveats

The data used in the present study to represent riverine inputs of nutrients and system concentrations for the PL box were collected two to three decades ago [Pereira 2003]. It is possible that DIP and DIN concentrations are underestimated due to the lower population density in the watershed during that time. The northern part of Patos Lagoon, where the city of Porto Alegre and its metropolitan regions are inserted, receives significant anthropogenic inputs. The population in the region increased ~50% [IBGE 2023] since the 1990's. The main cities of the PLE box region increased ~14% (Pelotas] and ~6% (Rio Grande) in the same period [IBGE 2023]. On the other hand, the data used to represent

inputs from the São Gonçalo Channel, which include water and effluents from the Mirim Lagoon and the city of Pelotas, were more current [de Souza 2015]. Similarly, concentrations in PLE and coastal areas were based on recent data from Bordin *et al.* [2023a], averaged with the dataset of Pereira [2003]. Another potential source of uncertainty arises from the inputs of the city of Rio Grande. The city is located in the southeasternmost section of PLE, where there are significant anthropogenic inputs from sewage, harbor activities, and industrial effluents from soy and fertilizer factories [Baumgarten *et al.* 1995; Niencheski *et al.* 2006; Wallner-Kersanach *et al.* 2016]. Baumgarten *et al.* [2021] identified 17 sites of effluent disposal along the margins of Mangueira bight, particularly for DIP. Although concentrations decrease significantly away from the margins [Spengler *et al.* 2007; Wallner-Kersanach *et al.* 2016; Marreto *et al.* 2017], these sources are likely to make a substantial contribution to nutrient budgets, especially during periods of longer residence time. However, it should be noted that an underestimation may be occurring due to the challenges involved in quantifying the actual water flux from diffuse sources. Niencheski & Windom [1994] estimated that approximately 3% of total produced DIP (5,850 t $year^{-1}$) was lost from Rio Grande factories, and could potentially enter the estuary. However, Wallner-Kersanach *et al.* [2016] did not observe a significant increase in nutrient contamination in the PLE region over the past decade. It is important to note that no fluxes of particulate or dissolved organic matter were considered in the present study, yet these may represent significant fluvial inputs to PLE [Niencheski & Windom, 1994].

PLE is a very complex and dynamic system. The hydrology is mainly affected by wind and river discharge [Möller *et al.* 2001], which affect nutrients [Wallner-Kersanach *et al.* 2016] and ecology over short to long timescales [Abreu *et al.* 2017]. Seasonally, high concentrations and variability of nutrients, chl-a [Abreu *et al.* 1994, 2010] and NEM [Bordin *et al.* 2023a,b] occur during increased river discharge in early spring, and higher temperatures towards summer. River discharge reaches its minimum during summer and fall, while chl-*a* [Abreu *et al.* 1994; Abreu *et al.* 2010] and metabolic rates reach their minimum during winter [Bordin *et al.* 2023a,b]. In addition to seasonal variation, long-term hydrological and biogeochemical features are also observed in PLE, including those

associated with El Niño Southern Oscillation (ENSO) [Távora *et al.* 2020; Bortolin *et al.* 2022; Bordin *et al.* 2023a,b]. During the positive phase (El Niño), precipitation [Grimm 2009] and river discharges increase, circulation patterns intensify and salinity decreases in the estuary [Fernandes *et al.* 2002]. This can result in the removal of nutrients from the water column due to the zero-salinity effect [Windom *et al.* 1999]. Conversely, during La Niña years (ENSO negative phase), low precipitation [Grimm 2009] and river discharges are expected, leading to salinization of PLE, longer residence times and higher concentrations of sewage products, such as ammonium, being retained in the estuary [Baumgarten *et al.* 1995; Abreu *et al.* 2010; Bordin *et al.* 2023a]. Despite these long-term trends, PLE exhibits significant variability on shorter timescales [Abreu *et al.* 2010; Bordin *et al.* 2023a,b], which can alter biogeochemical dynamics and nutrient budgets. Therefore, caution must be exercised to avoid misinterpretations.

8.6 Concluding remarks

This first attempt to estimate nutrient fluxes between the Patos Lagoon estuary and its adjacent continental shelf (aboveground) was useful. The utilization of hourly water flux data and daily averaged nutrient concentrations in the water column provided reliable estimates of nutrient fluxes, which were in line with LOICZ budget results. The estimates of exchange flux between the estuary and the coast are considered reliable, as station RS-2 is located at the estuary exit, where intense water flux results in a shorter residence time and fewer sinks and sources influenced by biogeochemical processes. Although the estimates were specific to the dry season, they are representative of ~8% (M1) of the climatology in the area. This study also represents the first attempt to estimate DIP and DIN budgets using the LOICZ box model approach, considering Patos Lagoon, its estuary and the adjacent coastal ocean. The findings indicate that the estuary exports DIP and DIN to the adjacent continental shelf, but also imports DIP, possibly from Plata Plume Water, which intrudes further across the boundary between the estuary and the limnic region of the lagoon. The budget analysis also allowed for the estimation of net ecosystem metabolism (NEM) and N-fixation and denitrification rates. Denitrification prevailed in both the limnic and estuarine

regions. The limnic region exhibited slight autotrophy, and the estuary net heterotrophy, under austral summer drought conditions. These outcomes were primarily attributed to nitrogen limitation resulting from low allochthonous nutrient supply, and losses through denitrification, particularly in the estuarine zone, characterized by a lower N:P ratio and a higher net heterotrophic rate. It is recommended that future studies incorporate as many nutrient sources as possible, including dissolved, particulate, organic and inorganic species, under different meteoceanographic conditions. Such an approach would provide more representative estimates of the entire system and throughout the year. Additionally, conducting NEM experiments in shoals and investigating N-cycling using more specific methodologies would further enhance our understanding of the system.

Capítulo IX:
Síntese da Discussão e Conclusões

Aqui serão destacados os principais pontos das discussões e das conclusões dos artigos científicos apresentados nos Capítulos IV, V e VI. Primeiramente, os artigos serão abordados um a um, de acordo com a sua escala de cobertura temporal e espacial. Por fim, será feito um fechamento geral concluindo a Tese através da verificação das hipóteses formuladas e das considerações finais.

9.1 Caracterização do metabolismo aquático do ecossistema do estuário da Lagoa dos Patos: variabilidade espacial e temporal de pequena escala

A primeira caracterização do metabolismo aquático do estuário da Lagoa dos Patos se deu através de uma metodologia *in situ,* discreta, i.e., através de amostragem de campo e experimentos de produção primária e R. A condução desta abordagem através de experimentos em escala diária foi inédita no estuário da Lagoa dos Patos, porém, restrita apenas ao período de duração da campanha amostral, entre fevereiro e março de 2021 (verão austral tardio), e às duas estações de coleta, representativas de ambientes de canal, com profundidade igual (estação 1) e maior (estação 2) que a profundidade média do estuário da Lagoa dos Patos, e de ambientes cujas características hidrodinâmicas e biogeoquímicas são distintas. A estação 1 cobriu um ambiente abrigado, interno ao estuário, onde o processo biogeoquímico predominante é a remineralização da matéria orgânica, enquanto a estação 2, localizado no canal de acesso principal ao estuário, próximo da sua desembocadura, cobriu um ambiente exposto à influência da água marinha, cuja biogeoquímica é dominada por mistura conservativa [Windom *et al.* 1999].

Apesar de se encontrarem em zonas hidrodinâmicas e biogeoquímicas distintas, o metabolismo se comportou de forma semelhante nas duas estações, ambas apresentando heterotrofia líquida, e flutuações concomitantes ao longo da campanha amostral. Embora o verão austral no estuário da Lagoa dos Patos

tenha apresentado maior transparência da água e, consequentemente, uma zona eufótica mais profunda em comparação com outros períodos do ano, a heterotrofia líquida foi atribuída principalmente à limitação por luz. Isso ocorreu devido à grande profundidade local, na qual uma grande parte da coluna de água ficou limitada por luz. Esse cenário resultou em uma taxa de respiração (R) maior do que a de produção primária, levando a um estado de heterotrofia líquida na coluna de água. Essa tendência foi corroborada quando comparadas as taxas de R e o metabolismo líquido entre as duas estações. Na estação 2, que possui o dobro da profundidade da estação 1, apesar de uma zona eufótica ligeiramente mais ampla, apenas as taxas respiratórias foram significativamente mais altas, resultando em uma maior heterotrofia líquida.

Entretanto, de acordo com o GAM, o principal mecanismo de controle da produção primária foi o nitrato, evidenciando uma limitação por este nutriente. Essa constatação é corroborada pelas baixas razões N:P, consistentemente menores que 16 ao longo de toda a campanha amostral. A limitação por nutrientes nitrogenados durante períodos de estiagem ocorre devido ao baixo suprimento proveniente de sua principal fonte, a drenagem continental. Por outro lado, o fosfato, que é limitante em períodos de maior aporte de água doce devido à sua adsorção favorecida pela baixa salinidade, e que resulta em seu sequestro nos sedimentos ao longo do seu percurso desde a foz dos rios até o estuário, não é limitante nessa época do ano. O fosfato sequestrado nos sedimentos é liberado (dessorção) devido à intrusão e predominância de água marinha no interior do estuário. Além disso, a intrusão de água marinha no estuário também representa um aporte de fosfato, possivelmente pela influência da Água da Pluma do Prata, que é transportada para o norte durante períodos de ventos do quadrante sul. Essa massa de água é rica em nutrientes, principalmente fosfato, e desempenha um papel importante na biogeoquímica da Lagoa dos Patos durante o verão austral. Este mecanismo também foi definido como importante pelo GAM, evidenciado pela maior significância dos parâmetros vento e salinidade em resposta à dinâmica de entrada/saída de água marinha/estuarina, induzida pela ação do vento no estuário da Lagoa dos Patos.

A radiação fotossinteticamente ativa foi o parâmetro que melhor explicou o processo de R, de acordo com o GAM. É provável que essa variável tenha sido

selecionada devido às maiores taxas respiratórias ao longo da zona afótica. No entanto, é curioso notar que esse parâmetro não se mostrou significativo no GAM quando a produção primária foi utilizada como variável dependente. Além disso, a temperatura foi outro fator importante no controle da R, uma vez que influencia a resposta fisiológica dos organismos heterotróficos.

Em relação à influência da composição e estrutura da comunidade fitoplanctônica no metabolismo, as diatomáceas foram o grupo que mais contribuiu para ambas as taxas metabólicas, produção primária e R, uma vez que foram o grupo dominante em ambas as estações amostrais. De acordo com o RDA, as criptófitas e prasinófitas parecem ter contribuído significativamente para as taxas de produção primária, enquanto as cianobactérias, dinoflagelados e criptófitas para a R. Entretanto, é importante ressaltar que o tamanho amostral (n) não foi suficiente para afirmar com certeza essas contribuições.

Apesar das evidências de que as diatomáceas tiveram uma contribuição significativa nas flutuações de carbono inorgânico dissolvido através da sua assimilação na produção primária, não foram encontradas relações diretas entre os demais parâmetros do sistema carbonato e as taxas metabólicas. A estação 1 se comportou principalmente como emissora de CO_2 para a atmosfera, enquanto a estação 2, atuou como um sumidouro. Foi constatado que o sistema carbonato foi principalmente controlado pela entrada/saída de água marinha/estuarina, induzida pelo vento.

9.2 Caracterização e variabilidade temporal do metabolismo aquático do ecossistema do estuário da Lagoa dos Patos: da escala diária à interannual

O método do oxigênio dissolvido livre foi a segunda abordagem aplicada nesta tese, também inédita para o estuário da Lagoa dos Patos. Apesar de aplicado apenas na estação 1 e com ausência de algumas variáveis suplementares tais como os nutrientes, fitoplâncton e parâmetros do sistema carbonato, essa abordagem permitiu expandir as estimativas do metabolismo para escalas de tempo mais amplas, desde diárias até interanuais. Além disso, houve ganhos significativos com a expansão vertical e abrangência para toda a

comunidade de organismos presentes na área subjacente à estação 1, representando efetivamente o metabolismo de todo o ecossistema. Além da comunidade planctônica pelágica, o método engloba os processos metabólicos do bentos e nécton, uma vez que os sinais de variação do oxigênio dissolvido são capturados de forma integrada. No entanto, é importante ressaltar que o pressuposto essencial do método é que haja homogeneidade horizontal, vertical e temporal da massa de água, o qual foi respeitado no estudo.

O metabolismo líquido do ecossistema na estação 1 foi heterotrófico durante todo o período analisado. Mais uma vez, as altas taxas de heterotrofia líquida foram atribuídas à grande profundidade local, na qual a maior parte da coluna de água fica abaixo da zona eufótica. Isso resulta em taxas respiratórias que excedem a produção primária de forma integrada para o ecossistema.

Ambas as taxas de GPP e R atingiram os seus valores máximos na primavera, diminuíram ligeiramente no verão e atingiram os seus valores mínimos no outono e inverno. Em escala diária o metabolismo foi controlado pela variabilidade da salinidade induzida pelo vento, com a entrada/saída de água marinha/estuarina, e pela variabilidade da radiação solar incidente, possivelmente devido à alternância entre dias nublados e ensolarados. Em escala sazonal, o regime de chuvas e descarga fluvial, que caracterizam os períodos de estiagem e cheias, foram os fatores determinantes, provavelmente devido ao controle do aporte de nutrientes e material em suspensão. Embora esses parâmetros não tenham sido medidos no estudo, eles estão de acordo com o que é descrito na literatura sobre o estuário da Lagoa dos Patos. Na primavera, há um grande aumento da drenagem continental, com um significativo aporte de nutrientes e material em suspensão. As taxas de GPP aumentam substancialmente na fina camada eufótica superficial, mas no restante da coluna de água, sob limitação de luz, as taxas respiratórias excedem a GPP integrada na coluna de água. O aporte de água doce diminui no verão, mas as taxas de GPP continuam elevadas, devido ao aumento da disponibilidade de luz, até que ocorra o exaurimento dos nutrientes na coluna de água, principalmente de nitrogênio. No outono, as taxas de GPP e R atingem o mínimo devido à escassez de nutrientes e à redução sazonal da disponibilidade de luz. No inverno, com o início da temporada de chuvas, as taxas aumentam, devido à

disponibilidade de nutrientes pela drenagem continental, mas são limitadas pela luz e pelas baixas temperaturas características dessa época do ano.

Apesar da série temporal abrangente, a análise interanual foi restrita aos dados das primaveras de cada ano. Isso se deve à distribuição desigual dos dados ao longo das diferentes épocas do ano, devido a lacunas existentes no conjunto original de dados, bem como às etapas de filtragem e seleção dos dias adequados para o método, a fim de cumprir os pressupostos de homogeneidade vertical, horizontal e temporal da massa de água por um período mínimo de 24 horas. Embora limitada às primaveras dos anos de 2016, 2017, 2019 e 2020, a análise permitiu capturar o efeito de um evento meteorológico extremo: a ocorrência de um ciclone extratropical sobre o sul do Brasil em 2016. Esse evento resultou em taxas elevadas de precipitação e aporte de água doce no estuário da Lagoa dos Patos, muito provavelmente carregadas de nutrientes e matéria orgânica. O efeito desse evento no metabolismo do estuário foi bastante conspícuo, pois aumentou substancialmente as taxas metabólicas, especialmente R. Esse incremento pode ser atribuído ao aumento da disponibilidade de nutrientes, mas principalmente à maior quantidade de matéria orgânica, cuja degradação resultou nas maiores taxas respiratórias observadas ao longo de todo o período analisado. Esses resultados evidenciam os potenciais impactos futuros associados às mudanças climáticas e seus eventos extremos na dinâmica biogeoquímica e no ecossistema do estuário da Lagoa dos Patos. No entanto, outros possíveis efeitos decorrentes deste evento não puderam ser avaliados neste trabalho, pois estão além de seu escopo e devido à limitação na disponibilidade de dados.

9.3 Caracterização do metabolismo aquático do ecossistema da Lagoa dos Patos e região estuarina em períodos de estiagem

O balanço de massa de água, sal e nutrientes realizado pelo modelo de caixas LOICZ foi o terceiro e último método utilizado nesta tese para estimar o metabolismo no estuário da Lagoa dos Patos. Este método foi capaz de fornecer estimativas integradas para todo o sistema, expandindo as estimativas dos dois primeiros métodos aplicados, os quais eram limitados espacialmente, uma vez

que forneciam o metabolismo apenas nos locais onde os experimentos foram realizados: método 1, estações 1 (RS-1) e 2 (RS-2); e método 2, estação 1 (RS-1). O modelo de caixas LOICZ exige uma quantidade significativa de dados que englobem os valores internos e as principais fontes e sumidouros de propriedades para cada caixa do modelo. Além disso, esses dados precisam estar bem distribuídos espacialmente, a fim de representar o sistema como um todo. Também é necessário que os dados utilizados sejam consistentes temporalmente, ou seja, coletados na mesma estação do ano, e/ou em condições meteoceanográficas semelhantes em relação aos principais fatores que contribuem para o controle dos processos metabólicos em um determinado ecossistema. Como observado no segundo método/artigo, em escala sazonal, o principal fator controlador do metabolismo no estuário da Lagoa dos Patos é o regime de chuvas/vazante nas bacias de drenagem/rios que compõem a totalidade da Lagoa dos Patos.

O período em que a disponibilidade de dados foi suficiente para representar o sistema de forma completa, foi o de verão/estiagem, o qual está em consonância com os dados coletados durante a campanha amostral que constituiu o primeiro método/artigo apresentado nesta tese. Além de fornecer informações sobre o metabolismo, o uso do modelo LOICZ para o balanço de massa permitiu obter os fluxos de nutrientes entre a região límnica da Lagoa dos Patos, a região estuarina e o oceano costeiro adjacente, bem como avaliar o equilíbrio entre os processos de nitrificação e desnitrificação em cada uma dessas regiões. É importante ressaltar que o balanço de massa realizado pelo modelo LOICZ e as estimativas geradas por esse método são inéditos para a Lagoa dos Patos, a região estuarina e a plataforma continental adjacente.

A região límnica apresentou um metabolismo líquido levemente autotrófico, enquanto a estuarina, heterotrófico. Embora tenha sido limitado aos períodos de verão/estiagem, o método utilizado permitiu caracterizar o estado metabólico de forma integrada para todo o sistema, em um período em que se acreditava que o estuário fosse autotrófico.

Tanto a região límnica quanto a estuarina da Lagoa dos Patos apresentaram desnitrificação líquida de nitrogênio. A região límnica, por estar

mais próxima da principal fonte de água doce e nutrientes para o sistema, apresentou uma menor taxa de desnitrificação e uma razão N:P mais elevada em comparação com a região estuarina. Isso resultou em um metabolismo líquido mais próximo da neutralidade. Por outro lado, na região estuarina a desnitrificação líquida foi mais acentuada, o que reduziu a disponibilidade de nutrientes nitrogenados para os organismos fotossintetizantes. Essa limitação potencial adicional aos produtores primários pode ter causado um leve aumento da heterotrofia líquida.

A região límnica da lagoa dos patos comportou-se como sumidouro de nitrogênio e fósforo inorgânicos dissolvidos. Enquanto isso, a região estuarina atuou como um sumidouro de nitrogênio, mas como fonte de fósforo inorgânico dissolvido. Isso pode ser atribuído aos aportes do município de Rio Grande, tais como efluentes domésticos, mas principalmente industriais, como as fábricas de fertilizantes localizadas em suas margens no setor sul do estuário. Entretanto, o comportamento como fonte de fósforo inorgânico dissolvido observado na região estuarina, também pode ter sido causado pelo fluxo positivo de fosfato entre o estuário e a costa. Isso representou em um influxo de fosfato da costa para o estuário, alcançando a região límnica da Lagoa dos Patos. A concentração de fosfato e os índices termohalinos na zona costeira são compatíveis com a Água da Pluma do Prata, o que evidencia a importância das intrusões dessa massa de água para o interior da Lagoa dos Patos. Essas intrusões representam uma fonte significativa de nutrientes e desempenham um papel importante na dinâmica biogeoquímica da maior laguna costeira do mundo.

9.4 Considerações finais e direcionamentos futuros

Essa Tese de Doutorado testou duas hipóteses ao longo do seu desenvolvimento. Em relação à hipótese (I), que afirmava que o metabolismo aquático no estuário da Lagoa dos Patos é predominantemente autotrófico em um ciclo anual, a hipótese foi parcialmente refutada. Por meio dos dois primeiros métodos e artigos apresentados, foi observada heterotrofia líquida em duas regiões de canais do estuário da Lagoa dos Patos. No entanto, não é possível assumir, com base apenas nestes dois locais analisados, que o sistema como um todo é heterotrófico. Isso ocorre porque a profundidade média do estuário é

menor do que a profundidade das duas estações amostradas, o que as torna não representativas de todo o sistema.

Através do modelo LOICZ, foi possível obter uma visão integrada de todo o ecossistema do estuário da Lagoa dos Patos, pelo menos para os períodos de verão/estiagem. De acordo com a literatura, esperava-se que apenas o período de inverno austral apresentasse heterotrofia líquida, sendo o verão o segundo mais autotrófico, logo após a primavera. Entretanto, o metabolismo líquido foi heterotrófico em períodos de verão/estiagem.

Para abordar de forma mais abrangente a questão do metabolismo do estuário da Lagoa dos Patos, é necessário realizar investigações adicionais, que possam solucionar esta questão de maneira integrada no tempo e no espaço. Para isso, são sugeridos experimentos semelhantes aos realizados nesta tese, em regiões rasas e mais amplamente distribuídas. Os resultados do segundo artigo destacaram o potencial de alterações ambientais e ecológicas decorrentes das mudanças climáticas. Esses efeitos devem ser estudados para fornecer subsídios para tomadas de decisões que possam mitigar suas consequências. Para atingir este objetivo, é necessário manter as boias meteoceanográficas a longo prazo e instalar novos sistemas para aumentar a cobertura e representatividade do estuário da Lagoa dos Patos, incluindo regiões rasas e embaiamentos, que possuem hidrodinâmica e biogeoquímica distintas. Sugere-se também realizar amostragens *in situ* de nutrientes, fitoplâncton e de parâmetros do sistema carbonato, com uma cobertura espacial mais abrangente, em conjunto com esses sistemas de amostragem operacional. Isso é essencial para obter conjuntos de dados suficientes para realizar análises estatísticas mais robustas. Tais análises são cruciais para estabelecer relações precisas entre os processos físicos e biogeoquímicos abordados, como a relação entre o metabolismo, a composição e a estrutura da comunidade fitoplanctônica, bem como os fluxos de CO_2 entre o estuário e a atmosfera.

Em relação à hipótese (II), de que o metabolismo aquático no estuário da Lagoa dos Patos varia principalmente em função da temperatura e radiação solar incidente em escala sazonal, e do vento em escalas menores, podemos concluir que ela foi parcialmente confirmada. A radiação solar incidente demonstrou ser

um fator importante em escala sazonal, enquanto a temperatura não foi incluída nas análises. Em escala diária, o vento foi o fator determinante, mas também se constatou a influência significativa da radiação solar incidente, temperatura e nitrato. Esses resultados contrastantes podem ser atribuídos à considerável variabilidade em pequena escala que interferiu nos padrões sazonais. Além disso, a amostragem desigual entre as estações do ano, conforme mencionado anteriormente, pode ter reduzido a capacidade do modelo GAM de estabelecer relações claras entre as variáveis explicativas e a resposta. Para resolver essas questões, sugerem-se mais experimentos e amostragens que cubram todas as variáveis de interesse de forma uniforme. Também é recomendada a instalação de mais boias meteoceanográficas, mantendo-as em operação por longos períodos. Isso permitirá a coleta de dados suficientes para análises estatísticas mais robustas e a alimentação de modelos numéricos de forma mais precisa.

Capítulo X:

Referências Bibliográficas

Abreu, PC [1992] Phytoplankton produktion and the microbial food web of the Patos Laggon estuary, southern Brazil. 100p (Doctoral dissertation, Ph. D. Thesis. Universität Bremen, Fed. Republic of Germany).

Abreu PC, Odebrecht C, Gonzalez A [1994). Particulate and dissolved phytoplankton production of the Patos Lagoon estuary, southern Brazil: comparison of methods and influencing factors. *Jour of Plank Res*, *16*(7), 737-753. https://doi.org/10.1093/plankt/16.7.737

Abreu PC, Hartmann C, Odebrecht C [1995] Nutrient-rich saltwater and its influence on the phytoplankton of the patos lagoon estuary, Southern Brazil. Est, Coa and She Sci 40(2): 219-229. https://doi.org/10.1016/S0272-7714(05)80006-X

Abreu PC, Costa CS, Bemvenuti C, Odebrecht C, Graneli W. Anesio AM [2006] Eutrophication processes and trophic interactions in a shallow estuary: Preliminary results based on stable isotope analysis (δ 13 C and δ 15 N). Est and Coa, 29, 277-285. https://doi.org/10.1007/BF02781996

Abreu PC, Bergesch M, Proença L A, Garcia CA, Odebrecht C [2010] Short-and long-term chlorophyll a variability in the shallow microtidal Patos Lagoon estuary, Southern Brazil. *Est-Coas*, *33*(2), 554-569. https://doi.org/10.1007/s12237-009-9181-9

Abreu PC, Marangoni J, Odebrecht C [2017] So close, so far: differences in long-term chlorophyll a variability in three nearby estuarine-coastal stations. *Mar Bio Res*, *13*(1), 9-21. https://doi.org/10.1080/17451000.2016.1189081

Acha EM, Mianzan H, Guerrero R, Carreto J, Giberto D, Montoya N, Carignan M [2008] An overview of physical and ecological processes in the Rio de la Plata Estuary. Cont she res. https://doi.org/10.1016/j.csr.2007.01.031

Aguiar VF, Baumgarten MGZ, Rodrigues H [2014] Identificação e diagnóstico dos locais de lançamento de efluentes nas margens da enseada estuarina Saco da mangueira (Rio Grande, RS). Anais do Congresso Brasileiro de Oceanografia (ISBN: 978-85-66184-03-7), pp. 1793-1792, Itajaí, Brazil. Available on line at http://www.aoceano.org.br/site/images/pdf/livro_de_resumos_cbo201 4.pdf

Altieri AH, Diaz RJ [2019] Dead zones: oxygen depletion in coastal ecosystems. In *World seas: An environmental evaluation* (pp. 453-473). Academic Press. https://doi.org/10.1016/B978-0-12-805052-1.00021-8

Atkinson MJ, & Smith SV [1983). C: N: P ratios of benthic marine plants 1. Limnology and Oceanography, 28(3), 568-574. https://doi.org/10.4319/lo.1983.28.3.0568

Akaike H [1974] A new look at the statistical model identification. IEEE Trans. Autom. Control 19 (6), 716–723.

Albuquerque C, Kerr R, Monteiro T, Orselli IBM, de Carvalho-Borges M, de Oliveira Carvalho, ADC, Mendes CRB, [2022] Seasonal variability of carbonate chemistry and its controls in a subtropical estuary. Estuarine, Coa and She Sci, 108020. http://doi.org/10.1016/j.ecss.2022.108020

Albuquerque C, [2022] Sistema Carbonato e Fluxos de Dióxido de Carbono no Estuário da Lagoa dos Patos. Tese de Doutorado – FURG. 137 p.

Almeida MA, Cunha MA, Alcântara F [2005] Relationship of bacterioplankton production with primary production and respiration in a shallow estuarine system (Ria de Aveiro, NW Portugal). Microbio Res, 160(3), 315-328. http://dx.doi.org/10.1016/j.micres.2005.02.005

Andrade CFF, Niencheski LFH, Attisano KK, Milani MR, Santos IR, Milani IC [2012] Fluxos de nutrientes associados às descargas de água subterrânea para a Lagoa Mangueira (Rio Grande do Sul, Brasil). Quim. Nova 35, 1–6. https://doi.org/10.1590/S0100-40422012000100002

Arndt S, Regnier P, Vanderborght JP, [2009] Seasonally-resolved nutrient export fluxes and filtering capacities in a macrotidal estuary. Jour of Mar Sys 78(1): 42–58. https://doi.org/10.1016/j.jmarsys.2009.02.008

Apple JK, Smith EM, Boyd TJ [2008] Temperature, salinity, nutrients, and the covariation of bacterial production and chlorophyll-a in estuarine ecosystems. Jour of Coas Res, (10055), 59-75. https://doi.org/10.2112/SI55-005.1

Aspila KI, Agemian H, Chau ASY [1976] A semi-automated method for the determination of inorganic, organic and total phosphate in sediments. *Analyst*, *101*(1200), 187-197. https://doi.org/10.1039/AN9760100187

Ávila RA, Orozco PMS, Andrade MM, Möller OO [2021] Temporal variability of suspended-solids concentration in the estuarine channel of patos lagoon, Southern Brazil. Water, 13(5), 646. http://doi.org/10.3390/w13050646

Azevedo IC, Duarte PM, Bordalo AA [2006). Pelagic metabolism of the Douro estuary (Portugal)–factors controlling primary production. Est, Coa and She-Sci, 69(1-2), 133-146. http://dx.doi.org/10.1016/j.ecss.2006.04.002

Baumgarten MGZ, Niencheski LFH, Kuroshima KN [1995] Qualidade das águas estuarinas que margeiam o município do Rio Grande (RS-Brasil): nutrientes e detergente dissolvidos. Atlântica, *17*(1), 17-34.

Baumgarten MGZ, Aguiar VF, Gonçalves V, da Costa JD [2021] Uma estratégia otimizada para diagnosticar a qualidade das águas da enseada estuarina Saco da Mangueira (Rio Grande/RS), que recebe aportes antrópicos. Revista FEPAM, 14, 17-32. https://leoquim.furg.br/images/arquivos/artigos/umaestrategiaotimizada.pdf

Bemvenuti CE [2012] Benthic Invertebrates. In Seeliger, U., Odebrecht, C., and Castello, J. P. (Eds.). (2012). Subtropical convergence environments: the coast and sea in the southwestern Atlantic. Springer Science and Business Media.

Beck, Marcus W, Hagy III, James D, Murrel MC [2015] Improving estimates of ecosystem metabolism by reducing effects of tidal advection on dissolved oxygen time series. Lim-Ocean: Met, v. 13, n. 12, p. 731-745. https://doi.org/10.1002/lom3.10062

Bianchi TS [2007] Biogeochemistry of estuaries. Oxford University Press on Demand.

Biddanda B, Opsahl S, Benner R [1994). Plankton respiration and carbon flux through bacterioplankton on the Louisiana shelf. Limn and Ocean, 39(6), 1259-1275. http://dx.doi.org/10.4319/lo.1994.39.6.1259

Bitencourt LP, Fernandes EH, da Silva PD, Möller, OO [2020). Spatio-temporal variability of suspended sediment concentrations in a shallow and turbid lagoon. Jour of Mar Sys. https://doi.org/10.1016/j.jmarsys.2020.103454

Benson BB, Krause Jr D [1984] The concentration and isotopic fractionation of oxygen dissolved in freshwater and seawater in equilibrium with the atmosphere 1. Limn and ocea. https://doi.org/10.4319/lo.1984.29.3.0620

Bordin LH, Machado EDC, Carvalho M, Freire AS, Fonseca AL [2019] Nutrient and carbon dynamics under the water mass seasonality on the continental shelf at the South Brazil Bight. Jour of Mar Sys. https://doi.org/10.1016/j.jmarsys.2018.09.006

Bordin LH, Machado EDC, Mendes CRB, Camargo M [2023a] Daily Variability of Pelagic Metabolism in a Subtropical Lagoonal Estuary. Jour of Mar Sys. https://doi.org/10.1016/j.jmarsys.2023.103861

Bordin LH, Machado EdaC, Mendes CRB, Fernandes EH, Camargo M [2023b] Total Ecosystem metabolism Variability in a Subtropical Lagoonal Estuary Channel Site. Est and Coas. https://doi.org/10.1007/s12237-023-01270-2

Borges AV, Vanderborght JP, Schiettecatte LS, Gazeau F, Ferrón-Smith S, Delille B, Frankignoulle M [2004] Variability of the gas transfer velocity of CO_2 in a macrotidal estuary (the Scheldt). Estuaries, *27*(4), 593-603. https://doi.org/10.1007/BF02907647

Borges A, Abril G, [2011] Carbon dioxide and methane dynamics in estuaries. Treatise on Estuarine and Coastal Science. Biogeo 5:119–161. https://hdl.handle.net/2268/81409

Bortolin EC, Távora J, Fernandes EH [2022] Long-term variability on suspended particulate matter loads from the tributaries of the world's largest choked lagoon. Front in Mar Sci. https://doi.org/10.3389/fmars.2022.836739

Braga ES, Chiozzini VC, Berbel GB, Maluf JC, Aguiar VM, Charo M, Eichler BB [2008] Nutrient distributions over the Southwestern South Atlantic continental

shelf from Mar del Plata (Argentina) to Itajaí (Brazil): Winter–summer aspects. Cont She Res, 28(13), 1649-1661. http://doi.org/10.1016/j.csr.2007.06.018

Brandini FP [1985] Ecological studies in the Bay of Paranaguá: I. horizontal distribution and seasonal dynamics of the phytoplankton. *Bol do Inst Oce*, *33*, 139-147. https://doi.org/10.1590/S0373-55241985000200004

Broecker, Wallace S, [1982] Tracers in the Sea. Lamont-Doherty Geological Observatory.

Bruesewitz DA, Gardner WS, Mooney RF, Pollard L, Buskey EJ [2013] Estuarine ecosystem function response to flood and drought in a shallow, semiarid estuary: Nitrogen cycling and ecosystem metabolism. Limn and Oce, https://doi.org10.4319/lo.2013.58.6.2293

Blauw, AN *et al.* [2009] GEM: a generic ecological model for estuaries and coastal waters. Hydrob 618(1): 175. https://doi.org/10.1007/s10750-008-9575-x

Bužančić M, Gladan ŽN, Marasović I, Kušpilić G, Grbec B [2016] Eutrophication influence on phytoplankton community composition in three bays on the eastern Adriatic coast. Oceanol, 58(4), 302-316. https://doi.org/10.1016/j.oceano.2016.05.003

Bukaveckas PA, Beck M, Devore D, Lee WM [2018] Climatic variability and its role in regulating C, N and P retention in the James River Estuary. Est, Coa and She Sci, 205, 161-173. https://doi.org/10.1016/j.ecss.2017.10.004

Cabral, A., & Fonseca, A. [2019). Coupled effects of anthropogenic nutrient sources and meteo-oceanographic events in the trophic state of a subtropical estuarine system. *Estu, Coa and She Sci*, *225*, 106228.

Caffrey JM [2004] Factors controlling net ecosystem metabolism in US estuaries. *Est* 27(1): 90-101. https://doi.org10.1007/BF02803563

Caffrey JM, Murrell MC, Amacker KS, Harper JW, Phipps S, Woodrey MS [2014] Seasonal and inter-annual patterns in primary production, respiration, and net ecosystem metabolism in three estuaries in the northeast Gulf of Mexico. Est and Coa, 37(1), 222-241. http://dx.doi.org/10.1007/s12237-013-9701-5

Calliari LJ, Seeliger U, Castello JP [1997] Geological Setting. Subtropical Convergence Environments. The Coast and Sea in the Southern Atlantic. Springer, Berlin Heidelberg, 117-121.

Carmouze JP, Knoppers B, Vasconcelos P [1991] Metabolism of a subtropical Brazilian lagoon. Biogeoc, *14*(2), 129-148.

Casartelli MR, Mirlean N, Peralba MC, Barrionuevo S, Gómez-Rey MX, Madeira M [2008] An assessment of the chemical composition of precipitation and throughfall in rural-industrial gradient in wet subtropics (southern Brazil). Environ monit-assessm, 144(1-3), 105-116. https://doi.org/10.1007/s10661-007-9949-y

Cloern JE [1991] Annual variations in river flow and primary production in the South San Francisco Bay Estuary (USA). Est and coa: Spat and temp intercomp 19(30): 91.

Cloern JE, Foster SQ, Kleckner AE [2014] Phytoplankton primary production in the world's estuarine-coastal ecosystems. Biogeosciences, 11(9), 2477. https://doi.org/10.5194/bg-11-2477-2014

Costa CSB, Seeliger U, Kinas PG [1988] The effect of wind velocity and direction on the salinity regime in the Patos Lagoon Estuary. Ciência e Cultura. 40(9): 909-912.

Closs D [1962] Foraminíferos e tecamebas na Lagoa dos Patos. Bol Esc Geol, Porto Alegre 11:1-30.

Coloso JJ, Cole JJ, Hanson PC, Pace ML [2008] Depth-integrated, continuous estimates of metabolism in a clear-water lake. Canad Jour of Fisher and Aqua Sci, 65(4), 712-722. https://doi.org/10.1139/f08-006

Copernicus Marine Service, Operational Mercator Global Ocean Analysis and Forecast System. Retrieved February 15, 2023, from www.resources.marine.copernicus.eu/products.

Copertino MS, Seeliger U [2010] Habitats de Ruppia maritima e de macroalgas. In Seeliger, U. & C. Odebrecht (eds), Estuário da Lagoa dos Patos: um século de transformações. Editora da FURG, 92–98.

Damashek J, Francis, CA [2018] Microbial nitrogen cycling in estuaries: from genes to ecosystem processes. Est and Coa, 41(3), 626-660. https://doi.org/10.1007/s12237-017-0306-2

Dan SF, Liu SM, Udoh EC, Ding S [2019] Nutrient biogeochemistry in the cross-river estuary system and adjacent Gulf of Guinea, south east nigeria (west africa). Cont She Res, 179, 1-17. https://doi.org/10.1016/j.csr.2019.04.001

Day JW, Yanez-Arancibia A, Kemp WM, Crump BC [2012] Introduction to estuarine ecology. Est ecol, 2, 1-19. https://doi.org/10.1002/9781118412787.ch1

Deltares Systems [2014] QUICKPLOT: Visualisation and animation program for analysis of simulation results User Manual. Deltares, Delft, The Netherlands, 110 p.

Deltares Systems [2019] Delft3D-FLOW, Simulation of multi-dimensional hydrodynamic flows and transport phenomena, including sediments User Manual. Delft, the Netherlands, 704 p.

Deltares Systems [2020] QUICKIN: Generation and manipulation of grid-related parameters such as bathymetry, initial conditions and roughness User Manual. Deltares, Delft, The Netherlands, 110 p.

Souza de FM [2015] Qualidade da água do canal de São Gonçalo-RS/Brasil – Uma avaliação hidroquímica considerando seus usos múltiplos. Master's dissertation. Universidade Federal de Pelotas, Pelotas. 105 p. http://guaiaca.ufpel.edu.br:8080/handle/ri/2830

Dickson AG, Sabine CL, Christian JR, [2007] Guide to Best Practices for Ocean CO_2 Measurements 3. PICES Special Publication, 191. http://dx.doi.org/10.25607/OBP-1342

Dodge Y [2008] Kruskal-Wallis Test. The Con Encyc of Stat, 288-290.

Domingues RB, Anselmo TP, Barbosa AB, Sommer U, Galvão HM [2011] Light as a driver of phytoplankton growth and production in the freshwater tidal zone of a turbid estuary. Est, Coa and She Sci, 91(4), 526-535. https://doi.org/10.1016/j.ecss.2010.12.008

Dyer KR [1997] Estuaries, 2nd Edition. Wiley, New York. Eguiguren, V., 1894. Las lluvias en Piura. Boletın de la Sociedad de Geografıa de Lima 4, 241–258. https://doi.org/10.1002/9781118412787

Egbert Gary D, Svetlana Y Erofeeva [2002] Efficient inverse modeling of barotropic ocean tides. Journal of Atmospheric and Oceanic Technology. p. 183-204. https://doi.org/10.1175/1520-0426(2002)019<0183:EIMOBO>2.0.CO;2

ECMWF [2023] European Center for Medium-Range Weather Forecasts. Retrieved on January 30, from www.ecmwf.int/en/forecasts/datasets/reanalysis-datasets/era5

Falkowski PG, Laws EA, Barber RT, Murray JW [2003] Phytoplankton and their role in primary, new, and export production. In Ocean biogeo (pp. 99-121). Springer, Berlin, Heidelberg. https://doi.org/10.1007/978-3-642-55844-3_5

Fahey TJ, Knapp AK [2007] Principles and standards for measuring primary production. Oxford University Press. https://doi.org/10.1093/acprof:oso/9780195168662.001.0001

Fernandes EHL, Dyer KR, Möller OO, Niencheski LFH [2002] The Patos lagoon hydrodynamics during an El Niño event (1998). Cont She Res. https://doi.org/10.1016/S0278-4343(02)00033-X

Fernandes EH, da Silva PD, Gonçalves GA, Möller OO [2021). Dispersion plumes in open ocean disposal sites of dredged sediment. *Water*, *13*(6), 808. https://doi.org/10.3390/w13060808

Franzen MO, Silva P, Siegle E, Fernandes EH [2023] Influence of long jetties on estuarine and coastal hydrodynamics in a microtidal estuary. Reg St in Mar Sci, 59, 102809. https://doi.org/10.1016/j.rsma.2022.102809

Fujita CC, Odebrecht C [2007] Short term variability of chlorophyll a and phytoplankton composition in a shallow area of the Patos Lagoon estuary (Southern Brazil). Atl (Rio Grande), 29(2), 93-106. https://doi.org/10.5088/atlântica.v29i2.694

Gazeau F, Gattuso JP, Middelburg JJ, Brion N, Schiettecatte LS, Frankignoulle M, Borges AV [2005] Planktonic and whole system metabolism in a nutrient-rich estuary (the Scheldt estuary). Est, 28(6). https://doi.org/10.1007/BF02696016

Grimm AM [2009] Variabilidade interanual do clima no Brasil. Tempo e Clima no Brasil. São Paulo: Oficina de Textos, 353-374.

Garcia CA, Baer SE, Garcia NS, Rauschenberg S, Twining BS, Lomas MW, Martiny AC [2018] Nutrient supply controls particulate elemental concentrations and ratios in the low latitude eastern Indias Oceasn. Na commu, 9(1), 1-10. https://doi.org/10.1038/s41467-018-06892-w

Giering SL, [2014] Reconciliation of the carbon budget in the ocean's twilight zone. Nature, 507: 7493:480. https://doi.org/10.1038/nature13123

Gieskes WWC, Kraay GW, Baars MA [1979] Current 14C methods for measuring primary production: gross underestimates in oceanic waters. Nethe Jour of Sea Res, 13(1), 58-78. https://doi.org/10.1016/0077-7579(79)90033-4

Giordani G, Austoni M, Zaldivar JM, Swaney DP, Viaroli P [2008). Modelling ecosystem functions and properties at different time and spatial scales in shallow coastal lagoons: an application of the LOICZ biogeochemical model. Est, Coa and She Sci, 77(2), 264-277. https://doi.org/doi:10.1016/j.ecss.2007.09.017

Gordon DC, Boudreau JR, Mann KH, Silvert WL, Smith SVG, Wattayakorn Wulff F, Yanagi T [1996] LOICZ BIOGEOCHEMICAL MODELLING GUIDELINES. LOICZ/R&S/95-5, VI +96 PP. LOICZ, Texel, The Netherlands. https://www.ferrybox.eu/imperia/md/content/loicz/print/rsreports/report5.pdf

Grasshoff K, Kremling K, Ehrhardt M [2007] Methods of seawater analysis. John Wiley & Sons. https://doi.org/10.1002/9783527613984

Haimovici M, Cardoso LG [2017] Long-term changes in the fisheries in the Patos Lagoon estuary and adjacent coastal waters in Southern Brazil. Mar Bio Res, 13(1), 135-150. https://doi.org/10.1080/17451000.2016.1228978

Harari J [2015] Fundamentos de modelagem numérica em Oceanografia. Ed. Salt, Sea & Limno Tech, São Paulo.

Hartmann C, Calliari LJ [1996] Composição e qualidade do material em suspensão durante alta turbidez na extremidade sul da Laguna dos Patos, RS, Brasil. Pesqui. Geo, 22, 74–83. http://repositorio.furg.br/handle/1/3215

Hartmann C, Schettini CAF [1991). Aspectos hidrológicos na região da desembocadura da Laguna dos Patos, RS. http://repositorio.furg.br/handle/1/3217

Haraguchi L, Carstensen J, Abreu PC, Odebrecht C [2015) Long-term changes of the phytoplankton community and biomass in the subtropical shallow Patos Lagoon Estuary, Brazil. Estu, Coa and She Sci, 162, 76 87. https://doi.org/10.1016/j.ecss.2015.03.007

Hopkinson CS, Jr EM Smith [2005] Estuarine respiration: an overview of benthic, pelagic, and whole system respiration. In Respiration in aquatic systems, ed. P.A. del Giorgio and P.J.l.B. Williams, 122–146. Oxford: Oxford University Press. https://doi.org/10.1093/acprof:oso/9780198527084.003.0008

Hopkinson BM, Dupont CL, Allen AE, Morel FMM [2011] Efficiency of the CO_2 concentrating Mechanism of Diatoms, vol. 10. Proceeding of the National Academy of Sciences of the United States of America, pp. 3830–3837. https://doi.org/10.1073/pnas.1018062108

Holm-Hansen O, Riemann B [1978] Chlorophyll-*a* determination: improvements in methodology. Oikos, 438–447. https://doi.org/10.2307/3543338

Hunter [2007] "Matplotlib: A 2D Graphics Environment", Computing in Science & Engin, vol. 9, no. 3, pp. 90-95. https://doi.ieeecomputersociety.org/10.1109/MCSE.2007.55

IBGE, 2022. Instituto Brasileiro de Geografia e Estatística. Monitoramento da Cobertura e Uso da Terra. Retrieved on 11/23/2022 from https://www.ibge.gov.br/geociencias/informacoes-ambientais/cobertura-e-uso-da-terra.html

INMET [2023] Instituto Nacional de Meteorologia. Retrieved on January 30 from https://portal.inmet.gov.br/normais.

Iriarte A, de Madariaga I, Diez-Garagarza F, Revilla M, Orive E [1997] Primary plankton production, respiration and nitrification in a shallow temperate estuary

during summer. Jour of Exp Mar Bio and Eco, 208(1-2), 127-151. https://doi.org/10.1016/S0022-0981(96)02672-X

Jiang LQ, Cai WJ, Wang Y [2008] A comparative study of carbon dioxide degassing in river-and marine-dominated estuaries. Limn and Oce. https://doi.org/10.4319/lo.2008.53.6.2603

Jickells TD, Andrews JE, Parkes DJ, Suratman S, Aziz AA, Hee YY [2014] Nutrient transport through estuaries: The importance of the estuarine geography. *Est, Coa and She Sci*, *150*, 215-229. https://doi.org/10.1016/j.ecss.2014.03.014

Jesus ARDS, Odebrecht C [2002] O impacto da herbivoria do microzooplâncton no fitoplâncton no estuário da Lagoa dos Patos. http://repositorio.furg.br/handle/1/5568

Juhl AR, Murrell MC [2008] Nutrient limitation of phytoplankton growth and physiology in a subtropical estuary (Pensacola Bay, Florida). Bull of Mar Sci, 82(1), 59-82.

Jutras M, Mucci A, Sundby B, Gratton Y, Katsev S [2020] Nutrient cycling in the Lower Station Lawrence Estuary: Response to environmental perturbations. Est, Coa and She Sci, 239, 106715. https://doi.org/10.1016/j.ecss.2020.106715

Kjerfve, B. [1986] Comparative oceanography of coastal lagoons. In Estuarine variability (pp. 63-81). Academic Press. https://doi.org/10.1016/B978-0-12-761890-6.50009-5

Kemp WM, Smith EM, Marvin-DiPasquale M, Boynton WR [1997] Organic carbon balance and net ecosystem metabolism in Chesapeake Bay. Mar Eco Prog Ser, 150, 229-248. https://doi.org/doi:10.3354/meps150229

Kirk J [2003] The vertical attenuation of irradiance as a function of the optical properties of the water. Limn and Oce, 48, 9-17. https://doi.org/10.4319/lo.2003.48.1.0009

Kocum E, Underwood GJ, Nedwell DB [2002] Simultaneous measurement of phytoplanktonic primary production, nutrient and light availability along a turbid,

eutrophic UK east coast estuary (the Colne Estuary). Mar eco prog ser, 231, 1-12. https://doi.org/10.3354/meps231001

Koroleff F, Palmork KH [1972] Report on the ICES/SCOR nutrient intercalibration experiment, September 1972. ICES. http://hdl.handle.net/11250/101628

Kovács L [2022] Feature selection algorithms in generalized additive models under concurvity. *Comput Stat*. https://doi-org.ez40.periodicos.capes.gov.br/10.1007/s00180-022-01292-7

Lanari M, Copertino M [2017] Drift macroalgae in the Patos Lagoon Estuary (southern Brazil): effects of climate, hydrology and wind action on the onset and magnitude of blooms. Mar Bio Res. https://doi.org/10.1080/17451000.2016.1225957

Landim de Souza WF, Knoppers B [2000] Araruama Lagoon, Rio de Janeiro State. In S. V. Smith, V. Dupra, J. I. Marshall Crossland, & C. J. Crossland (Eds.). Estuarine systems of the South American region: carbon, nitrogen and phosphorus fluxes (pp. 37– 39.). LOICZ Reports and Studies no. 15, ii+87 pages, LOICZ, Texel: The Netherlands.

Laruelle GG, Dürr HH, Lauerwald R, Hartmann J, Slomp CP, Goossens N, Regnier PAG [2013] Global multi-scale segmentation of continental and coastal waters from the watersheds to the continental margins. Hyd and Earth Sys Scie, 17, 2029-2051. https://doi.org/10.5194/hess-17-2029-2013

Lomas MW, Burke AL, Lomas DA, Bell DW, Shen C, Dyhrman ST, Ammerman JW [2010] Sargasso Sea phosphorus biogeochemistry: an important role for dissolved organic phosphorus (DOP). Biogeos *7*(2). https://doi.org/10.5194/bg-7-695-2010

Lovett GM, Cole JJ, Pace ML, [2006] Is net ecosystem production equal to ecosystem carbon accumulation? Ecosys, 9: 1152–155. https://doi.org/10.1007/s10021-005-0036-3

Lewis ER, Wallace DWR [1998] Program developed for CO_2 system calculations (No. cdiac: CDIAC-105). Environmental System Science Data Infrastructure for a Virtual Ecosystem.

Libes S [2009] Introduction to marine biogeochemistry. Academic Press. https://doi.org/10.1021/ed069pA251.2

Litchman E, Klausmeier CA [2008] Trait-based community ecology of phytoplankton. Ann rev of eco, evol, and sys, 39, 615-639. https://doi.org/10.1146/annurev.ecolsys.39.110707.173549

Legendre P, Anderson MJ [1999] Distance-based redundancy analysis: testing multispecies responses in multifactorial ecological experiments. Eco monog, 69(1), 1-24. https://doi.org/10.1890/0012-9615(1999)069[0001:DBRATM]2.0.CO;2

Lopes, J. F., Lopes, C. L., & Dias, J. M. 2021. Extreme Meteorological Events in a Coastal Lagoon Ecosystem: The Ria de Aveiro Lagoon (Portugal) Case Study. Jour of Mar Sci and Eng. https://doi.org/10.3390/jmse9070727

López-Sandoval DC, Rodríguez-Ramos T, Cermeño P, Sobrino C, Marañón E [2014] Photosynthesis and respiration in marine phytoplankton: relationship with cell size, taxonomic affiliation, and growth phase. Jour of exp mar bio and eco, 457, 151-159. https://doi.org/10.1016/j.jembe.2014.04.013

Los FJ, Villars MT, Van Der Tol, MWM [2008] A 3-dimensional primary production
model (BLOOM/GEM) and its applications to the (southern) North Sea (coupled physical–chemical–ecological model). Jour of Mar Sys,74(1-2): 259-294. https://doi.org/10.1016/j.jmarsys.2008.01.002

Mackenzie FT, Ver LM, Lerman A [2000] Coastal-zone biogeochemical dynamics under global warming. Internat Geol Rev, 42(3), 193-206. https://doi.org/10.1080/00206810009465077

Mackey MD, Mackey DJ, Higgins HW, Wright SW [1996] CHEMTAX-a program for estimating class abundances from chemical markers: application to HPLC measurements of phytoplankton. Mar Ecol Prog-Ser, 144, 265-283. https://doi.org/doi:10.3354/meps144265

Marreto RN, Baumgarten MDGZ, Wallner-Kersanach M [2017] Trophic quality of waters in the Patos Lagoon estuary: a comparison between its margins and

the port channel located in Rio Grande, RS, Braz Acta Limn Bras, 29. https://doi.org/10.1590/S2179-975X10716

MacIntyre HL, Geider RJ [1996] Regulation of Rubisco activity and its potential effect on photosynthesis during mixing in a turbid estuary. Mar Eco Prog Ser, 144, 247-264. https://doi.org/doi:10.3354/meps144247

Marañón E [2008] Inter-specific scaling of phytoplankton production and cell size in the field. Jour of plank res, 30(2), 157-163. https://doi.org/10.1093/plankt/fbm087

Marques WC, Möller OO [2008] Variabilidade temporal em longo período da descarga fluvial e níveis de água da Lagoa dos Patos, Rio Grande do Sul, Brasil. Rev Bras de Rec Híd 13, 155–163. https://repositorio.furg.br/handle/1/945

Marques WC, Fernandes EH, Monteiro IO, Möller OO [2009] Numerical modeling of the Patos Lagoon coastal plume, Brazil. Cont Shelf Res, 29(3), 556-571. https://doi.org/10.1016/j.csr.2008.09.022

Marques WC, Monteiro IO [2011] The Exchange Processes in the Patos Lagoon Estuarine Channel, Brazil. Int Jour of Geos, 2(03), 248. https://doi.org/10.4236/ijg.2012.34076

Martyr-Koller RC, Kernkamp HWJ, Van Dam A, Van Der Wegen M, Lucas LV, Knowles N, Fregoso TA [2017] Application of an unstructured 3D finite volume numerical model to flows and salinity dynamics in the San Francisco Bay-Delta. *Est, Coa and She Sci*, *192*, 86-107. https://doi.org/10.1016/j.ecss.2017.04.024

McSweeney JM, Chant RJ, Wilkin JL, Sommerfield CK [2017] Suspended-sediment impacts on light-limited productivity in the Delaware estuary. Est and Coa, 40(4), 977-993. http://doi.org/10.1007/s12237-016-0200-3

Middelburg JJ, Soetaert K, Hagens M [2020] Ocean alkalinity, buffering and biogeochemical processes. Rev of Geophy, 58(3), e2019RG000681. https://doi.org/10.1029/2019RG000681

Möller OO, Stech J, Mata MM [1996] The Patos Lagoon summertime circulation and dynamics. Conti She Res. https://doi.org/10.1016/0278-4343(95)00014-R

Möller OO, Castaing P [1999] Hydrographical characteristics of the estuarine area of Patos Lagoon (30 S, Brazil). In Estuaries of South America (pp. 83-100). Springer, Berlin, Heidelberg.

Möller OO, Castaing P, Salomon JC, Lazure P [2001] The influence of local and non-local forcing effects on the subtidal circulation of Patos Lagoon. Est, *24*(2), 297-311. https://doi.org/10.2307/1352953

Möller, OO, Piola AR, Freitas AC, Campos EJ [2008] The effects of river discharge and seasonal winds on the shelf off southeastern South America. Cont She Res. 28 (13), 1607–1624. https://doi.org/10.1016/j.csr.2008.03.012

Möller OO, Castello JP, Vaz AC [2009] The effect of river discharge and winds on the interannual variability of the pink shrimp Farfantepenaeus paulensis production in Patos Lagoon. Est and Coa. https://doi.org/10.1007/s12237-009-9168-6

Möller OO, Fernandes EH [2010] Hidrologia e hidrodinâmica. In: O Estuário da Lagoa dos Patos: Um século de transformações/Edição de U. Seeliger, C. Odebrecht. Rio Grande: FURG. P. 180.

Mendes CRB, Odebrecht C, Tavano VM, Abreu PC [2017] Pigment-based chemotaxonomy of phytoplankton in the Patos Lagoon estuary (Brazil) and adjacent coast. Mar Bio Res, 13(1), 22-35. https://doi.org/10.1080/17451000.2016.1189082

Millero FJ, Graham TB, Huang F, Bustos-Serrano H, Pierrot D [2006] Dissociation constants of carbonic acid in seawater as a function of salinity and temperature. Mar Chem, 100(1-2), 80-94. https://doi.org/10.1016/j.marchem.2005.12.001

Muraoka K, Hanson P, Frank E, Jiang M, Chiu K, Hamilton D [2018] A data mining approach to evaluate suitability of dissolved oxygen sensor observations for lake metabolism analysis. *Limn and Ocea: Met*. https://doi.org/10.1002/lom3.10283

Murrell MC, Hagy JD, Lores EM, Greene RM [2007] Phytoplankton production and nutrient distributions in a subtropical estuary: importance of freshwater flow. Est and Coa 30(3): 390-402. https://doi.org/10.1007/BF02819386

Murrell MC, Caffrey JM, Marcovich DT, Beck MW, Jarvis BM, Hagy JD [2018] Seasonal oxygen dynamics in a warm temperate estuary: effects of hydrologic variability on measurements of primary production, respiration, and net metabolism. Est and coas, 41(3), 690-707. https://doi.org/10.1007/s12237-017-0328-9

Nagy GJ, Gómez-Erache M, López CH, Perdomo AC [2002] Distribution patterns of nutrients and symptoms of eutrophication in the Rio de la Plata River Estuary System. In *Nutrients and eutrophication in estuaries and coastal waters* (pp. 125-139). Springer, Dordrecht.

Nixon SW [1995] Coastal marine eutrophication: a definition, social causes, and future concerns. Ophelia,41(1): 199–219. https://doi.org/10.1080/00785236.1995.10422044

Niencheski LF, Windom HL, Smith R [1994] Distribution of particulate trace metal in Patos Lagoon Estuary (Brazil). Mar Poll Bull, 28(2), 96-102. https://doi.org/10.1016/0025-326X(94)90545-2

Niencheski LF, Windom HL [1994] Nutrient flux and budget in Patos Lagoon estuary. Sci of the tot environ, 149(1-2), 53-60. https://doi.org/10.1016/0048-9697(94)90004-3

Niencheski LF, Baumgarten MZ, Fillmann G, Windom HL [1999] Nutrients and suspended matter behaviour in the Patos Lagoon Estuary (Brazil). In Estuaries of South America (pp. 67-81). Springer, Berlin, Heidelberg. https://doi.org/10.1007/978-3-642-60131-6

Niencheski LF, Jahnke RA [2002] Benthic respiration and inorganic nutrient fluxes in the estuarine region of Patos lagoon (Brazil). Aquat Geochem. 8 (3), 135–152. https://doi.org/10.1023/A:1024207220266

Niencheski LFH, Baumgarten MZ, Cabrera L, Juliano SK [2006] Patos Lagoon: indicators of organic pollution. Jour of Coa Res, 1356-1359. http://www.jstor.org/stable/25742975. Accessed 23 June 2023

Niencheski LF, Jahnke RA [2002] Benthic respiration and inorganic nutrient fluxes in the estuarine region of Patos Lagoon (Brazil). Aqua Geoch, 8(3), 135-152. https://doi.org/10.1023/A:1024207220266

National Weather Service, National Centers for Environmental Prediction, Climate Prediction Center [NOAA). Retrieved on May 19, 2022, from https://origin.cpc.ncep.noaa.gpv/products/analysis_monitoring/ensostuff/ONI_v5.php

Needoba JA, Peterson TD, Johnson KS [2012] Method for the quantification of aquatic primary production and net ecosystem metabolism using in situ dissolved oxygen sensors. In Molecular biological technologies for ocean sensing (pp. 73-101). Humana Press, Totowa, NJ. https://doi.org/10.1007/978-1-61779-915-0

Ocean Carbon and Acidification Data System (OCADS) [2022]. Retrieved on March 25, 2022, from https://www.ncei.noaa.gov/access/ocean-carbon-data-system

Oczkowski A, Hunt CW, Miller K, Oviatt C, Nixon S, Smith L [2016] Comparing measures of estuarine ecosystem production in a temperate New England estuary. Est and coa. https://doi.org/10.1007/s12237-016-0113-1

Oksanen JF, *et al.* 2018. Vegan: Community Ecology Package. R Package Version 2.5-2. https://CRAN.R-project.org/package=vegan

Odebrecht C, Seeliger U, Coutinho R, Torgan LC [1987] Florações de Microcystis (cianobactérias) na Lagoa dos Patos, RS. *Anais do Simpósio Ecossistemas Costeiros Sul e Sudeste do Brasil: Síntese do Conhecimento, Canaéia, SP, Brasil. 213p*, 11-16.

Odebrecht C, Abreu PC, Möller OO, Niencheski LF, Proença LA, Torgan LC [2005] Drought effects on pelagic properties in the shallow and turbid Patos Lagoon, Brazil. *Est*, *28*, 675-685. https://doi.org/10.1007/BF02732906

Odebrecht C, Abreu PC, Carstensen J [2015] Retention time generates short-term phytoplankton blooms in a shallow microtidal subtropical estuary. Estu, Coas and She Sci, 162, 35-44. http://dx.doi.org/10.1016/j.ecss.2015.03.004

Odum HT [1956] Primary production in flowing waters 1. Limn and oce, *1*(2), 102-117. https://doi.org/10.4319/lo.1956.1.2.0102

Oliveira H, Fernandes E, Möller OO, García-Rodríguez F [2019] Relationships between wind effect, hydrodynamics and water level in the world's largest coastal lagoonal system. https://doi.org/10.3390/w11112209

Parizzi RA, Machado EDC, Tavares CPDS, Fernandes LF, De Camargo MG, Mafra Jr, LL [2016] Primary productivity and phytoplankton dynamics in a subtropical estuary: a multiple timescale approach. *Sci Mar*. https://doi.org/10.3989/scimar.04358.26a

Patterson EW [2016] "Stocks and Sources of Carbon Buried in the Salt Marshes and Seagrass Beds of Patos Lagoon, Southern Brazil". Honors Theses. 170. https://scarab.bates.edu/honorstheses/170

Piedras FR, Odebrecht C [2012] The response of surf-zone phytoplankton to nutrient enrichment (Cassino Beach, Brazil). J Exp Mar Biol Ecol. 432–433, 156–161. https://doi.org/10.1016/j.jembe.2012.07.020.

Pasquini AI, Niencheski LF, Depetris PJ [2012). The ENSO signature and other hydrological characteristics in Patos and adjacent coastal lagoons, south-eastern Brazil. Est, Coa and She Sci. https://doi.org/10.1016/j.ecss.2012.07.004

Pereira, N., & D'Incao, F. 2012. Relationship between rainfall, pink shrimp harvest (Farfantepenaeus paulensis) and adult stock, associated with El Niño and La Niña phenomena in Patos Lagoon, southern Brazil. *Journal of the Marine Biological Association of the United Kingdom.* https://doi.org/10.1017/S0025315412000021

Pierrot DE, Lewis E, Wallace DWR [2006] MS Excel program developed for CO_2 system calculations. Carbon Dioxide Information Analysis Center, Oak Ridge National Laboratory, US Department of Energy. *ORNL/CDIAC-IOS*. https://10.3334/CDIAC/otg.CO2SYS_XLS_CDIAC105a

Piola AR, Matano RP, Palma ED, Möller OO, Campos EJ [2005] The influence of the Plata River discharge on the western South Atlantic shelf. Geop Res Let, 32(1). https://doi.org/10.1029/2004GL021638

Proença LDO, Hama LL, Odebrecht C [1994] Contribution of microalgae to particulate organic carbon in the shallow area of area of Lagoa dos Patos estuary, southern Brazil. Atlantica (Brazil).

Proença LAO [1990] Ciclo anual da produção primáiria, biomassa do fitoplâncton e carbono orgânico particulado em área rasa da porção sul da Lagoa dos Patos. M.Sc. Thesis, FURG - RS, Brazil, 81 pp.

Pokavanich T, Alosairi Y [2014] Summer flushing characteristics of Kuwait Bay. *Jour of Coa Res*, *30*(5), 1066-1073. https://doi.org/10.2112/JCOASTRES-D-13-00188.1.

Rede Brasileira de Pesquisa em Acidificação dos Oceanos (BrOA) [2022]. Retrieved May 31, 2022, from http://broa.furg.br

Ragueneau O, Savoye N, Del Amo Y, Cotten J, Tardiveau B, Leynaert A [2005] A new method for the measurement of biogenic silica in suspended matter of coastal waters: using Si: Al ratios to correct for the mineral interference. Cont She-Res, 25(5-6), 697-710. https://doi.org/10.1016/j.csr.2004.09.017

Redfield A, Ketchum B, Richards F [1963] The influence of organisms on the com- position of sea water. In: Hill, M.N. (Ed.), The Sea. The Composition of Sea-water Comparative and Descriptive Oceanography, vol. 2. Interscience Publishers, New York, pp. 26–77. https://www.scopus.com/record/display.uri?eid=2-s2.00003663268&origin=inward&txGid=2dfb25084f2813f557f81c48cdaed585

Regnier P [2013a] Modelling estuarine biogeochemical dynamics: from the local to the global scale. Aqua geochem, 19(5-6):591–626. https://doi.org/10.1007/s10498-013-9218-3

Regnier P, Friedlingstein P, Ciais P, Mackenzie FT, Gruber N, Janssens IA, Arndt S [2013b] Anthropogenic perturbation of the carbon fluxes from land to ocean. Nat geos, 6(8), 597-607. https://doi.org/10.1038/ngeo1830

Reynolds CS [2006] The ecology of phytoplankton. Cambridge University Press. https://doi.org/10.1017/CBO9780511542145

Risgaard-Petersen N [2004] Denitrification. In: Nielsen, S.L., Banta, G.T., Pedersen, M.F. (eds) Estuarine Nutrient Cycling: The Influence of Primary Producers. Aquatic Ecol B Ser, vol 2. Springer, Dordrecht. https://doi.org/10.1007/978-1-4020-3021-5_10

RG Pilots. Praticagem de Rio Grande [2022]. Retrieved February 17, 2022, from https://rgpilots.com.br

R Development Core Team [2022]. R: A Language and Environment for Statistical Computing. R Foundation for Statistical Computing, Vienna, Austria ISBN 3-900051- 07-0, URL. http://www.R-project.org

Ro KS, Hunt PG [2006] New unified equation for wind-driven surficial oxygen transfer into stationary water bodies. *Trans of the ASABE*. https://doi.org/10.13031/2013.22020

Santos L, Vaz L, Gomes NCM, Vaz N, Dias JM, Cunha Â, Almeida A [2014] Impact of freshwater inflow on bacterial abundance and activity in the estuarine system Ria de Aveiro. Est, Coa and She Sci, 138, 107-120. vier Ltd. https://doi.org/10.1016/j.ecss.2013.12.021

Schafer KVR, Tripathee F, Artigas TH, Morin, Bohrer G [2014] Carbon dioxide fluxes of an urban tidal marsh in the Hudson-Raritan estuary, J. Geophys. Res. Biogeosci.,119,2065–2081, http://doi.org/10.1002/2014JG002703

Scottá FC, Andrade MM, Silva Jr VO, Oliveira N, Weschenfelder J, Bortolin EC, Nunes JC [2019). Geoacoustic patterns of the Guaíba River bottom and sub-bottom and their relationship with sedimentary and hydrodynamic processes. *Brazilian* Jour of Geoph 37(1): 105-120. https://doi.org/10.22564/rbgf.v37i1.1991

Soares I, Möller OO [2001] Low-frequency currents and water mass spatial distribution on the southern Brazilian shelf. Cont She-Res, 21(16-17), 1785-1814. https://doi.org/10.1016/S0278-4343(01)00024-3

Souza RB, Copertino MS, Fisch G, Santini MF, Pinaya WH, Furlan FM, Pezzi LP [2022] Salt marsh-atmosphere CO2 exchanges in Patos Lagoon Estuary, Southern Brazil. Fron in Mar Sci, 9, 892857. http://doi.org/10.3389/fmars.2022.892857

Souza GK de CME, von Ahn LFH, Niencheski [2018] Effects of coastal lagoon water level on groundwater fluxes of nutrients to the coastal zone of southern Brazil, Jour of Mar Sys, https://doi.org/10.1016/j.jmarsys.2020.103459

Seiler LM, Fernandes EHL, Martins F, Abreu PC [2015] Evaluation of hydrologic influence on water quality variation in a coastal lagoon through numerical modeling. *Ecol Mod*. https://doi.org/10.1016/j.ecolmodel.2015.07.021

Seiler LM, Fernandes EHL, Siegle E [2020] Effect of wind and river discharge on water quality indicators of a coastal lagoon. *Reg Stu in Mar Sci*, *40*, 101513. https://doi.org/10.1016/j.rsma.2020.101513

Soares I, Möller OO [2001] Low-frequency currents and water mass spatial distribution on the southern Brazilian shelf. Cont She Res. https://doi.org/10.1016/S0278-4343(01)00024-3

Staehr PA, Bade D, Van de Bogert MC, Koch GR, Williamson C, Hanson P, Kratz T [2010] Lake metabolism and the diel oxygen technique: state of the science. Limnol and Ocean: Methods, 8(11), 628-644. https://doi.org/10.4319/lom.2010.8.0628

Staehr PA, Testa JM, Kemp WM, Cole JJ, Sand-Jensen K, Smith SV [2012] The metabolism of aquatic ecosystems: history, applications, and future challenges. Aqua Sci, 74(1), 15-29. https://link.springer.com/article/10.1007/s00027-011-0199-2

Statham PJ [2012] Nutrients in estuaries e an overview and the potential impacts of climate change. Sci. Tot Envir 434, 213-227. https://doi.org/10.1016/j.scitotenv.2011.09.088

Stech JL, Lorenzzetti JA [1992] The response of the South Brazil Bight to the passage of wintertime cold fronts. Jour of Geoph Res: Oce 97(C6): 9507-9520.

Stott P [2016] How climate change affects extreme weather events. *Sci.* https://doi.org/10.1126/science.aaf7271

Strickland JD [1968] A practical handbook of seawater analysis. Fish Res Bd 167:1–311. http://dx.doi.org/10.25607/OBP-1791

Sunda WG, Cai WJ [2012] Eutrophication induced CO_2-acidification of subsurface coastal waters: interactive effects of temperature, salinity, and atmospheric p CO_2. Env sci and tech, 46(19), 10651-10659. https://doi.org/10.1021/es300626f

Seeliger U [2001] The Patos Lagoon Estuary, Brazil. In *Coastal marine ecosystems of Latin America* (pp. 167-183). Springer, Berlin, Heidelberg.

SiMCosta. Sistema de Monitoramento da Costa Brasileira., 2022. Retrieved February 17, 2022, from https://simcosta.furg.br

Távora J, Fernandes EH, Bitencourt LP, Orozco PMS [2020] El-Niño Southern Oscillation (ENSO) effects on the variability of Patos Lagoon Suspended Particulate Matter. Reg St in Mar Sci, 40, 101495. https://doi.org/10.1016/j.rsma.2020.101495

Takahashi T, Sutherland SC, Wanninkhof R, Sweeney C, Feely RA, Chipman D W, De Baar HJ [2009] Climatological mean and decadal change in surface ocean pCO_2, and net sea–air CO_2 flux over the global oceans. Deep Sea Res Part II: Top Stu in Ocean, 56(8-10), 554-577. https://doi.org/10.1016/j.dsr2.2008.12.009

Testa JM, Kemp WM, Hopkinson, CS, Smith SV [2012] Ecosystem metabolism. Estu ecol: 381-416.

https://doi.org/10.1002/9781118412787.ch15

Thébault J, Schraga TS, Cloern JE, Dunlavey EG [2008] Primary production and carrying capacity of former salt ponds after reconnection to San Francisco Bay. Wetlands. https://doi.org/10.1672/07-190.1

They NH, Ferreira LMH, Marins LF, Abreu PC [2015] Bacterial community composition and physiological shifts associated with the El Niño Southern Oscillation (ENSO) in the Patos Lagoon Estuary. Mic ecol. https://doi.org/10.1007/s00248-014-0511-5

They NH, Marins LF, Möller OO, Abreu PC [2019] High bacterial activity in nutrient rich saltwater: Evidence from the uncoupling between salinity and nutrients in the Patos Lagoon estuary. Est, Coa and She-Sci, 216, 148-156. https://doi.org/10.1016/j.ecss.2018.09.001

Valiela I [2015] Marine ecological processes. New York: Springer. https://doi.org/10.1007/978-0-387-79070-1

van Rijn LC, Walstra DJ, Grasmeijer B, Sutherland J, Pan S, Sierra JP [2003] The predictability of cross-shore bed evolution of sandy beaches at the time

scale of storms and seasons using process-based profile models. *Coa Eng*, *47*(3), 295-327. https://doi.org/10.1016/S0378-3839(02)00120-5.

Vaz AC, Möller OO, Almeida TLD [2006] Análise quantitativa da descarga dos rios afluentes da Lagoa dos Patos. http://repositorio.furg.br/handle/1/694

Vaz L, Frankenbach S, Serôdio J, Dias JM [2019] New insights about the primary production dependence on abiotic factors: Ria de Aveiro case study. Ecol Ind, 106, 105555. https://doi.org/10.1016/j.ecolind.2019.105555

Vollenweider R, [1998] Characterization of the trophic conditions of marine coastal waters with special reference to the NW adriatic sea: proposal for a trophic scale, turbidity and generalized water quality index. Environ 9(3):329–357. https://doi.org/10.1002/(SICI)1099-095X(199805/06)9:3<329::AID-ENV308>3.0.CO;2-9

Yao H, Montagna PA, Wetz MS, Staryk CJ, Hu X [2022] Subtropical estuarine carbon budget under various hydrologic extremes and implications on the lateral carbon exchange from tidal wetlands. Wat Res, 217, 118436. https://doi.org/10.1016/j.watres.2022.118436.

Wang CF, Hsu MH, Kuo AY [2004] Residence time of the Danshuei River estuary, Taiwan. Est, Coa and She Sci, 60(3), 381-393. https://doi.org/10.1016/j.ecss.2004.01.013

Wallner-Kersanach M, Mirlean N, Baumgarten MZ, Costa LD.F, Baisch PRM [2015]. Temporal evolution of the contamination in the southern area of Patos Lagoon Estuary, RS, Brazil. http://repositorio.furg.br/handle/1/5973

Wallner-Kersanach M, Machado EC [2010] Amostragem e análise de carbono orgânico particulado (COP) e nitrogênio orgânico particulado (NOP). In: Baumgarten MGZ, Wallner-Kersanach M, Niencheski LFH (Org.) Manual de Análises em Oceanografia Química 2ed, Rio Grande, Editora da FURG, 156-166.

Walstra DJR, Van Rijn LC, Blogg H, Van Ormondt M [1999] Evaluation of a hydrodynamic area model based on the COAST3D data at Teignmouth 1999. In Proceedings of coastal dynamics 2001 conference, Lund D (Vol. 4, pp. 1-D4).

Weiss R [1974] Carbon dioxide in water and seawater: the solubility of a non-ideal gas. Mar chem 2(3), 203-215. https://doi.org/10.1016/0304-4203(74)90015-2

Windom HL, Niencheski LF, Smith Jr RG [1999] Biogeochemistry of nutrients and trace metals in the estuarine region of the Patos Lagoon (Brazil). Est, Coa and She-Sci, 48(1), 113-123. https://doi.org/10.1006/ecss.1998.0410

Wood SN [2017] Generalized additive models: an introduction with R (Second edition). chapman and hall/CRC. https://doi.org/10.1201/9781315370279

Wood S [2018] Mixed GAM computation vehicle with GCV/AIC/REML smoothness estimation and GAMMs by REML/PQL. *R package version*, 1-8.

Wolfe, D. A. (Ed.). [1986]. Estuarine variability. Elsevier.

Wright SW, Ishikawa A, Marchant HJ, Davidson AT, van den Enden RL, Nash GV [2009] Composition and significance of picophytoplankton in Antarctic waters. Pol Biol, 32(5), 797-808. https://doi.org/10.1007/s00300-009-0582-9

Wright SW, van den Enden RL, Pearce I, Davidson AT, Scott FJ, Westwood K J. [2010] Phytoplankton community structure and stocks in the Southern Ocean (30–80 E) determined by CHEMTAX analysis of HPLC pigment signatures. Deep Sea Res P II: Top St in Oce, *57*(9-10), 758-778. https://doi.org/10.1016/j.dsr2.2009.06.015

Wurtsbaugh WA, Paerl HW, Dodds WK [2019] Nutrients, eutrophication and harmful algal blooms along the freshwater to marine continuum. Wiley Int Rev: Wat, 6(5), e1373. https://doi.org/10.1002/wat2.1373.

Zapata M, Rodríguez F, Garrido JL [2000] Separation of chlorophylls and carotenoids from marine phytoplankton: a new HPLC method using a reversed phase C8 column and pyridine-containing mobile phases. Mar Ecol Prog Ser, 195, 29-45. https://doi.org/ doi:10.3354/meps195029

Zago MSA [1976] The planktonic Cladocera (Crust.) and aspects of the eutrophication of American Reservoir, Braz Bol Zool. 1:105-145. https://doi.org/10.11606/issn.2526-3358.bolzoo.1976.121561

Zhao Y, Quigg A [2014] Nutrient limitation in Northern Gulf of Mexico (NGOM): phytoplankton communities and photosynthesis respond to nutrient pulse. *PloS one*, *9*(2), e88732. https://doi.org/10.1371/journal.pone.0088732

Zeebe RE, Wolf-Gladrow D [2007] CO_2 in seawater: equilibrium, kinetics, isotopes (No. 65). Gulf Professional Publishing.

Zeldis JR, Swaney DP [2018] Balance of catchment and offshore nutrient loading and biogeochemical response in four New Zealand coastal systems: implications for resource management. Est and Coa, 41, 2240-2259. https://doi.org/10.1007/s12237-018-0432-5

Zuur AF [2012] A beginner's guide to generalized additive models with R (pp. 1-206). Newburgh: Highland Statistics Limited.

ANEXO A

Este anexo contém as seguintes figuras e tabelas mencionadas no capítulo IV: Table A.1, Table A.2, Table A.3, Table A.4, Figure A.1, Figure A.2, Table A.5, Table A.6, Figure A.3, Figure A.4, Figure A.5, Figure A.6 e Figura A.7.

Table A.1. Dates of the pelagic ecosystem metabolism experiments at stations 1 and 2 in the Patos Lagoon Estuary, Brazil.

Station	Dates
1	Fev-23, Fev-25, Fev-26, Fev-28, Mar-02, Mar-09, Mar-11, Mar-15, Mar-17, Mar-19, Mar-23
2	Fev-24, Fev-27, Mar-03, Mar-05, Mar-10, Mar-12, Mar-16, Mar-18, Mar-22

Table A.2. Minimum, maximum, mean ± standard deviation (SD) of salinity and temperature (°C) for the stations 1 and 2 in the Patos Lagoon Estuary at the surface, intermediate (only at station 2) and bottom layers from Feb-24-2021 to Mar-23-2021 (late austral summer). Kruskal-Wallis differences among means of the two stations (KWst) and among means of the layers (KWdp): p-value: <0.001 (***), <0.01 (**), <0.05 (*), <0.1 (.), >0.1 (x).

	Salinity					Temperature (°C)				
	Min.	Max.	Mean ± SD	KWdp	KWst	Min.	Max.	Mean ± SD	KWdp	KWst
St. 1										
Surface	5.2	26.6	17.9 ± 5.4	*	***	22.0	27.6	25.1 ± 1.2	x	x
Bottom	14.7	32.3	23.4 ± 5.0	*	***	23.4	27.1	24.9 ± 0.9	x	x
St. 2										
Surface	5.6	33.2	22.6 ± 9.5	***	***	24.2	26.6	25.2 ± 0.5	x	x
Interm.	6.9	33.2	26.0 ± 7.9	***	***	24.4	26.7	25.3 ± 0.5	x	x
Bottom	8.4	33.6	29.1 ± 6.9	***	***	24.4	26.0	25.2 ± 0.4	x	x

Table A.3. Minimum (Min), maximum (Max), mean ± standard deviation (SD) at the surface and bottom, for the dissolved inorganic nutrients (nitrite, nitrate, ammonium, phosphate and silicate (µM)), dissolved oxygen (DO – µmol), dissolved oxygen saturation (DOS) and TRIX (trophic index), for station 1 and 2 in the Patos Lagoon Estuary from Feb-24-2021 to Mar-23-2021 (late austral summer). Kruskal-Wallis differences between means of the two stations (KW_{st}) and among means of water column layer of same station (KW_{dp}): p-value: <0.001 (***), <0.01 (**), <0.05 (*), <0.1 (.), >0.1 (x), repeated (r). KW was not performed (-) for the station 2 intermediate layer due the lack of data in the station 1 intermediate layer. Sample n = 152.

	Min	Max	Mean ± SD	KW_{st}	KW_{dp}
St. 1 surface					
Nitrite	0.00	0.1	0.06 ± 0.04	*	.
Nitrate	0.3	6.4	1.8 ± 6.4	.	.
Ammonium	0.5	10.3	3.1 ± 2.4	x	.
Phosphate	1.0	2.6	1.6 ± 0.4	x	.
Silicate	20.7	222.9	95.9 ± 46.5	x	*
DO	196.9	298.4	250.1 ± 26.9	x	*
DOS	74.2	119.6	93.8 ± 10.5	*	**
TRIX	3.8	7.8	5.4 ± 1.0	x	.
St. 1 Bottom					
Nitrite	0.002	0.2	0.07 ± 0.05	.	r
Nitrate	0.3	6.6	2.6 ± 1.5	.	r
Ammonium	0.4	12.7	3.4 ± 2.7	.	r
Phosphate	1.0	4.6	1.7 ± 0.6	.	r
Silicate	31.2	98.7	69.1 ± 13.6	**	r
DO	180.1	298.8	228.1 ± 29.2	**	r
DOS	48.8	105.1	84.5 ± 14.1	*	r
TRIX	4.3	9.1	6.2 ± 1.2	.	r
St. 2 Surface					
Nitrite	0.01	0.2	0.09 ± 0.05	r	x
Nitrate	0.2	6.3	2.1 ± 1.6	r	*
Ammonium	0.3	7.6	2.3 ± 1.8	r	x
Phosphate	1.0	2.0	1.5 ± 0.2	r	x
Silicate	32.6	188.4	93.2 ± 50.0	r	*
DO	217.7	288.8	252.7 ± 19.7	r	**
DOS	90.7	105.9	95.8 ± 3.9	r	x
TRIX	3.5	6.3	5.0 ± 0.8	r	*
St. 2 Interm.					
Nitrite	0.0	0.3	0.1 ± 0.0	-	r
Nitrate	0.3	6.7	2.4 ± 1.6	-	r
Ammonium	0.3	5.8	2.1 ± 1.3	-	r
Phosphate	1.0	2.1	1.5 ± 0.2	-	r
Silicate	35.7	183.9	71.7 ± 39.6	-	r
DO	213.7	285.6	240.9 ± 16.2	-	r
DOS	84.1	109.0	94.0 ± 4.7	-	r
TRIX	3.6	6.2	5.2 ± 0.7	-	r
St. 2 Bottom					
Nitrite	0.01	0.2	0.1 ± 0.06	r	r
Nitrate	0.5	5.0	2.1 ± 1.2	r	r
Ammonium	0.6	5.7	2.3± 1.2	r	r
Phosphate	0.7	2.5	1.6 ± 0.3	r	r
Silicate	26.5	176.6	59.5 ± 33.4	r	r
DO	201.2	278.9	234.2 ± 17.6	r	r

DOS	82.0	103.8	92.3 ± 4.9	r	r
TRIX	4.3	6.6	5.5 ± 0.7	r	r

Table A.4. Minimum (Min), maximum (Max), mean ± standard deviation (SD) on the surface and bottom, for the variables hydrogenionic potential (pH - total scale), total alkalinity (TC - µmol/kg), total inorganic carbon (TC - µmol/kg), carbon dioxide partial pressure (pCO_2 µatm) and the air/water carbon dioxide net fluxes (FCO_2 – mmol C m^2 d^{-1}; positive values denote outgassing to the atmosphere, and negative, ingassing), for station 1 and 2, in the Patos Lagoon Estuary from Feb-24-2021 to Mar-23-2021 (late austral summer). Kruskal-Wallis among stations (KW_{st}) and among water column layers (KW_{dp}): p-value: <0.001 (***), <0.01 (**), <0.05 (*), <0.1 (.), >0.1 (x), repeated (r). Sample n = 76, (46 for FCO_2).

	Min	Max	Mean ± SD	KW_{st}	KW_{dp}
St. 1 Surface					
pH	7.4	8.1	7.8 ± 0.2	***	x
TC	777.1	1925.4	1539.8 ± 386.8	**	-
TA	572.2	2023.9	1376.2 ± 303.3	***	-
pCO_2	234.3	1,173.9	450.3 ± 302.3	*	-
FCO_2	–42.5	104.9	4.4 ± 41.2	x	-
St. 2 Surface					
pH	7.5	8.2	8.0 ± 0.17	r	x
TC	1124.3	1980.4	1761.9 ± 253.2	r	***
TA	786.3	2245.8	1685.3 ± 495.0	r	***
pCO_2	169.5	612.5	284.7 ± 85.6	r	.
FCO_2	–38.9	49.4	–15.4 ± 17.3	r	-
St. 2 Bottom					
pH	7.6	8.1	8.0 ± 0.1	***	r
TC	440.69	1816.5	1234.1 ± 333.3	***	r
TA	1268.8	2302.6	2076.4 ± 283.3	***	r
pCO_2	294.2	4207.8	581.4 ± 833.5	*	r

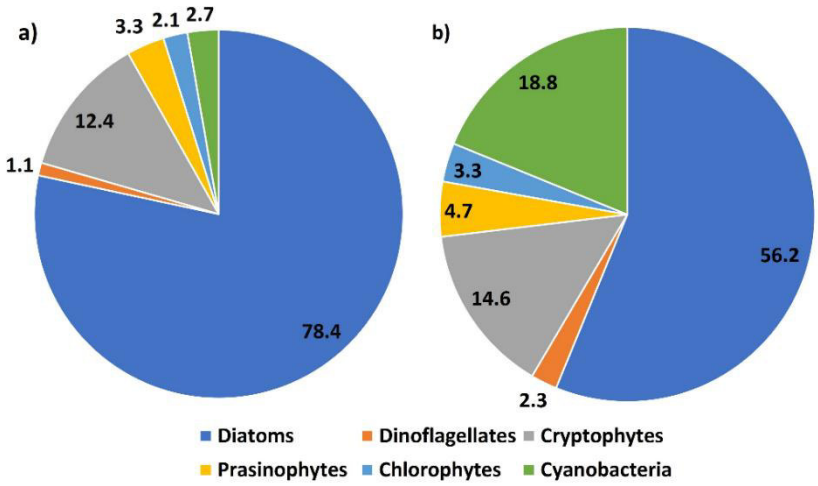

Figure A.1. Phytoplankton groups total contribution (%) at the surface layer of station 1 (a) and 2 (b), Patos Lagoon Estuary, from Feb-24-2021 to Mar-23-2021 (late austral summer).

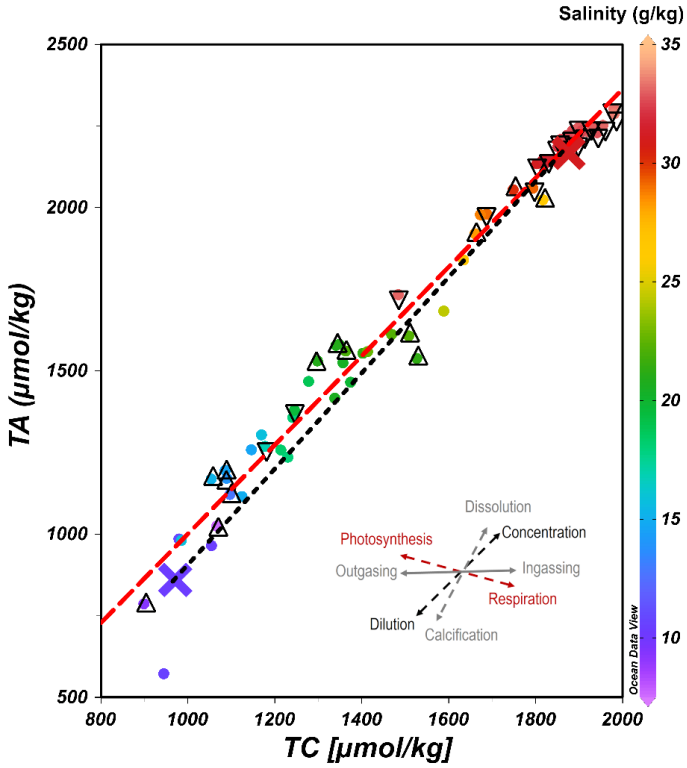

Figure A.2. Scatterplot of total dissolved inorganic carbon (TC) versus total alkalinity (TA), with salinity in the color gradient. Data for the station 1 and 2, in the Patos Lagoon Estuary, from Feb-24-2021 to Mar-23-2021 (late austral summer). The triangles represent the surface, and the inverted triangles represent the bottom for station 2, while the dots represent the surface for station 1. The color gradient inside the symbols represents the salinity. The main processes that drive the carbonate system in the Patos Lagoon Estuary are represented by the insert arrows, adapted from Zeebe and Wolf Gladrow [2007]. The data disposed along the linear regression (red dashed line), if on the bottom, represent a carbon dilution (low TC) condition, while on the top, a carbon concentrated condition. Those displaced on the bottom left-hand side represent the estuarine water behaving as a net source of CO_2 to the atmosphere, on the middle left-hand side the carbon uptake by photosynthesis, on the top left-hand side the carbonate dissolution. Otherwise, those data displaced on the top right-hand-side represent the estuarine water is acting as a net sink of CO_2 from the atmosphere, on the middle right-hand side, the organic matter respiration, returning the carbon to the estuarine water, and finally, on the bottom right-hand side, the carbon uptake by calcifying organisms. The dotted line depicts the theoretical conservative mixing line of riverine and oceanic waters, which indicate the effect of dilution and concentration of salt on changing the AT-CT concentrations. The purple and the red crosses represent the riverine and oceanic waters endmembers. Sample n = 65.

Table A.5. Details of the GAM (generalized additive model) for gross primary production (GPP) as the dependent variable, at station 1 and 2 in the Patos Lagoon Estuary**.** Data from Feb-24-2021 to Mar-23-2021 (late austral summer). As independent variables: temperature (Temp), salinity (Sal), nitrate (Nitra), phosphate (Phos), silicate (Sili), turbidity (Turb), trix trophic index (TRIX), photosynthetically active radiation (PAR), wind speed and direction (W), water flow rate (Flow). Others: Akaike information criterion (AIC), r squared (R^2), deviance explained (Dev.exp), bottom layer (Lay.Bot, intercept – itc), intermediate layer (Lay.Int), surface layer (Lay.Sup), standard error (SE), degrees of freedom (df), and F statistics (F). Sample n = 46.

Model and diagnostics	Term	Parametric coefficients			GAM analysis of variance		
		Estimate	SE	p.value	df	F	p.value
GPP ~ s(Flow) + s(Sal) + s(Nitra) +	Lay.Bot (itc)	3.29	0.10	2e-16			
s(Sili) + Lay	Lay.Int	1.07	0.17	6e-06			
AIC: 33.1 R2: 0.88; Dev.exp:	Lay.Sup	0.16	0.17	0.38			
95.3%	s(Flow)				7.37	4.37	4e-3
	s(Sal)				6.60	7.80	2e-4
	s(Nitra)				3.47	18.87	7e-6
	s(Sili)				7.75	5.19	0.002
GPP ~ s(W) + s(Sal) + s(Nitra) +	Lay.Bot (itc)	3.43	0.12	2e-16			
s(Sili) + Lay	Lay.Int	0.85	0.19	3e-4			
AIC: 45.3 R2: 0.85; Dev.exp: 93%	Lay.Sup	-0.05	0.21	0.79			
	s(W)				7.42	4.04	6e-3
	s(Sal)				4.40	8.58	3e-4
	s(Nitra)				3.50	17.35	3e-6
	s(Sili)				7.60	3.16	0.02
GPP ~ s(Temp) + s(Sal) + s(Chl-*a*)	Lay.Bot (itc)	3.30	0.13	3e-16			
+ s(Nitra) + Lay	Lay.Int	0.86	0.23	1e-3			
AIC: 47.4; R2: 0.84; Dev.exp:	Lay.Sup	0.19	0.21	0.37			
92.8%	s(Temp)				8.26	1.53	0.22
	s(Sal)				2.87	6.67	4e-3
	s(Chl-*a*)				5.77	5.68	1e-3
	s(Nitra)				6.42	3.59	0.01
GPP ~ s(Flow) + s(Sal) + s(Nitra) +	Lay.Bot (itc)	3.06	0.16	1e-14			
s(Turb) + Lay	Lay.Int	1.27	0.25	7e-5			
AIC: 55.0; R2: 0.81; Dev.exp:	Lay.Sup	0.64	0.27	0.02			
90.7%	s(Flow)				1.00	1.32	0.26
	s(Sal)				5.70	9.73	6e-5
	s(Nitra)				5.31	9.65	5e-5
	S(Turb)				8.92	2.79	0.02

Table A.6. Details of the GAM (generalized additive model) for respiration rate (R) as the dependent variable, for station 1 and 2 in the Patos Lagoon Estuary**.** Data from Feb-24-2021 to Mar-23-2021 (late austral summer). As independent variables: temperature (Temp), salinity (Sal), nitrate (Nitra), phosphate (Phos), silicate (Sili), turbidity (Turb), trix trophic index (TRIX), photosynthetically active radiation (PAR), wind speed and direction (W), water flow rate (Flow). Others: Akaike information criterion (AIC), r squared (R^2), deviance explained (Dev.exp), bottom layer (Lay.Bot, intercept – itc), intermediate layer (Lay.Int), surface layer (Lay.Sup), standard error (SE), degrees of freedom (df), and F statistics (F). Sample n = 46.

Model and diagnostics	Term	Parametric coefficients			GAM analysis of variance		
		Estimate	SE	p.value	df	F	p.value
R ~ s(Temp) + s(PAR) + s(W) +	Lay.Bot (itc)	1.64	0.07	6e-11			
s(Phos) + Lay	Lay.Int	-0.07	0.04	0.09			
AIC: –96.5; R2: 0.83; Dev.exp: 95.2%	Lay.Sup	-0.22	0.18	0.24			
	s(Temp)				7.82	7.87	1e-3
	s(PAR)				8.99	9.84	2e-4
	s(W)				8.95	5.30	3e-3
	s(Phos)				4.34	1.83	0.16
R ~ s(Temp) + s(PAR) + s(W) +	Lay.Bot (itc)	0.62	0.03	4e-13			
s(Flow) + Lay	Lay.Int	0.02	0.01	0.26			
AIC: –72.9; R2: 0.78; Dev.exp: 91.2%	Lay.Sup	0.12	0.07	0.13			
	s(Temp)				4.99	7.02	9e-4
	s(PAR)				8.43	8.76	8e-5
	s(W)				8.82	2.42	0.03
	s(Flow)				2.24	2.75	0.06
R ~ s(Temp) + s(Chl-a) + s(W) +	Lay.Bot (itc)	1.55	0.03	2e-16			
s(Turb) + Lay	Lay.Int	-0.06	0.04	0.22			
AIC: –70.8; R2: 0.76; Dev.exp: 90.5%	Lay.Sup	-4e-3	0.05	0.93			
	s(Temp)				7.17	2.68	0.07
	s(Chl-*a*)				3.17	2.21	0.11
	s(W)				8.14	2.91	0.02
	s(Turb)				6.57	7.92	3e-4
R ~ s(Temp) + s(Chl-*a*) + s(W) +	Lay.Bot (itc)	1.47	0.02	2e-16			
s(Nitra) + Lay	Lay.Int	0.02	0.05	0.61			
AIC: –66.0; R2: 0.73; Dev.exp: 89.2%	Lay.Sup	0.14	0.04	5e-3			
	s(Temp)				1.00	5.08	3e-3
	s(Chl-*a*)				8.99	5.19	1e-3
	s(W)				7.89	2.44	0.05
	s(Nitra)				6.23	7.13	5e-4

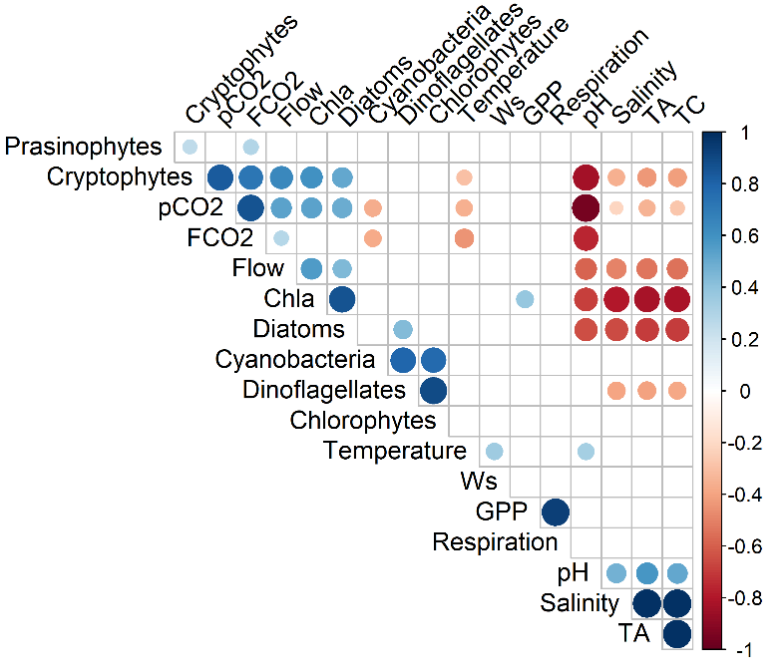

Figure A.3. Pearson's correlation matrix of the main meteoceanographic variables, carbonate system parameters, and phytoplankton groups, for station 1 and 2 surface layer (n= 18), in the Patos Lagoon Estuary, Brazil, from Feb-24-2021 to Mar-23-2021 (late austral summer). Only significant correlations are shown in the graph ($p < 0.05$). Positive correlations are indicated by blue circles, and negative by red circles. The color intensity represents the strength of the correlation from 0 to 1 for positive and 0 to -1 for negative correlations. Abbreviations: Gross primary production (GPP), total alkalinity (TA), total inorganic carbon (TC), water carbon dioxide partial pressure (pCO_2), and net CO_2 fluxes between air/water (FCO_2), chlorophyll-a (chla), wind speed and direction (Ws), and water flow rate (Flow).

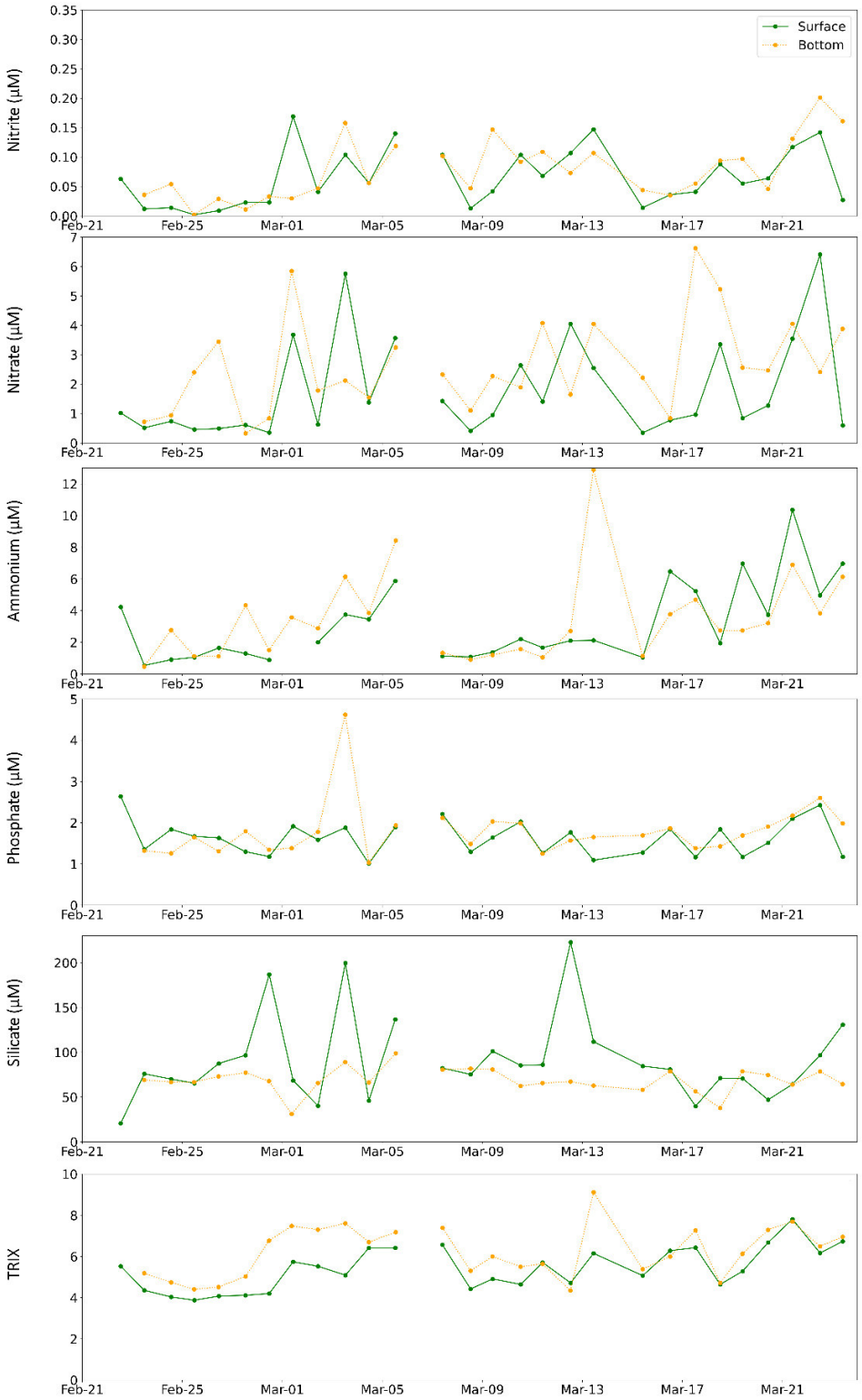

Figure A.4. Time series of dissolved inorganic nutrients (nitrite, nitrate, ammonium, phosphate, silicate) and TRIX trophic index, for station 1 in the Patos Lagoon Estuary from Feb-23-2021 to Mar-23-2021 (late austral summer). Continuous line (surface), dotted (bottom).

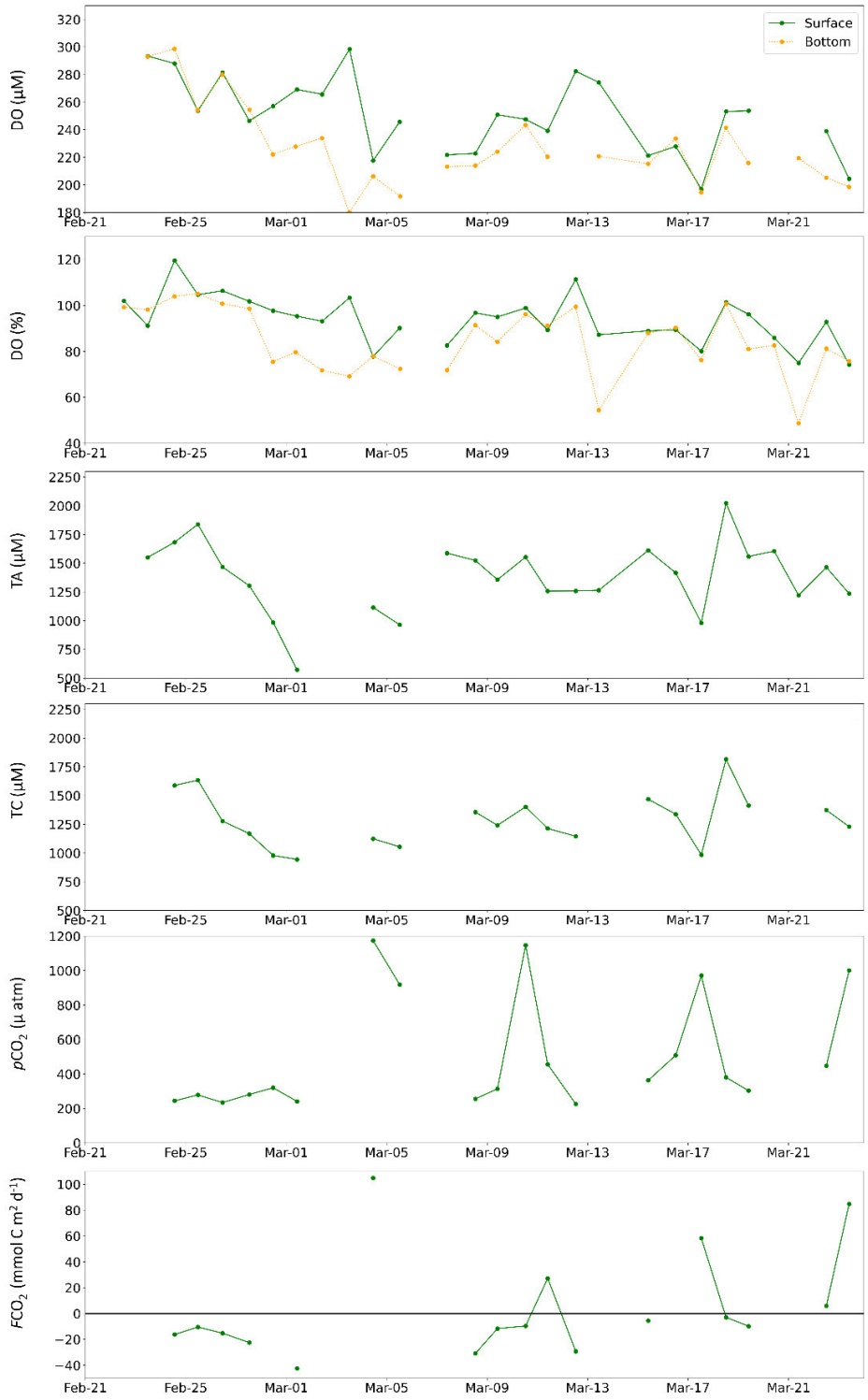

Figure A.5. Time series of dissolved oxygen (DO) and its saturation index (DOS), total alkalinity (TA), total carbon (TC), water partial pressure of carbon dioxide (pCO_2) and water-air net carbon dioxide fluxes (FCO_2), for station 1 in the Patos Lagoon Estuary from Feb-23-2021 to Mar-23-2021 (late austral summer). Continuous line (surface), dotted (bottom).

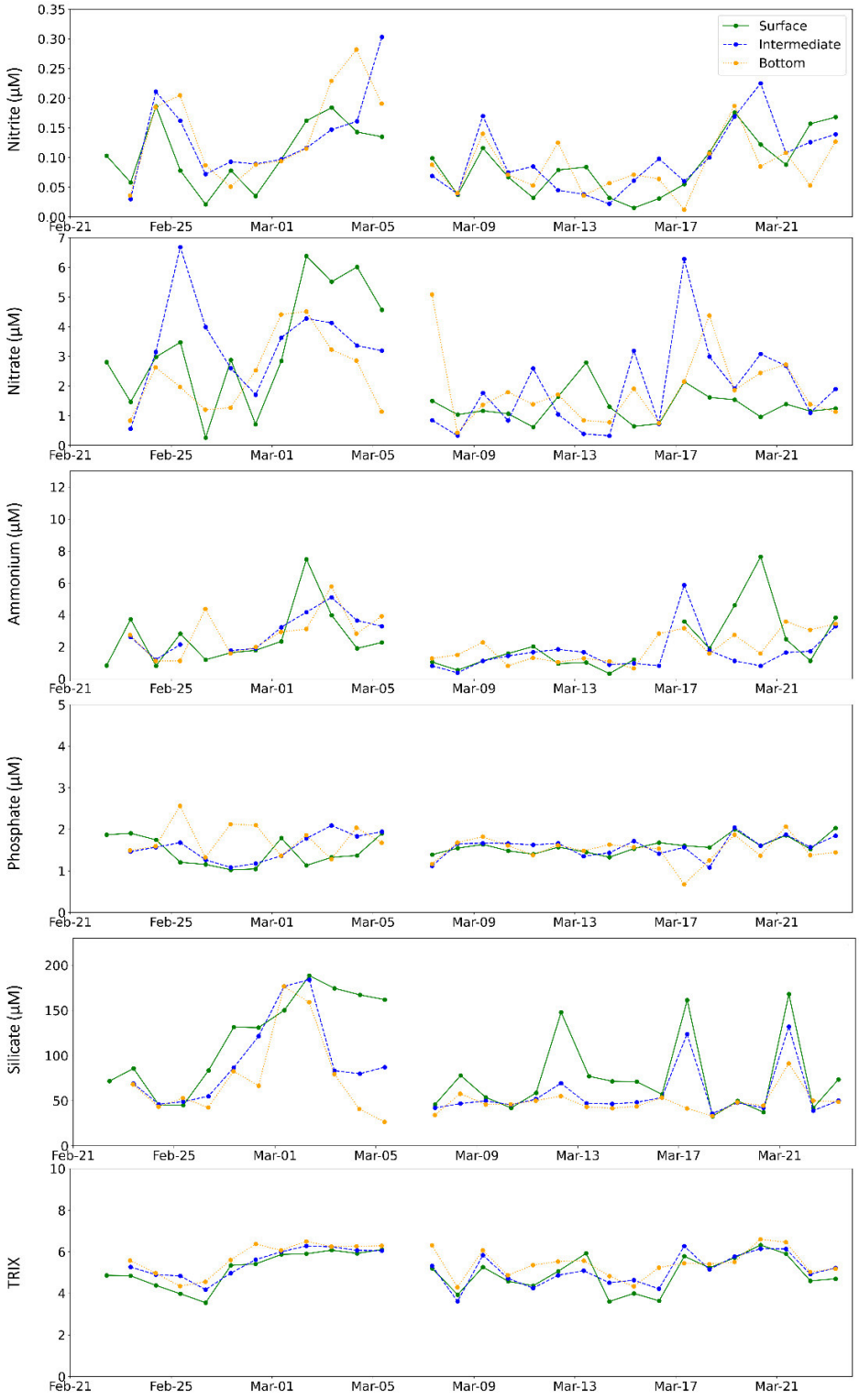

Figure A.6. Time series of dissolved inorganic nutrients (nitrite, nitrate, ammonium, phosphate, silicate) and TRIX trophic index, for station 2 in the Patos Lagoon Estuary from Febr-23-2021 to Mar-23-2021 (late austral summer). Continuous line (surface), dashed (intermediate), dotted (bottom).

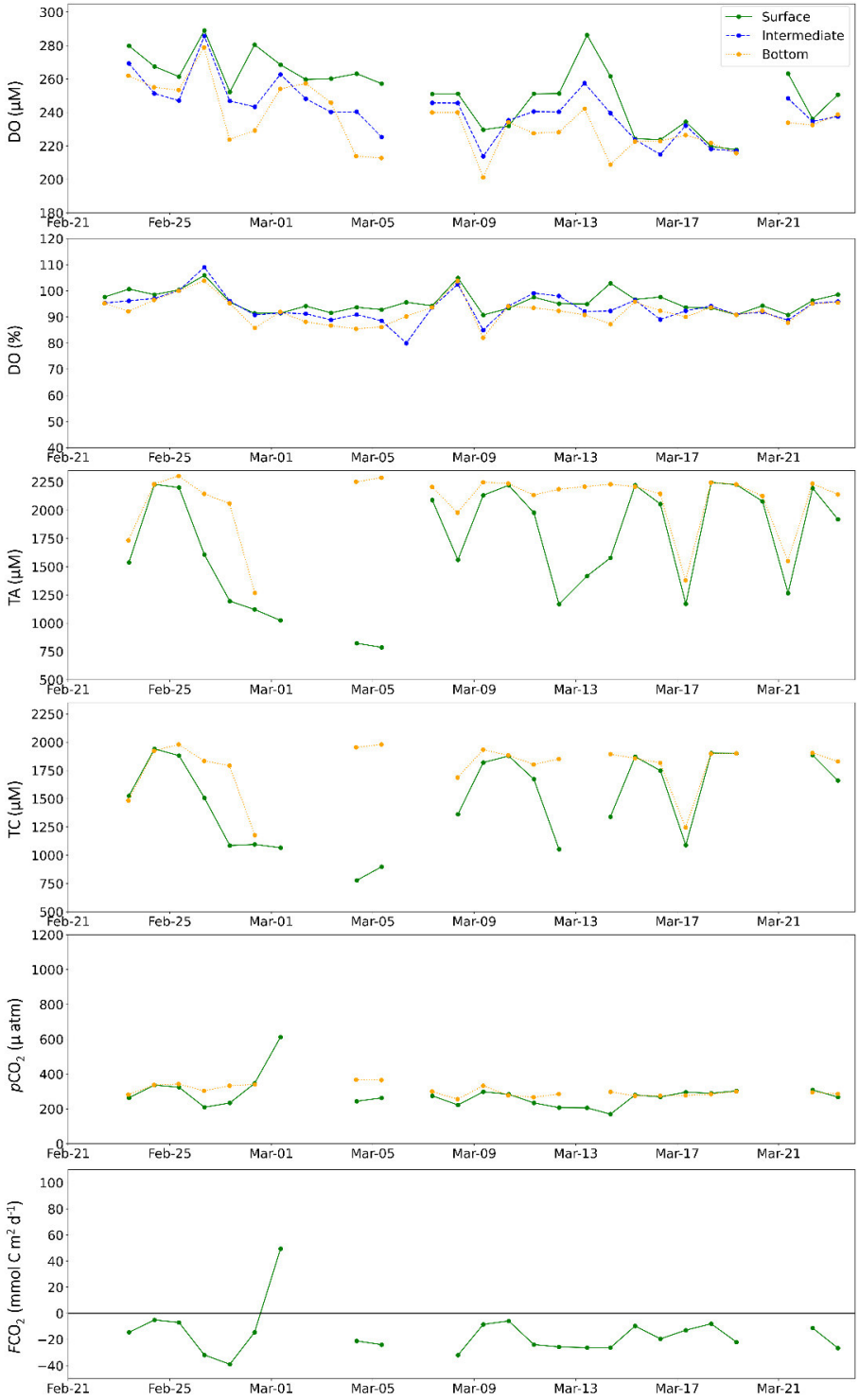

Figure A.7. Time series of dissolved oxygen (DO) and its saturation index (DOS), total alkalinity (TA), total carbon (TC), partial pressure of carbon dioxide (pCO_2) and water-air net carbon dioxide fluxes (FCO_2), for station 2 in the Patos Lagoon Estuary from Febr-23-2021 to Mar-23-2021 (late austral summer). Continuous line (surface), dashed (intermediate), dotted (bottom).

ANEXO B

Este anexo contém as seguintes figuras e tabelas mencionadas no capítulo VIII: Figure B.1., Table B.1., Table B.2., Figure, B.2., Figure B.3., Figure B.4, Figure B.5. e Figure B.6.

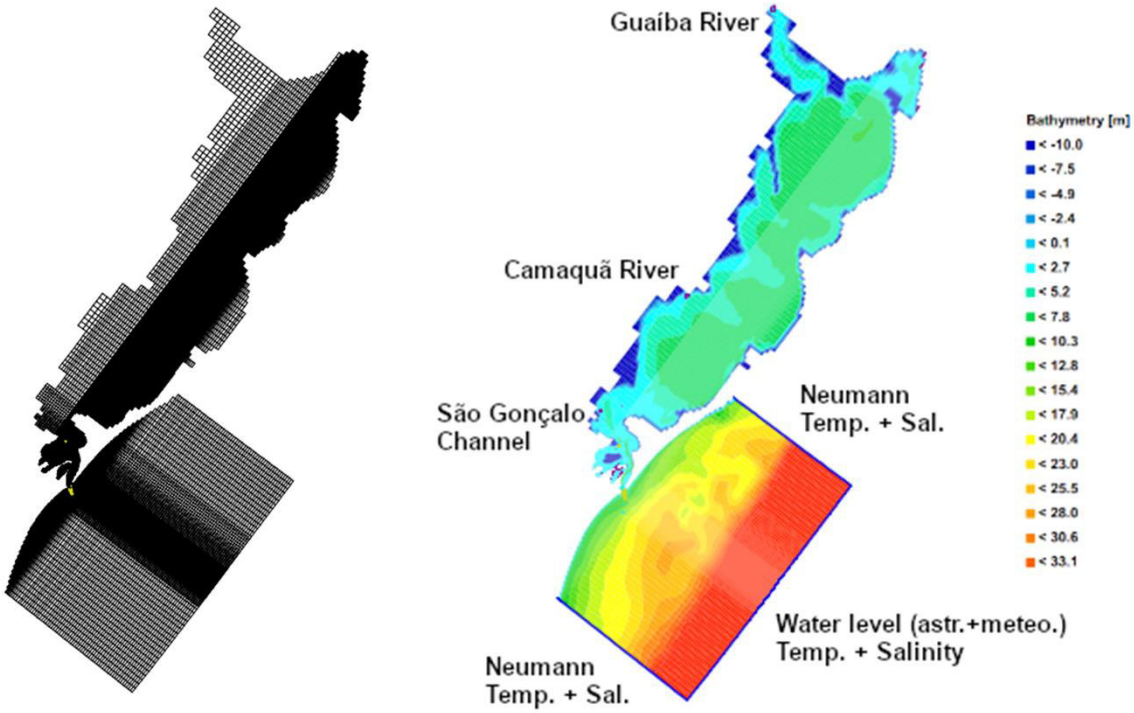

Figure B.1. The Patos Lagoon Delft3D-FLOW regular mesh (left hand-side), and the bathymetric map (right hand-side) showing the oceanic open boundaries and rivers.

Table B.1. Demonstrative resume of Delft3D D-FLOW hydrodynamic model set-up. The first four simulations were for sensitivity analysis, in which the processes were being added one at a time, in order, tides (astronomical + meteorological), winds, river discharge, temperature and salinity. The root mean absolute error (RMAE) was not estimated on this phase (simulations 1 to 4). Only one process was calibrated at each phase (simulations 5 to 25, phases intercalated shadow and non-shadow lines).

Simul. n°	Period MM/YY	Roughness	Horizontal Eddy viscosity	Vertical Eddy Viscosity	Horizontal Eddy diffusivity	Vertical Eddy diffusivity	Model for 3D turbulence	Wind drag coefficient	RMAE water level	RMAE current velocity
1	02/19	Default White-Colebrook	Default	Default	Default	Default	Default K-Epsilon	Default	x	x
2	02/19	Default White-Colebrook	Default	Default	Default	Default	Default K-Epsilon	Default	x	x
3	02/19	Default White-Colebrook	Default	Default	Default	Default	Default K-Epsilon	Default	x	x
4	02/19	Default White-Colebrook	Default	Default	Default	Default	Default K-Epsilon	Default	x	x
5	02/19	Chezy Default	Default	Default	Default	Default	Default K-Epsilon	Default	SL = 0.57 Prat. = 0.59	RS-1 = 0.81 RS-2 = 0.76 RS-4 = 0.89
6	02/19	Manning Default	Default	Default	Default	Default	Default K-Epsilon	Default	SL = 0.63 Prat. = 0.60	RS-1 = 0.79 RS-2 = 0.77 RS-4 = 0.82
7	02/19	Z0 Default	Default	Default	Default	Default	Default K-Epsilon	Default	SL = 0.68 Prat. = 0.64	RS-1 = 0.89 RS-2 = 0.82 RS-4 = 0.91
8	02/19	White-Colebrook Default	Default	Default	Default	Default	Default K-Epsilon	Default	SL = 0.51 Prat. = 0.55	RS-1 = 0.77 RS-2 = 0.70 RS-4 = 0.85
9	02/19	White-Colebrook U=0.1 m V=0.1 m	Default	Default	Default	Default	Default K-Epsilon	Default	SL = 0.47 Prat. = 0.50	RS-1 = 0.74 RS-2 = 0.68 RS-4 = 0.86
10	02/19	White-Colebrook U=0.001 m V=0.001 m	Default	Default	Default	Default	Default K-Epsilon	Default	SL = 0.41 Prat. = 0.46	RS-1 = 0.71 RS-2 = 0.65 RS-4 = 0.82
11	02/19	White-Colebrook U=0.00001 m V=0.00001 m	Defalut	Default	Default	Default	Default K-Epsilon	Default	SL = 0.39 Prat. = 0.43	RS-1 = 0.69 RS-2 = 0.62 RS-4 = 0.77
12	02/19	White-Colebrook U=0.00001 m V=0.00001 m	15	Default	Default	Default	Default K-Epsilon	Default	SL = 0.37 Prat. = 0.41	RS-1 = 0.67 RS-2 = 0.60 RS-4 = 0.74
13	02/19	White-Colebrook U=0.00001 m V=0.00001 m	12.50	Default	Default	Default	Default K-Epsilon	Default	SL = 0.39 Prat. = 0.45	RS-1 = 0.78 RS-2 = 0.66 RS-4 = 0.83
14	02/19	White-Colebrook U=0.00001 m V=0.00001 m	11.25	Default	Default	Default	Default K-Epsilon	Default	SL = 0.34 Prat. = 0.40	RS-1 = 0.65 RS-2 = 0.60 RS-4 = 0.71

15	02/19	White-Colebrook U=0.00001 m V=0.00001 m	11.25	75	Default	Default	Default K-Epsilon	Default	SL = 0.31 Prat. = 0.37	RS-1 = 0.61 RS-2 = 0.57 RS-4 = 0.70
16	02/19	White-Colebrook U=0.00001 m V=0.00001 m	11.25	50	Default	Default	Default K-Epsilon	Default	SL = 0.28 Prat. = 0.34	RS-1 = 0.58 RS-2 = 0.60 RS-4 = 0.69
17	02/19	White-Colebrook U=0.00001 m V=0.00001 m	11.25	25	Default	Default	Default K-Epsilon	Default	SL = 0.25 Prat. = 0.30	RS-1 = 0.55 RS-2 = 0.59 RS-4 = 0.65
18	02/19	White-Colebrook U=0.00001 m V=0.00001 m	11.25	25	0.0001	0.01	Default K-Epsilon	Default	SL = 0.21 Prat. = 0.38	RS-1 = 0.51 RS-2 = 0.56 RS-4 = 0.62
19	02/19	White-Colebrook U=0.00001 m V=0.00001 m	11.25	25	0.0001	0.001	Default K-Epsilon	Default	SL = 0.20 Prat. = 0.36	RS-1 = 0.49 RS-2 = 0.53 RS-4 = 0.61
20	02/19	White-Colebrook U=0.00001 m V=0.00001 m	11.25	25	0.0001	0.00001	Default K-Epsilon	Default	SL = 0.20 Prat. = 0.35	RS-1 = 0.49 RS-2 = 0.53 RS-4 = 0.60
21	02/19	White-Colebrook U=0.00001 m V=0.00001 m	11.25	25	0.0001	0.00001	Constant	Default	SL = 0.24 Prat. = 0.37	RS-1 = 0.55 RS-2 = 0.58 RS-4 = 0.64
22	02/19	White-Colebrook U=0.00001 m V=0.00001 m	11.25	25	0.0001	0.00001	K-L	Default	SL = 0.25 Prat. = 0.38	RS-1 = 0.54 RS-2 = 0.57 RS-4 = 0.67
22	02/19	White-Colebrook U=0.00001 m V=0.00001 m	11.25	25	0.0001	0.00001	Algebraic	Default	SL = 0.19 Prat. = 0.25	RS-1 = 0.43 RS-2 = 0.47 RS-4 = 0.53
23	02/19	White-Colebrook U=0.00001 m V=0.00001 m	11.25	25	0.0001	0.00001	Algebraic	A=0.00155/0 B=0.003/19.22 C=0.003/19.22	SL = 0.15 Prat. = 0.21	RS-1 = 0.35 RS-2 = 0.38 RS-4 = 0.49
24	02/19	White-Colebrook U=0.00001 m V=0.00001 m	11.25	25	0.0001	0.00001	Algebraic	A=0.00155/0 B=0.003/19.22 C=0.003/19.22	SL = 0.09 Prat. = 0.17	RS-1 = 0.24 RS-2 = 0.26 RS-4 = 0.42
25	02/19	White-Colebrook U=0.00001 m V=0.00001 m	11.25	25	0.0001	0.00001	Algebraic	A=0.00155/0 B=0.00855/19.22 C=0.00855/19.22	SL = 0.05 Prat. = 0.19	RS-1 = 0.22 RS-2 = 0.19 RS-4 = 0.33

Table B.2. LOICZ box model budget table as in the toolbox, with input values (plain) and output (bold), for the two compartments, limnic Patos Lagoon (PL box) and Patos Lagoon Estuary (PLE box).

Compartment / Concentration / Fluxes / Budgets	Unity	Value entered by user (plain) or calculated by the toolbox (bold)	SD	References
PL BOX – LIMNIC PATOS LAGOON				
System area (A)	km2	9660.0	0.0	Quikin [this study]
System volume (V)	10^6 m^3	49100.0	0.0	Quikin [this study]
Average system depth (D)	**m**	**5.1**	**0.0**	**LOICZ toolbox**
Precipitation (Vp)	10^6 m^3 d^{-1}	37.1	1.1	INMET [2023]
Evaporation (Ve)	10^6 m^3 d^{-1}	-34.8	1.2	INMET [2023]
Freshwater River flow (Vq)	10^6 m^3 d^{-1}	116.0	3.6	ANA [2023]
Residual flow (Vr)	**10^6 m^3 d^{-1}**	**-118.3**	**4.0**	**LOICZ toolbox**
System Salinity (Ssys)	psu	2.0	0.1	Pereira [2003]
Downstream (Next Compartment) System Salinity (Socn=Ssysx)	psu	18.5	0.4	Pereira [2003]
Residual flux Salinity (Sr = [Socn+Ssys]/2)	**psu**	**10.2**	**0.2**	**LOICZ toolbox**
Salinity Flux of Residual flow (VrxSr)	**10^6 psu m^3 d^{-1}**	**-1207.9**	**49.0**	**LOICZ toolbox**
Salinity Flux of Exchange flow (Vx x (Socn-Ssys))	**10^6 psu m^3 d^{-1}**	**1207.9**	**49.0**	**LOICZ toolbox**
Exchange flow (Vx)	**10^6 m^3 d^{-1}**	**73.3**	**2.5**	**LOICZ toolbox**
Exchange time (tx)	**d**	**256.7**	**8.8**	**LOICZ toolbox**
Phosphorus concentration (DIP) of Precipitation (DIPp)	mmol m^{-3}	3.4	0.2	Casartelli *et al.* [2008]
Phosphorus concentration (DIP) of River flow (DIPq)	mmol m^{-3}	0.8	0.1	Pereira [2003]
System Phosphorus concentration (DIPsys)	mmol m^{-3}	1.3	0.1	Pereira [2003]
Downstream (Next Compartment) System Phosphorus concentration (DIPocn=DIPsysx)	mmol m^{-3}	1.5	0.1	Pereira [2003]
Residual flux Phosphorus concentration (DIPr = [DIPocn+DIPsys]/2)	**mmol m^{-3}**	**1.4**	**0.0**	**LOICZ toolbox**
Phosphorus Flux in Precipitation (VpxPp)	**10^3 mol d^{-1}**	**126.4**	**6.7**	**LOICZ toolbox**
	10^3 mol m^{-2} d^{-1}	**$1.3x10^{-8}$**	**$7.2x10^{-10}$**	**LOICZ toolbox**
Phosphorus Flux of River flow (VqxPq)	**10^3 mol d^{-1}**	**95.1**	**7.7**	**LOICZ toolbox**
	10^3 mol m^{-2} d^{-1}	**$9.9x10^{-9}$**	**$8x10^{-10}$**	**LOICZ toolbox**
Phosphorus Flux of Groundwater flow (VgxPg)	**10^3 mol d^{-1}**	**0.0**	**0.0**	**LOICZ toolbox**
Phosphorus Flux of Other Freshwater flows (VoxPo)	**10^3 mol d^{-1}**	**0.0**	**0.0**	**LOICZ toolbox**
Phosphorus Flux of Residual flows (VrxPr)	**10^3 mol d^{-1}**	**-161.0**	**8.0**	**LOICZ toolbox**
Phosphorus Flux of Residual flows (VrxPr)	**10^3 mol m^{-2} d^{-1}**	**$1.6x10^{-8}$**	**$8x10^{-10}$**	**LOICZ toolbox**
Net Phosphorus Flux of Exchange flow	**10^3 mol d^{-1}**	**14.4**	**7.7**	**LOICZ toolbox**
Net Phosphorus Flux of Exchange flow	**10^3 mol m^{-2} d^{-1}**	**$1.5x10^{-9}$**	**$8x10^{-10}$**	**LOICZ toolbox**
Net Phosphorus Flux across boundaries	**10^3 mol d^{-1}**	**74.9**	**12.2**	**LOICZ toolbox**
∆DIP	**10^3 mol d^{-1}**	**-74.9**	**12.2**	**LOICZ toolbox**
Nitrogen concentration (DIN) of Precipitation (DINp)	mmol m^{-3}	41.6	1.6	Casartelli *et al.* [2008]
Nitrogen concentration (DIN) of River flow (DINq)	mmol m^{-3}	26.5	0.6	Pereira [2003]
System Nitrogen concentration (DINsys)	mmol m^{-3}	15.0	0.6	Pereira [2003]
Downstream (Next Compartment) System Nitrogen concentration (DINocn=DINsysx)	mmol m^{-3}	6.7	0.2	Pereira [2003]
Residual flux Nitrogen concentration (DINr = [DINocn+DINsys]/2)	**mmol m^{-3}**	**10.8**	**0.3**	**LOICZ toolbox**

Nitrogen Flux in Precipitation (VpxNp)	**10^3 mol d^{-1}**	**1542.8**	**78.4**	**LOICZ toolbox**
	10^3 mol m^{-2} d^{-1}	**$1.5x10^{-7}$**	**$7.5x10^{-9}$**	**LOICZ toolbox**
Nitrogen Flux of River flow (VqxDINq)	**10^3 mol d^{-1}**	**3080.5**	**118.3**	**LOICZ toolbox**
	10^3 mol m^{-2} d^{-1}	**$3.2x10^{-7}$**	**$1.2x10^{-8}$**	**LOICZ toolbox**
Nitrogen Flux of Groundwater flow (VgxDINg)	**10^3 mol d^{-1}**	**0.0**	**0.0**	**LOICZ toolbox**
Nitrogen Flux of Other Freshwater flows (VoxDINo)	**10^3 mol d^{-1}**	**0.0**	**0.0**	**LOICZ toolbox**
Nitrogen Flux of Residual flows (VrxDINr)	**10^3 mol d^{-1}**	**-1281.8**	**57.5**	**LOICZ toolbox**
Nitrogen Flux of Residual flows (VrxDINr)	**10^3 mol m^{-2} d^{-1}**	**$-1.3x10^{-7}$**	**$5.9*10^{-9}$**	**LOICZ toolbox**
Net Nitrogen Flux of Exchange flow	**10^3 mol d^{-1}**	**-611.1**	**46.9**	**LOICZ toolbox**
Net Nitrogen Flux of Exchange flow	**10^3 mol m^{-2} d^{-1}**	**$-6.3x10^{-8}$**	**$4.9x10^{-9}$**	**LOICZ toolbox**
Net Nitrogen Flux across boundaries	**10^3 mol d^{-1}**	**2730.4**	**124.4**	**LOICZ toolbox**
∆DIN	**10^3 mol d^{-1}**	**-2730.4**	**124.4**	**LOICZ toolbox**
Local C:P molar ratio (ie Redfield C:P ratio)	unitless	106	0.0	Default
Local N:P molar ratio (ie Redfield N:P ratio)	unitless	16	0.0	Mean of all concentrations
Estimated Net Ecosystem Metabolism	**10^3 mol C d^{-1}**	**7935.3**	**1294.8**	**LOICZ toolbox**
Estimated Net Ecosystem Metabolism (Standard Unit)	**mmol C m^{-2} d^{-1}**	**0.8**	**0.1**	**LOICZ toolbox**
Expected DDIN	**10^3 mol d^{-1}**	**-1197.8**	**195.4**	**LOICZ toolbox**
Estimated N fixation - Denitrification (Standard Unit)	**mmol m^{-2} d^{-1}**	**-0.16**	**0.02**	**LOICZ toolbox**
Estimated N fixation - Denitrification	**10^3 mol d^{-1}**	**-1532.6**	**228.5**	**LOICZ toolbox**

Compartment / Concentration / Fluxes / Budgets	**Unity**	**Value entered by user (plain) or calculated by the toolbox (bold)**	**SD**	**References**
PLE BOX – PATOS LAGOON ESTUARY				
System area (A)	km^2	879.0	0.0	Quikin
System volume (V)	106 m^3	1680.0	0.0	Quikin
Average system depth (D)	**m**	**1.9**	**0.0**	**LOICZ toolbox**
Precipitation (Vp)	10^6 m^3 d^{-1}	3.4	0.2	INMET [2023]
Evaporation (Ve)	10^6 m^3 d^{-1}	-4.1	0.1	INMET [2023]
Freshwater River flow (Vq)	10^6 m^3 d^{-1}	35.8	0.9	ANA [2023]
Other Freshwater flows (Vo)	10^6 m^3 d^{-1}	0.0	0.0	Seiler *et al.* [2020]
Residual flow (Vr)	**10^6 m^3 d^{-1}**	**-153.4**	**4.1**	**LOICZ toolbox**
Upstream Residual flow (Vr)	**10^6 m^3 d^{-1}**	**118.3**	**4.0**	**LOICZ toolbox**
Upstream Exchange flow (Vx)	**10^6 m^3 d^{-1}**	**73.3**	**2.5**	**LOICZ toolbox**
System Salinity (Ssys)	**psu**	**18.5**	**0.4**	**LOICZ toolbox**
Ocean Salinity (Socn)	psu	32.2	1.0	Mean of Pereira [2003] and Bordin *et al.* [2023a]
Residual flux Salinity (Sr = [Socn+Ssys]/2)	**psu**	**25.4**	**0.6**	**LOICZ toolbox**
Salinity Flux in Precipitation (VpxSp)	**10^6 psu m^3 d^{-1}**	**0.0**	**0.0**	**LOICZ toolbox**
Salinity Flux of River flow (VqxSq)	**10^6 psu m^3 d^{-1}**	**0.0**	**0.0**	**LOICZ toolbox**
Salinity Flux of Groundwater flow (VgxSg)	**10^6 psu m^3 d^{-1}**	**0.0**	**0.0**	**LOICZ toolbox**
Salinity Flux of Other Freshwater flows (VoxSo)	**10^6 psu m^3 d^{-1}**	**0.0**	**0.0**	**LOICZ toolbox**
Salinity Flux of Residual flow (VrxSr)	**10^6 psu m^3 d^{-1}**	**-3888.8**	**145.3**	**LOICZ toolbox**
Salinity Flux of Exchange flow (Vx x (Socn-Ssys))	**10^6 psu m^3 d^{-1}**	**3888.8**	**145.3**	**LOICZ toolbox**
Exchange flow (Vx)	**10^6 psu m^3 d^{-1}**	**283.5**	**20.5**	**LOICZ toolbox**
Exchange time (tx)	**d**	**3.3**	**0.1**	**LOICZ toolbox**
Phosphorus concentration (DIP) of Precipitation (DIPp)	mmol m^{-3}	3.8	0.1	Casartelli *et al.* [2008]
Phosphorus concentration (DIP) of River flow (DIPq)	mmol m^{-3}	0.6	0.0	Pereira [2003]
Phosphorus concentration of Other Freshwater flows (DIPo)	mmol m^{-3}	18.2	0.0	Seiler *et al.* [2020]

System Phosphorus concentration (DIPsys)	**mmol m^{-3}**	**1.5**	**0.1**	**LOICZ toolbox**
Ocean Phosphorus concentration (DIPocn)	mmol m^{-3}	1.5	0.0	Mean of Pereira [2003] and Bordin *et al.* [2023a]
Residual flux Phosphorus concentration (DIPr = [DIPocn+DIPsys]/2)	**mmol m^{-3}**	**1.5**	**0.1**	**LOICZ toolbox**
Phosphorus Flux in Precipitation (VpxPp)	**10^3 mol d^{-1}**	**12.8**	**0.9**	**LOICZ toolbox**
	10^3 mol m^{-2} d^{-1}			**LOICZ toolbox**
Phosphorus Flux of River flow (VqxPq)	**10^3 mol d^{-1}**	**22.6**	**1.5**	**LOICZ toolbox**
	10^3 mol m^{-2} d^{-1}			**LOICZ toolbox**
Phosphorus Flux of Other Freshwater flows (VoxPo)	**10^3 mol d^{-1}**	**0.35**	**0.0**	**LOICZ toolbox**
	10^3 mol m^{-2} d^{-1}			**LOICZ toolbox**
Phosphorus Flux of Residual flows (VrxPr)	**10^3 mol d^{-1}**	**-226.6**	**10.0**	**LOICZ toolbox**
Phosphorus Flux of Residual flows (VrxPr)	**10^3 mol m^{-2} d^{-1}**	**$-2.6x10^{-7}$**	**$1.1x10^{-8}$**	**LOICZ toolbox**
Net Phosphorus Flux of Exchange flow	**10^3 mol d^{-1}**	**10.4**	**28.6**	**LOICZ toolbox**
Net Phosphorus Flux of Exchange flow	**10^3 mol m^{-2} d^{-1}**	**$1.2x10^{-8}$**	**$3.3x10^{-8}$**	**LOICZ toolbox**
Net Phosphorus Flux across boundaries	**10^3 mol d^{-1}**	**-33.9**	**35.9**	**LOICZ toolbox**
∆DIP	**10^3 mol d^{-1}**	**33.9**	**35.9**	**LOICZ toolbox**
Nitrogen concentration (DIN) of Precipitation (DINp)	mmol m^{-3}	41.2	0.5	Casartelli *et al.* [2008]
Nitrogen concentration (DIN) of River flow (DINq)	mmol m^{-3}	31.7	0.4	Pereira [2003]
Nitrogen concentration of Other Freshwater flows (DINo)	mmol m^{-3}	1428.0	0.0	Seiler *et al.* [2020]
System Nitrogen concentration (DINsys)	**mmol m^{-3}**	**6.7**	**0.2**	**LOICZ toolbox**
Ocean Nitrogen concentration (DINocn)	mmol m^{-3}	4.0	0.2	Mean of Pereira [2003] and Bordin *et al.* [2023a]
Residual flux Nitrogen concentration (DINr = [DINocn+DINsys]/2)	**mmol m^{-3}**	**5.3**	**0.1**	**LOICZ toolbox**
Nitrogen Flux in Precipitation (VpxNp)	**10^3 mol d^{-1}**	**138.1**	**7.8**	**LOICZ toolbox**
	10^3 mol m^{-2} d^{-1}			**LOICZ toolbox**
Nitrogen Flux of River flow (VqxDINq)	**10^3 mol d^{-1}**	**1134.5**	**30.7**	**LOICZ toolbox**
	10^3 mol m^{-2} d^{-1}			**LOICZ toolbox**
Nitrogen Flux of Groundwater flow (VgxDINg)	**10^3 mol d^{-1}**	**0.0**	**0.0**	**LOICZ toolbox**
Nitrogen Flux of Other Freshwater flows (VoxDINo)	**10^3 mol d^{-1}**	**27.1**	**0.0**	**LOICZ toolbox**
	10^3 mol m^{-2} d^{-1}			**LOICZ toolbox**
Nitrogen Flux of Residual flows (VrxDINr)	**10^3 mol d^{-1}**	**-816.4**	**31.1**	**LOICZ toolbox**
Nitrogen Flux of Residual flows (VrxDINr)	**10^3 mol m^{-2} d^{-1}**	**$-9.3x10^{-7}$**	**$3.5x10^{-8}$**	**LOICZ toolbox**
Net Nitrogen Flux of Exchange flow	**10^3 mol d^{-1}**	**-761.6**	**88.4**	**LOICZ toolbox**
Net Nitrogen Flux of Exchange flow	**10^3 mol m^{-2} d^{-1}**	**$-8.7x10^{-7}$**	**$1x10^{-7}$**	**LOICZ toolbox**
Net Nitrogen Flux across boundaries	**10^3 mol d^{-1}**	**1614.8**	**125.5**	**LOICZ toolbox**
∆DIN	**10^3 mol d^{-1}**	**-1614.8**	**125.5**	**LOICZ toolbox**
Local C:P molar ratio (ie Redfield C:P ratio)	unitless	106.0	0.0	Default
Local N:P molar ratio (ie Redfield N:P ratio)	unitless	16.0	0.0	Mean of all concentrations
Estimated Net Ecosystem Metabolism (Phytoplankton)	**10^3 mol d^{-1}**	**-3329.8**	**3288.7**	**LOICZ toolbox**
Estimated Net Ecosystem Metabolism (Seagrasses)	**10^3 mol d^{-1}**	**-1744.8**	**1689.4**	**LOICZ toolbox**
Estimated Net Ecosystem Metabolism (Average)	**10^3 mol d^{-1}**	**-5074.6**		**LOICZ toolbox**
Estimated Net Ecosystem Metabolism (Phytoplankton)	**mmol C m^{-2} d^{-1}**	**-4.4**	**4.3**	**LOICZ toolbox**
Estimated Net Ecosystem Metabolism (Seagrasses)	**mmol C m^{-2} d^{-1}**	**-14.5**	**14.0**	**LOICZ toolbox**
Estimated Net Ecosystem Metabolism (Average)	**mmol C m^{-2} d^{-1}**	**-5.7**	**5.6**	**LOICZ toolbox**
Expected DDIN	**10^3 mol d^{-1}**	**542.5**	**574.9**	**LOICZ toolbox**
Estimated N fixation - Denitrification (Standard Unit)	**mmol m^{-2} d^{-1}**	**-2.5**	**0.7**	**LOICZ toolbox**
Estimated N fixation - Denitrification	**10^3 mol d^{-1}**	**-2157.3**	**595.0**	**LOICZ toolbox**

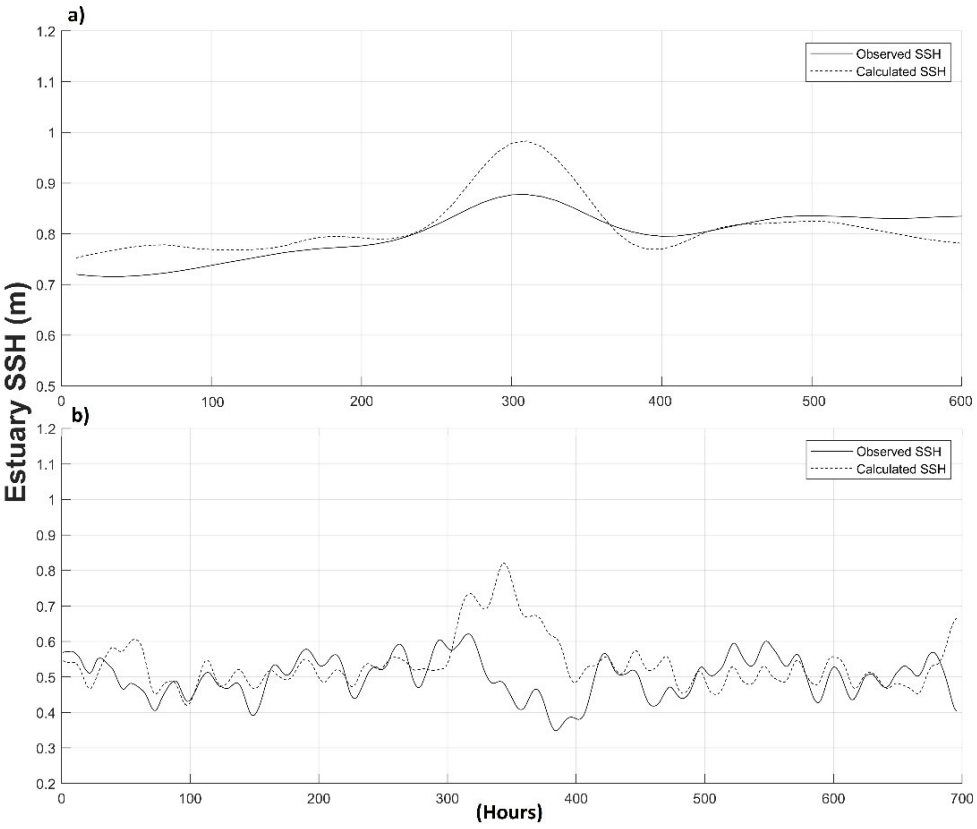

Figure B.2. Temporal series of the observed and calculated estuary surface height (SSH) at a) São Lourenço do Sul (SL) and b) Rio Grande Port Pilotage (RGP) stations.

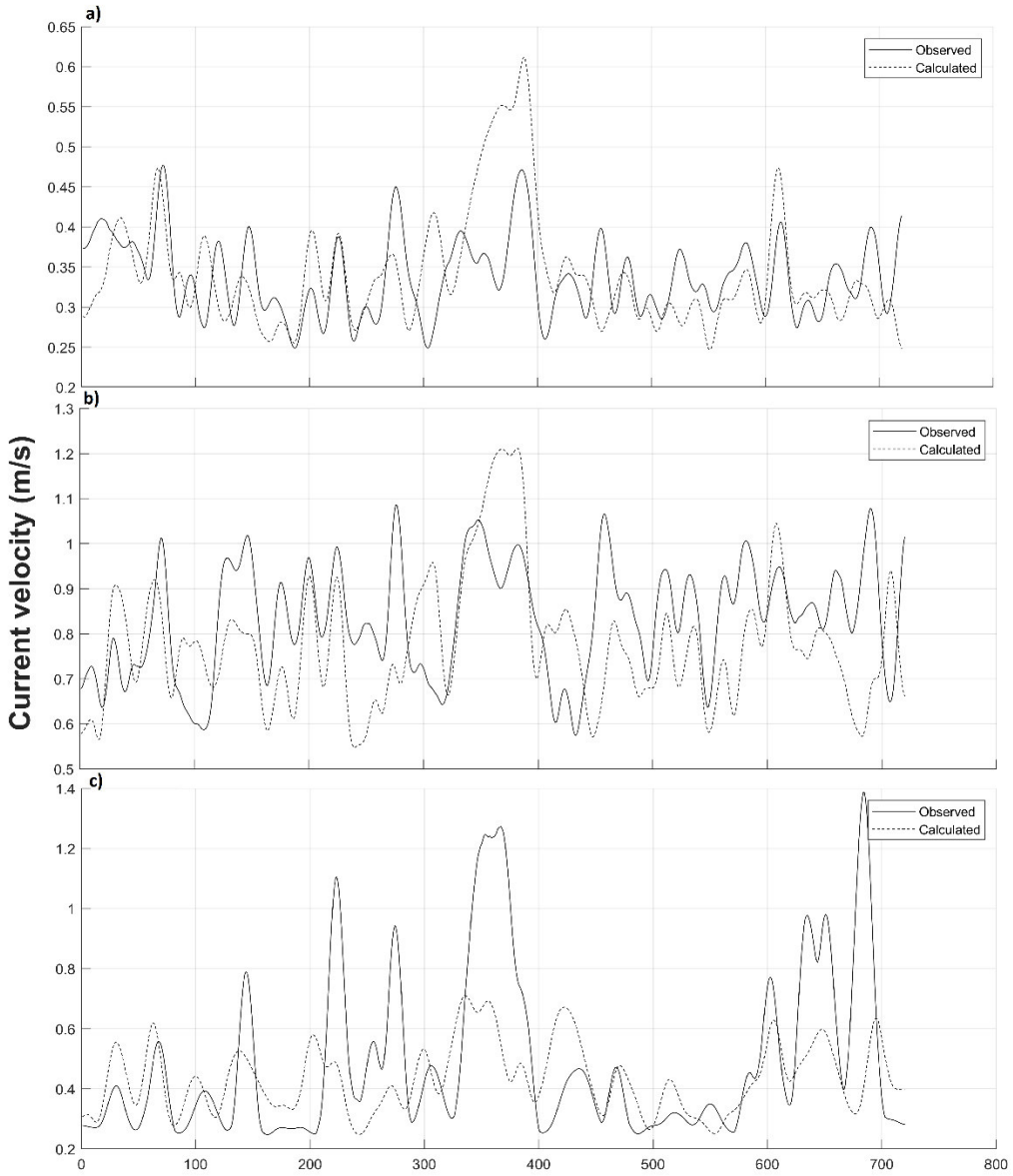

Figure B.3. Temporal series of the observed and calculated longitudinal current velocity at the stations a) 1, b) 2 and c) 4.

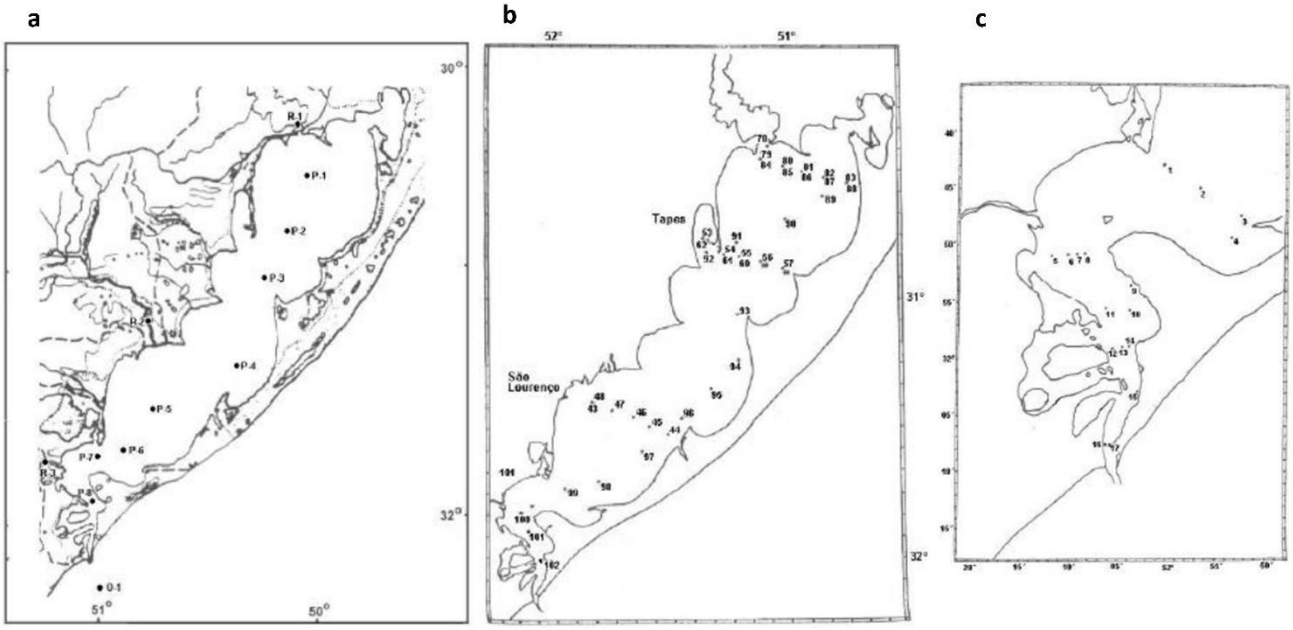

Figure B.4. Map of Patos Lagoon (a, b) and its estuarine zone (c), with sampling stations on N-S axis from Projeto Mar de Dentro (a), N-S and E-W axis from Projeto Espinha (b, c). Figure adapted from Pereira [2003].

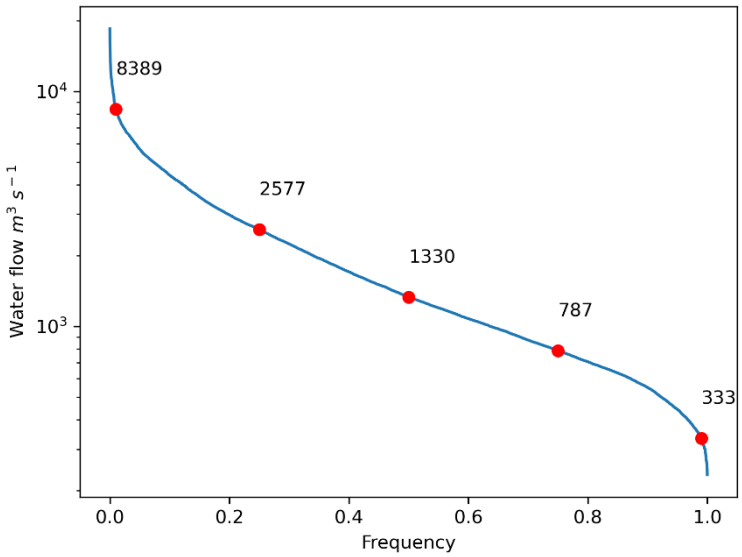

Figure B.5. Total river discharge $m^3 s^{-1}$ from Guaíba and Camaquã rivers into the Patos Lagoon Estuary, at 0.01, 0.25, 0.5, 0.75 and 0.99 (x10 = %) frequencies, estimated from climatological data [ANA, 2023].

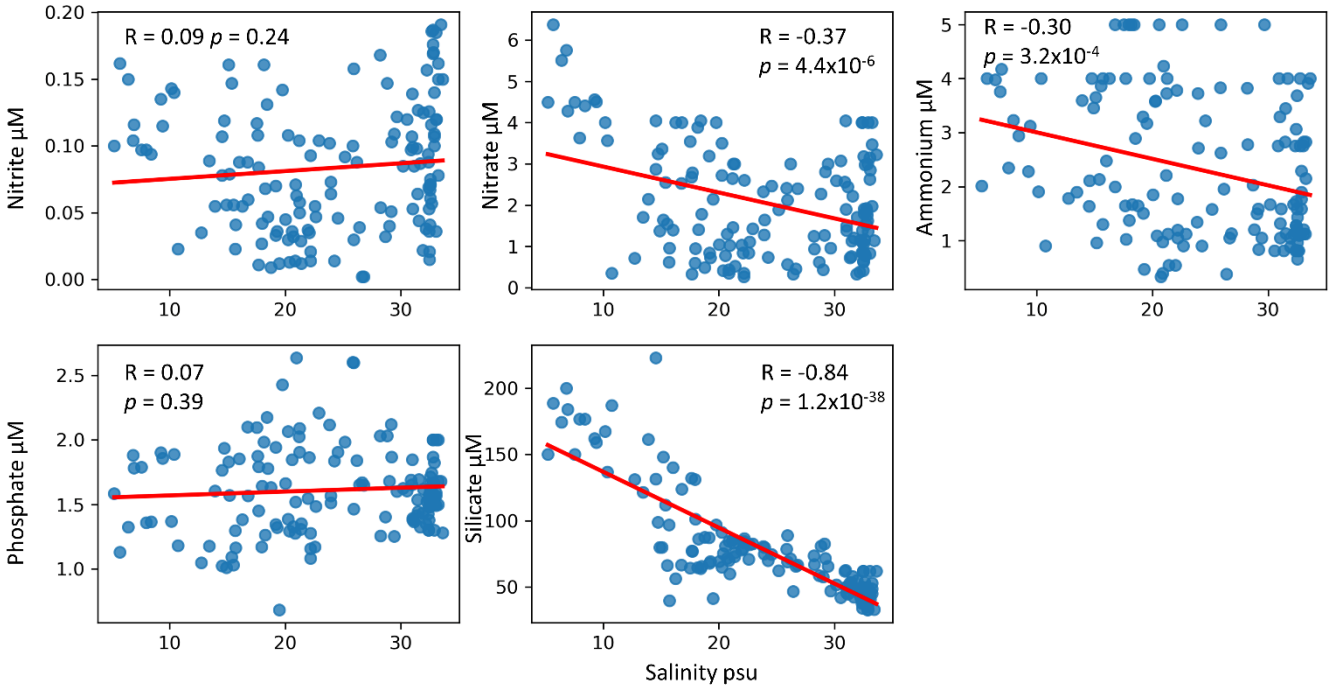

Figure B.6. Scatterplot of salinity vs. dissolved inorganic nutrients nitrite, nitrate, ammonium, phosphate and silicate, with trendline (red line), Pearson's correlation coefficient (R) and p-value (p). Data for Stations RS-1 and RS-2 [Bordin *et al.* 2023a].